UiT The Arctic University of Norway

Faculty of Health Sciences

Novel insights into the fenestrated scavenger endothelium of the liver sinusoid

A study on the fenestrations and endocytic function of liver sinusoidal endothelium

Christopher Florian Holte

A dissertation for the degree of Philosophia Doctor January 2024

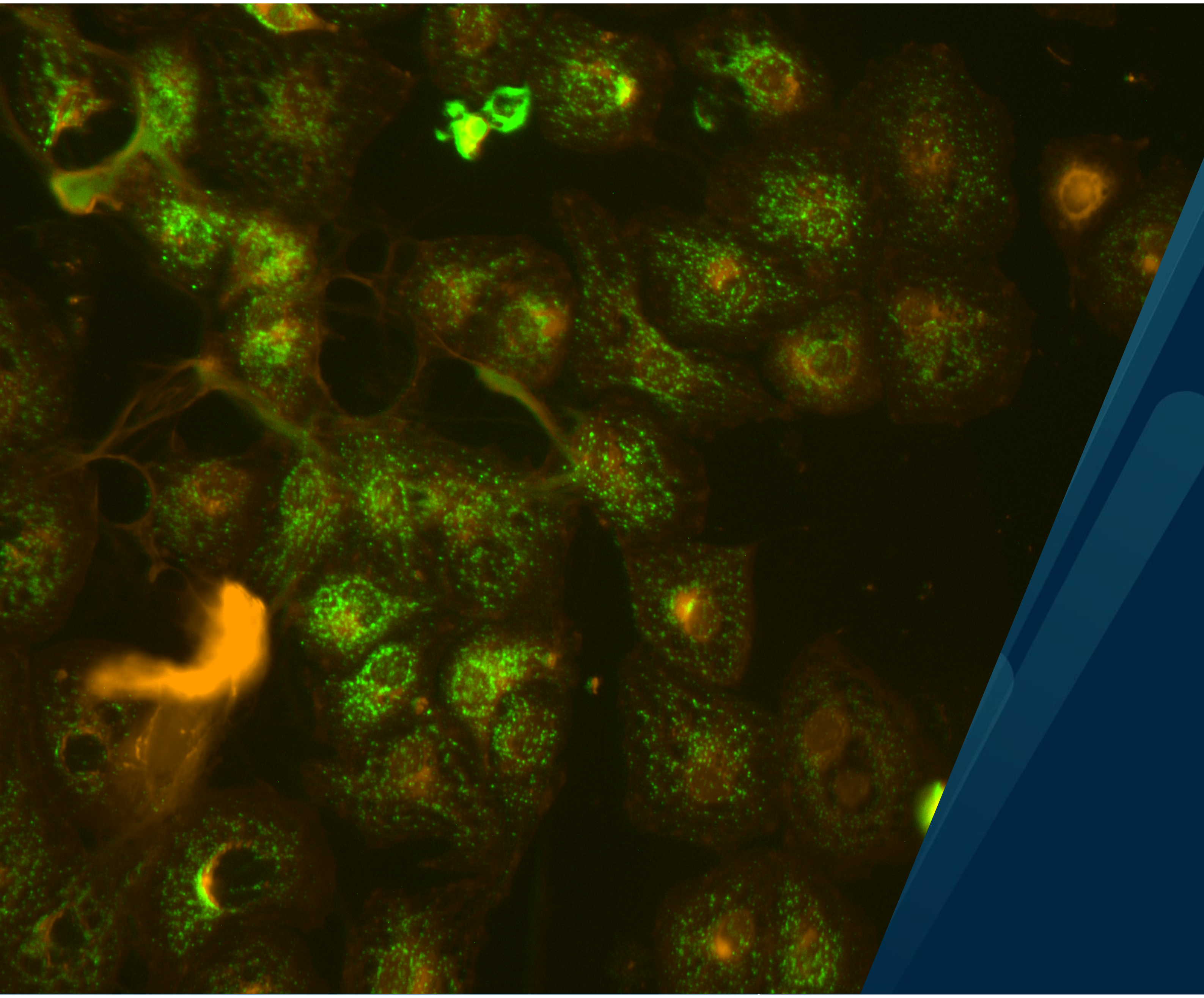

Novel insights into the fenestrated scavenger endothelium of the liver sinusoid

A study on the fenestrations and endocytic function of liver sinusoidal endothelium

Christopher Florian Holte

A dissertation for the degree of Philosophiae Doctor

Vascular Biology Research Group
Institute of Medical Biology
Faculty of Health Sciences
UiT – The Arctic University of Norway

January 2024

Table of Contents

Title Page image: mouse LSEC treated with Alexa Fluor 488 labelled oxHSA (green) and counterstained with cell mask orange (orange).

“The purpose of a system is what it does.”

S. Beer

“The story so far: In the beginning the Universe was created. This has made a lot of people very angry and been widely regarded as a bad move.”

D. Adams

Acknowledgements

This thesis has been made possible through the generous financial support from a number of esteemed institutions. I am profoundly grateful for the funding provided by UiT - The Arctic University of Norway, the Research Council of Norway, and the European Union, which collectively formed the financial backbone of this research endeavour.

The journey of this thesis was navigated under the expert guidance of Professor Peter AG McCourt, whose supervision was both an honour and a privilege. His wisdom and mentorship have been invaluable throughout this process. Additionally, I owe a debt of gratitude to Associate Professor Anett K Larsen for her co-supervision, insightful feedback, and unwavering support.

My heartfelt appreciation goes out to the engineering wizards of our team—Gianina, Jaione, and Ruomei. Their technical prowess and innovative problem-solving skills were instrumental in the success of this work. Their contributions were nothing short of magical, and I am deeply thankful for their involvement.

I am also indebted to the scientific staff within the vascular biology research group. Karen, Bård, Kjell, Javier and Cristina have been a source of inspiration and knowledge. Their collaborative spirit and willingness to share their expertise have greatly enriched my research experience over the course of these years.

A special note of thanks is extended to the 'McTeam'—Karolina, Larissa, Tanja, Kuba, and our honorary members Eike and Philip, as well as our past member Hong and our new member Kanji. Your camaraderie and support have been a cornerstone of my journey.

Karolina deserves a special mention for her enduring patience and support over the last five years. Her strength and encouragement have been a constant source of comfort and motivation, for which I am eternally grateful. I must also express my gratitude to Enya and Ellie, whose ability to lift my spirits and brighten even the most challenging days has been a true gift.

My sincere thanks are extended to our collaborators who have invested their time and expertise. Matteo, in particular, for his pivotal role in the realization of **Paper II**. Dmitiri for his HPLC expertise in **Paper III**. Tom, Randi and the other staff at KAM, for invaluable assistance with the microscopes. I am also grateful to our Australian colleagues—David, Victoria, Nick, and Glenn—for their warm hospitality and the enriching experience provided in their laboratory in Sydney. Furthermore, I would like to acknowledge the valuable contributions of Bartek, Balpreet, Deanna, and Louise, whose collaborative efforts have been essential to our research.

Finally my thanks go out to my friends and my parents for support and encouragement, when I needed it.

In summary, this thesis is not just a reflection of my efforts, but a tapestry woven from the contributions of many. To all who have been a part of this journey, I extend my deepest thanks.

Summary

The sinusoids (specialized small blood vessels) of the liver are covered by endothelium (blood vessel wall cells) with open transcellular pores (holes that go from one side to the other) called fenestrations. This allows for efficient bidirectional transfer of solutes between the blood and the hepatocytes (main metabolic liver cell). These fenestrations can disappear or reduce in number and size in disease states or in ageing. We therefore sought to map the literature on compounds, that affect these fenestrations, and to hypothesize how the mechanism regulating them operates.

The fenestrations are unevenly distributed along the sinusoid, with there being a greater fraction of the cell surfaces covered by these pores towards the end (the pericentral area) compared with the start of the vessel (the periportal area). There are also lymphatic vessels in the periportal area, in a space behind the portal vein and hepatic artery, which is often omitted from consideration in anatomical illustrations and flow models of the liver. We therefore sought to make a digital model at the single sinusoid level, including these ultrastructural details, to assess their influence on fluid flow parameters.

The liver endothelium is a scavenging endothelium, that is to say high capacity waste removal cells specialized in macromolecular and nanoparticle sized waste from the blood stream. Albumin is the single most abundant protein in blood, with chemically modified forms of it being found in several pathologies, especially diabetes or liver disease. It was found by a Japanese research group, Iwao et al., that when albumin is highly oxidized, it is rapidly removed from the blood stream, mainly by the liver. The properties of the liver sinusoidal endothelium as a scavenger endothelium, and the clearance kinetics led us to believe this was done by the liver sinusoidal endothelium and its stabilin receptors, because of the functions of these in respect to other modified albumins. We indeed found that this was the case.

The analysis of fenestrations from microscopy images is a laborious process, and contains the possibility of introducing user bias into quantifications. We assessed three different methods of image analysis for the purpose of quantifying fenestration parameters. These were manual, semi-automated/thresholding based, and fully automated/neural network based approaches. The manual classification method had little bias with regards to number, whilst showing significant user bias for diameter/size of fenestration. The semi-automated was the least biased with regard to diameter/size, but significantly biased with regards to number. The fully automated also showed considerable user bias for all parameters, however it can be used for batch processing. The methods are roughly ordered by speed (manual, semi-automated, fully automated), with regards to larger data sets.

List of Publications

Paper I

Karolina Szafranska*, Larissa D. Kruse*, **Christopher Florian Holte***, Peter McCourt, and Bartlomiej Zapotoczny. "The wHole story about fenestrations in LSEC." Frontiers in physiology 12 (2021): 735573.

*shared first authorship

Paper II

Matteo Boninsegna, Peter AG McCourt, and **Christopher Florian Holte†**. "The Computed Sinusoid." Livers 3, no. 4 (2023): 657-673.

† corresponding author

Paper III

Christopher Holte†, Karolina Szafranska, Larissa Kruse, Jaione Simon-Santamaria, Ruomei Li, Dmitri Svistounov, and Peter McCourt. "Highly oxidized albumin is cleared by liver sinusoidal endothelial cells via the receptors stabilin-1 and-2." Scientific Reports 13, no. 1 (2023): 19121.

† corresponding author

Paper IV

Karolina Szafranska, **Christopher Florian Holte**, Larissa Dorothea Kruse, Hong Mao, Cristina Ionica Øie, M. Szymonski, Bartlomiej Zapotoczny, and P. A. G. McCourt. "Quantitative analysis methods for studying fenestrations in liver sinusoidal endothelial cells. A comparative study." Micron 150 (2021): 103121.

Additional publications not included in this thesis:

V Karolina Szafranska, Tanja Neuman, Zbigniew Baster, Zenon Rajfur, Oskar Szelest, **Christopher Holte**, Agata Kubisiak et al. "From fixed-dried to wet-fixed to live–comparative super-resolution microscopy of liver sinusoidal endothelial cell fenestrations." Nanophotonics 11, no. 10 (2022): 2253-2270.

VI Hong Mao, Karolina Szafranska, Larissa Kruse, **Christopher Holte**, Deanna L. Wolfson, Balpreet Singh Ahluwalia, Cynthia B. Whitchurch et al. "Effect of caffeine and other xanthines on liver sinusoidal endothelial cell ultrastructure." Scientific Reports 13, no. 1 (2023): 13390.

List of Abbreviations

«CD» - Cluster of Differentiation

«SR» - Scavenger Receptor

µCT - Micro Computed Tomography

AcLDL - Acetylated LDL

AFM - Atomic Force Microscopy

AGE - Advanced Glycation End Product

AOPP - Advanced Oxidation Protein Product

BSA - Bovine Serum Albumin

cAMP - cyclic Adenosine Mono Phosphate

cGMP - cyclic Guanosine Mono Phosphate

Coll. - Collagen

CV - Central Vein

dSTORM - direct Stochastic Optical Reconstruction Microscopy

EC-LDL - Endothelial Cell (modified) LDL

EGF - Endothelial Growth Factor

eNOS - endothelial Nitrous Oxidase

FITC - Fluorescein Iso Thio Cyanate

FSA - Formylated Serum Albumin

GTP - Guanosine Tri Phosphate

HA - Hepatic Artery

HC - Hepatocyte

HDL - High Density Lipoprotein

HEK - Human Embryonic Kidney (Cell Line)

Hep. - Hepatocyte

HIV - Human Immunodeficiency Virus

HSA - Human Serum Albumin

HSC - Hepatic Stellate Cell

LDL - Low Density Lipoprotein

LIMK1 – LIM domain Kinase 1

LSEC - Liver Sinusoidal Endothelial Cell

LV - Lymphatic Vasculature

MAPK – Mitogen Activated Protein Kinase

MK2 – Mitogen activated protein kinase Kinase 2

MLCK - Myosin Light Chain Kinase

Nuc. - Nucleus

oxHSA - (highly) oxidized HSA

oxLDL - oxidized LDL

PIINP – Procollagen II N-terminal propeptide

PINP – Procollagen I N-terminal propeptide

PV - Portal Vein

RBC - Red Blood Cell

RES - Reticulo-Endothelial System

RhoA/ROCK – Ras family homologue member A/ Rho associated coiled coil containing protein kinase

SC - Stellate Cell

SD - Space (of) Disse

SEC - Scavenger Endothelial Cell

SEM - Scanning Electron Microscopy

SIM - Structured Illumination Microscopy

siRNA - silencing Ribo Nucleic Acid(s)

SoD - Space of Disse

SPARC - secreted protein acidic and rich in cysteine

STED - Stimulated Emission Depletion (Microscopy)

SV40 - Simian Virus 40

$t_{1/2}$ - half-life, half time

TEM - Transmission Electron Microscopy

TRITC - Tetramethylrhodamine

TAA - Thioacetamide

VitE - Vitamin E

VLVL - Very Low Density Lipoprotein

1 Introduction

1.1 The liver

The liver is the largest of the internal organs, coming in at around 2% of total body weight in the normal healthy adult. The perfused colour of the liver is burgundy/red, indicative of its extensive vascularization, and a light shade of brown when washed free of blood. It is situated at the top of the peritoneum in the right hypochondrial, a space of which it occupies the majority of, and epigastric regions. To retain its elevated position it is secured in place by a number of ligaments, attaching the organ to its surrounding and the venous attachments to the inferior vena cava. The liver extends from the fifth intercostal to just before the costal margin, its surface covered by a connective tissue layer named Glisson's capsule with convex upper and concave lower surfaces. The functional anatomy of the liver subdivides the organ in ways that are not readily observable from the surface. Subdivisions are in accordance with blood and biliary vasculature, the first level of subdivision divides the liver into two hemi-livers, the second divides these into four sections and these further into a total of 8 segments. The segments have their own blood-supply and biliary drainage, allowing for isolated resections of these. The liver's blood supply - the portal vein and hepatic artery - together with the bile-duct and nerves enter into the liver from its hilus the porta hepatis, with blood outflow draining into three main separate hepatic veins and further into the inferior vena cava. The liver's lymphatics drain through several different routes, some adjacent to the hepatic veins, and some through the porta hepatis, all eventually draining into the thoracic duct. The liver's blood supply consists of 70-80% venous low oxygenated blood, from the portal vein, and 20-30% highly oxygenated arterial blood from the hepatic artery. In the normal healthy adult approximately 1.5L of blood circulates through the liver every minute, constituting about a quarter of cardiac output [1, 2, 3].

1.1.1 Main functions of the liver

The canonical main functions of the liver, are metabolic, performed by its parenchymal cells the hepatocytes. These include:

Bile formation: bile acids which aid lipid absorption by emulsifying lipids in the small intestine, are formed from cholesterol by hepatocytes and secreted into bile canaliculi, which drain into bile ducts which drain into the gall bladder and from there is secreted into the small intestine. Bilirubin formed by the metabolism of heme is excreted through this route, it reaches the liver conjugated to albumin, and is converted into its soluble form by the hepatocytes before excretion via the biliary system.

Protein synthesis: hepatocytes synthesize the major plasma proteins, save for immunoglobulins, such as albumin, fibrinogen, prothrombin, transferrin and lipoproteins.

Glucose homeostasis: hepatocytes synthesize or break into glucose their glycogen storage in response to pancreatic hormones insulin and glucagon. Further the hepatocytes can also form glucose out of other carbohydrates, and from amino acids.

Lipid metabolism: oxidation of triglycerides for energy, synthesizing plasma lipoproteins and cholesterol and phospholipids.

Drugs and xenotoxins: hepatocytes metabolize a wide host of exogenous compounds, such as drugs and toxicants, largely via cytochrome complexes [4,3,5].

1.1.2 Microanatomy and ultrastructure of the liver

The liver vasculature branches out extensively, into a tortuous network of special capillaries dubbed sinusoids. The terminal parts of the portal veins and hepatic arteries drain into the sinusoids, which in turn drain into the central vein, flowing out of the liver into the inferior vena cava [5,4].

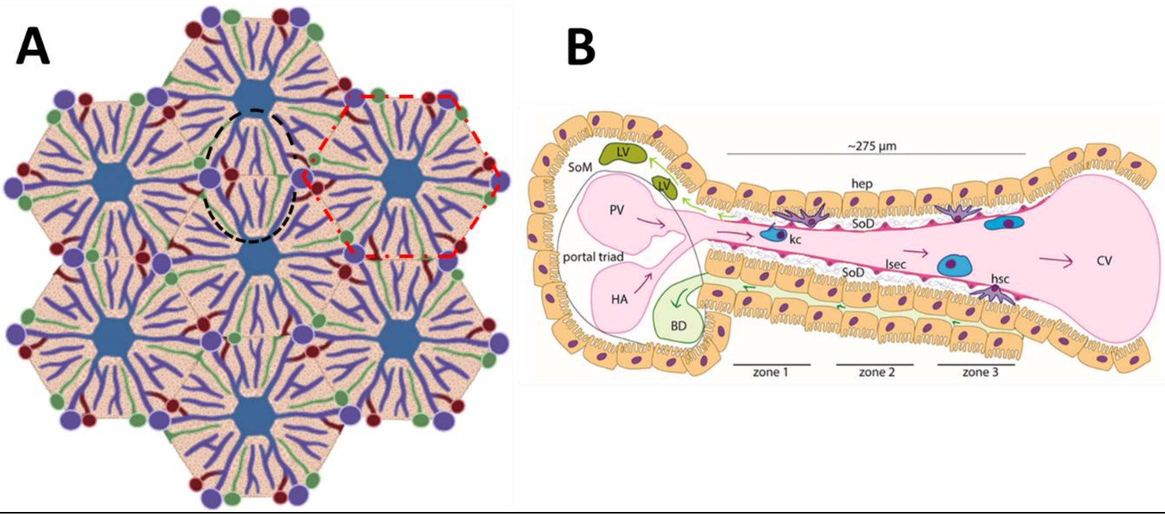

Figure 1.1: **A** Schematic of liver architecture with classical lobules, example indicated by red dashed line, and example of liver acinus indicated by black dashed line. Portal vein and sinusoids in purple, hepatic artery in red, central vein blue, and bile ducts in green (lymphatics omitted). (Schema created using BioRender.com) **B** Schematic of a single liver sinusoid showing direction of flow from portal vein (PV) and hepatic artery (HA) to central vein (CV). SoD=Space of Disse, KC=Kupffer cell, hsc=Hepatic Stellate cell, SoM=Space of Mall, hep=Hepatocytes, BD=Bile Duct, LV=Lymphatic Vasculature. Illustration from **Paper II**.

The sinusoids form a complex three dimensional network, best appreciated by observing vascular corrosion casts under scanning electron microscopy (SEM) or micro computed tomography (µ-CT) [6,7,8,9]. These are often divided into structurally repeating segments, such as classical hepatic lobules, consisting of a central vein, and the surrounding sinusoids and portal triads (portal vein, hepatic artery, bile duct) flowing into it, these have the appearance of repeating hexagons. Alternatively, the liver can be divided into functional units, the more modern concept of the hepatic acini. The acinus lies between two or more venules, with blood flowing from portal tracts through sinusoids towards the venules. This functional unit is somewhat more difficult to discern in histological preparations, but is more accurate in regard to the perfusion of the liver sinusoids [5].

1.2 Fenestrations, what they are and where they are found

1.2.1 What fenestrations are

Fenestrations (trans-cellular pores) are not uncommon in the body with sites of absorption, excretion or endocrine glands being sites with fenestrations. There are other definitions of transcellular pores, where fenestrations are considered but one type of these, however as this is not fully standardized terminology, for the purpose of this introduction all transcellular channels shall be considered ‘fenestrations’.

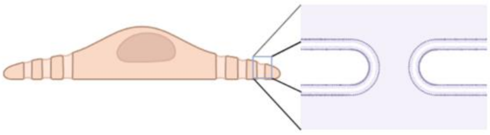

Figure 1.2: Fenestrations are transcellular pores, connecting the luminal to abluminal sides of a cell, typically an endothelial cell. (Created with BioRender.com)

The existence of such structures had been theorised on account of permeabilities of fluids and certain solutes in capillaries [10]. However being structures smaller than the diffraction limit of visible spectrum light [11], they could not be observed directly until the development of super-resolved microscopies (those that can resolve finer details than diffraction limited visible light microscopies), the first of which was the electron microscope [12].

The confirmation of the existence of these structures was only possible with advances in tissue preservation and sectioning for transmission electron microscopy (TEM)[12] which occurred in the late 1940’s and early 1950’s [13,14,15,16,17]. Prior to the advances in sample preparation, while the electron microscope possessed the necessary resolution, the tissue sections were of too poor quality or too thick to correctly identify ultrastructural details such as fenestrations [18].

1.2.2 Where fenestrations are found

The following section will describe the different organs, tissues and vascular beds where fenestrations have been found.

Endocrine / hormone secreting glands

Hormone secreting glands mostly contain fenestrated endothelium, presumably to allow more rapid distribution to the bloodstream of hormones from the secretory cells. The anterior pituitary gland [5,19,20], the adrenal gland [5], including the adrenal cortex [21,22,23] and adrenal medulla [24], the pineal gland [25], thyroid gland [26,27,28,29], parathyroid [30], pancreatic island capillaries [31], neurohypophysis [32,33], corpus luteum [34] have fenestrated endothelial beds. Testicular endothelium likewise is fenestrated [4], specifically type IV endothelium [35].

Other vascular beds

The choriocapillaris (capillaries in the eyes, over the retinal pigment epithelium) endothelium is fenestrated [36,37]. Synovial membrane (in bone) endothelium is described as fenestrated [4,38,39]. Bone marrow sinusoidal endothelium forms large fenestrations to allow the passage of blood cells, and there are also occasionally smaller fenestrations vaguely similar to that in other fenestrated endothelium, though this form is very rarely observed [experimental and reviewed in 40]. Senior angioma (aka cherry angiomas) were found to contain fenestrated capillaries [41,42]. Tongue endothelium was found to be fenestrated in frogs [43]. Gingival terminal vascular bed capillaries of rabbits are 30% fenestrated [44]. The splenic sinusoids are notable for having very large open fenestrations on the reticular/rod cells [45], as well as intercellular gaps between endothelia of the vascular sinus, which are presumed to filter out rigid red blood cells [46]. In the lymph nodes it has been theorized there are also fenestrations on account of permeabilities of certain solutes [reviewed in [47]], and larger fenestrations allowing macrophages behind to access the lumen [[48]].

Mesentery/Peritoneum

The human parietal and rabbit diaphragmatic peritoneum contain fenestrated capillaries [[49]]. Mesentery capillaries are 26.6% of the fenestrated type [[50]].

Muscle capillaries

The soleus muscle capillaries were found to be fenestrated, though to a lesser extent than other fenestrated capillaries, with 1 in 60 ultra-thin sections showing fenestrations [[51]]. The number of fenestrations was found significantly increased in animals with immobilized hind-legs in a SEM study [[52]], indicating they may be induced in instances of remodelling or atrophy. Indeed it was found that the capillaries of the extensor digitorum longus became increasingly fenestrated with increasing age in rats [[53],[54]]. The atrioventricular node (AV-node) in the heart, confirmed in rats, cats, mice, rabbit, primates also possesses fenestrated endothelium [[55],[56]], which Shimada et al. [[56]] take to be in connection with the heart's lymphatic vasculature, and connected with signalling to the node.

Skin

The terminal capillaries of rat skin exhibit fenestrated endothelium [[57]], this is another area in which fenestrated endothelium is in proximity to lymphatic vasculature, as distribution studies on LPS have shown, the murine footpad extracellular extravascular space drains into proximal lymph nodes [[58]]. This may differentiate the interstitial spaces [[59]] in different anatomical locations, as the presence of fenestrated endothelium suggests a greater localized flow-rate in certain areas, which should have nowhere else to go than into the lymphatic vasculature, except in secretory organs or glands, and these fenestrations may be inducible under different conditions, as was found for muscle tissue [[53],[54]].

Absorption / excretion related

Kidney glomerular capillaries [[5],[60],[61]], capillaries of the lamina propria of the intestinal villi [[62]], lymphatic endothelium below enterocytes [[5]], the intestinal villi epithelial basal lamina [[63],[64]] are fenestrated. Last but not least, the sinusoids of the liver are lined with fenestrated endothelium [[65],[66],[67],[62],[68],[69]]. The liver being one of the more fragile organs with respect to fixation artefacts and perfusion pressure [[70]], was only observed in a well preserved manner from Yamagishi's 1959 [[68]] paper onwards, with earlier work showing extensive tissue damage, which made interpretations substantially more difficult. Unified nomenclature and standardization of fixation pressures and technique were introduced by Wisse in his 1970 paper [[69]]. There exists some confusion in literature, as nomenclature was not standardized early on, and still misleading terminology such as "discontinuous endothelium" "intercellular gaps" are used about fenestrations. This confusion is likely a holdover from the aforementioned poor fixation and tissue preparation, indeed it was found that immersion fixation of blocks of liver tissue showed examples of this very artefact [[69]], though perfusion pressures also greatly affect tissue preservation [[69],[71]].

Open or diaphragmed fenestrations

Fenestrations can further be diaphragmed or un-diaphragmed and have dense or sparse glycocalyx depending on the tissue and function. However, not all fenestrated tissues have been investigated this thoroughly.

The endothelium of the pituitary [72,73,74] is an example of diaphragmed fenestrated endothelium, with a PLVAP (Plasmalemma vesicle associated protein) "plug" and diaphragm across its fenestrations. The endothelium of the choriocapillaris is plugged by a PLVAP membrane. Glomerular endothelium, and exocrine pancreatic endothelium likewise are diaphragmed fenestrated endothelium, with PLVAP associated diaphragms. Knock out models (PLVAP -/-) showed there were still endothelial fenestrations but now without diaphragms, and of less uniform sizes [75]. Solus muscle and AV-node fenestrations also contain diaphragms [51].

Function of fenestration diaphragms

The diaphragm of fenestra serves a role in restricting the size of solutes passing through, as was found for the endothelium of the choriocapillaris, where tracers above a certain size were excluded, horseradish peroxidase (Einstein-Stokes Radius (ESR): 30Å, MW: 44kDa) could cross while haemoglobin (ESR: 32Å, MW: 64.5kDa) and lactoperoxidase (ESR: 40Å, MW: 78kDa) could not [76]. This shows that diaphragmed fenestrations are not permeable to many serum proteins, albumin for example (ESR: 35Å) [77]. Diaphragms are found also in caveola [75,78], suggesting a size exclusion mechanism for caveola mediated uptake.

The endothelium of the liver sinusoids is the preeminent example of completely open pores, that is un-diaphragmed fenestrations that allow completely free passage to fluid, solutes, particulates and colloids [69]. However the fenestrations of the liver may obtain diaphragms under diseased conditions [71], this would greatly limit the access of solutes to the space of Disse compared with the normal healthy state, and presents the aberrant transformations of fenestrations as a mechanism of disease.

In summary, there are numerous sites in the body possessing fenestrations, even in non-endothelial cells, such as the epithelial cells of the intestinal villi. The formation of fenestrations in endothelial cells seems to follow an underlying 'program' independent of which 'type' of endothelial fenestration, certainly with regards to glomerular/pituitary/liver sinusoidal endothelial cell fenestrations, which seem differentiated only by the expression of PLVAP with regard to their structures. Their induction may be through similar stimuli from their underlying parenchyma or vessel flow characteristics and oxygen tensions. The presence of fenestrations can also be pathological, or the result of degeneration related as shown in ageing and immobilization experiments.

1.3 LSEC and fenestrations

Evolutionary conservation of fenestrated liver sinusoids

The fenestrations of the liver sinusoid are a highly evolutionarily conserved feature, having been found in seemingly all species examined that have livers. Of the following (non-exhaustive) list; mammals such as humans [79, 80, 81], macaques [82], rabbits [68], rats [69], bats [83] and even more evolutionarily distant species such as chickens [84], quail, pigeons, society finches [85], soft shelled turtles [86], Japanese grass lizards, tiger keelback snakes [87] carps [88], flatfish [89], grass-puffer fish, Tana lungfish, Japanese eels [90] Atlantic croakers [91], and all the way down to Atlantic hagfish [92] and sea lamprey [93], have fenestrated liver sinusoids. The fenestrated endothelium appears to be an integral part of the functional vertebrate liver and seem to be found in all species examined. Presumably fenestrations do not occur in invertebrates, as these lack proper endothelium [94].

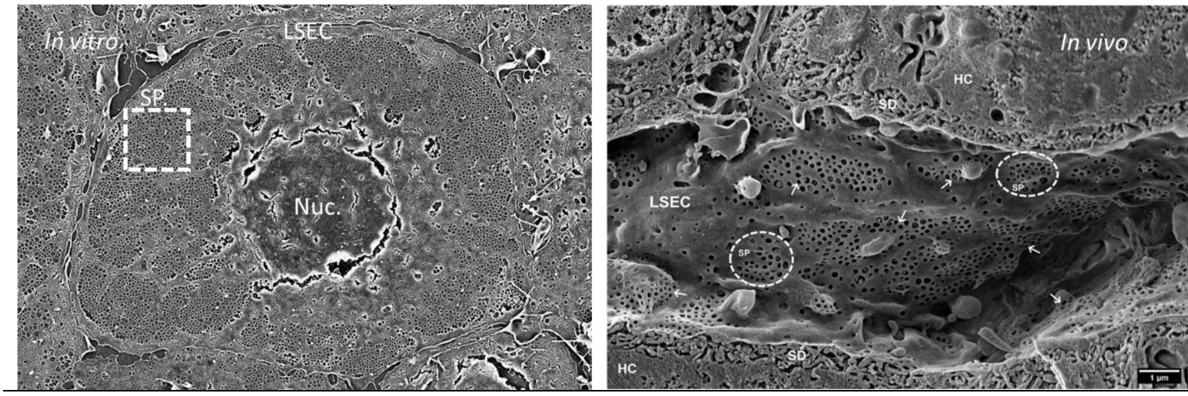

Figure 1.3: Left panel: Scanning electron micrograph of *in vitro* cultured rat LSEC, fenestrations in sieve plate (SP) indicated by dashed line, nuc.=nucleus. Right panel: Scanning electron micrograph of freeze fracture of rat liver, showing a liver sinusoid, dashed line indicates fenestrations in sieve plate, HC=Hepatocyte, SD=Space of Disse. Image reproduced from **Paper I** (courtesy of Prof. Karen K. Sørensen).

Nature and distribution of fenestrations in liver sinusoids

The fenestrations of the liver sinusoids are non-diaphragmed fenestrations, with diameters in the order of 0.05-0.3µm with most being around 0.075-0.15µm in diameter [69,68,95]. Importantly the type of microscopy used and the tissue preparation, or cell preparation for *in vitro*, does affect the size distributions of fenestrations in a systematic way [96,97], such that comparisons should be made between the same mode of imaging.

Fenestrations are modified by numerous stimuli, such as drugs, hormones, toxins but also pathological conditions and ageing [98]. The changes in fenestrations, opening and closing of the pores, was in recent studies by a Krakow group, using live-cell atomic force microscopy (AFM), found to be a very rapid process, in the order of seconds. The cells will even to some extent cycle fenestrations through open and closed states in the absence of any obvious stimuli [99–101]. This dynamic nature raises interesting questions with regard to how and why they are thus regulated, rather than being more static structures.

Function of liver sinusoidal fenestrations, chylomicron sieving and size exclusion

The size range of fenestrations directly affect the sizes of solutes that can access the space of Disse and hepatocytes, [102,103], this is likely a critical component of liver function, especially given its very high degree of evolutionary conservation (reviewed in the previous section). Electron microscopic observations by Naito and Wisse on the size distribution of chylomicrons present in the space of Disse and the diameters of fenestrations in suckling neonatal rats, which are naturally rich in serum chylomicrons, showed the distributions overlapped to a great extent [104]. A repeat study on adult rats given corn-oil showed the same tendency [105].

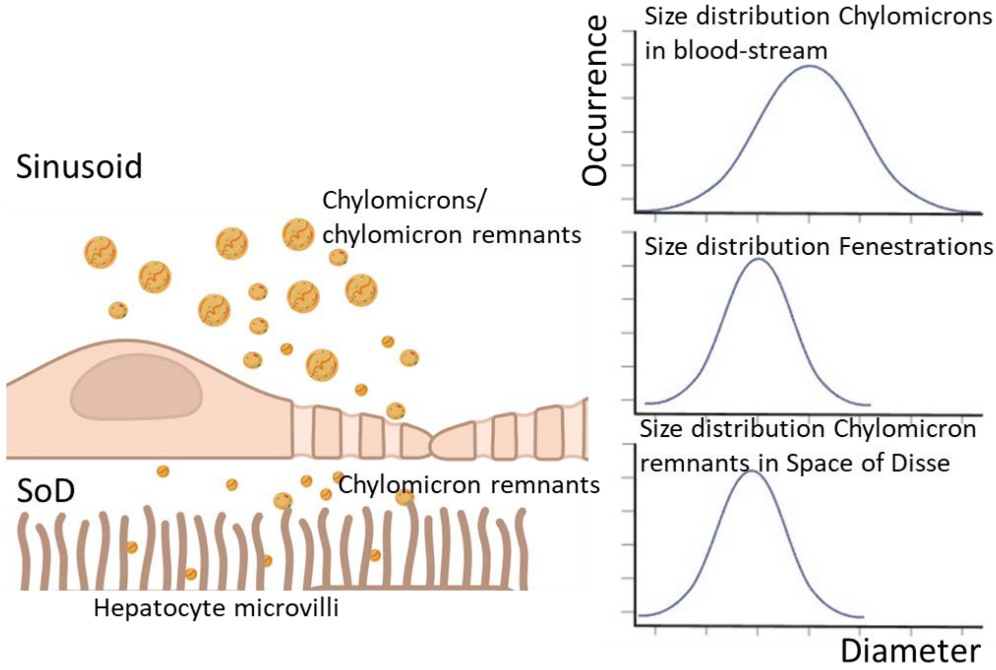

Figure 1.4: Relationship between fenestra diameters and chylomicron access to the space of Disse, and hepatocytes. Left panel: Illustration of section through sinusoidal wall, and of relation between fenestration size and lipoprotein size. Right panel: Graph of overlap in size distribution between chylmicrons found in Space of Disse and fenestration diameters (adapted from Naito et al., 1978, De Zanger et al., 1982). (Created with BioRender.com)

Distribution of fenestrations along the sinusoids and fluid flow within the sinusoids

The liver sinusoids expand gradually along their length starting with diameters of about 4, 6.4, 8.8 μm (as measured by SEM, TEM, μ-CT) and terminating with diameters of about 5.7, 7.6, 13.7μm (as measured by SEM, TEM, μ-CT) [96,106] (likely the μ-CT method adds the Disse space to the sinusoidal diameter).

Fenestrations are unequally distributed along the sinusoids, with higher porosity (% of area that is fenestrations) towards the ends/ pericentral area compared with the periportal region, the pericentral area having either 33% more according to Wisse et al., or 2-3X the porosity of the periportal area, according to Vidal-Vanaclocha & Barbera-Guillem [107,108]. The exact reason for this is not yet known, though we aim to investigate the influence of porosity on pressure and fluid velocity in **Paper II**.

Pathological alterations to LSEC fenestrations/ sinusoidal porosity

'Pseudocapillarization' is the loss of/or great reduction in number of fenestrations, of the sinusoidal lining of the liver, the term 'capillarization' has also been used for this phenomenon, usually in the more extreme cases, as in cirrhosis models. Hepatic pseudocapillarization, a term coined by Le Couteur, is a notable effect of ageing, where the liver sinusoidal endothelium loses fenestrations and grows thicker [[109]]. It is observed in seemingly all mammalians investigated, such as rat [[110]], mouse [[111], [112]], non-human primate (baboon) [[113]], and human [[114]].

Loss of fenestrations has been observed in numerous models of cirrhosis/fibrosis, including thioacetamide models [[115]], CCl_4 [[116]], dimethyl nitrosamine [[117]], N-diethyl nitrosamine [[118]], and cross species serum injection [[119]]. Mouse hepatitis virus 3 infection was also found to cause loss of fenestrations [[120]], it would stand to reason other liver pathogens may elicit similar changes, though this is not well described. Moreover, loss of fenestrations was observed in livers of alcoholics [[121],[122]], being found to happen prior to connective tissue deposition.

Importantly some of these effects are likely at least partially mediated by Kupffer cell activation, as demonstrated by $GdCl_3$/Glycine mediated killing/inactivation of Kupffer cells. It was found that the effect of bacterial LPS (overload) on liver sinusoidal vasculature was effected by Kupffer cells, by ablating these with gadolinium chloride [[123]] and the toxic effect of traditional medicine plant Piper methysticum active ingredient kvalatone on sinusoidal endothelium was similarly ameliorated by $GdCl_3$ [[124]].

The involvement of LPS and Kupffer cell activation provides a plausible intersection of the endocytic/clearance function of LSEC with inflammation and loss of fenestrations. The mechanism would likely be either loss of LSEC endocytic ability or inhibition by ligand overload leads to an accumulation of noxious ligands that stimulate immune cell and Kupffer cell activation. The release of cytokines and reactive oxygen species from activated Kupffer and other immune cells subsequently injure or signal to LSEC to close their fenestrations.

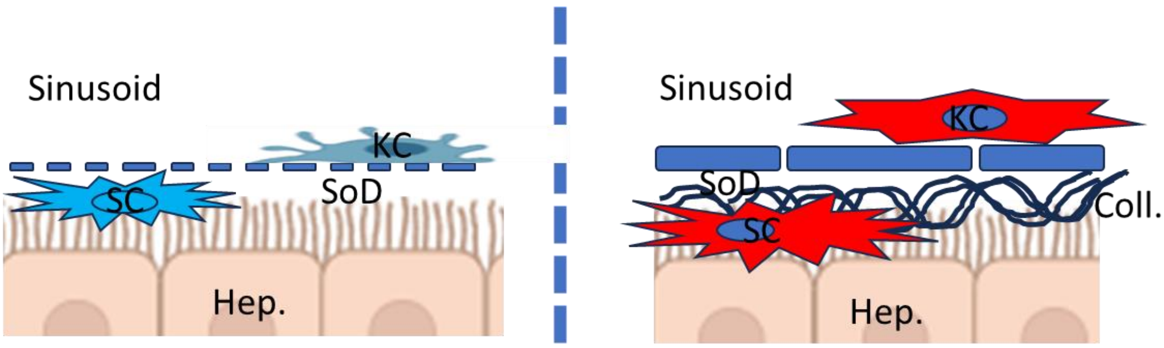

Figure 1.5: Pathological alterations to liver sinusoidal endothelium. Left panel: Normal/healthy/young morphology, endothelium is well fenestrated, allowing efficient exchange between sinusoid and the space of Disse (SoD) and hepatocytes (Hep.), Kupffer cells (KC) and stellate cells (SC) are quiescent. Right panel: Sinusoidal endothelium is thickened, with fewer and smaller fenestrations than in the healthy/normal case, impairing exchange between the sinusoid and the space of Disse/hepatocytes. Kupffer cells and stellate cells are shown as activated here, and collagen deposition (Coll.) in the space of Disse further impairs exchange. (Created with BioRender.com)

Connections to dyslipidaemia, atherosclerosis, fibrosis, glucose transport and insulin sensitivity

The young or healthy liver has rapid and efficient transport across open fenestrations, intuitively a reduction or loss of these would impede liver function, and indeed this has been found.

The diameters of fenestrations were by Fraser et al. suggested to be a driver of atherosclerosis and dyslipidaemia [103], based upon their findings of species susceptibility compared with LSEC fenestration diameters. For example chickens [125] and rabbits [126] were prone to developing atherosclerosis under high cholesterol diets, while rats, having wider fenestrations, were not, but could be made prone by nicotine treatment which reduced their fenestration diameters [127]. Pseudocapillarization was also proposed as the mechanism for ageing related dyslipidaemia [128].

Beyond the impairment of lipoprotein uptake by hepatocytes, reduction or loss of fenestrations also impairs vitamin-A transport, as the hepatic stellate cells residing in the space of Disse no longer can be reached. This was confirmed experimentally in a rat cirrhosis model, where hepatic retinol uptake was impaired [129]. Vitamin-A deficiency activates stellate cells, and induces fibrosis on its own [130,131].

Furthermore the loss of fenestrations impairs glucose transport [132], reduces hepatic insulin sensitivity [133], and reduces hepatic extraction of drugs such as; diazepam [134] and acetaminophen [135]. Hepatic extraction of other drugs is impaired as well, as pharmacological kinetics of hepatically converted drugs in ageing individuals can be notably altered [136].

Computational models of the liver sinusoids

As the pressure of individual sinusoids cannot be measured directly, and flow velocity only with great difficulty by intravital microscopy [137], modelling the fluid flow in the liver has been of great interest.

However the majority of models tend towards modelling larger areas of the liver in more generalized ways and those at single sinusoid level scale tend to not fully incorporate ultrastructural detail [138–149], such as the gradient of porosity that is found in liver sinusoids [107,108].

Incorporating these structural details; porosity, geometry and lymphatic drainage into a model of the liver sinusoid in order to evaluate their influence on flow-parameters is the rationale for **Paper II**.

1.4 The Reticuloendothelial system and the scavenger endothelium concept

The reticuloendothelial system can be said to consist of two distinct cell populations specialized in distinct but overlapping clearance functions. The divide between functions is specialization either towards phagocytosis or pinocytosis. In mammals the RES consists of mononuclear phagocytes, the macrophages, and the scavenger endothelium, found in liver sinusoids, but also bone marrow sinusoids, spleen, choriocapillaris, lymph nodes and other sites [150, 151,152]. In fish the scavenger endothelia are found in several other anatomical locations, such as endocardium, or head kidney depending on the species. In calliphora (blowflies) the system appears to be split into haemocytes and nephrocytes [151]. The most prominent receptors for endocytosis in LSEC (stabilin-1 & -2 and the mannose receptor) are also highly conserved in vertebrates, with stabilin-2 [151] and the mannose receptor [153] being found in cod endocardium.

Both in cod [154] and in mice [155] the SEC, in cod endocardium, in mice as in other mammals the liver sinusoidal endothelium, removed bacterial lipopolysaccharide from circulation.

A brief history of the discovery of the RES/ SEC

The cells of the "reticuloendothelium" were originally observationally characterized as the cells taking up the dye lithium-carmine (a vital-stain) *in vivo* [156] The concept the reticuloendothelial system (RES) was developed from these observations [157].

The subdivision of RES cells of the liver by their size range preferences was detailed by Lison & Smulders in 1948, where they found that what they termed G-cells, have a preference for electronegative dyes with larger diameters - they used Prussian blue (228Å) - whilst smaller diameter dye ammonium carmine (20.5Å) distributed to what they termed F-cells [158]. A source of future confusion can be seen here, as they call all 'athrocytic' (historic term for endocytic) cells in the liver "Kupffer cells" (G-type and F-type Kupffer cells). The heterogeneity of nomenclature came to have downstream effects once it was standardized later, and attributes from different classifications migrated to contemporary definitions.

The term RES fell out of favour towards the later part of the 20th century, much due to van Furth and associates [159], who argued in favour of the term "mononuclear phagocyte system" and insisted it only include the Kupffer cells of the liver. This term is still in use, with many medical textbooks and pharmacological research articles ascribing most non-hepatocyte liver uptake to the MPS/ liver macrophages /Kupffer cells/ liver "white blood cells".

A repeat of the lithium carmine injection experiment found that in the liver the LSEC took up the majority of the dye, more than Kupffer cells per cell and in total, as determined by histological examination, colocalization with denatured collagen (a known LSEC ligand), and electron microscopic evaluation [160]. The concept of the scavenger endothelial cell (SEC) was launched around this time, at the 9th Kupffer cell symposium.

The confusion seems in large part to have originated in the uncertainty in the original nomenclature, where subsequent authors were uncertain about which cell type was which and whereby they were characterized [Reviewed in Wisse 1970[69]]. Confusion with regards to the nomenclature was not only in regards to which were the endocytic cells of the liver, or the nature of the lining, but also what was originally meant by von Kupffer by "sternzellen" (stellate cells), referring to either Kupffer cells or stellate cells (the confusion originating from von Kupffer himself), with the term Kupfferian stellate cells having being used at a time (Kupffersche sternzellen) [161]. The old terminology has bled over into some of modern research and literature and continues to be a source of misunderstanding.

Impairment of RES function in disease states

Impaired RES clearance of damaged erythrocytes occurs in active rheumatoid arthritis patients [162], based upon that stabilins clear damaged red blood cells (RBCs)/cell corpses [163,164] this implies a sensitivity to ligand overload /competitive inhibition of the system [165,166]. Similarly whole body irradiation diminished the clearance of damaged RBCs [167].

The uptake of colloidal albumin [168] which was used historically to assess RES function *in vivo*, even clinically [reviewed in 169,150] has later identified as a ligand of the LSEC [170], hence this particular probe was in fact an LSEC test primarily. (The RES was not originally considered to consist of functionally distinctive cell populations; therefore caution is required when reviewing older publications on the subject matter. These publications do however still contain useful data if one accounts for this.)

AGE-modified proteins are taken up by the choriocapillaris in the eye [171], this is suggested as a possible mechanism for diabetic blindness, either directly from AGE accumulation, or from the impaired scavenging AGE-albumin causes [165].

Similarly hyaluronan clearance (principally by lymph nodes, liver, spleen (in this order of importance)) [172,173] is impaired by rheumatoid arthritis, cirrhosis, and is a symptom of impending liver transplant rejection [174].

1.5 Endocytosis, focus on clathrin/receptor mediated endocytosis, and LSEC

In addition to clathrin and caveolin mediated endocytosis, other forms of endocytosis can be further classified by dynamin dependence. RhoA regulated endocytosis is an example of dynamin dependent endocytosis, while ARF6 regulated and CDC42 regulated endocytosis, are examples of dynamin independent endocytosis [175].

Phagocytosis

Phagocytosis was coined and first described by Metchnikoff in 1883, his later work on phagocytosis in infection and immunity [176,177] leading to his 1908 Nobel prize in Medicine and Physiology. Phagocytosis is qualitatively described as the engulfment of larger particulate matter, such as bacteria [178,179].

Macropinocytosis, pinocytosis or cell drinking was first observed by time-lapse microscopy in the 1930s [180,181], being first discovered in macrophages. Pinocytosis came to be the term for fluid phase endocytosis, compared to phagocytosis for particulate uptake [182].

Clathrin-Coated Pits / Coated Vesicles

Coated pits/vesicles were first described by electron microscopic observations [183], and from the beginning were believed to be sites of protein internalization, which was indeed confirmed shortly thereafter [184,185]. Coated pits are known to be sites of receptor mediated endocytosis and were found in nearly all types of cells studied [186]. The earliest evidence of such trafficking by coated vesicles, was the finding that ferritin was taken up in neurons in such a manner [187]. The structure of clathrin coated vesicles, and their conformational change on internalization were first described by Kanaseki and Kadota [188], describing a basket like pattern of repeating pentagons and hexagons. The principal protein of clathrin coated vesicles, namely clathrin, was isolated and characterized by Pearse in the following decade [189]. Clathrin coated pits and caveola were originally/ alternatively referred to as bristle coated pits, coated pits and uncoated pits, or non-coated membrane invaginations [190] based upon their appearance in electron micrographs.

Caveola

Caveola were, as clathrin coated vesicles, first observed by electron microscopy [191,192] these were found to be related to uptake of several ligands, notable ones include simian virus 40 (SV40) [193], cholera and tetanus toxin [190]. Caveolae are formed by/through the actions of the associated proteins; caveolins, mainly caveolin-1 [194]. Caveolins were discovered considerably later than clathrins, most likely on account of their being much less visible in electron micrographs (therefore caveola were often described as "uncoated vesicles"). Caveolae are often found to be bridged by a diaphragm, similar to how fenestrations in many fenestrated endothelial capillary beds are [78,195].

Receptor cycling vs activated internalization

There are two ways in which cell surface receptors for endocytosis can cycle, either constitutively or by ligand activation, this was first found by Hopkins et al. in the 1980's using the examples of the receptor systems for endocytosis of transferrin and EGF [196]. The process of caveola mediated endo/transcytosis is noted to be triggered, as opposed to being constitutive, which characterizes clathrin-mediated processes [194]; gp60/albondin mediated albumin transcytosis for example is caveola mediated, and tyrosine kinase dependent [197].

Dynamin Constriction

The GTPase dynamin is required for the pinching off of endocytotic vesicles from the cell membrane, presenting a rate limiting step, in clathrin- and caveolin-mediated, and likely other endocytic processes [198]. Dynamin localizes to the neck of caveolae and mediates their budding off [199]. Antibodies to dynamin inhibited clathrin-mediated and caveolae-mediated endocytosis when micro-injected into cultured hepatocytes [200].

1.6 LSEC mediated uptake

The LSEC are cells specialized in clathrin mediated endocytosis [reviewed in [151], [201], [202]] and thus with constitutively cycling cell surface receptors. That the cell surface of LSEC are covered by bristle covered micropinocytotic vesicles (clathrin-coated pits) was described by Wisse in his seminal 1970 electron microscopy study of the rat liver sinusoids [69] and in later EM studies as well [203,204,205,189]. LSEC contain relatively high amounts of the clathrin endocytosis related machinery proteins compared with other cell types, such as Rabs 5&7, α&β-adaptin and rabadaptin [206]. In general LSEC express high levels of genes associated with endocytosis, internalization, and vesicle transport [207], indicative of their scavenger cell function.

The tubulin cytoskeleton of LSEC is the transport 'high way' for endocytosed ligands, with clathrin heavy chains distributing along continuous microtubules in the cells. The tubulin network of LSEC is visually distinctive compared with other cell types, indicating its part in the functional specialization of LSEC as scavenger cells [205].

LSEC are responsible for the clearance from systemic circulation of a wide range of macromolecules, especially connective tissue components and denatured serum proteins. Studies on clearance where cellular distribution was performed showed the often predominant involvement of the LSEC in uptake.

Table 1.1: A non-exhaustive list of ligands of receptors LSEC express:

Receptor	Ligands	References
Stabilin-1 (MS-1, CLEVER-1, Feel-1, SR-H1)	FSA, AcLDL, oxLDL (EC-LDL), AGE-BSA, nidogen, LPS, oxHSA, phosphatidyl serine, bacteria (e.coli, s.aureus), phosphorothioate antisense oligonucleotides, SPARC, Placental lactogen, heparin, GDF-15	Nagelkerke 1983,1984[208,209], Blomhoff 1984[210], Van Berkel 1991[211], Smedsrød 1997[212], Hansen 2002[213], Adachi 2002[214], Tamura 2003[215], Malovic 2010[216], Kzhyshkowska 2006[217,218], 2008[219], Li 2011[220], Lee 2011[221], Schledzewski 2011[222], Pempe 2012[223], Miller 2016[224], Cabral 2021[155], Holte 2023[166]
Stabilin-2 (HA/S-R, MS-2, CLEVER-2, Feel-2, HARE, SR-H2)	Hyaluronan, chondroitin sulfate, nidogen, heparin, N-terminal propeptides of procollagen (I, III), oxLDL (EC-LDL), AGE-BSA, FSA, Ac-LDL, LPS, oxHSA, phosphatidyl serine, VWF-FVIII, phosphothioate antisense oligonucleotides, GDF-15, serglycine	Nagelkerke 1983[208], Blomhoff 1984[210], Smedsrød 1984[225], Van Berkel 1991[211], Melkko 1994[226], Smedsrød 1997[212], McCourt 1999[227], Øynebråten 2000[228], Tamura 2003[215], Harris 2004[229], Harris&Weigel 2008[230], Øie 2008[231], Malovic 2010[216], Li 2011[220], Lee 2011[221], Schledzewski 2011[222], Miller 2016[224], Swystun 2018[232], Cabral 2021[155], Holte 2023[166],
Mannose Receptor (Mrc1, SR-E3, CD-206)	Collagen alpha chains (I, II, III, IV, V, XI), C-terminal propeptide of procollagen type I, tissue plasminogen activator, lysosomal enzymes, salivary amylase, invertase, mannan, terminal mannose/L-fucose/GlcNAc, ovalbumin, ricin, horseradish peroxidase, agalacto-orsomucoid, ahexosamino-orsomucoid, lutropin, bacteria and yeast, influenza, herpes, HIV	Hubbard 1979[233], Isaksson 1983[234], Smedsrød 1985[235], 1988[236], 1990a[237], 1990b[238], Eskild 1986[239], Praaning-van Dalen 1987[240], Magnusson&Berg 1989[241],1993[242], Ezekowitz 1990[243], Taylor 1992[244], Asumendi 1996[245], Stahl&Ezekowitz 1998[246], Milone&Fitzgerald-Bocarsly 1998[247], Roseman&Baenziger 2000[248], Reading 2000[249], Gordon 2002[250], Turville 2002[251], Allavena 2004[252], Malovic 2007[253], Elvevold 2008[254], Brocheriou 2011[255]
Fc Gamma RIIb2	IgG immune complexes	Mousavi 2007[256]
SR-A1	AcLDL, oxLDL, β-amyloid fibrils, AGEs, LPS, lipoteichoic acid, MDA-albumin	Hampton 1991[257], Dunne 1994[258], Araki 1995[259], El Khoury 1996[260], Suzuki 1997[261], Kunjathoor 2002[262]
SR-B1	LDL, oxLDL, VLDL, HDL, VitE, carotenoids, silica	Acton 1996[263], Kozarsky 1997[264], Varban 1998[265], During 2005[266], Reboul 2006[267], Brundert 2011[268], Tsugita 2017[269]
LOX-1 (SR-E1)	oxLDL, apoptotic bodies, CRP, bacteria, platelets, anionic phospholipids, MAA-albumin	Oka 1998[270], Li&Mehta 2000[271], Chen 2001a[272],2001b[273], Shih 2009[274]
LSIGN (CD209L)	HIV, SARS-CoV, SARS-CoV2, HCV, VWF-FVIII	Gardner 2003[275], Jeffers 2004[276], Boily-Larouche 2012[277], Swystun 2019[278], Kondo 2021[279]
LSECTIN (CLEC4G)	Mannose oligosaccharides, terminal GlcNAc, mannose, fucose	Feinberg 2001[280], Liu 2004[281]
LRP-1	ApoE, tissue plasminogen activator, receptor associated protein, α2M, lactoferrin, FVIII	Hussain 1999[282], Herz&Strickland 2001[283], Prasad 2016[284], Salama 2019[285]
LYVE-1	Hyaluronan	Banerji 1999[286]
CD-36	HDL, LDL, VLDL, anionic phospholipids, apoptotic bodies, collagen, aldehyde modified proteins	Tandon 1989[287], Savill 1991[288], Rigotti 1995[289], Calvo 1998[290], Duryee 2005[291], Brundert 2011[268]

Hubbard et al. in 1979 [233] describe the liver carbohydrate recognition system, using ^{125}I labelled ligands and autoradiographic electron microscopy, and oligosaccharide terminating proteins. Those terminating in galactose were found to be taken up predominantly by hepatocytes, while those terminating in N-acetyl-glucosamine (agalacto-orsomucoid), mannose (a-hexosamino-orsomucoid), preputial β-glucoronindase, mannobiosaminated RNase A were taken up predominantly by the sinusoid lining cells (LSEC and Kupffer cells), with LSEC taking up 2-6 times more per cell. Competition studies showed the N-acetyl-glucosamine and mannose terminating proteins competed with one another, indicating a common receptor [233]. This was the first study on what became known as the mannose receptor. The mannose receptor binds and enables internalization of mannose, fucose [292], the LSEC mannose receptor takes up a wide host of ligands including ovalbumin [241], tissue plasminogen activator [238] and lutropin hormone [293,294].

Lysosomal enzymes, mannose receptor

Macrophages internalize lysosomal enzymes via their mannose receptor [295,292,296], in the liver however it was found that sinusoidal endothelial cells are the most active in uptake of mannose receptor ligands [233,297]. Indeed the LSEC take up, and are dependent upon the mannose receptor mediated uptake of, lysosomal enzymes for proper catabolic function, as found by the use of mannose receptor knock out mice by Elvevold et al. LSEC MR ligands cathepsin-D, α-mannosidase, α-hexosaminidase and aryl-sulphatase were confirmed totally dependent on mannose receptor activity [254].

Connective tissue ligands

Soluble collagen alpha chains were found to be cleared by the liver, with uptake predominantly by LSEC [235]. The receptor for endocytosis for denatured collagen on LSEC was subsequently found to be the mannose receptor (Mrc1) [253]. The mannose receptor and collagen receptor were previously thought to be separate entities, one may come across this nomenclature in articles predating this discovery.

Hyaluronan was found to be cleared extremely rapidly (2.5-4.5 minutes) from systemic circulation by mainly the liver with contribution by the spleen, (a pattern we shall see recurring). The non-parenchymal cells were further found to be the site of uptake, with virtually nothing taken up in hepatocytes [298]. *In vitro* studies confirmed the uptake was by LSEC [299,225,239]. The uptake receptor for hyaluronan was definitely described by McCourt et al. in 1999, as being what is now known as stabilin-2 [227,300]. Studies on the uptake of hyaluronate (= hyaluronan) in LSEC further demonstrated their rapidly cycling cell surface receptors [301]. Laminin, nidogen and laminin-nidogen complexes were found to be cleared by the liver, most was taken up by LSEC, but Kupffer cells had a higher per cell uptake for laminin and laminin-nidogen complexes [302]. Chondroitin sulphate proteoglycan was similarly found to be taken up by LSEC [303], with EM studies of this uptake demonstrating the kinetics of LSEC endocytosis, with internalization occurring in the range of 1 minute, and transfer to lysosomal compartments after a 40-60 minute lag [304]. The receptor for serglycin, a form of chondroitin sulphate proteoglycan, was found to also be stabilin-2 [305, 228]. Amino-terminal propetides of type I and III procollagen, are cleared by the liver with a $t_{1/2}$ of 0.6 minues, the majority (78%) is taken up by LSEC. Cross competition *in vitro* showed inhibition of PINP or PIIINP by formaldehyde treated serum albumin (FSA), acetylated LDL (AcLDL) and poly-I, but not hyaluronan [306].

The non-overlap of ligand binding domains made certain identification fraught, with stabilin-2 being originally considered as several receptors.

Modified protein ligands

It was discovered early that *in vivo* Ac-LDL was taken up mostly by LSEC, with uptake 4X higher per mg cell protein than in Kupffer cells, this was confirmed *in vitro* as well [208,210]. Uptake of modified LDLs was shown by KO-studies to be independent of SR class A, but susceptible to competitive inhibition by poly-I [307]. The uptake of oxLDL is via the receptors stabilin-1 and -2, was later shown by Li et al. in 2011 [220].

FSA now a canonical model ligand of the LSEC, was found to be taken up by LSEC by Eskild et al. in 1984 [308], the same group also found that Ac-LDL, endothelial cell modified LDL, and FSA were taken up by the same receptor(s) by competitive inhibition studies [309].

Advanced glycation end-product BSA (AGE-BSA) showed rapid clearance *in vivo*, distributing nearly exclusively to liver, with modest uptake in spleen and kidney. Most of the liver uptake (60%) distributed to the LSEC. *In vitro* competitive studies showed modest inhibition by FSA and poly-I. [212]. AGE-BSA was also found to reduce the endocytic ability of LSEC in culture, in pulse-chase experiments [165]. The receptors stabilin-1 and -2 (called FEEL-1 and -2 by Tamura et al.) were identified as receptors for endocytosis of AGE-BSA [215].

Immune Complexes

Small soluble immunogloblin G immune complexes are endocytosed by LSEC and Kupffer cells, but in a manner much slower than other ligands (FSA, collagen fragments) [310], it is primarily the FcγRIIb2 on LSEC responsible for this uptake [256].

Virus uptake

Viral uptake in the liver and viral clearance by the liver has been known of for considerable time - rapid clearance by liver reticuloendothelial system is seen for Vesicular Stomatitis virus and Newcastle disease virus, notably virus with antiserum is cleared much faster [311]. The same is the case for Moscow strain ectromelia virus, which is cleared in few minutes by 'the littoral cells lining the liver' [312]. Many of these are attributed to the Kupffer cells by authors, though there are sure to be misattributions, and archaic uses of nomenclature (the sinusoidal lining was by some considered entirely of Kupffer cells, thus the term "Kupffer cell" in very old publications becomes somewhat fraught).

BK and JC polyoma viruses are cleared by the LSEC *in vivo*, by receptors not yet known [313]. HIV-like particles (virus like particles consisting of some of HIV proteins) were rapidly cleared by the LSEC [314]. Adenovirus rAd5 is rapidly cleared by LSEC (90%) [315]. Enterobacterial virus (T4-phage) is avidly endocytosed by LSEC in culture, degradation is mildly inhibited by FSA, suggesting some similarity in entry/endosomal processing [316].

Infectious uptake

Murine betaherpesvirus-1 is able to infect (murine) LSEC via binding to neuropilin-1, and dynamin dependent endocytosis and monensin sensitive endosomal maturation - by all appearances hijacking of the LSEC endocytic machinery [317]. SARS-CoV2 binds to LSIGN on LSEC, and the virus was found inside LSEC from Covid patient autopsies, indicating it may be infectious uptake [279]. The LSEC are a site for latency and reactivation of cytomegalovirus, indicative that these are taken up by LSEC and escape degradation in some way [318]. There is also evidence to suggest LSEC transcytosis may be part of hepatitis virus infection of hepatocytes [319,320] via L-SIGN and DC-SIGN [321].

Interference with clearance / Immune responses

LSECtin based binding/uptake by LSEC downregulated local immune responses and prolonged hepatitis viral presence, another example of viral appropriation of LSEC normal functions, in this case the tolerogenic effect of LSEC [322].

Bacterial enterotoxin

Bacterial lipopolysaccharide (LPS) is cleared from circulation by the liver [323], in a manner inhibitable by fucoidan and poly-I, [324], in distribution studies by Van Oosten et al. Kupffer cells took up more LPS per cell than LSEC, whilst in a study by Yao et al. more LPS injected was associated with LSEC (75%) than Kupffer cells(25%) [325]. Uptake in LSEC is via the receptors for endocytosis stabilin-1 and -2 [155]. The differences in distribution between LSEC and Kupffer cells, are likely in part due to the heterogeneity of LPS, being more of a class of molecule than a specific molecule. LSEC themselves are relatively insensitive to LPS stimulation [123], but their clearance thereof and presumably the immune tolerance they can effect [326] is crucial to maintain homeostasis [155].

Binding without endocytosis

Candida albicans is bound but not killed in the absence of Kupffer cells by the liver sinusoids, in a manner inhibitable by mannose, indicating the mannose receptor for binding activity [327].

Bacteria as well as cell-corpses and senescent red blood cells attach to the receptors stabilin-1/-2 on LSEC while the uptake of the bound ligands is performed by the Kupffer cells. Binding of phosphatidyl-serine by stabilins is responsible for this binding, of which stabilin-1 in some macrophages, importantly not those of the liver, also facilitates endocytosis and degradation [328,163,164]. Seemingly LSEC serve to capture/immobilize and in some way ‘hand over’ these ‘macro-ligands’ to the Kupffer cells [329,330,221,164,163,331]. This immobilization without uptake may confuse kinetics studies of microorganism/bacteria clearance.

Transcytosis

Transcytosis, whereby ligands internalized are released again, likely on the abluminal side, with or without modification, also occurs in LSEC. Ceruloplasmin and Transferrin are both; taken up, desialated, and released by LSEC with subsequent hepatocyte uptake [332,333, 334].

Endosome uptake and degradation kinetics of LSEC, exemplified by some more well studied ligands

Studies by Eskild et al., on the internalization kinetics of FSA in LSEC, in *in vitro* EM studies gold labelled FSA was found associated with coated pits in LSEC, and the discovery that pH 6.0 would dissociate surface bound ligand, allowed the $t_{1/2}$ for internalization to be estimated as 24 seconds. Pronase treatment, destruction of cell surface proteins, demonstrated a 40% reduction in receptors, indicative of a large internal pool and rapid cycling. Endosomes with FSA mature into lysosomes after about 9-12 minutes [335].

The *in vivo* clearance kinetics of FITC labelled, heat denatured collagen were found to adhere to a bi-phasic clearance, with a $t_{½}\alpha$ of 0.8 minutes and a $t_{½}\beta$ of 3.7 minutes, distributing 89% to liver. Using collagens labelled with different fluorophores the speed of trafficking to lysosomes was studied. TRITC labelled heat denatured collagen was injected into animals, after 24 hours cells from these animals were cultured, and FITC labelled heat denatured collagen added, and fluorescence time course experiment performed. It was found to take 8 h after addition of FITC-collagen for a partial overlap of fluorescence to be observed, and a full 18 hours until overlap was complete (i.e. both being in the same compartment). *In vitro* pulse-chase studies showed collagen reaching early endosomes by 20 minutes, and prelysosomal compartments after 60 minutes [336]. Further studies using fluorescent and electron microscopy confirmed the sequential sorting and rough time-frames, going from early endosome (0-20min), to late endosome (20min-2h) and lysosome (2h+) [337].

Impairment of LSEC endocytosis

LSEC endocytic activity becomes impaired under certain pathological conditions, for some the effect is definitely ascribed to the LSEC, while for others it can be likely ascribed but has not been validated. In general impairments of reticuloendothelial function by the classic definition, most probably involves some manner of impaired binding and or uptake by LSEC or would have an effect upon their uptake function.

In ageing models it was found the endocytic capacity of LSEC was clearly reduced, by performing capacity studies on isolated cells from aged animals [338]. This is probably related to the observed endothelial thickening and pseudocapillarization in ageing [109]. The loss of endocytic activity with senescence of LSEC has been proposed as a mechanism leading to death in ageing [339].

In cirrhosis and other liver injury or disease there is often elevated levels of scavenger receptor ligands such as hyaluronan [174] and oxidized albumin [340,341]. This is expected as these conditions involve extensive liver cell death and inflammation, which would lead to inactivation of the LSEC scavenging function. Other pathological states also see elevated scavenger receptor ligands, such as AGEs and AOPPs in diabetes [342], or oxLDL [343] and oxidized albumin in atherosclerosis [344].

The pro-athrogenic ligand oxLDL was found to cause endothelial thickening and reduction in fenestration frequency in the centrilobular area of the sinusoid [345].

AGE-BSA was found to impair scavenging function in isolated LSEC for prolonged periods of time [165], and the glucose moiety of AGE-BSA was not removed from the LSEC *in vivo* for weeks after injection in another study, with removal of this moiety being much slower in post-pubescent animals [346].

2 Aims of the study:

The LSEC of the liver are highly fenestrated with non-diaphragmed fenestrations that are crucial to normal lipoprotein transport, and evolutionarily conserved across all species with livers. We sought to evaluate all previous research on LSEC fenestrations, summarize all compounds found to modulate them and hypothesize a mechanism for their regulation.

Further we sought to evaluate the influence of LSEC fenestrations, their typical distribution, as well as other relevant parameters on the flow parameters of the liver sinusoid.

LSECs are also avid scavenger cells that remove macromolecular waste, among which are modified albumins FSA, and AGE-BSA both of which are taken up via the receptors stabilin-1 and -2. We hypothesized that LSEC/stabilins were the site of uptake/endocytic receptors for highly oxidized albumin, and sought to determine if this was the case.

Finally, super resolved microscopy is required to visualize the fenestrations of LSEC, and large image sets need to analyzed to be able to conclude about their regulation. We therefore sought to evaluate methods for image analysis, and segmenting out fenestrations from these images, to demonstrate strengths, weaknesses and susceptibility to user bias.

3 Summary of Papers

3.1 Paper I

The wHole story about fenestrations in LSEC

Objectives:

The objective of this paper was to review the available literature on what chemical compounds affect the fenestrations on LSEC, assess the evidence presented (*in vitro/ in vivo*, species, microscopy used) and to map out which direction the changes went.

Methods:

The paper is a non-systematic review, going over all literature that could be found concerned with alterations to LSEC fenestrations. The evidence presented by each article was then assessed for reliability, several works were of too poor quality with regards to microscopy/ sample preparations to support their claims, these were excluded from the review. The works deemed sufficiently well performed were summarized over class of molecule, e.g. recreational drug, pharmaceutical drug, hormone, lab-tools and experimental models.

Results:

A wide host of compounds had been found to have effects upon the fenestrations of LSEC. Recreational drugs, mostly caused reductions in fenestrations. Vasodilators/constrictors and actin scaffold modifying compounds were notable in their ability to affect fenestrations. Vasodilating compounds in general increased the diameters of fenestrations, and vasoconstrictors decreased diameters. Actin disrupting toxins caused an increase in the numbers of fenestrations, with no effect or decrease to diameters. Numerous medical drugs affected fenestrations, including; metformin- increased numbers, sildenafil- increased numbers, amlodipine- increased numbers, among others. An expanded model for how fenestration may be regulated was also generated based on these various compounds and their modes of action.

Conclusion(s):

Many compounds can affect the porosity of the liver sinusoids. These have implications for both liver focused interventions and intoxication/ off target effects of other interventions. The exact mechanism of fenestration regulation is not yet known, nor are all constituent components of the fenestra associated cytoskeleton. Actin, spectrin, myosin, nitrous oxide regulated pathways, cAMP and/or cGMP regulated pathways seem nearly certainly involved. We summarized the literature of the field over a long period of time, and added data from a book-series which does (to date) not exist in digital form in its entirety, “Cells of the Hepatic Sinusoid” by the Kupffer Cell Foundation. This we believe will allow these results to be known, and incorporated into newer research.

3.2 Paper II

The Computed Sinusoid

Objectives:

The aim of this study was to use fluid dynamics simulation to investigate the influence fenestration distribution, vessel shape and lymphatic drainage have upon the liver sinusoid.

Methods:

Computational fluid dynamics simulations were carried out on 2D models of the liver sinusoids, with varied features (cylindrical/conical, constant high (20%), low (5%) or increasing variable (5, 6, 20%) porosity), to investigate their contributions to pressures and flow velocities in the sinusoid, across the LSEC, and in the space of Disse.

Results:

The overall shape of the vessel had the single largest effect on flow parameters, with velocity magnitudes 2 fold lower in divergent radii models, and pressures 5-8% reduced in comparison with constant radius models. The addition of a lymphatic drainage significantly affected flow in the space of Disse, with 2-4 fold increases to velocity magnitude, and 6-12% reductions in pressure. Porosity made only small contributions to luminal pressure, while higher porosity models had lower velocity magnitudes and pressures across fenestrations, flow velocity in the space of Disse was higher in higher porosity models.

Conclusion:

The included parameters did show effects on flow parameters, though some unexpectedly modest. Porosity appears to be able to modify flow in the space of Disse, given the rapid nature of fenestration regulation, this may be a way in which the liver regulates this flow.

3.3 Paper III

Highly oxidized albumin is cleared by liver sinusoidal endothelial cells via the receptors stabilin - 1 and - 2

Objectives:

Highly oxidized albumin is a modified serum protein associated with several pathologies, such as atherosclerosis, liver disease and diabetes. LSEC are scavenger endothelial cells specialized in the clearance of macromolecular waste. The fact that very oxidized albumin was cleared by the liver and spleen, with a very short half life, as found in a study by Iwao et al., led us to suspect the LSEC and their stabilins were involved, based upon previous work by this group and others on the subject. We therefore sought to demonstrate that highly oxidized albumin (oxHSA) is in fact cleared by LSEC *in vivo*, and that binding and uptake is via the receptors stabilin-1 and -2.

Methods:

In vivo: organ and hepatocellular distribution by way of Iodine-125 labelled oxHSA.

In vitro: Uptake of ^{125}I-oxHSA in isolated LSEC, Kupffer cells, hepatocytes, HEK293 overexpressing either stabilin-1 or -2 respectively, and competitive inhibition studies in LSEC and HEK293 expressing stabilin-1 or -2. Affinity chromatography of LSEC detergent lysates, with Sepharose 4B immobilized oxHSA, native albumin and 'empty' Sepharose 4B followed by mass spectrometry identification of eluted proteins. Viability, EM level morphology and recovery of endocytosis (pulse-chase) experiments.

Results:

oxHSA is cleared extremely rapidly by the liver and spleen, and in the liver distributed overwhelmingly to the LSEC. Cultured LSEC endocytosed much more oxHSA than either Kupffer cells or hepatocytes, further this uptake was inhibitable by ligands of the stabilins (oxLDL, FSA, AGE-BSA). HEK293 cells expressing either stabilin (-1 or -2) endocytosed oxHSA to a much greater extent than vector control cells. oxHSA could also inhibit the uptake of other stabilin ligands in LSEC and HEK293 (stabilin-1 or -2) cells. oxHSA did not decrease cell viability (as measured by amar-blue or lactate dehydrogenase assays) in cultured LSEC, nor did morphology change perceivably in the cells at any concentration tested. oxHSA did however decrease the endocytic activity of LSEC for prolonged periods of time in pulse-chase experiments.

Conclusion:

LSEC and their stabilins are the primary clearance site and system for highly oxidized albumin, this highly oxidized albumin can depress their normal scavenger function plausibly contributing to the pathogenesis of conditions where oxHSA is formed. Ablation of the stabilin receptor system has been shown previously by others to have severe deleterious effects on health and lifespan in model animals. Thus, elevated levels of circulating ligands of the stabilins, such as oxHSA, are a prognostic marker of reticuloendothelial dysfunction, and indicative of poorer prognoses.

3.4 Paper IV

Quantitative analysis methods for studying fenestrations in liver sinusoidal endothelial cells. A comparative study

Objectives:

The diameters and numbers of fenestrations are both important parameters of LSEC, where porosity determines the exchange rate with the bloodstream, and the diameters present a size exclusion filter for what size of particle or colloid may enter the space of Disse and access the hepatocytes. We sought to evaluate three different ways of quantifying these parameters (diameters and frequency), i) the original manual image segmentation, ii) a semi-automated thresholding-based approach in ImageJ, and iii) a fully automated neural-network based approach, using the Ilsatik software package.

Methods:

Three super-resolved microscopies were used to generate images of rat LSEC, i) Atomic Force Microscopy, ii) Structured Illumination Microscopy and iii) Scanning Electron Microscopy. The image sets from these were then segmented by either method; manually measuring parameters in ImageJ, extracting features with thresholding in ImageJ, or classified by a pre-trained neural-network, using Ilastik. Outputs from these were then compared, and user bias from five different users of the methods.

Results:

The impact of user bias could be seen in all methods evaluated, but the impact was different in each. Out of the methods manual counting was the most accurate for numbers (frequency) of fenestrations, while the semi-automated method (thresholding) was the most accurate for diameters. The semi-automated method also showed the least amount of user bias. The fully automated method depended more than the others on high image quality/ resolution.

Conclusion:

Manual classification is very accurate for frequencies, less accurate for diameters, whilst containing considerable user bias compared to semi-automatic classification (thresholding). The semi-automatic approach is the least sensitive to user bias, and has the best accuracy for diameters. The fully automated method is the fastest, with the qualification that it must be trained first, such that this applies to larger sets of homogenous images (wrt. Resolution and image size). The optimal approach is best decided by the data-set at hand, largely size of data set and image quality.

4 Discussion

4.1 Methodological considerations

Paper I: In **Paper I** we conducted a non-systematic review, this is on account of the very long time-span from which we collected articles. Many were not very well indexed, some were from books of conference proceedings we only serendipitously had access to. For old articles (pre-internet) the use of 'modern' search terms would also likely not have worked, as terminology has shifted over the last 50 years, and far from everything has been properly indexed. The difficulty was more in finding the articles at all, rather than to narrow down search terms in order to exclude spurious results, given the age of some of the work, as well as the niche character of the field. Exclusion was done by assessing the methodology and quality of images produced, if preservation of tissue or sample preparation looked sub-par, we excluded on this basis.

The inclusion criteria were that the papers had quantitative results pertaining to fenestra number, diameters or porosity (area fraction), imaging modalities and sample preparations that make it likely the results are valid.

Paper II: **Paper II** is an *in-silico* study, using experimentally determined input parameters to model the fluid flow velocity magnitude and pressure in a 2D sinusoid. There were several different versions of this model generated, with variations to shape (conical/cylindrical) outlets (with/without lymphatic drainage) and input parameters (normal or elevated pressure).

For computational, and hardware related reasons, simplifications had to be made. We modelled the sinusoids as a 2D half-section for computing time and hardware constraint reasons. We compared this 2D model with a smaller 3D model, to ensure the simplification we had made was valid. The sinusoids also leave out several important parameters from physiology, that were not trivial to include. The flow was modelled as continuous, whilst the real case is of pulsatile flow as in blood vessels in general, with starts and stops. The tissue *in vivo* is also elastic and compressible, whilst our model was made to be rigid. These parameters are however computationally expensive, and we felt our primary inquiry into the function of the sinusoidal ultrastructure could still be done to satisfaction even with the aforementioned simplifications.

Paper III: **Paper III** is a study on the uptake of a modified protein ligand *in vivo* and *in vitro*, characterization of its receptor *in vitro* and its effects on LSEC *in vitro*.

Ligand radioiodination was the main method of the paper: oxHSA and other ligands were labelled with 125-Iodine (^{125}I) by the oxidative Iodogen™ method. To be sure that the labelling did not greatly alter the molecule, competitive inhibition studies with ^{125}I-oxHSA against unlabelled oxHSA were performed. Unlabelled oxHSA could inhibit the uptake of ^{125}I-oxHSA, indicating that the receptor system had not changed. oxHSA is also highly oxidized, with the fairly gentle oxidation of the labelling procedure unlikely to contribute much. Experiments with similarly labelled native albumin has shown that this labelling technique does not predispose albumin for clearance.

In vitro uptake studies were performed with excess of native albumin in the culture media, there would also have been excess albumin *in vivo* as albumin constitutes a large fraction of serum proteins. This blocking was done to minimize non-specific binding to the culture wells and assist in precipitation for quantitation of degradation. Quantification of degradation was done by precipitating intact protein with trichloroacetic acid, bringing the solution below the pI of albumin, a method that has worked for all soluble modified version of albumin (formylated albumin: FSA, glycated albumin: AGE-BSA), and is separately validated by cell free control wells in the experiments, in which the amount of precipitated radiation is taken to be the intact fraction.

Affinity chromatography was performed to identify the receptors for endocytosis, oxHSA, native albumin were separately coupled to Sepharose4B. As a further control Sepharose4B without attached protein was used. Only proteins very strongly attached to the columns were eluted, less strong associations would have washed off in the extensive washing steps of the procedure. Thus the method could determine stabilin-1 and -2 were strongly bound to oxHSA, but other receptors with weaker affinity may have been overlooked.

Primary cell isolation, culture

LSEC, as a cell type lose phenotype and functions rapidly in culture [231,347], effectively placing a limit on the time-frame of experiments. There are currently no existing cell lines that replicate LSEC morphology and function to an acceptable level, these are therefore not a useful replacement. Expanding the time in culture LSEC preserve their characteristics is therefore an important pursuit in liver research. Until this point in time a useful timeframe of 2-3 days in culture is the maximum, severely limiting what can be done, for example siRNA experiments have not been feasible [personal communication; Sørensen & Smedsrød].

There are of course limitations to using cultured cells, as they have been removed from the context of their organ, and the systemic circulation wherein they resided. Organs as most things in physiology are highly dynamic in nature, with cycles and fluctuations across multitudes of parameters (hormones, nutrients, pressure, and more). Improving culture conditions, to more closely mimic physiological parameters is an important direction of research, allowing better *in vitro* modelling, as well as disentangling the downstream effects of these parameters in isolation, allowing for a better understanding of the underlying physiology.

Caveats regarding the use of model organisms

It has been documented extensively that primary LSEC (and likely other specialized cell types) lose phenotype and functions rapidly in culture such that only freshly isolated primary cells are of any use in their study. One should also not underestimate the confounder presented by species differences between model organisms (mice, rats, pigs and so forth) and humans. Highly conserved mechanisms found in most vertebrate or mammalian species can be adequately modelled in rodent models, however care should be taken in extrapolation, their cross-talk and interactions could be significantly different. The organ and cell population, -specific responses are likely to be different between certain species [348].

For disease models there should also be caution in comparing pathologies not intrinsically similar, such as for example intoxicant caused liver injury as models for steatohepatosis/ cirrhosis (e.g. CCl_4, TAA), being of different aetiologies they likely are not functionally similar in all respects, despite being often chosen for time constraint reasons. The lifespan of model organisms is another important source of discrepancy, compensatory systems found in long lived organism such as humans may not be present in small animals with typically short life-spans, complicating comparison [349]. It is imperative to perform comparative tissue transcriptomic and proteomic studies, comparing especially model organisms and humans, to assess the validity of a model for its application.

Paper IV: **Paper IV** is a methodological study on techniques used in image classification when quantifying LSEC fenestrations. The topic had not seen comparative analysis performed before, comparing different methods of image analysis. The paper further adds detail by comparing these across multiple modalities (AFM, SIM, SEM).

There were not many known techniques besides manual classification, though some uses of thresholding deconvolution and automated classification had been made. We demonstrate how these methods compare, and how user bias affects each, as well as how they interact with different modalities. This allows future users to make a much more informed decision about which method to choose, and the potential pitfalls (mainly user bias).

The methods examined were the best available methods at the time of publication, but now it would be of considerable interest to revisit artificial intelligence-based approaches given their recent rapid and considerable developments.

4.2 General Discussion

Fenestration regulation

Cellular messengers involved in fenestration regulation

The actin cytoskeleton is an important part of fenestrations and their associated cytoskeletal structure. NO, Calcium ions, cyclic GMP and cyclic AMP are all in some way involved in regulating fenestrations.

Inferred mechanisms of LSEC fenestrations regulation

In **Paper I** we propose that the integral parts of the fenestration associated structures are actin, spectrin and myosin, and these regulate fenestrations via RhoA/ROCK, Calcium Calmodulin, eNOS NO and cyclic AMP/GMP involving pathways. There are undoubtedly more complexities to the pathways that regulate fenestrations, and all components or directions of contribution (i.e. increase/decrease diameter/numbers) may not be correctly ascribed, we do however believe that our schema is mostly correct.

The fenestration associated cytoskeleton

There exists a cytoskeletal structure which appears to hold open the fenestrations on LSEC, as seen by cytoskeleton buffer extracted and membrane stripped, or TEM of whole-mounted, cytoskeleton buffer extracted LSEC. The structure was first described by Braet et al. [350] and more recently Zapotoczny et al. [351] using optical nanoscopy, found it to be in part at least made up of actin and spectrin. Thus actin cytoskeleton related and regulating proteins are of particular interest with regards to fenestration regulation.

Further developments upon the hypothesis developed in Paper I

Zapotoczny et al. in a 2022 study [352] further tested the hypothesis formulated in **Paper I**, with the aid of various inhibitors and cytoskeleton modulating compounds. The Rho-ROCK pathway is identified as regulating fenestration diameters and MLCK is identified as critical to the formation of fenestrations.

Zhang et al. [353] demonstrate how substrate stiffness both maintains phenotype (soft) or causes loss of fenestrations (stiff) *in vitro*, and by which pathways. They show that the focal adhesion kinase (FAK) via the p38 MAPK MK2 pathway, causes actin remodelling mediated by LIMK1 and Cofilin. eNOS and other LSEC typical markers (Stab1/2, Fcgr2b, Gata4) are found downregulated in the stiff substrate cells, suggesting generalized dedifferentiation. This is of further interest beyond merely understanding LSEC fenestration regulation, but also seems linked with defenestration seen in disease state, e.g. fibrosis. The authors suggest connective tissue component cross-linking as an important mediator.

Paper VI, "Effect of caffeine and other xanthines on liver sinusoidal endothelial cell ultrastructure." also extends the knowledgebase of **Paper I**, adding the xanthines as a class of compounds which can modulate fenestrations.

Fenestration alterations *in vitro* vs *in vivo*

It should be noted that in the *in vivo* case interactions with other cell types in the liver (and conceivably elsewhere) in response to stimuli complicates discerning the mechanism of action of a compound upon fenestrations. This is of course the most realistic way to assess whether a compound can alter fenestrations, as *in vitro* studies remove much of the anatomical context of the cells. However, for discerning the mechanisms behind, and cell type specific responses, to compounds, *in vitro* studies on freshly isolated primary cells will be a good choice. In **Paper I** we list whether experiments were *in vivo* or *in vitro,* that future experimenters may know whether the mechanism could involve additional cell types (though for the in vitro case the incidence of contaminating other NPCs is rarely zero).

Fenestration modulation in pathological states

Caloric restriction was found to improve the sinusoidal endothelial phenotype *in vivo*, with thinner endothelium, with greater porosity found in aged animals on a calorically restricted diet [128,354]. An every-other-day feeding regimen in mice was found to lower oxidative stress markers in mouse livers compared with ad libitum mice [355], which is likely a contributing factor to observed pseudocapillarization, based on liver sinusoidal changes elicited by oxidative stress [356]. Presumably ad libitum feeding is a sub-optimal feeding regimen across species, on account of the rarity of this situation in evolutionary history. As effective as caloric restriction is, it is unlikely to see widespread adoption (possibly with the exception of liraglutide users) for obvious reasons.

Therefore there is a need for therapeutic interventions that can address ageing (and other pathology) related pseudocapillarization/ capillarization.

Our review sought to collect the known literature on the subject matter, that it may be systematized and interventions could be derived from it.

Assessing pseudocapillarization *in vivo* / clinically

As stated in **Paper I**, pseudocapillarization is a major motivating factor for studying fenestration affecting compounds. Hence it would be immensely valuable to be able to asses *in vivo*/ clinically when such an intervention would be beneficial/required, and whether the intervention is working. Le Couteur et al. demonstrated the utility of the multiple indicator dilution technique in assessing hepatic porosity [132]. Based upon these findings and those of Naito et al. [104] findings on the size restricting effect of fenestrations *in vivo*, a method for assessing liver sinusoidal pseudocapillarization may be inferred. Kinetics and possibly distribution, of radiotracer labelled lipoprotein could be used to estimate if the liver sinusoid is comparatively normal, with bidirectional transfer happening at a normal/healthy rate, or if the reduction of fenestrations has begun to impede transfer. This would allow for a relatively simple method of assessing accessibility of the space of Disse clinically. Importantly this would not distinguish between connective tissue deposition-based loss of access, compared with pseudocapillariation/ defenestration of the sinusoids. Adding a separate tracer of a different photon-energy or being in some other way distinguishable, connected to antibodies against collagen could facilitate this. Gadolinium based contrast agent uptake by hepatocytes has also been proposed as a method for estimating liver function using dynamic MRI [357], this would also measure sinusoidal endothelial permeability, similarly to indocyanine-green clearance [358], though the small size of these agents make them likely less sensitive than lipoproteins which are closer in size to fenestration diameters.

Further, a computational model, such as we developed in **Paper II**, could with slight modifications be used to simulate expected parameters given certain porosities and resulting uptake kinetics.

Liver sinusoid *in silico* models, level of detail

Our *in silico* model contains relevant ultrastructural details of the liver sinusoids [106, 107, 108] modestly simplified for computation. We however did have to make some simplifications in the model still. For example the model is completely rigid, as opposed to elastic as normal liver tissue would be. We also simplify the flow as constant, while in reality it is of course pulsatile. The lymphatic drain outlet pressure was set to an estimated value, as there is no good way to measure it directly. We believe the simplifications are both necessary, for computational reasons, and do not detract much from what we sought to investigate. It would still be worthwhile to implement the model with added details, to make it even more accurate.

The distribution of fenestrations in the sinusoid, lymphatic drainage and their contribution to sinusoidal flow

In our model, the flow in the lumen of the sinusoid was modulated nigh exclusively by the shape of the vessel, while flow in the space of Disse was modulated by fenestrations and lymphatic drainage. This indicates the lymphatic outflow as an important factor determining flow, with implications for obstruction of lymph in the liver. The presence and geometry of the liver lymphatics have been described and studied by electron microscopy by Ohtani et al. [359] and with immunolabeling and fluorescence by Kiefer et al. [360].

LSEC scavenger cell function

When to suspect LSEC mediated uptake

LSEC as scavenger endothelium are specialized towards macromolecular waste clearance [151,361], thus ligands for endocytosis by LSEC fall into a size range typically less than 1μm, usually even smaller [201]. LSEC can however immobilize larger solutes such as bacteria [328,331] or damaged / senescent red blood cells [221,329,330], however they do not endocytose these, this is done by the Kupffer cells in this case. On account of their very high endocytic capacity, if the disappearance from the blood-stream is very rapid, this alone should make the LSEC a prime candidate site for uptake, or binding if too large for LSEC endocytosis. If in addition the uptake distributes to mainly liver (and secondly spleen), they are likely to be involved in some capacity. Thus, a clearance, biodistribution-experiment that displays I) rapid clearance II) high % distribution to the liver; should lead to the LSEC being investigated as the likely site of uptake.

Caution: Biodistribution experiments carried out without blood clearance measurements, and with a too long time-frame (LSEC uptake is typically rapid and has 2-5 min $t_{1/2}$, with degradation beginning shortly thereafter [308,309]), may misattribute the uptake, as much of the ligand may have become degradation products after few hours.

It would be prudent to always determine the clearance kinetics, and should they be in the range that LSEC typically operate in, with distribution to the liver; extracting the liver a similar time after injection as 2 half-lives will be prudent. With fluorescent labelling one can visually determine if uptake is via LSEC in frozen sections (and counter-staining with an LSEC marker e.g. stabilin-2), otherwise for radiolabelled (or by other methods measurable) ligands, performing a liver cell separation within this time-frame and measuring activities per cell (or some other measurable parameter relating to the ligand).

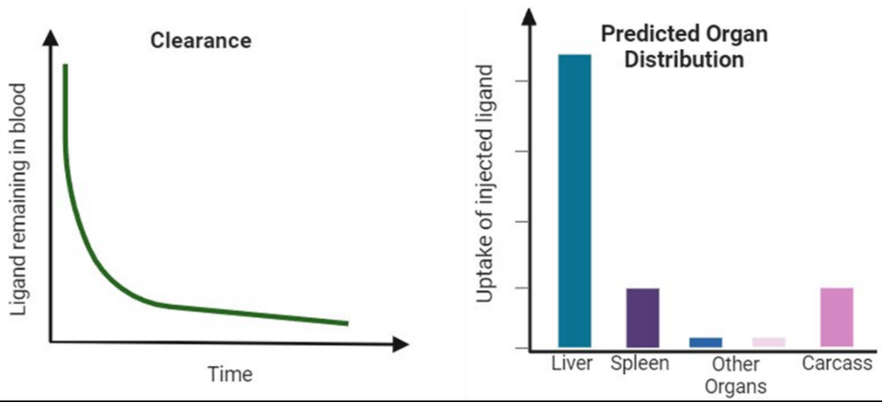

Figure 3.1: Illustration of characteristics that indicate LSEC involvement; Left panel: Rapid clearance, Right panel: Distributes mainly to liver. (Created with BioRender.com)

Albumin charge and conformational change and clearance

Based upon previous findings on formylated (FSA)[308], glycated (AGE-BSA)[212] and now highly oxidized, **Paper III**, albumin; charge and conformational changes drive the affinity for scavenger receptors, mostly stabilins, and lead to clearance from circulation. Observations made by Svistounov using HPLC on formylated, glycated, and highly oxidized albumins, indicate a conformational change [personal communications D. Svistounov, **Paper III**], and higher propensity towards dimerization. This presumably relates to receptor affinity and clearance. Further binding studies using receptor cell-lines could elucidate which modifications and conformational changes.

oxHSA presence in disease states

The very efficient uptake of oxHSA by LSEC that we document both *in vivo* and *in vitro*, shows that the presence of this modified protein in circulation is a strong marker for severe impairment of LSEC (and probably RES in general) mediated clearance functions. This, as it would otherwise be rapidly removed, and that it can depress endocytic activity on its own in LSEC for prolonged periods of time.

oxHSA may not be very specific as a marker, given the various pathologies that can lead to its accumulation [362], we however believe there may be value in screening for it, as appreciable quantities of oxHSA would indicate critical failure of the scavenging/RE system. High levels of oxHSA would further indicate liver involvement, in whichever pathology it is found.

Implications to impaired scavenging

The LSEC are responsible for the removal of a wide host of macromolecular waste from the blood-stream [201,202], some of which e.g. LPS [155] and oxLDL [220] are known mediators of inflammation and pathological development. If the scavenger cell system is overwhelmed or impaired this may set off a cascade of inflammation across the body. The production of reactive oxygen species by activated immune cells [363] suggests a potential loop, whereby oxidation protein products stimulate inflammation and additional ROS formation [340], as well as impair scavenger cell uptake, as seen in our work.

Discussing targeted delivery to LSEC in diseased states

Targeting LSEC for delivering therapeutics to the liver is a promising approach given their avid endocytic nature, and well characterized receptor systems (see sections on endocytosis and receptor table). There exist promising developments using nanocarriers to deliver therapeutic cargo to LSEC, or the liver in general via the LSEC [364,365,366,367,368,369]. This would be useful to deliver drugs specifically to the liver, or more specifically to LSEC. This may be done in order to deliver therapeutics to LSEC such as those described in **Paper I**.

Endocytosis in diseased states and implications for liver targeting with nanoparticles and the like (e.g. nanocarriers, drug-targeting moiety conjugates etc.)

Decreased uptake: Uptake of colloidal carbon (India ink) was found decreased in the ageing rat [150,370,371,372,373, reviewed 109], and uptake of sulfanilate-azo-albumin was reduced by half in aged rats [374]. A study by Ito et al. in 2007, similarly found reduced uptake of FSA and AGE-BSA in aged rats [112]. LSEC isolated from aged rats showed reduced endocytotic capacity relative to cells from young animals [338] but there was still considerable LSEC mediated scavenging in aged rat LSEC in this study. Expression of the important scavenger receptor stabilin-2 was also found decreased in aged mice [375]. There are also other considerations to be had when using nanotheraputics (or similar targeted approaches) in the elderly [reviewed in 376]. Interestingly scavenger receptor targeting may be more effective than hepatocyte targeting approaches, which may be slowed considerably by age related pseudocapillarization (reviewed in section on fenestrations).

Circulating scavenger receptor ligands will also render certain targeting strategies will be less effective. In advanced liver disease [340,341] circulating oxidized albumin is often seen, which is in of itself a potent SR ligand and will likely displace stabilin receptor targeting moieties, and renders reduced scavenging in general on account of its own high affinity as described in **Paper III** [166]. Oxidized LDL, also a stabilin ligand and nanoparticle, taken up by LSEC [220], may also displace stabilin ligands, and other scavenger receptor targeting nanoparticles. Similarly advanged glycation end products (AGEs) as seen in diabetes [377] may impair uptake via the stabilins of LSECs [378,215]. Additionally increased levels of circulating ligands would have the potential to overwhelm the uptake and degradation systems of the LSEC (or other highly endocytotic cell types) as noted by Hansen et al. [165], and slow down and or redirect the nanoparticles elsewhere.

Kupfer cell impairment: Chronic liver disease was found to impair clearance of bacteria in humans [379]. Intravital microscopy of uptake of 1.1μm latex beads, canonically taken up by Kupffer cells, however showed no impairment with age in rats [380].

Increased uptake: murine LSEC isolated from thioacetamide induced fibrosis animals showed increased uptake of dextran, albumin and mannose-albumin [381]. It was also found [382] that inflammatory cytokines and lipopolysaccharide increased uptake of ^{125}I-FSA and ^{125}I-mannan in cultured rat LSEC.

A recent paper details a two-step process of treating liver fibrosis, by administering first nanoparticles targeting LSEC via a surface hyaluronan moiety, containing a refenestrating agent (simvastatin) to reopen the pores through the LSEC layer to access the cells behind, and secondly nanoparticles targeting to stellate cells containing siRNA against collagen alpha chain and collagenase attached to their surface to remove already formed collagen [364]. This shows the method of targeting works for the CCl_4 induced model of fibrosis, and therefore fibrosis cases with similar pathological development.

Overall, caution should be applied when targeting diseased states with nanoparticles, as if uptake is severely reduced, such as for example can occur in ageing or late-stage cirrhosis, little of the relevant cargo would reach its intended target, while an unknown secondary site may be strongly affected. Conversely, if a condition, as in early inflammation, increases the endocytic capacity of the target cell type, the dosage may have to be lowered, and a slow-release strategy adopted, to avoid target site toxicity. Whether the intervention has dose-dependent toxic effects close to the therapeutic dose used, should determine the level of caution required.

Ideally primary cells from the relevant disease conditions, or relevant model thereof, should be tested, and matched to circulating serum markers to evaluate appropriate strategies for administration of therapeutic nanoparticles in the clinic. It may be beneficial to screen liver uptake kinetics in patients, perhaps using the classical method of radiolabelled colloidal albumin [168] which has been used to asses reticuloendothelial function in humans in ageing historically [reviewed in 169,150], which was found to taken up by LSEC *in vivo* [170], and Albunex type air-filled microspheres could similarly assess Kupffer cell (macrophage) function [383].

A note of caution when modifying liver uptake for the purpose of systemic delivery

The liver and RES uptake are crucial systems, especially with regard to LPS and bacterial clearance (LSEC/ Kupffer cell & splenic red pulp cells) [155,30,31]. Considerable quantities of LPS are measurable in the blood after mastication [384] and defecation [385], especially in conditions impacting gut barrier integrity. Impairing these clearance systems to enable e.g. prolonging the circulation time of nanoparticles or similar, which are often stabilin/ scavenger receptor ligands [386,387], and whose liver clearance constitutes somewhat of a challenge in nanomedicine [388–390], may thus lead to systemic inflammation. This would be unfortunate especially in cancer patients which are already frail, from chemotherapy or old age [391,392]. Irradiation has also been found to diminish the clearance of damaged red blood cells [167], while this function is largely performed by the spleen, it is via the same receptor system (stabilin-1/-2) [163,164] that LSEC use for much of their clearance functions [227,230,202]. A plausible solution could be to have patients be fasting for the duration of the treatment, such that little LPS and bacteria will come into the bloodstream, and the consequence of impaired clearance thereby reduced. Another could be haemophoresis, where noxious elements are removed from the blood extraneously. It seems unlikely inhibition of the RES can be done for prolonged periods of time without considerable side-effects.

Imaging and Image analysis

Fenestration analysis/ Image classification

The choice for the optimal strategy/ method for classifying images to segment out fenestrations should, based on our results, be adjusted to the type of study, image quality and size of dataset to be analysed.

Manual techniques are more robust, and less prone to misclassification, if the user knows the cell type and feature, and can be well applied for small datasets where there are large differences. In such cases it is most expedient to analyse the data thus, especially if the image quality is less than excellent. On noisier images of lower resolution, especially electron microscopy images, it is better to invest the time to perform manual classification, rather than attempt to optimize an approach that may or may not yield results or produce artefacts in the data. Perhaps recently developed AI based denoising could allow for use of more automated approaches. One significant drawback of manual classification, beyond the time requirement, is that user bias can skew data, and ideally analysis should be done by only one user for consistency. For simple counting, the frequencies of fenestrations, this method is relatively unbiased in our data (**Paper IV**).

Semi-automated approaches are by our estimation the most likely to be of use for measuring diameters or fenestration sizes, with acceptable image quality and somewhat large datasets, the semi-automated approach allows for analysis of diameters mostly uncompromised by user-bias. This allows multiple individuals to analyse a dataset, allowing for parallelization of image analysis. It is however more biased across users for the number of fenestrations than the other two methods. It may therefore be required to have analysis be performed by a single person, for counting fenestration numbers with this method.

Fully automated, machine-learning based approaches require very good and consistent image quality, this may change with AI based postprocessing [393]. However the homogeneity of the dataset is likely still of great importance, such that images ought ideally be from the same instrument with the same settings. The strength of this method is allowing for batch-processing of very large datasets. The dataset presumably needs to be above a certain size to justify, as we found training the software took significant amounts of time. The benefit of a trained classifier is however that it should work with all future datasets of the same resolution and magnification. There is considerable bias from the user training the model, and therefore optimal to assign one user to the training.

In summary, manual classification is still optimal for very small datasets, ideally with large differences, or images of poorer quality where artefacts would be an issue. Semi-automatic classification is the best suited for measuring diameters, and relatively fast and easy to apply, suitable for medium sized datasets, with average and above image quality. Automatic classification requires good quality images, but can classify very large sets of images, if using the same pretraining with identical biases throughout.

Imaging and imaging modalities

The imaging modality used and the processing of samples required for these naturally alter the dimensions of structures imaged to varying degrees. For example, transmission electron microscopy and scanning electron microscopy alter tissue and cells to different degrees, as demonstrated by Wisse [96] comparing liver sinusoids, LSEC fenestrations and red blood cells. It was found that TEM causes noticeably less shrinkage, presumably due to plastic infiltration expanding the tissue/cells back a bit after desiccation.

Modalities that do not require desiccation/work on wet samples will inherently have less shrinkage artefacts. They must however have comparable resolution for this to matter.

Optical nanoscopy techniques, such as; SIM [394], STED [395], dSTORM [396], are performed on wet samples and therefore avoid shrinkage artefacts as are inevitable for conventional electron microscopy. One major downside of these is that they can as of yet only be applied to *in vitro* specimens, with tissue optical nanoscopy being a while away still (at least with regards to fenestration analysis).

Atomic force microscopy is similar or better in resolution than optical nanoscopy techniques, with the added benefit of live-cell dynamic imaging, visualizing fenestrations dynamics in living cells [100] (SIM and STED could in principle be applied to live cell imaging, but membrane dyes present a challenge [personal correspondence: Szafranska & Zapotoczny]). Similarly to optical nanoscopy it can also only be done on cultured cells, to observe fenestrations.

Cryo-electron microscopy also avoid the problem of shrinkage artefacts, while retaining electron microscopy level resolution [397,398], the equipment however is prohibitively expensive and relatively rare. This modality also for obvious reasons precludes live cell imaging.

We compared the modalities of SEM, STED, SIM and AFM in **Paper V**, on cultured LSEC, and found sample dehydration for SEM shifts the size distribution upwards towards larger diameters compared with all other modalities. This shift is notable with regards to the “true size" of fenestrations, and physiological interpretations of their size from SEM micrographs. However the shift appears to be of the entire distribution such that comparisons between treatments and matched controls still should be valid. The resolution of electron microscopy compared with other forms of microscopy, also means that smaller differences can be detected with this modality compared with others. Ease of use, speed of acquisition and cost are also relevant factors, and conventional SEM still holds up well in this regard.

Imaging modalities also impact which method of image analysis is best suited to the task, fluorescence-based methods such as SIM, STED and dSTORM produce images with clear contrast to background and are easily segmentable by thresholding (semi-automated approach), making for easy analysis (at the cost of resolution or acquisition time). AFM also yields images readily segmentable by thresholding. SEM has the best resolution of the modalities, but lower contrast between cell and background, the images thus require more careful processing.

Neural network approaches to classifying fenestrations, as was successfully adapted to SEM, SIM and AFM images by us (**Paper IV**), were also used on AFM images [399] by Li et al., though a different tool (We used Ilastik, Li et al. used an in-house coded method). Semi-automated approaches have also been used for STED [395], SIM [400], an earlier version of the method using the Kentron-Zeiss IBAS system on SEM images [108].

LSEC endocytic functions and fenestrations

LSEC possess two distinct functional phenotypes, one as a highly efficient scavenger cell, the other as the dynamic filter providing access to the liver parenchyma. It has been much discussed, by rarely published on the topic of whether these functions are interconnected or related. It seems likely the two programs are distinctive, on account of the non-fenestrated scavenger endothelium that can be found in fish e.g cod and zebrafish [151,386], and the multitudes of fenestrated non-scavenger endothelia (reviewed in the introduction). Experiments by Zapotoczny et al. also found no decrease in endocytosis beyond that which corresponded to toxicity for several fenestration affecting compounds [352]. It should be possible to disentangle these transcriptional programs by isolating and analysing these cell populations. There also seem to be distinct types of fenestrations, the larger type as found in spleen [4] and intestine [64] appear significantly different from the smaller types in other tissues. These smaller types on the other hand appear more similar, and as Herrnberger et al. found, knocking down the diaphragm protein PLVAP transforms kidney and other diaphragmed fenestrations into a type more resembling that in liver [75]. It is highly likely the underlying mechanisms, at least those involved in the formation and maintenance of fenestrations, are similar for the fenestrations of the liver, kidney, choriocapillaris and other capillary fenestration. Perchance an increased understanding of the underlying mechanism may be useful in designing interventions later as well.

Noxious ligands of LSEC and pathological alterations

Though there are certain ways in which the topics overlap, toxic and inflammatory ligands such as oxLDL [345] can cause loss of fenestrations in LSEC. One idea was that indigestible ligands also can contribute to endothelial thickening, and in such a manner the scavenging function becomes key to understanding chronic illness / ageing related loss of / reduction in fenestrations. If so this also opens up new avenues of therapies and treatments. A gastric K/H^+

pump inhibitor, soraprazan, has been successfully repurposed for the treatment of lipofuscin related blindness (Stargardt's disease) [401,402], and it and similar drugs should more be found, could then potentially be applied to ameliorate age and illness related endothelial thickening, reductions in endocytic activity and defenestration in the liver. Speculating somewhat on the aetiology of ageing related endothelial thickening, exploring such therapeutics, that remove lipofuscin/indigestible material from cells, should be worth looking further into. There also exists a possibility for a relationship to vitamin-A cross linking products and lipofuscinosis. this is seemingly the case in Stargardts disease [403], and stellate cells in the liver are vitamin-A storing cells [404], creating a possible if tenuous connection, as LSEC isolated from elderly humans [405] have considerable lipofuscin-like autofluorescence. How or if this connects with LSEC phenotype and function bears exploring.

5 Concluding remarks and Future perspectives

5.1 Concluding remarks

In **Paper I** we summarize the available literature over the topic of fenestration affecting compounds, what compounds are known to affect fenestrations and in what way these affect the fenestrations. We review at times obscure literature covering over 50 years of liver research, with some references existing only as printed books. This is to our knowledge the most comprehensive and up to date summary of the field of LSEC fenestration modulators. Our review allows for future researchers to have a systematized list of compounds and categories, with which to modulate fenestrations.

In **Paper II** we model the hepatic sinusoid as a simplified 2D model, to investigate the relative contributions to flow properties of ultrastructural parameters; distribution of fenestrations, shape of vessel, presence or absence of lymphatic drainage. We found the influence on flow in the sinusoidal lumen is predominantly affected by the overall shape of the sinusoid, with little contribution from fenestrations. The flow in the space of Disse however was to a certain extent modulated by fenestrations, both overall porosity and distribution. The addition of a lymphatic drainage at the periportal area also affected the flow through the space of Disse. Our model also demonstrates an easy way to include more realistic ultrastructural details, such as those mentioned above, in a fluid flow model that we hope can be built further upon.

In **Paper III** we investigated the uptake of a highly oxidized form of albumin, oxHSA. We found that this was taken up principally by LSEC *in vivo* and in isolated primary cells from the liver. Further we identified the receptors for endocytosis, stabilins -1 and -2, by uptake and competitive inhibition studies in isolated LSEC, stabilin -1 or -2 overexpressing cell lines, and affinity chromatography of LSEC detergent lysates. We found that oxHSA was non-toxic to LSEC, and did not modify their fenestrations, however oxHSA depressed LSEC endocytic ability for prolonged periods of time.

The methods examined in **Paper IV** allow users to select their optimal method, based on image quality, data set size, and user bias. Automated and semi-automated methods allow for larger datasets to be analyzed, as would be required for elucidating smaller effects in studies, while requiring better quality microscopy images. The manual approach is still applicable, though ideally for large effects in smaller data sets, or when image quality is poor.

5.2 Future perspectives

The compounds we summarize can be used in for example the design of targeted interventions, for example drug conjugates or nano-encapsulations. Further compounds can be hypothesized and tested for fenestration modulating activity based upon classes of compounds, e.g. vasodilators seem to dilate fenestrations in general, and VEGF, NO, cyclic nucleotides (cAMP/cGMP) seem involved in upregulation of fenestrations. Building from these historical insights and our theory of fenestration regulation, hypotheses concerned with the true mechanism of fenestral regulation may be developed and tested. Obvious candidates for compounds to test would be stable cyclic nucleotides, and inducers and inhibitors of nucleotide cyclases and downstream protein kinases e.g. PKA.

Our computational model integrates ultrastructural details, often omitted from fluid models of the liver, with efficient simplicity, allowing more complex models to be adapted from it. We should like to see the model adapted with intermittent pulsatile flow, blood cells passing through and elastic deformable walls, parameters we had to simplify away for time and computational reasons, but which for users with more advanced hardware would be well worth implementing.

Highly oxidized albumin is cleared extremely rapidly by LSEC, which we believe implies that finding it in blood tests at detectable levels is likely an indicator of severe scavenger cell dysfunction, possibly advanced liver disease. We also found that the receptors for endocytosis are the stabilins, implying, based on previous findings (AGE-BSA, FSA), that there is a structural reorganization of modified albumin rendering it ligand of the aforementioned. Other modified varieties of albumin, especially denatured types, are thus likely taken up by these receptors. We believe this can be used to design delivery to stabilin expressing cells, such as albumin nanocarriers, of which there exist some.

The image analysis methods examined allow for an easy assessment of which methods would suit users best, given their data. The automated method already showed great promise in our study, and we believe with recent advances in machine learning, this method will become even more powerful. Artificial intelligence assisted image denoising will soon be able to improve nigh any image set such that fully automated classification can be made the standard method of classification.

6 References:

(1) Mahadevan, V. Anatomy of the Liver. *Surg. (United Kingdom)* **2020**, *38* (8), 427–431. https://doi.org/10.1016/j.mpsur.2014.10.004.

(2) Ellis, H. Anatomy of the Liver. *Surgery* **2011**, *29* (12), 589–592. https://doi.org/10.1016/j.mpsur.2011.09.012.

(3) McCuskey, R. S. Anatomy of the Liver. In *Zakim & Boyer's HEPATOLOGY*; Boyer, T. D., Manns, M. P., Sanyal, A. J., Eds.; ELSEVIER, 2012; pp 3–20.

(4) Junqueria, L. C.; Carneiro, J.; Long, J. A. *Basic Histology*, 5th ed.; Appleton & Lange, 1986.

(5) Young, B.; O'Dowd, G.; Woodford, P. *Wheater's Funtional Histology A Text and Colour Atlas*, 6th ed.; ELSEVIER: CHURCHILL LIVINGSTONE, 2013.

(6) Debbaut, C.; Segers, P.; Cornillie, P.; Casteleyn, C.; Dierick, M.; Laleman, W.; Monbaliu, D. Analyzing the Human Liver Vascular Architecture by Combining Vascular Corrosion Casting and Micro-CT Scanning: A Feasibility Study. *J. Anat.* **2014**, *224* (4), 509–517. https://doi.org/10.1111/joa.12156.

(7) Eberlova, L.; Liska, V.; Mirka, H.; Gregor, T.; Tonar, Z.; Palek, R.; Skala, M.; Bruha, J.; Vycital, O.; Kalusova, K.; Haviar, S.; Kralickova, M.; Lametschwandtner, A. Porcine Liver Vascular Bed in Biodur E20 Corrosion Casts. *Folia Morphol.* **2016**, *75* (2), 154–161. https://doi.org/10.5603/FM.a2015.0094.

(8) Lametschwandtner, A.; Spornitz, U.; Minnich, B. Microvascular Anatomy of the Non-Lobulated Liver of Adult Xenopus Laevis: A Scanning Electron Microscopic Study of Vascular Casts. *Anat. Rec.* **2022**, *305* (2), 243–253. https://doi.org/10.1002/ar.24649.

(9) Wack, K. E.; Ross, M. A.; Zegarra, V.; Sysko, L. R.; Watkins, S. C.; Stolz, D. B. Sinusoidal Ultrastructure Evaluated during the Revascularization of Regenerating Rat Liver. *Hepatology* **2001**, *33* (2), 363–378. https://doi.org/10.1053/jhep.2001.21998.

(10) Pappenheimer, J. R.; Renkin, E. M.; Borrero, L. M. Filtration, Diffusion and Molecular Sieving Through Peripheral Capillary Membranes A Contribution to the Pore Theory of Capillary Permeability. *Am. J. Pathol.* **1951**, *167*.

(11) Abbe, E. VII.-On the Estimation of Aperture in the Microscope. *J. R. Microsc. Soc.* **1881**, *1* (3), 388–423. https://doi.org/10.1111/j.1365-2818.1881.tb05909.x.

(12) Ruska, E.; Knoll, M. Das Elektronenmikroskop. *Zeitschrift für Phys.* **1932**, *78*, 318–337. https://doi.org/10.1055/s-0028-1122268.

(13) Dalton, A. J. Electron Microscopy of Tissue Sections; 1953; pp 403–417. https://doi.org/10.1016/S0074-7696(08)61039-6.

(14) PALADE, G. E. A Study of Fixation for Electron Microscopy. *J. Exp. Med.* **1952**, *95* (3), 285–298. https://doi.org/10.1084/jem.95.3.285.

(15) Porter, K.; Blum, J. A STUDY IN MICROTOMY FOR ELECTRON MICROSCOPY. *Anat. Rec.* **1953**, *117* (4), 685–709.

(16) SJÖSTRAND, F. ULTRA-THIN TISSUE SECTIONS FOR ELECTRON MICROSCOPY. *Nature* **1951**, *168*, 646–647.

(17) SJöstrand, F. S. A New Microtome for Ultrathin Sectioning for High Resolution Electron Microscopy. *Experientia* **1953**, *9* (3), 114–115. https://doi.org/10.1007/BF02178346.

(18) Claude, B. Y. A.; Fullam, E. F. THE PREPARATION OF SECTIONS OF GUINEA PIG LIVER FOR ELECTRON MICROSCOPY (Received for Publication , February 13 , 1946) The High Resolving Power of the Electron Microscope Offers an Opportunity to Extend the Study of Intracellular Organization to The ' . *Microscopy* **1946**.

(19) Farquhar, M. G. Fine Structure and Function in Capillaries of the Anterior Pituitary Gland. *Angiology* **1961**, *12* (7), 270–292. https://doi.org/10.1177/000331976101200704.

(20) Rinehart, J. F.; Farquhar, M. G. The Fine Vascular Organization of the Anterior Pituitary Gland. An Electron Microscopic Study with Histochemical Correlations. *Anat. Rec.* **1955**, *121* (2), 207–239. https://doi.org/10.1002/ar.1091210206.

(21) Zelander, T. Ultrastructure of the Mouse Adrenal Cortex. An Electron Microscopical Study in Intact and Hydrocortisone-Treated Male Adults. *J. Ultrastruct. Res.* **1959**, *3* (SUPPL. 1), 1–111. https://doi.org/10.1016/S0889-1605(59)80004-5.

(22) Belt, W. Electron Microscopy of the Adrenal Cortex of the Rat. *Anat. Rec.* **1956**, *124* (2).

(23) Lever, B. Y. J. D. FINE STRUCTURAL APPEARANCES IN THE RAT PARATHYROID. **1955**.

(24) LEVER, J. D. ELECTRON MICROSCOPIC OBSERVATIONS ON THE NORMAL AND DENERVATED ADRENAL MEDULLA OF THE RAT 1. *Endocrinology* **1955**, *57* (5), 621–635. https://doi.org/10.1210/endo-57-5-621.

(25) Møller, M.; van Deurs, B.; Westergaard, E. Vascular Permeability to Proteins and Peptides in the Mouse Pineal Gland. *Cell Tissue Res.* **1978**, *195* (1), 1–15. https://doi.org/10.1007/BF00233673.

(26) Ekholm, R. THE ULTRASTRUCTURE OF THE BLOOD CAPILLARIES IN THE MOUSE THYROID GLAND. *Zeitschrift für Zellforsch.* **1957**, *46*, 139–146.

(27) Monroe, B. G. Electron Microscopy of the Thyroid. *Anat. Rec.* **1953**, *116* (3).

(28) DEMPSEY, E. W.; PETERSON, R. R. ELECTRON MICROSCOPIC OBSERVATIONS ON THE THYROID GLANDS OF NORMAL, HYPOPHYSECTOMIZED, COLD-EXPOSED AND THIOURACIL-TREATED RATS 1. *Endocrinology* **1955**, *56* (1), 46–58. https://doi.org/10.1210/endo-56-1-46.

(29) Heimann, P. Ultrastructure of Human Thyroid. *Eur. J. Endocrinol.* **1966**, *53*.

(30) TRIER, J. S. The Fine Structure of the Parathyroid Gland. *J. Biophys. Biochem. Cytol.* **1958**, *4* (1), 13–22. https://doi.org/10.1083/jcb.4.1.13.

(31) Bencosme, S. A.; Pease, D. C. Electron Microscopy of the Pancreatic Islets. *Endocrinology* **1958**, *63* (1).

(32) Hartmann, J. F. ELECTRON MICROSCOPY OF THE NEUROHYPOPHYSIS IN NORMAL AND HISTAMINE TREATED RATS. *Zeitschrift für Zellforsch.* **1958**, *48*, 291–308.
(33) Palay, S. The Fine Structure of the Neurohypophysis. In *Ultrastructure and cellular chemistry of neuron and tissue.*; Waelsh, H., Ed.; Paul B Hoeber Inc., Harper & Brothers New York, 1957.
(34) Lever, J. D. Remarks on the Electron Microscopy of the Rat Luteum and Comparison with Earlier Observations on the Adrenal Cortex. *Anat. Rec.* **1956**, *124* (1), 111–125. https://doi.org/10.1002/ar.1091240109.
(35) RERKAMNUAYCHOKE, W.; NISHIDA, T.; KUROHMARU, M.; HAYASHI, Y. Morphological Studies on the Vascular Architechture in the Boar Spermatic Cord. *J. Vetrinary Med. Sci.* **1991**, *53* (2), 233–239.
(36) Garron, L. K. The Ultrastructure of the Retinal Pigment Epithelium with Observations on the Choriocapillaris and Bruch's Membrane. *Trans. Am. Ophthalmol. Soc.* **1963**, *61*, 545–588.
(37) Carlson, E. C. Fenestrated Subendothelial Basement Membranes in Human Retinal Capillaries. *Investig. Ophthalmol. Vis. Sci.* **1989**, *30* (9), 1923–1932.
(38) Dryll, A.; Lansaman, J.; Cazalis, P.; Peletier, A. P.; De Seze, S. Light and Electron Microscopiy Study of Capillaries in Normal and Inflammatory Human Synovial Membrane. *J. Clin. Pathol.* **1977**, *30*, 556–562.
(39) Norton, W. L.; Ziff, M. Electron Microscopic Observations on the Rheumatoid Synovial Membrane. *Arthritis Rheum.* **1966**, *9* (4), 589–610. https://doi.org/10.1002/art.1780090405.
(40) Muto, M. A Scanning and Transmission Electron Microscopic Study on Rat Bone Marrow Sinuses and Transmural Migration of Blood Cells. *Arch. Histol. Jpn.* **1976**, *39* (1), 51–66.
(41) Stehbens, W. E.; Ludatscher, R. M. Fine Structure of Senile Angiomas of Human Skin. *Angiology* **1968**, *19* (10), 581–592. https://doi.org/10.1177/000331976801901002.
(42) Ludatscher, R. M.; Stehbens, W. E. Vesicles of Fenestrated and Non-Fenestrated Endothelium. *Zeitschrift für Zellforsch. und Mikroskopische Anat.* **1969**, *97* (2), 169–177. https://doi.org/10.1007/BF00344755.
(43) Stehbens, W. E. ULTRASTRUCTURE OF VASCULAR ENDOTHELIUM IN THE FROG. *Q. J. Exp. Physiol. Cogn. Med. Sci.* **1965**, *50* (4), 375–384. https://doi.org/10.1113/expphysiol.1965.sp001804.
(44) Mohamed, A. H.; Waterhouse, J. P.; Friederici, H. H. R. The Fine Structure of Gingival Terminal Vascular Bed. *Microvasc. Res.* **1973**, *6* (2), 137–152. https://doi.org/10.1016/0026-2862(73)90016-2.
(45) MIYOSHI, M.; FUJITA, T. Stereo-Fine Structure of the Splenic Red Pulp. A Combined Scanning and Transmission Electron Microscope Study on Dog and Rat Spleen. *Arch. Histol. Jpn.* **1971**, *33* (3), 225–246. https://doi.org/10.1679/aohc1950.33.225.
(46) Uehara, K.; Uehara, A. Vimentin Intermediate Filaments: The Central Base in Sinus Endothelial Cells of the Rat Spleen. *Anat. Rec.* **2010**, *293* (12), 2034–2043. https://doi.org/10.1002/ar.21210.
(47) Jalkanen, S.; Salmi, M. Lymphatic Endothelial Cells of the Lymph Node. *Nat. Rev. Immunol.* **2020**, *20* (9), 566–578. https://doi.org/10.1038/s41577-020-0281-x.
(48) Spalding, H. J.; Heath, T. J. Inguinal Lymph Centre in the Pig. **1989**, 43–54.
(49) Gotloib, L.; Shustak, A.; Bar-Sella, P.; Eiali, V. Fenestrated Capillaries in Human Parietal and Rabbit Diaphragmatic Peritoneum. *Nephron* **1985**, *41* (2), 200–202. https://doi.org/10.1159/000183581.
(50) Gotloib, L.; Shustak, A.; Jaichenko, J. Fenestrated Capillaries in Mice Submesothelial Mesenteric Microvasculature. *Int. J. Artif. Organs* **1989**, *12* (1), 20–24. https://doi.org/10.1177/039139888901200103.
(51) Korneliussen, H. Fenestrated Blood Capillaries and Lymphatic Capillaries in Rat Skeletal Muscle. *Cell Tissue Res.* **1975**, *163* (2), 169–174. https://doi.org/10.1007/BF00221724.
(52) Seki, T.; Sakai, Y.; Taira, K. Occurrence of Fenestrated Capillaries in the Rat Tibialis Anterior Muscles after the Hindlimb Cast Immobilization: Scanning Electron Microscopy. *KITAKANTO Med. J.* **2004**, *54* (2), 87–91. https://doi.org/10.2974/kmj.54.87.
(53) Desaki, J.; Oki, S.; Matsuda, Y.; Sakanaka, M. Morphological Changes of Capillaries in the Rat Soleus Muscle Following Experimental Tenotomy. *J. Electron Microsc. (Tokyo).* **2000**, *49* (1), 185–193. https://doi.org/10.1093/oxfordjournals.jmicro.a023785.
(54) Desaki, J.; Oki, S.; Matsuda, Y. Morphological Changes of Capillaries Associated with Muscle-Fiber Atrophy in the Extensor Digitorum Longus Muscle of Aged Rats. *J. Electron Microsc. (Tokyo).* **1996**, *45* (5), 364–371. https://doi.org/10.1093/oxfordjournals.jmicro.a023453.
(55) Weihe, E.; Kalmbach, P. Ultrastructure of Capillaries in the Conduction System of the Heart in Various Mammals. *Cell Tissue Res.* **1978**, *192* (1), 77–87. https://doi.org/10.1007/BF00231024.
(56) Shimada, T.; Noguchi, T.; Kitamura, H.; Matsufuji, Y.; Campbell, G. R. Structure and Distribution of Lymphatic Capillaries and Fenestrated Blood Capillaries in the Conduction System of the Rabbit Heart. *Heart Vessels* **1988**, *4* (3), 123–127. https://doi.org/10.1007/BF02058423.
(57) Imayama, S. Scanning and Transmission Electron Microscope Study on the Terminal Blood Vessels of the Rat Skin. *J. Invest. Dermatol.* **1981**, *76* (3), 151–157. https://doi.org/10.1111/1523-1747.ep12525558.
(58) Lu, M.; Munford, R. S. The Transport and Inactivation Kinetics of Bacterial Lipopolysaccharide Influence Its Immunological Potency In Vivo. *J. Immunol.* **2011**, *187* (6), 3314–3320. https://doi.org/10.4049/jimmunol.1004087.
(59) Wiig, H.; Swartz, M. A. Interstitial Fluid and Lymph Formation and Transport: Physiological Regulation and Roles in Inflammation and Cancer. *Physiol. Rev.* **2012**, *92* (3), 1005–1060. https://doi.org/10.1152/physrev.00037.2011.
(60) Latta, H.; Maunsbach, A. B.; Madden, S. C. The Centrolobular Region of the Renal Glomerulus Studied by Electron Microscopy. *J. Ultrasructure Res.* **1960**, *4* (3–4), 455–472. https://doi.org/10.1016/S0022-5320(60)80033-0.
(61) Rhodin, J. Electron Microscopy of the Glomerular Capillary Wall. *Exp. Cell Res.* **1955**, *8*, 572–574.
(62) BENNETT, H. S.; LUFT, J. H.; HAMPTON, J. C. Morphological Classifications of Vertebrate Blood Capillaries. *Am. J. Physiol.* **1959**, *196* (2), 381–390. https://doi.org/10.1152/ajplegacy.1959.196.2.381.
(63) Azumi, R.; Morita, K.; Mizutani, Y.; Hayatsu, M.; Terai, S.; Ushiki, T. Dynamics of Basal Lamina Fenestrations in the Rat Intestinal Villous Epithelium in Response to Dietary Conditions. *Biomed. Res.* **2018**, *39* (2), 65–74.

https://doi.org/10.2220/biomedres.39.65.
(64) Komuro, T. Fenestrations of the Basal Lamina of Intestinal Villi of the Rat. *Cell Tissue Res.* **1985**, *239*, 183–188.
(65) ROUILLER, C. LES CANNICULES BILLIARES. *Acta Anat. (Basel).* **1956**, *26*.
(66) Dalton, A. J.; Felix, M. D. THE ELECTRON MICROSCOPY OF NORMAL AND MALIGNANT CELLS. *Ann. N. Y. Acad. Sci.* **1956**, *63* (6), 1117–1140.
(67) Wassermann, F. The Structure of the Wall of the Hepatic Sinusoids in the Electron Microscope. *Zeitschrift für Zellforsch. und Mikroskopische Anat.* **1958**, *49* (1), 13–32. https://doi.org/10.1007/BF00335060.
(68) Yamagishi, M. Electron Microscope Studies on the Fine Structure of the Sinusoidal Wall and Fat-Storing Cells of Rabbit Livers. *Arch. Histol. Jpn.* **1959**, *18* (2).
(69) Wisse, E. An Electron Microscopic Study of the Fenestrated Endothelial Lining of Rat Liver Sinusoids. *J. Ultrasructure Res.* **1970**, *31* (1–2), 125–150. https://doi.org/10.1016/S0022-5320(70)90150-4.
(70) ATERMAN, K. *The Structure of the Liver Sinusoids and the Sinusoidal Cells*; ACADEMIC PRESS INC., 1963. https://doi.org/10.1016/b978-1-4832-2824-2.50009-1.
(71) Wisse, E.; Braet, F.; Duimel, H.; Vreuls, C.; Koek, G.; Wm, S.; Damink, O.; Broek, M. A. J. Van Den; Geest, B. De; Dejong, C. H. C.; Tateno, C.; Frederik, P.; Wisse, E.; Duimel, H.; Vreuls, C.; Frederik, P. Fixation Methods for Electron Microscopy of Human and Other Liver. **2010**, *16* (23), 2851–2866. https://doi.org/10.3748/wjg.v16.i23.2851.
(72) Nakakura, T.; Suzuki, T.; Horiguchi, K.; Tanaka, H.; Arisawa, K.; Miyashita, T.; Nekooki-Machida, Y.; Hagiwara, H. Fibronectin-Integrin Signaling Regulates PLVAP Localization at Endothelial Fenestrae by Microtubule Stabilization. *Cell Tissue Res.* **2021**, *384* (2), 449–463. https://doi.org/10.1007/s00441-020-03326-2.
(73) Nakakura, T.; Suzuki, T.; Tanaka, H.; Arisawa, K.; Miyashita, T.; Nekooki-Machida, Y.; Kurosawa, T.; Tega, Y.; Deguchi, Y.; Hagiwara, H. Fibronectin Is Essential for Formation of Fenestrae in Endothelial Cells of the Fenestrated Capillary. *Cell Tissue Res.* **2021**, *383* (2), 823–833. https://doi.org/10.1007/s00441-020-03273-y.
(74) Nakakura, T.; Tanaka, H.; Suzuki, T. Regulation of Fenestra Formation via Actin-Dynamin2 Interaction in Rat Pituitary Endothelial Cells. *Cell Tissue Res.* **2022**, *390* (3), 441–451. https://doi.org/10.1007/s00441-022-03685-y.
(75) Herrnberger, L.; Seitz, R.; Kuespert, S.; Bösl, M. R.; Fuchshofer, R.; Tamm, E. R. Lack of Endothelial Diaphragms in Fenestrae and Caveolae of Mutant Plvap-Deficient Mice. *Histochem. Cell Biol.* **2012**, *138* (5), 709–724. https://doi.org/10.1007/s00418-012-0987-3.
(76) Pino, R. M.; Essner, E. Permeability of Rat Choriocapillaris to Hemeproteins. Restriction of Tracers by a Fenestrated Endothelium. *J. Histochem. Cytochem.* **1981**, *29* (2), 281–290. https://doi.org/10.1177/29.2.7252121.
(77) Axelsson, I. Characterization of Proteins and Other Macromolecules by Agarose Gel Chromatography. *J. Chromatogr. A* **1978**, *152* (1), 21–32. https://doi.org/10.1016/S0021-9673(00)85330-3.
(78) Herrnberger, L.; Ebner, K.; Junglas, B.; Tamm, E. R. The Role of Plasmalemma Vesicle-Associated Protein (PLVAP) in Endothelial Cells of Schlemm's Canal and Ocular Capillaries. *Exp. Eye Res.* **2012**, *105*, 27–33. https://doi.org/10.1016/j.exer.2012.09.011.
(79) ITO, T.; SHIBASAKI, S. Electron Microscopic Study on the Hepatic Sinusoidal Wall and the Fat-Storing Cells in the Normal Human Liver. *Arch. Histol. Jpn.* **1968**, *29* (2), 137–192.
(80) TANUMA, Y.; ITO, T.; SHIBASAKI, S. Further Electron-Microscope Studies on the Human Hepatic Sinusoidal Wall with Special Reference to the Fat-Storing Cell. *Arch. Histol. Jpn.* **1982**, *45* (3), 263–274. https://doi.org/10.1679/aohc.45.263.
(81) MUTO, M.; NISHI, M.; Tsuneo, F. Scanning Electron Microscopy of Human Liver Sinusoids. *Arch. histol. jap.*, **1977**, *40* (2), 137–151.
(82) Tanuma, Y.; Ohata, M.; Ito, T.; Uchida, K. Electron Microscopic Studies on the Sinusoidal Cells in the Monkey Liver. *Arch. Histol. Jpn.* **1983**, *46* (3), 401–426. https://doi.org/10.1679/aohc.46.401.
(83) Tanuma, Y.; Ito, T. Electron Microscope Study on the Hepatic Sinusoidal Wall and Fat-Storing Cells in the Bat. *Arch. Histol. Jpn.* **1978**, *41* (1), 1–39.
(84) Ohata, M.; Ito, T. Experimental Study on the Fine Structure of Chicken Liver Parenchyme with Special References to Extra-Sinusoidal Macrophages and Sinusoidal Blood Cells. Part 1. Sinusoidal Cells and Macrophages in the Normal and India Ink-Perfused Livers. *Arch. Histol. Jpn.* **1986**, *49* (1), 83–103. https://doi.org/10.1679/aohc.49.83.
(85) Ohata, M.; Tanuma, Y.; Ito, T. Electron Microscopic on the Study Fine on Avian Livers with Special Remarks on the Fine Structure of Sinusoidal. *Okajimas Folia Anat. Jpn.* **1982**, *58* (March), 325–368.
(86) Tanuma, Y. Electron Microscopic Study on the Hepatic Sinusoidal Wall of the Soft-Shelled Turtle (Amyda Japonica) with Special Remarks on the Smooth Muscle Cells. *Arch. Histol. Jpn.* **1987**, *50* (3), 251–272. https://doi.org/10.1679/aohc.50.251.
(87) Taira, K.; Mutoh, H. Comparative Ultrastructural Study of the Ito Cells in the Liver in Some Reptiles. *Arch. Histol. Jpn.* **1981**, *44* (4), 373–384. https://doi.org/10.1679/aohc1950.44.373.
(88) TANUMA, Y.; ITO, T. Electron Microscopic Study on the Sinusoidal Wall of the Liver of the Crucian, Carassius Carassius, with Special Remarks on the Fat-Storing Cell (FSC). *Arch. Histol. Jpn.* **1980**, *43* (3), 241–263. https://doi.org/10.1679/aohc1950.43.241.
(89) Tanuma, Y.; Ohata, M.; Ito, T. Electron Microscopic Study on the Sinusoidal Wall of the Liver in the Flatfish, Kareius Bicoloratus: Demonstration of Numerous Desmosomes along the Sinusoidal Wall. *Arch. Histol. Jpn.* **1982**, *45* (5), 453–471. https://doi.org/10.1679/aohc.45.453.
(90) Shiojiri, N.; Kametani, H.; Ota, N.; Akai, Y.; Fukuchi, T.; Abo, T.; Tanaka, S.; Sekiguchi, J.; Matsubara, S.; Kawakami, H. Phylogenetic Analyses of the Hepatic Architecture in Vertebrates. *J. Anat.* **2018**, *232* (2), 200–213. https://doi.org/10.1111/joa.12749.
(91) Eurell, J. A.; Haensly, W. E. The Histology and Ultrastructure of the Liver of Atlantic Croaker Micropogon Undulatus L. *J. Fish Biol.* **1982**, *21* (1), 113–125. https://doi.org/10.1111/j.1095-8649.1982.tb02829.x.

(92) Mugnaini, E.; Harboe, S. B. The Liver of Myxine Glutinosa: A True Tubular Gland. *Zeitschrift f�r Zellforsch. und Mikroskopische Anat.* **1967**, *78* (3), 341–369. https://doi.org/10.1007/BF00325318.
(93) Youson, J. H.; Yamamoto, K.; Shivers, R. R. Nonparenchymal Liver Cells in a Vertebrate without Bile Ducts. *Anat. Embryol. (Berl).* **1985**, *172* (1), 89–96. https://doi.org/10.1007/BF00318947.
(94) Monahan-Earley, R.; Dvorak, A. M.; Aird, W. C. Evolutionary Origins of the Blood Vascular System and Endothelium. *J. Thromb. Haemost.* **2013**, *11* (SUPPL.1), 46–66. https://doi.org/10.1111/jth.12253.
(95) Wisse, E.; De Zanger, R.; Charles, K.; Van Der Smissen, P.; McCuskey, R. The Liver Sieve : Considerations Concerning the Structure and Function of Endothelial Fenestrae , the Sinusoidal Wall and the Space of Disse. *Hepatology* **1985**, *5* (4).
(96) Wisse, E.; Charles, K.; Vandersmissen, P.; De Zanger, R. B. Comparative Morphometry on Rat Liver Sinusoids, Endothelial Fenestrae, and Red Blood Cells Fixed by Constant Low Pressure Perfusion Fixation. *Proceedings, Annu. Meet. Electron Microsc. Soc. Am.* **1984**, *42* (February 2022), 208–209. https://doi.org/10.1017/s042482010011115x.
(97) Szafranska, K.; Neuman, T.; Baster, Z.; Rajfur, Z.; Szelest, O.; Holte, C.; Kubisiak, A.; Kus, E.; Wolfson, D. L.; Chlopicki, S.; Ahluwalia, B. S.; Lekka, M.; Szymonski, M.; McCourt, P.; Zapotoczny, B. From Fixed-Dried to Wet-Fixed to Live – Comparative Super-Resolution Microscopy of Liver Sinusoidal Endothelial Cell Fenestrations. *Nanophotonics* **2022**, *11* (10), 2253–2270. https://doi.org/10.1515/nanoph-2021-0818.
(98) Szafranska, K.; Kruse, L. D.; Holte, C. F.; McCourt, P.; Zapotoczny, B. The WHole Story About Fenestrations in LSEC. *Front. Physiol.* **2021**, *12* (September). https://doi.org/10.3389/fphys.2021.735573.
(99) Zapotoczny, B.; Braet, F.; Wisse, E.; Lekka, M.; Szymonski, M. Biophysical Nanocharacterization of Liver Sinusoidal Endothelial Cells through Atomic Force Microscopy. *Biophys. Rev.* **2020**, *12* (3), 625–636. https://doi.org/10.1007/s12551-020-00699-0.
(100) Zapotoczny, B.; Szafranska, K.; Kus, E.; Braet, F.; Wisse, E.; Chlopicki, S.; Szymonski, M. Tracking Fenestrae Dynamics in Live Murine Liver Sinusoidal Endothelial Cells. *Hepatology* **2019**, *69* (2), 876–888. https://doi.org/10.1002/hep.30232.
(101) Zapotoczny, B.; Szafranska, K.; Owczarczyk, K. AFM Reveals Dynamic Morphology of Fenestrations in Living Liver Sinusoidal Endothelial Cells. *Sci. Rep.* **2017**, No. July, 1–6. https://doi.org/10.1038/s41598-017-08555-0.
(102) Wisse, E.; de Zanger, R. B.; Charels, K.; van der Smissen, P.; McCuskey, R. S. The Liver Sieve: Considerations Concerning the Structure and Function of Endothelial Fenestrae, the Sinusoidal Wall and the Space of Disse. *Hepatology* **1985**, *5* (4), 683–692. https://doi.org/10.1002/hep.1840050427.
(103) Fraser, R.; Dobbs, B. R.; Rogers, G. W. T. Lipoproteins and the Liver Sieve: The Role of the Fenestrated Sinusoidal Endothelium in Lipoprotein Metabolism, Atherosclerosis, and Cirrhosis. *Hepatology* **1995**, *21* (3), 863–874. https://doi.org/10.1016/0270-9139(95)90542-1.
(104) Naito, M.; Wisse, E. Filtration Effect of Endothelial Fenestrations on Chylomicron Transport in Neonatal Rat Liver Sinusoids. *Cell Tissue Res.* **1978**, *190* (3), 371–382. https://doi.org/10.1007/BF00219553.
(105) De Zanger, R.; Wisse, E. The Filtration Effect of Rat Liver Fenestrated Sinusoidal Endothelium on the Passage of (Remnant) Chylomicrons to The ... *Sinusoidal liver cells* **1982**, No. January.
(106) Yoon, Y. J.; Chang, S.; Kim, O. Y.; Kang, B. K.; Park, J.; Lim, J. H.; Yun Huang, J.; Kim, Y. K.; Byun, J. H.; Gho, Y. S. Three-Dimensional Imaging of Hepatic Sinusoids in Mice Using Synchrotron Radiation Micro-Computed Tomography. *PLoS One* **2013**, *8* (7), 1–10. https://doi.org/10.1371/journal.pone.0068600.
(107) Wisse, E.; De Zanger, R. B.; Jacobs, R.; McCuskey, R. S. Scanning Electron Microscope Observations on the Structure of Portal Veins, Sinusoids and Central Veins in Rat Liver. *Scan. Electron Microsc.* **1983**, No. pt 3, 1441–1452.
(108) Vidal-Vanaclocha, F.; Barberá-Guillem, E. Fenestration Patterns in Endothelial Cells of Rat Liver Sinusoids. *J. Ultrastruct. Res. Mol. Struct. Res.* **1985**, *90* (2), 115–123. https://doi.org/10.1016/0889-1605(85)90102-8.
(109) Le Couteur, D. G.; Warren, A.; Cogger, V. C.; Smedsrød, B.; Sørensen, K. K.; De Cabo, R.; Fraser, R.; McCuskey, R. S. Old Age and the Hepatic Sinusoid. *Anat. Rec.* **2008**, *291* (6), 672–683. https://doi.org/10.1002/ar.20661.
(110) Le Couteur, D. G.; Cogger, V. C.; Markus, A. M. A.; Harvey, P. J.; Yin, Z. L.; Ansselin, A. D.; McLean, A. J. Pseudocapillarization and Associated Energy Limitation in the Aged Rat Liver. *Hepatology* **2001**, *33* (3), 537–543. https://doi.org/10.1053/jhep.2001.22754.
(111) Warren, A.; Bertolino, P.; Cogger, V. C.; McLean, A. J.; Fraser, R.; Le Couteur, D. G. Hepatic Pseudocapillarization in Aged Mice. *Exp. Gerontol.* **2005**, *40* (10), 807–812. https://doi.org/10.1016/j.exger.2005.06.012.
(112) Ito, Y.; Sørensen, K. K.; Bethea, N. W.; Svistounov, D.; McCuskey, M. K.; Smedsrød, B. H.; McCuskey, R. S. Age-Related Changes in the Hepatic Microcirculation in Mice. *Exp. Gerontol.* **2007**, *42* (8), 789–797. https://doi.org/10.1016/j.exger.2007.04.008.
(113) Cogger, V. C.; Warren, A.; Fraser, R.; Ngu, M.; McLean, A. J.; Le Couteur, D. G. Hepatic Sinusoidal Pseudocapillarization with Aging in the Non-Human Primate. *Exp. Gerontol.* **2003**, *38* (10), 1101–1107. https://doi.org/10.1016/j.exger.2003.07.002.
(114) McLean, A. J.; Cogger, V. C.; Chong, G. C.; Warren, A.; Markus, A. M. A.; Dahlstrom, J. E.; Le Couteur, D. G. Age-Related Pseudocapillarization of the Human Liver. *J. Pathol.* **2003**, *200* (1), 112–117. https://doi.org/10.1002/path.1328.
(115) Mori, T.; Okanoue, T.; Sawa, Y.; Hori, N.; Ohta, M.; Kagawa, K. Defenestration of the Sinusoidal Endothelial-Cell in a Rat Model of Cirrhosis. *Hepatology* **1993**, *17* (5), 891–897.
(116) Martinez-Hernandez, A.; Martinez, J. The Role of Capillarization in Hepatic Failure: Studies in Carbon Tetrachloride-induced Cirrhosis. *Hepatology* **1991**, *14* (5), 864–874. https://doi.org/10.1002/hep.1840140519.
(117) Jézéquel, A. M.; Mancini, R.; Rinaldesi, M. L.; Macarri, G.; Venturini, C.; Orlandi, F. A Morphological Study of the

Early Stages of Hepatic Fibrosis Induced by Low Doses of Dimethylnitrosamine in the Rat. *J. Hepatol.* **1987**, *5* (2), 174–181. https://doi.org/10.1016/S0168-8278(87)80570-6.
(118) Haratake, J.; Hisaoka, M.; Yamamoto, O.; Horie, A. Morphological Changes of Hepatic Microcirculation in Experimental Rat Cirrhosis: A Scanning Electron Microscopic Study. *Hepatology* **1991**, *13* (5), 952–956. https://doi.org/10.1002/hep.1840130525.
(119) Bhunchet, E.; Fujieda, K. Capillarization and Venularization of Hepatic Sinusoids in Porcine Serum-induced Rat Liver Fibrosis: A Mechanism to Maintain Liver Blood Flow. *Hepatology* **1993**, *18* (6), 1450–1458. https://doi.org/10.1002/hep.1840180626.
(120) Steffan, A. M.; Pereira, C. A.; Bingen, A.; Valle, M.; Martin, J. P.; Koehren, F.; Royer, C.; Gendrault, J. L.; Kirn, A. Mouse Hepatitis Virus Type 3 Infection Provokes a Decrease in the Number of Sinusoidal Endothelial Cell Fenestrae Both in Vivo and in Vitro. *Hepatology* **1995**, *22* (2), 395–401. https://doi.org/10.1016/0270-9139(95)90556-1.
(121) Horn, T.; Christoffersen, P.; Henriksen, J. H. Alcoholic Liver Injury: Defenestration in Noncirrhotic Livers-a Scanning Electron Microscopic Study. *Hepatology* **1987**, *7* (1), 77–82.
(122) Clark, S. A.; Bramwell Cook, H.; Oxner, R. B. G.; Angus, H. B.; George, P. M.; Fraser, R. Defenestration of Hepatic Sinusoids As a Cause of Hyperlipoproteinaemia in Alcoholics. *Lancet* **1988**, *332* (8622), 1225–1227. https://doi.org/10.1016/S0140-6736(88)90813-6.
(123) Sarphie, T. G.; D'Souza, N. B.; Deaciuc, I. V. Kupffer Cell Inactivation Prevents Lipopolysaccharide-Induced Structural Changes in the Rat Liver Sinusoid: An Electron-Microscopic Study. *Hepatology* **1996**, *23* (4), 788–796. https://doi.org/10.1053/jhep.1996.v23.pm0008666333.
(124) Zhang, L.; Rowe, A.; Braet, F.; Ramzan, I. Macrophage Depletion Ameliorates Kavalactone Damage in the Isolated Perfused Rat Liver. *J. Toxicol. Sci.* **2012**, *37* (2), 447–453. https://doi.org/10.2131/jts.37.447.
(125) Fraser, R.; Heslop, V. R.; Murray, F. E. M.; Day, W. A. Ultrastructural Studies of the Portal Transport of Fat in Chickens. *Br. J. Exp. Pathol.* **1986**, *67* (6), 783–791.
(126) Wright, P. L.; Smith, K. F.; Day, W. A.; Fraser, R. Small Liver Fenestrae May Explain the Susceptibility of Rabbits to Atherosclerosis. **1983**.
(127) Fraser, R.; Clark, S. A.; Day, W. A.; Murray, F. E. Nicotine Decreases the Porosity of the Rat Liver Sieve: A Possible Mechanism for Hypercholesterolaemia. *Br. J. Exp. Pathol.* **1988**, *69* (3), 345–350.
(128) Le Couteur, D. G.; Cogger, V. C.; McCuskey, R. S.; De Cabo, R.; Smedsrød, B.; Sorensen, K. K.; Warren, A.; Fraser, R. Age-Related Changes in the Liver Sinusoidal Endothelium: A Mechanism for Dyslipidemia. *Ann. N. Y. Acad. Sci.* **2007**, *1114*, 79–87. https://doi.org/10.1196/annals.1396.003.
(129) Rogers, G. W. T.; Dobbs, B. R.; Fraser, R. Decreased Hepatic Uptake of Cholesterol and Retinol in the Dimethylnitrosamine Rat Model of Cirrhosis. *Liver* **1992**, *12* (5), 326–329. https://doi.org/10.1111/j.1600-0676.1992.tb00581.x.
(130) Seifert, W. F.; Bosma, A.; Brouwer, A.; Hendriks, H. F. J.; Roholl, P. J. M.; van Leeuwen, R. E. W.; van Thiel-De Ruiter, G. C. F.; Seifert-Bock, I.; Knook, D. L. Vitamin A Deficiency Potentiates Carbon Tetrachloride-Induced Liver Fibrosis in Rats. *Hepatology* **1994**, *19* (1), 193–201. https://doi.org/10.1002/hep.1840190129.
(131) Shiratori, Y.; Ichida, T.; Geerts, A.; Wisse, E. Modulation of Collagen Synthesis by Fat-Storing Cells, Isolated from CCl4-or Vitamin A-Treated Rats. *Dig. Dis. Sci.* **1987**, *32* (11), 1281–1289. https://doi.org/10.1007/BF01296379.
(132) Le Couteur, D. G.; Rivory, L. P.; Yi, C.; Pond, S. M. Aging, Acute Oxidative Injury and Hepatocellular Glucose Transport in the Rat. *Int. Hepatol. Commun.* **1995**, *3* (5), 244–253. https://doi.org/10.1016/0928-4346(94)00186-9.
(133) Mohamad, M.; Mitchell, S. J.; Wu, L. E.; White, M. Y.; Cordwell, S. J.; Mach, J.; Solon-Biet, S. M.; Boyer, D.; Nines, D.; Das, A.; Catherine Li, S. Y.; Warren, A.; Hilmer, S. N.; Fraser, R.; Sinclair, D. A.; Simpson, S. J.; de Cabo, R.; Le Couteur, D. G.; Cogger, V. C. Ultrastructure of the Liver Microcirculation Influences Hepatic and Systemic Insulin Activity and Provides a Mechanism for Age-Related Insulin Resistance. *Aging Cell* **2016**, *15* (4), 706–715. https://doi.org/10.1111/acel.12481.
(134) Mitchell, S. J.; Huizer-Pajkos, A.; Cogger, V. C.; McLachlan, A. J.; Le Couteur, D. G.; Jones, B.; De Cabo, R.; Hilmer, S. N. The Influence of Old Age and Poloxamer-407 on the Hepatic Disposition of Diazepam in the Isolated Perfused Rat Liver. *Pharmacology* **2012**, *90* (5–6), 233–241. https://doi.org/10.1159/000341724.
(135) Mitchell, S. J.; Huizer-Pajkos, A.; Cogger, V. C.; McLachlan, A. J.; Le Couteur, D. G.; Hilmer, S. N. Poloxamer 407 Increases the Recovery of Paracetamol in the Isolated Perfused Rat Liver. *J. Pharm. Sci.* **2011**, *100* (1), 334–340. https://doi.org/10.1002/jps.22235.
(136) McLean, A. J.; Le Couteur, D. G. Aging Biology and Geriatric Clinical Pharmacology. *Pharmacol. Rev.* **2004**, *56* (2), 163–184. https://doi.org/10.1124/pr.56.2.4.
(137) Komatsu, H.; Koo, A.; Guth, P. H. Leukocyte Flow Dynamics in the Rat Liver Microcirculation. *Microvasc. Res.* **1990**, *40* (1), 1–13. https://doi.org/10.1016/0026-2862(90)90002-9.
(138) Bonfiglio, A.; Leungchavaphongse, K.; Repetto, R.; Siggers, J. H. Mathematical Modeling of the Circulation in the Liver Lobule. *J. Biomech. Eng.* **2010**, *132* (11). https://doi.org/10.1115/1.4002563.
(139) Siggers, J. H.; Leungchavaphongse, K.; Ho, C. H.; Repetto, R. Mathematical Model of Blood and Interstitial Flow and Lymph Production in the Liver. *Biomech. Model. Mechanobiol.* **2014**, *13* (2), 363–378. https://doi.org/10.1007/s10237-013-0516-x.
(140) Barléon, N.; Clarke, R. J.; Ho, H. Novel Methods for Segment-Specific Blood Flow Simulation for the Liver. *Comput. Methods Biomech. Biomed. Engin.* **2018**, *21* (15), 780–783. https://doi.org/10.1080/10255842.2018.1520224.
(141) Rezania, V.; Coombe, D.; Tuszynski, J. A. A Physiologically-Based Flow Network Model for Hepatic Drug Elimination III: 2D/3D DLA Lobule Models. *Theor. Biol. Med. Model.* **2016**, *13* (1), 1–22. https://doi.org/10.1186/s12976-016-0034-5.

(142) Debbaut, C.; Monbaliu, D.; Casteleyn, C.; Cornillie, P.; Van Loo, D.; Van Hoorebeke, L.; Simoens, P.; Pirenne, J.; Segers, P. Multiscale Modeling of the Blood Circulation in the Human Liver Using Vascular Corrosion Casting and Micro-CT Imaging Techniques. In *ASME 2011 Summer Bioengineering Conference, Parts A and B*; American Society of Mechanical Engineers, 2011; pp 451–452. https://doi.org/10.1115/SBC2011-53389.
(143) Piergiovanni, M.; Bianchi, E.; Capitani, G.; Li Piani, I.; Ganzer, L.; Guidotti, L. G.; Iannacone, M.; Dubini, G. Microcirculation in the Murine Liver: A Computational Fluid Dynamic Model Based on 3D Reconstruction from in Vivo Microscopy. *J. Biomech.* **2017**, *63*, 125–134. https://doi.org/10.1016/j.jbiomech.2017.08.011.
(144) Hu, J.; Lü, S.; Feng, S.; Long, M. Flow Dynamics Analyses of Pathophysiological Liver Lobules Using Porous Media Theory. *Acta Mech. Sin. Xuebao* **2017**, *33* (4), 823–832. https://doi.org/10.1007/s10409-017-0674-7.
(145) Rani, H. P.; Sheu, T. W. H.; Chang, T. M.; Liang, P. C. Numerical Investigation of Non-Newtonian Microcirculatory Blood Flow in Hepatic Lobule. *J. Biomech.* **2006**, *39* (3), 551–563. https://doi.org/10.1016/j.jbiomech.2004.11.029.
(146) Rohan, E.; Turjanicová, J.; Lukeš, V. Multiscale Modelling of Liver Perfusion. *15th Int. Conf. Comput. Plast. Fundam. Appl. COMPLAS 2019* **2019**, 343–353.
(147) Ahmadi-Badejani, R.; Mosharaf-Dehkordi, M.; Ahmadikia, H. An Image-Based Geometric Model for Numerical Simulation of Blood Perfusion within the Liver Lobules. *Comput. Methods Biomech. Biomed. Engin.* **2020**, *23* (13), 987–1004. https://doi.org/10.1080/10255842.2020.1782389.
(148) Mosharaf-Dehkordi, M. A Fully Coupled Porous Media and Channels Flow Approach for Simulation of Blood and Bile Flow through the Liver Lobules. *Comput. Methods Biomech. Biomed. Engin.* **2019**, *22* (9), 901–915. https://doi.org/10.1080/10255842.2019.1601180.
(149) Schwen, L. O.; Schenk, A.; Kreutz, C.; Timmer, J.; Rodríguez, M. M. B.; Kuepfer, L.; Preusser, T. Representative Sinusoids for Hepatic Four-Scale Pharmacokinetics Simulations. *PLoS One* **2015**, *10* (7), 1–39. https://doi.org/10.1371/journal.pone.0133653.
(150) Brouwer, A.; Knook, D. L. THE RETICULOENDOTHELIAL SYSTEM AND AGEING: A REVIEW. *Mech. Ageing Dev.* **1983**, *21*, 205–228.
(151) Sørensen, K. K.; McCourt, P.; Berg, T.; Crossley, C.; Le Couteur, D.; Wake, K.; Smedsrød, B. The Scavenger Endothelial Cell: A New Player in Homeostasis and Immunity. *Am. J. Physiol. - Regul. Integr. Comp. Physiol.* **2012**, *303* (12). https://doi.org/10.1152/ajpregu.00686.2011.
(152) Sørensen, K. K.; Simon-Santamaria, J.; McCuskey, R. S.; Smedsrød, B. Liver Sinusoidal Endothelial Cells. *Compr. Physiol.* **2015**, *5* (4), 1751–1774. https://doi.org/10.1002/cphy.c140078.
(153) Sorensen, K. K.; Tollersrud, O. K.; Evjen, G.; Smedsrod, B. Mannose-Receptor-Mediated Clearance of Lysosomal α-Mannosidase in Scavenger Endothelium of Cod Endocardium. *Comp. Biochem. Physiol. - A Mol. Integr. Physiol.* **2001**, *129* (2–3), 615–630. https://doi.org/10.1016/S1095-6433(01)00300-2.
(154) Seternes, T.; Sørensen, K.; Smedsrød, B. Scavenger Endothelial Cells of Vertebrates: A Nonperipheral Leukocyte System for High-Capacity Elimination of Waste Macromolecules. *Proc. Natl. Acad. Sci. U. S. A.* **2002**, *99* (11), 7594–7597. https://doi.org/10.1073/pnas.102173299.
(155) Cabral, F.; Al-Rahem, M.; Skaggs, J.; Thomas, T. A.; Kumar, N.; Wu, Q.; Fadda, P.; Yu, L.; Robinson, J. M.; Kim, J.; Pandey, E.; Sun, X.; Jarjour, W. N.; Rajaram, M. V. S.; Harris, E. N.; Ganesan, L. P. Stabilin Receptors Clear LPS and Control Systemic Inflammation. *iScience* **2021**, *24* (11), 103337. https://doi.org/10.1016/j.isci.2021.103337.
(156) Kiyono, K. *Die Vitale Karminspeicherung : Ein Beitrag Zur Lehre von Der Vitalen Färbung Mit Besonderer Berücksichtigung Der Zelldifferenzierungen Im Entzündeten Gewebe*; Gustav Fischer, Jena, 1914.
(157) Aschoff, L. Vorträge Uber Pathologie: Das Retikulo-Endotheliale System. Verlag von Gustav Fischer 1925.
(158) Lison, L.; Smulders, J. Discriminating ' Athrocytes ' in the Reticulo- Endothelial System. *Nature* **1948**, *162* (4106), 65–66.
(159) van Furth, R.; Cohn, Z. A.; Hirsch, J. G.; Humphrey, J. H.; Spector, W. G.; Langevoort, H. L. The Mononuclear Phagocyte System: A New Classification of Macrophages, Monocytes, and Their Precursor Cells. *Bull. World Health Organ.* **1972**, *46* (6), 845–852.
(160) Kawai, Y.; Smedsrød, B.; Elvevold, K.; Wake, K. Uptake of Lithium Carmine by Sinusoidal Endothelial and Kupffer Cells of the Rat Liver: New Insights into the Classical Vital Staining and the Reticulo-Endothelial System. *Cell Tissue Res.* **1998**, *292* (2), 395–410. https://doi.org/10.1007/s004410051069.
(161) Terao, K. LIVER INJURIES INDUCED BY FREE RADICALS. *J. Toxicol. Pathol.* **1989**, *2* (1), 11–18. https://doi.org/10.1293/tox.2.11.
(162) Williams, B.; Pussel, B.; Lockwood, C.; Cotton, C. DEFECTIVE RETICULOENDOTHELIAL SYSTEM FUNCTION IN RHEUMATOID ARTHRITIS. *Lancet* **1979**, 1311–1314.
(163) Park, S. Y.; Jung, M. Y.; Kim, H. J.; Lee, S. J.; Kim, S. Y.; Lee, B. H.; Kwon, T. H.; Park, R. W.; Kim, I. S. Rapid Cell Corpse Clearance by Stabilin-2, a Membrane Phosphatidylserine Receptor. *Cell Death Differ.* **2008**, *15* (1), 192–201. https://doi.org/10.1038/sj.cdd.4402242.
(164) Park, S. Y.; Jung, M. Y.; Lee, S. J.; Kang, K. B.; Gratchev, A.; Riabov, V.; Kzhyshkowska, J.; Kim, I. S. Stabilin-1 Mediates Phosphatidylserine-Dependent Clearance of Cell Cropses in Alternatively Activated Macrophages. *J. Cell Sci.* **2009**, *122* (18), 3365–3373. https://doi.org/10.1242/jcs.049569.
(165) Hansen, B.; Svistounov, D.; Olsen, R.; Nagai, R.; Horiuchi, S.; Smedsrød, B. Advanced Glycation End Products Impair the Scavenger Function of Rat Hepatic Sinusoidal Endothelial Cells. *Diabetologia* **2002**, *45* (10), 1379–1388. https://doi.org/10.1007/s00125-002-0912-8.
(166) Holte, C.; Szafranska, K.; Kruse, L.; Santamaria, J. S.; Li, R.; Svistounov, D.; Mccourt, P. Highly Oxidized Albumin Is Cleared by Liver Sinusoidal Endothelial Cells via the Receptors Stabilin - 1 and - 2. *Sci. Rep.* **2023**, No. 1, 1–11. https://doi.org/10.1038/s41598-023-46462-9.

(167) Schildt, B. E.; Eriksson, K. H. Function of the Reticuloendothelial System in Whole-Body Irradiated Mice. *Acta Oncol. (Madr).* **1972**, *11* (1), 48–58. https://doi.org/10.3109/02841867209129777.
(168) BENACERRAF, B.; BIOZZI, G.; HALPERN, B. N.; STIFFEL, C.; MOUTON, D. Phagocytosis of Heat-Denatured Human Serum Albumin Labelled with 131I and Its Use as a Means of Investigating Liver Blood Flow. *Br. J. Exp. Pathol.* **1957**, *38* (1), 35–48.
(169) Brouwer, A.; Horan, M. A.; Barelds, R. J.; Knook, D. L. Cellular Aging of the Reticuloendothelial System. *Arch. Gerontol. Geriatr.* **1986**, *5* (4), 317–324. https://doi.org/10.1016/0167-4943(86)90034-8.
(170) Praaning-van Dalen, D. P.; Knook, D. L. Quantitative Determination of in Vivo Endocytosis by Rat Liver Kupffer and Endothelial Cells Facilitated by an Improved Cell Isolation Method (1982) FEBS Letters 141, 229-232. *FEBS Lett.* **1982**, *148* (1), 167–169. https://doi.org/10.1016/0014-5793(82)81281-7.
(171) Li, R.; McCourt, P.; Schledzewski, K.; Goerdt, S.; Moldenhauer, G.; Liu, X.; Smedsrød, B.; Sørensen, K. K. Endocytosis of Advanced Glycation End-Products in Bovine Choriocapillaris Endothelial Cells. *Microcirculation* **2009**, *16* (7), 640–655. https://doi.org/10.1080/10739680903133185.
(172) Fraser, J. R. E.; Laurent, T. C.; Laurent, U. B. G. Hyaluronan: Its Nature, Distribution, Functions and Turnover. *J. Intern. Med.* **1997**, *242* (1), 27–33. https://doi.org/10.1046/j.1365-2796.1997.00170.x.
(173) Fraser, J. R. E.; Appelgren, L. E.; Laurent, T. C. Tissue Uptake of Circulating Hyaluronic Acid - A Whole Body Autoradiographic Study. *Cell Tissue Res.* **1983**, *233* (2), 285–293. https://doi.org/10.1007/BF00238296.
(174) Laurent, T. C.; Laurent, U. B. G.; Fraser, J. R. E. Serum Hyaluronan as a Disease Marker. *Ann. Med.* **1996**, *28* (3), 241–253. https://doi.org/10.3109/07853899609033126.
(175) Mayor, S.; Pagano, R. E. Pathways of Clathrin-Independent Endocytosis. *Nat. Rev. Mol. Cell Biol.* **2007**, *8* (8), 603–612. https://doi.org/10.1038/nrm2216.
(176) Metschnikoff, E. The Ancestral History of the Inflammatory Process. *J. Cell Sci.* **1884**, *S2-24* (93), 112–117. https://doi.org/10.1242/jcs.s2-24.93.112.
(177) Metschnikoff, E. Lecture on Phagocytosis and Immunity. *Br. Med. J.* **1891**, *1* (1570), 213–217. https://doi.org/10.1136/bmj.1.1570.213.
(178) Botelho, R. J.; Grinstein, S. Phagocytosis. *Curr. Biol.* **2011**, *21* (14), 533–538. https://doi.org/10.1016/j.cub.2011.05.053.
(179) Doherty, G. J.; McMahon, H. T. Mechanisms of Endocytosis. *Annu. Rev. Biochem.* **2009**, *78*, 857–902. https://doi.org/10.1146/annurev.biochem.78.081307.110540.
(180) LEWIS, W. H. PINOCYTOSIS BY MALIGNANT CELLS. *Am. J. CANCER* **1937**, *29* (4), 666–679. https://doi.org/https://doi.org/10.1158/ajc.1937.666.
(181) Lewis, W. H. Locomotion of Lymphocytes. *Bull. Johns Hopkins Hosp.* **1931**, *49*.
(182) Silverstein, S. C.; Cohn, Z. A.; Steinman, R. M. ENDOCYTOSIS. *Annu. Rev. Biochem.* **1977**, *46*, 669–722.
(183) ROTH, T. F.; PORTER, K. R. Yolk Protein Uptake in the Oocyte of the Mosquito Aedes Aegypti. L. *J. Cell Biol.* **1964**, *20*, 313–332. https://doi.org/10.1083/jcb.20.2.313.
(184) Fawcett, D. W. HISTOCHEMICAL SOCIETY SYMPOSIUM ON STRUCTURE AND FUNCTION AT CELL SURFACES, CHICAGO ILLINOIS, APRIL 12 1964 SURFACE SPECIALIZATION OF ABSORBING CELLS. *J. Histochem. Cytochem.* **1965**, *13* (2).
(185) Friend, D. S.; Farquhar, M. G. Functions of Coated Vesicles during Protein Absorption in the Rat Vas Deferens. *J. Cell Biol.* **1967**, *35* (2), 357–376. https://doi.org/10.1083/jcb.35.2.357.
(186) Goldstein, J. L.; Anderson, R. G. W.; Brown, M. S. Coated Pits, Coated Vesicles, and Receptor-Mediated Endocytosis. *Nature* **1979**, *279*, 679–685.
(187) Rosenbluth, J.; Wissig, S. L. THE DISTRIBUTION OF EXOGENOUS FERRITIN IN TOAD SPINAL GANGLIA AND THE MECHANISM OF ITS UPTAKE BY NEURONS. *J. Cell Biol.* **1964**, *23*.
(188) Kanaseki, T.; Kadota, K. The "Vesicle in a Basket". A Morphological Study of the Coated Vesicle Isolated from the Nerve Endings of the Guinea Pig Brain, with Special Reference to the Mechanism of Membrane Movements. *J. Cell Biol.* **1969**, *42* (1), 202–220. https://doi.org/10.1083/jcb.42.1.202.
(189) Pearse, B. M. F. Clathrin: A Unique Protein Associated with Intracellular Transfer of Membrane by Coated Vesicles. *Proc. Natl. Acad. Sci. U. S. A.* **1976**, *73* (4), 1255–1259. https://doi.org/10.1073/pnas.73.4.1255.
(190) Montesano, R.; Roth, J.; Robert, A.; Orci, L. Non-Coated Membrane Invaginations Are Involved in Binding and Internalization of Cholera and Tetanus Toxins. *Nature* **1982**, *296* (5858), 651–653. https://doi.org/10.1038/296651a0.
(191) Palade, G. E. Fine Structure of Blood Capillaries. *J. Apllied Phys.* **1953**, *24*, 1424.
(192) Yamada, E. Some Aspects of the Fine Structure of the Gall Bladder Epithelium of the Mouse. *J. Biophys. Biochem. Cytol.* **1955**, *1* (5). https://doi.org/10.2535/ofaj1936.45.1_11.
(193) Hummeler, K.; Tomassini, N.; Sokol, F. Morphological Aspects of the Uptake of Simian Virus 40 by Permissive Cells. *J. Virol.* **1970**, *6* (1), 87–93. https://doi.org/10.1128/jvi.6.1.87-93.1970.
(194) Sverdlov, M.; Shajahan, A. N.; Minshall, R. D. Tyrosine Phosphorylation-Dependence of Caveolae-Mediated Endocytosis: Caveolae Review Series. *J. Cell. Mol. Med.* **2007**, *11* (6), 1239–1250. https://doi.org/10.1111/j.1582-4934.2007.00127.x.
(195) Denzer, L.; Muranyi, W.; Schroten, H.; Schwerk, C. The Role of PLVAP in Endothelial Cells. *Cell Tissue Res.* **2023**, *392* (2), 393–412. https://doi.org/10.1007/s00441-023-03741-1.
(196) Hopkins, C. R.; Miller, K.; Beardmore, J. M. Receptor-Mediated Endocytosis of Transferrin and Epidermal Growth Factor Receptors: A Comparison of Constitutive and Ligand-Induced Uptake. *J. Cell Sci.* **1985**, *SUPPL. 3*, 173–186. https://doi.org/10.1242/jcs.1985.supplement_3.17.
(197) Tiruppathi, C.; Song, W.; Bergenfeldt, M.; Sass, P.; Malik, A. B. Gp60 Activation Mediates Albumin Transcytosis in Endothelial Cells by Tyrosine Kinase-Dependent Pathway. *J. Biol. Chem.* **1997**, *272* (41), 25968–25975.

https://doi.org/10.1074/jbc.272.41.25968.
(198) Sever, S.; Damke, H.; Schmid, S. L. Dynamin: GTP Controls the Formation of Constricted Coated Pits, the Rate Limiting Step in Clathrin-Mediated Endocytosis. *J. Cell Biol.* **2000**, *150* (5), 1137–1147. https://doi.org/10.1083/jcb.150.5.1137.
(199) Oh, P.; McIntosh, D. P.; Schnitzer, J. E. Dynamin at the Neck of Caveolae Mediates Their Budding to Form Transport Vesicles by GTP-Driven Fission from the Plasma Membrane of Endothelium. *J. Cell Biol.* **1998**, *141* (1), 101–114. https://doi.org/10.1083/jcb.141.1.101.
(200) Henley, J. R.; Krueger, E. W. A.; Oswald, B. J.; McNiven, M. A. Dynamin-Mediated Internalization of Caveolae. *J. Cell Biol.* **1998**, *141* (1), 85–99. https://doi.org/10.1083/jcb.141.1.85.
(201) Bhandari, S.; Larsen, A. K.; McCourt, P.; Smedsrød, B.; Sørensen, K. K. The Scavenger Function of Liver Sinusoidal Endothelial Cells in Health and Disease. *Front. Physiol.* **2021**, *12* (October), 1–23. https://doi.org/10.3389/fphys.2021.757469.
(202) Pandey, E.; Nour, A. S.; Harris, E. N. Prominent Receptors of Liver Sinusoidal Endothelial Cells in Liver Homeostasis and Disease. *Front. Physiol.* **2020**, *11* (July), 1–21. https://doi.org/10.3389/fphys.2020.00873.
(203) Wisse, E. An Ultrastructural Characterization of the Endothelial Cell in the Rat Liver Sinusoid under Normal and Various Experimental Conditions, as a Contribution to the Distinction between Endothelial and Kupffer Cells. *J. Ultrasructure Res.* **1972**, *38* (5–6), 528–562. https://doi.org/10.1016/0022-5320(72)90089-5.
(204) Kjeken, R.; Mousavi, S. A.; Brech, A.; Gjøen, T.; Berg, T. Fluid Phase Endocytosis of [125I]Iodixanol in Rat Liver Parenchymal, Endothelial and Kupffer Cells. *Cell Tissue Res.* **2001**, *304* (2), 221–230. https://doi.org/10.1007/s004410100348.
(205) Falkowska-Hansen, B.; Falkowski, M.; Metharom, P.; Krunic, D.; Goerdt, S. Clathrin-Coated Vesicles Form a Unique Net-like Structure in Liver Sinusoidal Endothelial Cells by Assembling along Undisrupted Microtubules. *Exp. Cell Res.* **2007**, *313* (9), 1745–1757. https://doi.org/10.1016/j.yexcr.2007.02.026.
(206) Juvet, L. K.; Berg, T.; Gjøen, T. The Expression of Endosomal Rab Proteins Correlates with Endocytic Rate in Rat Liver Cells. *Hepatology* **1997**, *25* (5), 1204–1212. https://doi.org/10.1002/hep.510250524.
(207) Bhandari, S.; Li, R.; Simón-Santamaría, J.; McCourt, P.; Johansen, S. D.; Smedsrød, B.; Martinez-Zubiaurre, I.; Sørensen, K. K. Transcriptome and Proteome Profiling Reveal Complementary Scavenger and Immune Features of Rat Liver Sinusoidal Endothelial Cells and Liver Macrophages. *BMC Mol. Cell Biol.* **2020**, *21* (1), 1–26. https://doi.org/10.1186/s12860-020-00331-9.
(208) Nagelkerke, J. F.; Barto, K. P.; van Berkel, T. J. In Vivo and in Vitro Uptake and Degradation of Acetylated Low Density Lipoprotein by Rat Liver Endothelial, Kupffer, and Parenchymal Cells. *J. Biol. Chem.* **1983**, *258* (20), 12221–12227. https://doi.org/10.1016/S0021-9258(17)44160-3.
(209) Nagelkerke, J. F.; Havekes, L.; Van Hinsbergh, V. W. M.; Van Berkel, T. J. C. In Vivo Catabolism of Biologically Modified LDL. *Arteriosclerosis* **1984**, *4* (3), 256–264. https://doi.org/10.1161/01.atv.4.3.256.
(210) Blomhoff, R.; Eskild, W.; Berg, T. Endocytosis of Formaldehyde-Treated Serum Albumin via Scavenger Pathway in Liver Endothelial Cells. *Biochem. J.* **1984**, *218* (1), 81–86. https://doi.org/10.1042/bj2180081.
(211) Van Berkel, T. J.; De Rijke, Y. B.; Kruijt, J. K. Different Fate in Vivo of Oxidatively Modified Low Density Lipoprotein and Acetylated Low Density Lipoprotein in Rats. Recognition by Various Scavenger Receptors on Kupffer and Endothelial Liver Cells. *J. Biol. Chem.* **1991**, *266* (4), 2282–2289. https://doi.org/10.1016/S0021-9258(18)52241-9.
(212) Smedsrød, B.; Melkko, J.; Araki, N.; Sano, H.; Horiuchi, S. Advanced Glycation End Products Are Eliminated by Scavenger-Receptor-Mediated Endocytosis in Hepatic Sinusoidal Kupffer and Endothelial Cells. *Biochem. J.* **1997**, *322* (2), 567–573. https://doi.org/10.1042/bj3220567.
(213) Hansen, B.; Arteta, B.; Smedsrød, B. The Physiological Scavenger Receptor Function of Hepatic Sinusoidal Endothelial and Kupffer Cells Is Independent of Scavenger Receptor Class A Type I and II. *Mol. Cell. Biochem.* **2002**, *240* (1–2), 1–8. https://doi.org/10.1023/A:1020660303855.
(214) Adachi, H.; Tsujimoto, M. FEEL-1, a Novel Scavenger Receptor with in Vitro Bacteria-Binding and Angiogenesis-Modulating Activities. *J. Biol. Chem.* **2002**, *277* (37), 34264–34270. https://doi.org/10.1074/jbc.M204277200.
(215) Tamura, Y.; Adachi, H.; Osuga, J. I.; Ohashi, K.; Yahagi, N.; Sekiya, M.; Okazaki, H.; Tomita, S.; Iizuka, Y.; Shimano, H.; Nagai, R.; Kimura, S.; Tsujimoto, M.; Ishibashi, S. FEEL-1 and FEEL-2 Are Endocytic Receptors for Advanced Glycation End Products. *J. Biol. Chem.* **2003**, *278* (15), 12613–12617. https://doi.org/10.1074/jbc.M210211200.
(216) Malovic, I.; Johansson, S.; Melkko, J.; Mayer, U.; Smedsrød, B.; McCourt, P. A. Nidogen Is a Physiological Ligand for Stabilin Receptors in Liver Sinusoidal Endothelial Cells. In *15th International Symposium on Cells of the Hepatic Sinusoid*; 2010.
(217) Kzhyshkowska, J.; Workman, G.; Cardó-Vila, M.; Arap, W.; Pasqualini, R.; Gratchev, A.; Krusell, L.; Goerdt, S.; Sage, E. H. Novel Function of Alternatively Activated Macrophages: Stabilin-1-Mediated Clearance of SPARC. *J. Immunol.* **2006**, *176* (10), 5825–5832. https://doi.org/10.4049/jimmunol.176.10.5825.
(218) Kzhyshkowska, J. Stabilin-1, a Homeostatic Scavenger Receptor with Multiple Functions. *J. Cell. Mol. Med.* **2006**, *10* (3). https://doi.org/10.2755/jcmm010.003.08.
(219) Kzhyshkowska, J.; Gratchev, A.; Schmuttermaier, C.; Brundiers, H.; Krusell, L.; Mamidi, S.; Zhang, J.; Workman, G.; Sage, E. H.; Anderle, C.; Sedlmayr, P.; Goerdt, S. Alternatively Activated Macrophages Regulate Extracellular Levels of the Hormone Placental Lactogen via Receptor-Mediated Uptake and Transcytosis. *J. Immunol.* **2008**, *180* (5), 3028–3037. https://doi.org/10.4049/jimmunol.180.5.3028.
(220) Li, R.; Oteiza, A.; Sørensen, K. K.; McCourt, P.; Olsen, R.; Smedsrød, B.; Svistounov, D. Role of Liver Sinusoidal Endothelial Cells and Stabilins in Elimination of Oxidized Low-Density Lipoproteins. *Am. J. Physiol. - Gastrointest. Liver Physiol.* **2011**, *300* (1), 71–81. https://doi.org/10.1152/ajpgi.00215.2010.

(221) Lee, S. J.; Park, S. Y.; Jung, M. Y.; Bae, S. M.; Kim, I. S. Mechanism for Phosphatidylserine-Dependent Erythrophagocytosis in Mouse Liver. *Blood* **2011**, *117* (19), 5215–5223. https://doi.org/10.1182/blood-2010-10-313239.
(222) Schledzewski, K.; Géraud, C.; Arnold, B.; Wang, S.; Gröne, H. J.; Kempf, T.; Wollert, K. C.; Straub, B. K.; Schirmacher, P.; Demory, A.; Schönhaber, H.; Gratchev, A.; Dietz, L.; Thierse, H. J.; Kzhyshkowska, J.; Goerdt, S. Deficiency of Liver Sinusoidal Scavenger Receptors Stabilin-1 and -2 in Mice Causes Glomerulofibrotic Nephropathy via Impaired Hepatic Clearance of Noxious Blood Factors. *J. Clin. Invest.* **2011**, *121* (2), 703–714. https://doi.org/10.1172/JCI44740.
(223) Pempe, E. H.; Xu, Y.; Gopalakrishnan, S.; Liu, J.; Harris, E. N. Probing Structural Selectivity of Synthetic Heparin Binding to Stabilin Protein Receptors. *J. Biol. Chem.* **2012**, *287* (25), 20774–20783. https://doi.org/10.1074/jbc.M111.320069.
(224) Miller, C. M.; Donner, A. J.; Blank, E. E.; Egger, A. W.; Kellar, B. M.; Østergaard, M. E.; Seth, P. P.; Harris, E. N. Stabilin-1 and Stabilin-2 Are Specific Receptors for the Cellular Internalization of Phosphorothioate-Modified Antisense Oligonucleotides (ASOs) in the Liver. *Nucleic Acids Res.* **2016**, *44* (6), 2782–2794. https://doi.org/10.1093/nar/gkw112.
(225) Smedsrød, B.; Pertoft, H.; Eriksson, S.; Fraser, J. R.; Laurent, T. C. Studies in Vitro on the Uptake and Degradation of Sodium Hyaluronate in Rat Liver Endothelial Cells. *Biochem. J.* **1984**, *223* (3), 617–626. https://doi.org/10.1042/bj2230617.
(226) Melkko, J.; Hellevik, T.; Risteli, L.; Risteli, J.; Smedsrød, B. Clearance of NH2-Terminal Propeptides of Types I and III Procollagen Is a Physiological Function of the Scavenger Receptor in Liver Endothelial Cells. *J. Exp. Med.* **1994**, *179* (2), 405–412. https://doi.org/10.1084/jem.179.2.405.
(227) McCourt, P.; Smedsrød, B.; Melkko, J.; Johansson, S. Characterization of a Hyaluronan Receptor on Rat Sinusoidal Liver Endothelial Cells and Its Functional Relationship to Scavenger Receptors. *Hepatology* **1999**, *30* (5).
(228) Oynebraten, I.; Hansen, B.; Smedsrod, B.; Uhlin-Hansen, L. Serglycin Secreted by Leukocytes Is Efficiently Eliminated from the Circulation by Sinusoidal Scavenger Endothelial Cells in the Liver. *J. Leukoc. Biol.* **2000**, *67* (2), 183–188. https://doi.org/10.1002/jlb.67.2.183.
(229) Harris, E. N.; Weigel, J. A.; Weigel, P. H. Endocytic Function, Glycosaminoglycan Specificity, and Antibody Sensitivity of the Recombinant Human 190-KDa Hyaluronan Receptor for Endocytosis (HARE). *J. Biol. Chem.* **2004**, *279* (35), 36201–36209. https://doi.org/10.1074/jbc.M405322200.
(230) Harris, E. N.; Weigel, P. H. The Ligand-Binding Profile of HARE: Hyaluronan and Chondroitin Sulfates A, C, and D Bind to Overlapping Sites Distinct from the Sites for Heparin, Acetylated Low-Density Lipoprotein, Dermatan Sulfate, and CS-E. *Glycobiology* **2008**, *18* (8), 638–648. https://doi.org/10.1093/glycob/cwn045.
(231) Martinez, I.; Nedredal, G. I.; Øie, C. I.; Warren, A.; Johansen, O.; Le Couteur, D. G.; Smedsrød, B. The Influence of Oxygen Tension on the Structure and Function of Isolated Liver Sinusoidal Endothelial Cells. *Comp. Hepatol.* **2008**, *7*, 1–11. https://doi.org/10.1186/1476-5926-7-4.
(232) Swystun, L. L.; Lai, J. D.; Notley, C.; Georgescu, I.; Paine, A. S.; Mewburn, J.; Nesbitt, K.; Schledzewski, K.; Géraud, C.; Kzhyshkowska, J.; Goerdt, S.; Hopman, W.; Montgomery, R. R.; James, P. D.; Lillicrap, D. The Endothelial Cell Receptor Stabilin-2 Regulates VWF-FVIII Complex Half-Life and Immunogenicity. *J. Clin. Invest.* **2018**, *128* (9), 4057–4073. https://doi.org/10.1172/JCI96400.
(233) Hubbard, A. L.; Wilson, G.; Ashwell, G.; Stukenbrok, H. An Electron Microscope Autoradiographic Study of the Carbohydrate Recognition Systems in Rat Liver. I. Distribution of 125I-Ligands among the Liver Cell Types. *J. Cell Biol.* **1979**, *83* (1), 47–64. https://doi.org/10.1083/jcb.83.1.47.
(234) Isaksson, A.; Hultberg, B.; Sundler, R.; Åkesson, B. Uptake of β-Hexosaminidase by Nonparenchymal Liver Cells and Peritoneal Macrophages. *Enzyme* **1983**, *30* (4), 230–238. https://doi.org/10.1159/000469582.
(235) Smedsrød, B.; Johansson, S.; Pertoft, H. Studies in Vivo and in Vitro on the Uptake and Degradation of Soluble Collagen A1(I) Chains in Rat Liver Endothelial and Kupffer Cells. *Biochem. J.* **1985**, *228* (2), 415–424. https://doi.org/10.1042/bj2280415.
(236) Smedsrød, B. Aminoterminal Propeptide of Type III Procollagen Is Cleared from the Circulation by Receptor-Mediated Endocytosis in Liver Endothelial Cells. *Coll. Relat. Res.* **1988**, *8* (4), 375–388. https://doi.org/10.1016/S0174-173X(88)80008-6.
(237) Smedsrød, B.; Melkko, J.; Risteli, L.; Risteli, J. Circulating C -Terminal Propeptide of Type I Procollagen Is Cleared Mainly via the Mannose Receptor in Liver Endothelial Cells. *Biochem. J.* **1990**, *271* (2), 345–350. https://doi.org/10.1042/bj2710345.
(238) Smedsrød, B.; Einarsson, M. Clearance of Tissue Plasminogen Activator by Mannose and Galactose Receptors in the Liver. *Thromb. Haemost.* **1990**, *63* (01), 060–066. https://doi.org/10.1055/s-0038-1645687.
(239) Eskild, W.; Smedsrød, B.; Berg, T. Receptor Mediated Endocytosis of Formaldehyde Treated Albumin, Yeast Invertase and Chondroitin Sulfate in Suspensions of Rat Liver Endothelial Cells. *Int. J. Biochem.* **1986**, *18* (7), 647–651. https://doi.org/10.1016/0020-711X(86)90295-8.
(240) Dalen, D. P. P.-V.; De Leeuw, A. M.; Brouwer, A.; Knook, D. L. Rat Liver Endothelial Cells Have a Greater Capacity than Kupffer Cells to EndocytoseN-Acetylglucosamine- and Mannose-Terminated Glycoproteins. *Hepatology* **1987**, *7* (4), 672–679. https://doi.org/10.1002/hep.1840070410.
(241) Magnusson, S.; Berg, T. Extremely Rapid Endocytosis Mediated by the Mannose Receptor of Sinusoidal Endothelial Rat Liver Cells. *Biochem. J.* **1989**, *257* (3), 651–656. https://doi.org/10.1042/bj2570651.
(242) Kindberg, G. M.; Magnusson, S.; Berg, T.; Smedsrød, B. Receptor-Mediated Endocytosis of Ovalbumin by Two Carbohydrate-Specific Receptors in Rat Liver Cells. The Intracellular Transport of Ovalbumin to Lysosomes Is Faster in Liver Endothelial Cells than in Parenchymal Cells. *Biochem. J.* **1990**, *270* (1), 197–203. https://doi.org/10.1042/bj2700197.

(243) Ezekowitz, R. A. B.; Sastry, K.; Bailly, P.; Warner, A. Molecular Characterization of the Human Macrophage Mannose Receptor: Demonstration of Multiple Carbohydrate Recognition-like Domains and Phagocytosis of Yeasts in Cos-1 Cells. *J. Exp. Med.* **1990**, *172* (6), 1785–1794. https://doi.org/10.1084/jem.172.6.1785.
(244) Taylor, M. E.; Bezouska, K.; Drickamer, K. Contribution to Ligand Binding by Multiple Carbohydrate-Recognition Domains in the Macrophage Mannose Receptor. *J. Biol. Chem.* **1992**, *267* (3), 1719–1726. https://doi.org/10.1016/s0021-9258(18)46005-x.
(245) Asumendi, A.; Alvarez, A.; Martinez, I.; Smedsrød, B.; Vidal-Vanaclocha, F. Hepatic Sinusoidal Endothelium Heterogeneity with Respect to Mannose Receptor Activity Is Interleukin-1 Dependent. *Hepatology* **1996**, *23* (6), 1521–1529. https://doi.org/10.1053/jhep.1996.v23.pm0008675173.
(246) Stahl, P. D.; Ezekowitz, R. A. B. The Mannose Receptor Is a Pattern Recognition Receptor Involved in Host Defense. *Curr. Opin. Immunol.* **1998**, *10* (1), 50–55. https://doi.org/10.1016/S0952-7915(98)80031-9.
(247) Milone, M. C.; Fitzgerald-Bocarsly, P. The Mannose Receptor Mediates Induction of IFN-α in Peripheral Blood Dendritic Cells by Enveloped RNA and DNA Viruses. *J. Immunol.* **1998**, *161* (5), 2391–2399. https://doi.org/10.4049/jimmunol.161.5.2391.
(248) Roseman, D. S.; Baenziger, J. U. Molecular Basis of Lutropin Recognition by the Mannose/GalNAc-4-S04 Receptor. *Proc. Natl. Acad. Sci. U. S. A.* **2000**, *97* (18), 9949–9954. https://doi.org/10.1073/pnas.170184597.
(249) Reading, P. C.; Miller, J. L.; Anders, E. M. Involvement of the Mannose Receptor in Infection of Macrophages by Influenza Virus. *J. Virol.* **2000**, *74* (11), 5190–5197. https://doi.org/10.1128/jvi.74.11.5190-5197.2000.
(250) Gordon, S. Pattern Recognition Receptors: Doubling up for the Innate Immune Response. *Cell* **2002**, *111* (7), 927–930. https://doi.org/10.1016/S0092-8674(02)01201-1.
(251) Turville, S. G.; Cameron, P. U.; Handley, A.; Lin, G.; Pöhlmann, S.; Doms, R. W.; Cunningham, A. L. Diversity of Receptors Binding HIV on Dendritic Cell Subsets. *Nat. Immunol.* **2002**, *3* (10), 975–983. https://doi.org/10.1038/ni841.
(252) Allavena, P.; Chieppa, M.; Monti, P.; Piemonti, L. From Pattern Recognition Receptor to Regulator of Homeostasis: The Double-Faced Macrophage Mannose Receptor. *Crit. Rev. Immunol.* **2004**, *24* (3), 179–192. https://doi.org/10.1615/CritRevImmunol.v24.i3.20.
(253) Malovic, I.; Sørensen, K. K.; Elvevold, K. H.; Nedredal, G. I.; Paulsen, S.; Erofeev, A. V.; Smedsrød, B. H.; McCourt, P. A. G. The Mannose Receptor on Murine Liver Sinusoidal Endothelial Cells Is the Main Denatured Collagen Clearance Receptor. *Hepatology* **2007**, *45* (6), 1454–1461. https://doi.org/10.1002/hep.21639.
(254) Elvevold, K.; Simon-Santamaria, J.; Hasvold, H.; McCourt, P.; Smedsrød, B.; Sørensen, K. K. Liver Sinusoidal Endothelial Cells Depend on Mannose Receptor-Mediated Recruitment of Lysosomal Enzymes for Normal Degradation Capacity. *Hepatology* **2008**, *48* (6), 2007–2015. https://doi.org/10.1002/hep.22527.
(255) Brochériou, I.; Maouche, S.; Durand, H.; Braunersreuther, V.; Le Naour, G.; Gratchev, A.; Koskas, F.; Mach, F.; Kzhyshkowska, J.; Ninio, E. Antagonistic Regulation of Macrophage Phenotype by M-CSF and GM-CSF: Implication in Atherosclerosis. *Atherosclerosis* **2011**, *214* (2), 316–324. https://doi.org/10.1016/j.atherosclerosis.2010.11.023.
(256) Mousavi, S. A.; Sporstøl, M.; Fladeby, C.; Kjeken, R.; Barois, N.; Berg, T. Receptor-Mediated Endocytosis of Immune Complexes in Rat Liver Sinusoidal Endothelial Cells Is Mediated by FcγRIIb2. *Hepatology* **2007**, *46* (3), 871–884. https://doi.org/10.1002/hep.21748.
(257) Hampton, R. Y.; Golenbockt, D. T.; Penman, M.; Krieger, M.; Raetzt, C. R. H. Recognition and Plasma Clearance of Endotoxin by Scavenger Receptors. *Nature* **1991**, *352* (July), 342–344.
(258) Dunne, D. W.; Resnick, D.; Greenberg, J.; Krieger, M.; Joiner, K. A. The Type I Macrophage Scavenger Receptor Binds to Gram-Positive Bacteria and Recognizes Lipoteichoic Acid. *Proc. Natl. Acad. Sci. U. S. A.* **1994**, *91* (5), 1863–1867. https://doi.org/10.1073/pnas.91.5.1863.
(259) Araki, N.; Higashi, T.; Mori, T.; Shibayama, R.; Kawabe, Y.; Kodama, T.; Takahashi, K.; Shichiri, M.; Horiuchi, S. Macrophage Scavenger Receptor Mediates the Endocytic Uptake and Degradation of Advanced Glycation End Products of the Maillard Reaction. *Eur. J. Biochem.* **1995**, *230* (2), 408–415. https://doi.org/10.1111/j.1432-1033.1995.0408h.x.
(260) El Khoury, J.; Hickman, S. E.; Thomas, C. A.; Cao, L.; Silverstein, S. C.; Loike, J. D. Scavenger Receptor-Mediated Adhesion of Microglia to β-Amyloid Fibrils. *Nature* **1996**, *382* (6593), 716–719. https://doi.org/10.1038/382716a0.
(261) Suzuki, H.; Kurihara, Y.; Takeya, M.; Kamada, N.; Kataoka, M.; Jishage, K.; Ueda, O.; Sakaguchi, H.; Higashi, T.; Suzuki, T.; Takashima, Y.; Kawabe, Y.; Cynshi, O.; Wada, Y.; Honda, M.; Kurihara, H.; Aburatani, H.; Doi, T.; Matsumoto, A.; Azuma, S.; Noda, T.; Toyoda, Y.; Itakura, H.; Yazaki, Y.; Horiuchi, S.; Takahashi, K.; Kruijt, J. K.; van Berkel, T. J. C.; Steinbrecher, U. P.; Ishibashi, S.; Maeda, N.; Gordon, S.; Kodama, T. A Role for Macrophage Scavenger Receptors in Atherosclerosis and Susceptibility to Infection. *Nature* **1997**, *386* (6622), 292–296. https://doi.org/10.1038/386292a0.
(262) Kunjathoor, V. V.; Febbraio, M.; Podrez, E. A.; Moore, K. J.; Andersson, L.; Koehn, S.; Rhee, J. S.; Silverstein, R.; Hoff, H. F.; Freeman, M. W. Scavenger Receptors Class A-I/II and CD36 Are the Principal Receptors Responsible for the Uptake of Modified Low Density Lipoprotein Leading to Lipid Loading in Macrophages. *J. Biol. Chem.* **2002**, *277* (51), 49982–49988. https://doi.org/10.1074/jbc.M209649200.
(263) Acton, S.; Rigotti, A.; Landschulz, K. T.; Xu, S.; Hobbs, H. H.; Krieger, M. Identification of Scavenger Receptor SR-BI as a High Density Lipoprotein Receptor. *Science (80-.).* **1996**, *271* (5248), 518–520. https://doi.org/10.1126/science.271.5248.518.
(264) Kozarsky, K. F.; Donahee, M. H.; Rigotti, A.; Iqbal, S. N.; Edelman, E. R.; Krieger, M. Overexpression of the HDL Receptor SR-BI Alters Plasma HDL and Bile Cholesterol Levels. *Nature* **1997**, *387* (6631), 414–417. https://doi.org/10.1038/387414a0.
(265) Varban, M. L.; Rinninger, F.; Wang, N.; Fairchild-Huntress, V.; Dunmore, J. H.; Fang, Q.; Gosselin, M. L.; Dixon,

K. L.; Deeds, J. D.; Acton, S. L.; Tall, A. R.; Huszar, D. Targeted Mutation Reveals a Central Role for SR-BI in Hepatic Selective Uptake of High Density Lipoprotein Cholesterol. *Proc. Natl. Acad. Sci. U. S. A.* **1998**, *95* (8), 4619–4624. https://doi.org/10.1073/pnas.95.8.4619.
(266) During, A.; Dawson, H. D.; Harrison, E. H. Carotenoid Transport Is Decreased and Expression of the Lipid Transporters SR-BI, NPC1L1, and ABCA1 Is Downregulated in Caco-2 Cells Treated with Ezetimibe. *J. Nutr.* **2005**, *135* (10), 2305–2312. https://doi.org/10.1093/jn/135.10.2305.
(267) Reboul, E.; Klein, A.; Bietrix, F.; Gleize, B.; Malezet-Desmoulins, C.; Schneider, M.; Margotat, A.; Lagrost, L.; Collet, X.; Borel, P. Scavenger Receptor Class B Type I (SR-BI) Is Involved in Vitamin E Transport across the Enterocyte. *J. Biol. Chem.* **2006**, *281* (8), 4739–4745. https://doi.org/10.1074/jbc.M509042200.
(268) Brundert, M.; Heeren, J.; Merkel, M.; Carambia, A.; Herkel, J.; Groitl, P.; Dobner, T.; Ramakrishnan, R.; Moore, K. J.; Rinninger, F. Scavenger Receptor CD36 Mediates Uptake of High Density Lipoproteins in Mice and by Cultured Cells. *J. Lipid Res.* **2011**, *52* (4), 745–758. https://doi.org/10.1194/jlr.M011981.
(269) Tsugita, M.; Morimoto, N.; Tashiro, M.; Kinoshita, K.; Nakayama, M. SR-B1 Is a Silica Receptor That Mediates Canonical Inflammasome Activation. *Cell Rep.* **2017**, *18* (5), 1298–1311. https://doi.org/10.1016/j.celrep.2017.01.004.
(270) Oka, K.; Sawamura, T.; Kikuta, K. I.; Itokawa, S.; Kume, N.; Kita, T.; Masaki, T. Lectin-like Oxidized Low-Density Lipoprotein Receptor 1 Mediates Phagocytosis of Aged/Apoptotic Cells in Endothelial Cells. *Proc. Natl. Acad. Sci. U. S. A.* **1998**, *95* (16), 9535–9540. https://doi.org/10.1073/pnas.95.16.9535.
(271) Li, D.; Mehta, J. L. Upregulation of Endothelial Receptor for Oxidized LDL (LOX-1) by Oxidized LDL and Implications in Apoptosis of Coronary Artery Endothelial Cells: Evidence from Use of Antisense LOX-1 MRNA and Chemical Inhibitors. *Arterioscler. Thromb. Vasc. Biol.* **2000**, *20* (4), 1116–1122. https://doi.org/10.1161/01.ATV.20.4.1116.
(272) Chen, M.; Kakutani, M.; Masaki, T.; Sawamura, T.; Chen, M.; Narumiya, S.; Naruko, T.; Ueda, M.; Sawamura, T. Activation-Dependent Surface Expression of LOX-1 in Human Platelets. *Biochem. Biophys. Res. Commun.* **2001**, *282* (1), 153–158. https://doi.org/10.1006/bbrc.2001.4516.
(273) CHEN, M.; NARUMIYA, S.; MASAKI, T.; SAWAMURA, T. Conserved C-Terminal Residues within the Lectin-like Domain of LOX-1 Are Essential for Oxidized Low-Density-Lipoprotein Binding. *Biochem. J.* **2001**, *355* (2), 289–296. https://doi.org/10.1042/bj3550289.
(274) Shih, H. H.; Zhang, S.; Cao, W.; Hahn, A.; Wang, J.; Paulsen, J. E.; Harnish, D. C. CRP Is a Novel Ligand for the Oxidized LDL Receptor LOX-1. *Am. J. Physiol. - Hear. Circ. Physiol.* **2009**, *296* (5), 1643–1650. https://doi.org/10.1152/ajpheart.00938.2008.
(275) Gardner, J. P.; Durso, R. J.; Arrigale, R. R.; Donovan, G. P.; Maddon, P. J.; Dragic, T.; Olson, W. C. L-SIGN (CD 209L) Is a Liver-Specific Capture Receptor for Hepatitis C Virus. *Proc. Natl. Acad. Sci.* **2003**, *100* (8), 4498–4503. https://doi.org/10.1073/pnas.0831128100.
(276) Jeffers, S. A.; Tusell, S. M.; Gillim-Ross, L.; Hemmila, E. M.; Achenbach, J. E.; Babcock, G. J.; Thomas, W. D.; Thackray, L. B.; Young, M. D.; Mason, R. J.; Ambrosino, D. M.; Wentworth, D. E.; DeMartini, J. C.; Holmes, K. V. CD209L (L-SIGN) Is a Receptor for Severe Acute Respiratory Syndrome Coronavirus. *Proc. Natl. Acad. Sci. U. S. A.* **2004**, *101* (44), 15748–15753. https://doi.org/10.1073/pnas.0403812101.
(277) Boily-Larouche, G.; Milev, M. P.; Zijenah, L. S.; Labbé, A. C.; Zannou, D. M.; Humphrey, J. H.; Ward, B. J.; Poudrier, J.; Mouland, A. J.; Cohen, É. A.; Roger, M. Naturally-Occurring Genetic Variants in Human DC-SIGN Increase HIV-1 Capture, Cell-Transfer and Risk of Mother-to-Child Transmission. *PLoS One* **2012**, *7* (7). https://doi.org/10.1371/journal.pone.0040706.
(278) Swystun, L. L.; Notley, C.; Georgescu, I.; Lai, J. D.; Nesbitt, K.; James, P. D.; Lillicrap, D. The Endothelial Lectin Clearance Receptor CLEC4M Binds and Internalizes Factor VIII in a VWF-Dependent and Independent Manner. *J. Thromb. Haemost.* **2019**, *17* (4), 681–694. https://doi.org/10.1111/jth.14404.
(279) Kondo, Y.; Larabee, J. L.; Gao, L.; Shi, H.; Shao, B.; Hoover, C. M.; McDaniel, J. M.; Ho, Y. C.; Silasi-Mansat, R.; Archer-Hartmann, S. A.; Azadi, P.; Srinivasan, R. S.; Rezaie, A. R.; Borczuk, A.; Laurence, J. C.; Lupu, F.; Ahamed, J.; McEver, R. P.; Papin, J. F.; Yu, Z.; Xia, L. L-SIGN Is a Receptor on Liver Sinusoidal Endothelial Cells for SARS-CoV-2 Virus. *JCI Insight* **2021**, *6* (14), 1–15. https://doi.org/10.1172/jci.insight.148999.
(280) Feinberg, H.; Mitchell, D. A.; Drickamer, K.; Weis, W. I. Structural Basis for Selective Recognition of Oligosaccharides by DC-SIGN and DC-SIGNR. *Science (80-.).* **2001**, *294* (5549), 2163–2166. https://doi.org/10.1126/science.1066371.
(281) Liu, W.; Tang, L.; Zhang, G.; Wei, H.; Cui, Y.; Guo, L.; Gou, Z.; Chen, X.; Jiang, D.; Zhu, Y.; Kang, G.; He, F. Characterization of a Novel C-Type Lectin-like Gene, LSECtin: Demonstration of Carbohydrate Binding and Expression in Sinusoidal Endothelial Cells of Liver and Lymph Node. *J. Biol. Chem.* **2004**, *279* (18), 18748–18758. https://doi.org/10.1074/jbc.M311227200.
(282) Hussain, M. M.; Strickland, D. K.; Bakillah, A. The Mammalian Low-Density Lipoprotein Receptor Family. *Annu. Rev. Nutr.* **1999**, *19*, 141–172. https://doi.org/10.1146/annurev.nutr.19.1.141.
(283) Herz, J.; Strickland, D. K.; Herz, J.; Strickland, D. K. LRP : A Multifunctional Scavenger and Signaling Receptor Find the Latest Version : Multiligand Receptors LRP : A Multifunctional Scavenger and Signaling Receptor. *J. Clin. Invest.* **2001**, *108* (6), 779–784. https://doi.org/10.1172/JCI200113992.Introduction.
(284) Prasad, J. M.; Young, P. A.; Strickland, D. K. High Affinity Binding of the Receptor-Associated Protein D1D2 Domains with the Low Density Lipoprotein Receptorrelated Protein (LRP1) Involves Bivalent Complex Formation: Critical Roles of Lysines 60 and 191. *J. Biol. Chem.* **2016**, *291* (35), 18430–18439. https://doi.org/10.1074/jbc.M116.744904.
(285) Salama, Y.; Lin, S. Y.; Dhahri, D.; Hattori, K.; Heissig, B. The Fibrinolytic Factor TPA Drives LRP1-Mediated Melanoma Growth and Metastasis. *FASEB J.* **2019**, *33* (3), 3465–3480. https://doi.org/10.1096/fj.201801339RRR.

(286) Banerji, S.; Ni, J.; Wang, S. X.; Clasper, S.; Su, J.; Tammi, R.; Jones, M.; Jackson, D. G. LYVE-1, a New Homologue of the CD44 Glycoprotein, Is a Lymph-Specific Receptor for Hyaluronan. *J. Cell Biol.* **1999**, *144* (4), 789–801. https://doi.org/10.1083/jcb.144.4.789.
(287) Tandon, N. N.; Lipsky, R. H.; Burgess, W. H.; Jamieson, G. A. Isolation and Characterization of Platelet Glycoprotein IV (CD36). *J. Biol. Chem.* **1989**, *264* (13), 7570–7575. https://doi.org/10.1016/s0021-9258(18)83272-0.
(288) Savill, J.; Hogg, N.; Haslett, C. Macrophage Vitronectin Receptor, CD36, and Thrombospondin Cooperate in Recognition of Neutrophils Undergoing Programmed Cell Death. *Chest* **1991**, *99* (3 SUPPL.), 6S-7S. https://doi.org/10.1378/chest.99.3_Supplement.6S-a.
(289) Rigotti, A.; Acton, S. L.; Krieger, M. The Class B Scavenger Receptors SR-BI and CD36 Are Receptors for Anionic Phospholipids. *J. Biol. Chem.* **1995**, *270* (27), 16221–16224. https://doi.org/10.1074/jbc.270.27.16221.
(290) Calvo, D.; Gómez-Coronado, D.; Suárez, Y.; Lasunción, M. A.; Vega, M. A. Human CD36 Is a High Affinity Receptor for the Native Lipoproteins HDL, LDL, and VLDL. *J. Lipid Res.* **1998**, *39* (4), 777–788. https://doi.org/10.1016/s0022-2275(20)32566-9.
(291) Michael J. Duryee, M.S. Thomas L. Freeman Ph.D. Monte S. Willis, M.D., Ph.D. Carlos D. Hunter, B. S.; Bartlett C. Hamilton III, B.S. Hiroshi Suzuki, Ph.D. Dean J. Tuma, P. D.; Lynell W. Klassen, M.D. Geoffrey M. Thiele, P. D. Scavenger Receptors on Sinusoidal Liver Endothelial Cells (SECs) Are Involved in the Uptake of Aldehyde-Modified Proteins. *Mol. Pharmacol. Fast Forw.* **2005**. https://doi.org/10.1124/mol.105.016121.
(292) Shepherd, V. L.; Lee, Y. C.; Schlesinger, P. H.; Stahl, P. D. L-Fucose-Terminated Glycoconjugates Are Recognized by Pinocytosis Receptors on Macrophages. *Proc. Natl. Acad. Sci. U. S. A.* **1981**, *78* (2 II), 1019–1022. https://doi.org/10.1073/pnas.78.2.1019.
(293) Fiete, D.; Srivastava, V.; Hindsgaul, O.; Baenziger, J. U. A Hepatic Reticuloendothelial Cell Receptor Specific for SO4-4GalNAcβ1, 4GlcNAcβ1,2Manα That Mediates Rapid Clearance of Lutropin. *Cell* **1991**, *67* (6), 1103–1110. https://doi.org/10.1016/0092-8674(91)90287-9.
(294) Mi, Y.; Shapiro, S. D.; Baenziger, J. U. Regulation of Lutropin Circulatory Half-Life by the Mannose/N-Acetylgalactosamine-4-SO4 Receptor Is Critical for Implantation in Vivo. *J. Clin. Invest.* **2002**, *109* (2), 269–276. https://doi.org/10.1172/JCI13997.
(295) Stahl, P. D.; Rodman, J. S.; Miller, M. J.; Schlesinger, P. H. Evidence for Receptor-Mediated Binding of Glycoproteins, Glycoconjugates, and Lysosomal Glycosidases by Alveolar Macrophages. *Proc. Natl. Acad. Sci. U. S. A.* **1978**, *75* (3), 1399–1403. https://doi.org/10.1073/pnas.75.3.1399.
(296) Stahl, P.; Gordon, S. Expression of a Mannosyl-Fucosyl Receptor for Endocytosis on Cultured Primary Macrophages and Their Hybrids. *J. Cell Biol.* **1982**, *93* (1), 49–56. https://doi.org/10.1083/jcb.93.1.49.
(297) Summerfield, J. A.; Vergalla, J.; Jones, E. A. Modulation of a Glycoprotein Recognition System on Rat Hepatic Endothelial Cells by Glucose and Diabetes Mellitus. *J. Clin. Invest.* **1982**, *69* (6), 1337–1347. https://doi.org/10.1172/JCI110573.
(298) Fraser, J. R. F.; Laurent, T. C.; Pertoft, H.; Baxter, E. Plasma Clearance, Tissue Distribution and Metabolism of Hyaluronic Acid Injected Intravenously in the Rabbit. *Biochem. J.* **1981**, *200* (2), 415–424. https://doi.org/10.1042/bj2000415.
(299) Smedsrød, B.; Eriksson, S.; Fraser, J.; Laurent, T.; Pertoft, H. Properties of Liver Endothelial Cells in Primary Monolayer Cultures. *Sinusoidal Liver Cells* **1982**.
(300) POLITZ, O.; GRATCHEV, A.; McCOURT, P. A. G.; SCHLEDZEWSKI, K.; GUILLOT, P.; JOHANSSON, S.; SVINENG, G.; FRANKE, P.; KANNICHT, C.; KZHYSHKOWSKA, J.; LONGATI, P.; VELTEN, F. W.; JOHANSSON, S.; GOERDT, S. Stabilin-1 and −2 Constitute a Novel Family of Fasciclin-like Hyaluronan Receptor Homologues. *Biochem. J.* **2002**, *362* (1), 155–164. https://doi.org/10.1042/bj3620155.
(301) Smedsrød, B. Cellular Events in the Uptake and Degradation of Hyaluronan. *Adv. Drug Deliv. Rev.* **1991**, *7* (2), 265–278. https://doi.org/10.1016/0169-409X(91)90006-X.
(302) Smedsrod, B.; Paulsson, M.; Johansson, S. Uptake and Degradation in Vivo and in Vitro of Laminin and Nidogen by Rat Liver Cells. *Biochem. J.* **1989**, *261* (1), 37–42. https://doi.org/10.1042/bj2610037.
(303) Smedsrød, B.; Kjellén, L.; Pertoft, H. Endocytosis and Degradation of Chondroitin Sulphate by Liver Endothelial Cells. *Biochem. J.* **1985**, *229* (1), 63–71. https://doi.org/10.1042/bj2290063.
(304) Smedsrød, B.; Malmgren, M.; Ericsson, J.; Laurent, T. C. Morphological Studies on Endocytosis of Chondroitin Sulphate Proteoglycan by Rat Liver Endothelial Cells. *Cell Tissue Res.* **1988**, *253* (1), 39–45. https://doi.org/10.1007/BF00221737.
(305) Falkowska-Hansen, B.; Øynebråten, I.; Uhlin-Hansen, L.; Smedsrød, B. Endocytosis and Degradation of Serglycin in Liver Sinusoidal Endothelial Cells. *Mol. Cell. Biochem.* **2006**, *287* (1–2), 43–52. https://doi.org/10.1007/s11010-005-9024-3.
(306) Melkko, J.; Hellevik, T.; Risteli, L.; Risteli, J.; Smedsrød, B. Clearance of NH2-Terminal Propeptides of Types I and III Procollagen Is a Physiological Function of the Scavenger Receptor in Liver Endothelial Cells. *J. Exp. Med.* **1994**, *179* (2), 405–412. https://doi.org/10.1084/jem.179.2.405.
(307) VAN BERKEL, T. J. C.; VAN VELZEN, A.; KRUIJT, J. K.; SUZUKI, H.; KODAMA, T. Uptake and Catabolism of Modified LDL in Scavenger-Receptor Class A Type I/II Knock-out Mice. *Biochem. J.* **1998**, *331* (1), 29–35. https://doi.org/10.1042/bj3310029.
(308) Eskild, W.; Berg, T. Endocytosis of Formaldehyde-Denatured Serum Albumin by Nonparenchymal Liver Cells in Vitro. *BBA - Mol. Cell Res.* **1984**, *803* (1–2), 63–70. https://doi.org/10.1016/0167-4889(84)90055-7.
(309) Eskild, W.; Henriksen, T.; Skreiting, G.; Blomhoff, R.; Berg, T. Endocytosis of Acetylated Low-Density Lipoprotein, Endothelial Cell-Modified Low-Density Lipoprotein, and Formaldehyde-Treated Serum Albumin by Rat Liver Endothelial Cells Evidence of Uptake via a Common Receptor. *Scand. J. Gastroenterol.* **1987**, *22* (10),

1263–1269. https://doi.org/10.3109/00365528708996474.
(310) Lovdal, T.; Andersen, E.; Brech, A.; Berg, T. Fc Receptor Mediated Endocytosis of Small Soluble Immunoglobulin G Immune Complexes in Kupffer and Endothelial Cells from Rat Liver. *J. Cell Sci.* **2000**, *113* (18), 3255–3266. https://doi.org/10.1242/jcs.113.18.3255.
(311) Brunner, K. T.; Hurez, D.; McCluskey, R. T.; Benacerraf, B. Blood Clearance of P32-Labeled Vesicular Stomatitis and Newcastle Disease Viruses by the Reticuloendothelial System in Mice. *J. Immunol.* **1960**, *85* (1), 99–105. https://doi.org/10.4049/jimmunol.85.1.99.
(312) MIMS, C. A. The Response of Mice to Large Intravenous Injections of Ectromelia Virus. I. The Fate of Injected Virus. *Br. J. Exp. Pathol.* **1959**, *40* (1936), 533–542.
(313) Simon-Santamaria, J.; Rinaldo, C. H.; Kardas, P.; Li, R.; Malovic, I.; Elvevold, K.; McCourt, P.; Smedsrød, B.; Hirsch, H. H.; Sørensen, K. K. Efficient Uptake of Blood-Borne BK and JC Polyomavirus-like Particles in Endothelial Cells of Liver Sinusoids and Renal Vasa Recta. *PLoS One* **2014**, *9* (11). https://doi.org/10.1371/journal.pone.0111762.
(314) Mates, J. M.; Yao, Z.; Cheplowitz, A. M.; Suer, O.; Phillips, G. S.; Kwiek, J. J.; Rajaram, M. V. S.; Kim, J.; Robinson, J. M.; Ganesan, L. P.; Anderson, C. L. Mouse Liver Sinusoidal Endothelium Eliminates HIV-like Particles from Blood at a Rate of 100 Million per Minute by a Second-Order Kinetic Process. *Front. Immunol.* **2017**, *8* (JAN), 1–9. https://doi.org/10.3389/fimmu.2017.00035.
(315) Ganesan, L. P.; Mohanty, S.; Kim, J.; Clark, K. R.; Robinson, J. M.; Anderson, C. L. Rapid and Efficient Clearance of Blood-Borne Virus by Liver Sinusoidal Endothelium. *PLoS Pathog.* **2011**, *7* (9). https://doi.org/10.1371/journal.ppat.1002281.
(316) Øie, C. I.; Wolfson, D. L.; Yasunori, T.; Dumitriu, G.; Sørensen, K. K.; McCourt, P. A.; Ahluwalia, B. S.; Smedsrød, B. Liver Sinusoidal Endothelial Cells Contribute to the Uptake and Degradation of Entero Bacterial Viruses. *Sci. Rep.* **2020**, *10* (1), 1–9. https://doi.org/10.1038/s41598-020-57652-0.
(317) Kyrrestad, I.; Larsen, A. K.; Sánchez Romano, J.; Simón-Santamaría, J.; Li, R.; Sørensen, K. K. Infection of Liver Sinusoidal Endothelial Cells with Muromegalovirus Muridbeta1 Involves Binding to Neuropilin-1 and Is Dynamin-Dependent. *Front. Cell. Infect. Microbiol.* **2023**, *13* (November), 1–16. https://doi.org/10.3389/fcimb.2023.1249894.
(318) Seckert, C. K.; Renzaho, A.; Tervo, H.-M.; Krause, C.; Deegen, P.; Kühnapfel, B.; Reddehase, M. J.; Grzimek, N. K. A. Liver Sinusoidal Endothelial Cells Are a Site of Murine Cytomegalovirus Latency and Reactivation. *J. Virol.* **2009**, *83* (17), 8869–8884. https://doi.org/10.1128/jvi.00870-09.
(319) Ludwig, I. S.; Lekkerkerker, A. N.; Depla, E.; Bosman, F.; Musters, R. J. P.; Depraetere, S.; van Kooyk, Y.; Geijtenbeek, T. B. H. Hepatitis C Virus Targets DC-SIGN and L-SIGN To Escape Lysosomal Degradation. *J. Virol.* **2004**, *78* (15), 8322–8332. https://doi.org/10.1128/JVI.78.15.8322-8332.2004.
(320) Breiner, K. M.; Schaller, H.; Knolle, P. A. Endothelial Cell-Mediated Uptake of a Hepatitis B Virus: A New Concept of Liver Targeting of Hepatotropic Microorganisms. *Hepatology* **2001**, *34* (4 I), 803–808. https://doi.org/10.1053/jhep.2001.27810.
(321) Lozach, P. Y.; Amara, A.; Bartosch, B.; Virelizier, J. L.; Arenzana-Seisdedos, F.; Cosset, F. L.; Altmeyer, R. C-Type Lectins L-SIGN and DC-SIGN Capture and Transmit Infectious Hepatitis C Virus Pseudotype Particles. *J. Biol. Chem.* **2004**, *279* (31), 32035–32045. https://doi.org/10.1074/jbc.M402296200.
(322) Liu, Y.; Gardner, C. R.; Laskin, J. D.; Laskin, D. L. Classical and Alternative Activation of Rat Hepatic Sinusoidal Endothelial Cells by Inflammatory Stimuli. *Exp. Mol. Pathol.* **2013**, *94* (1), 160–167. https://doi.org/10.1016/j.yexmp.2012.10.015.
(323) Mathison, J. C.; Ulevitch, R. J. The Clearance, Tissue Distribution, and Cellular Localization of Intravenously Injected Lipopolysaccharide in Rabbits. *J. Immunol.* **1979**, *123* (5), 2133–2143. https://doi.org/10.4049/jimmunol.123.5.2133.
(324) Van Oosten, M.; Van De Bilt, E.; Van Berkel, T. J. C.; Kuiper, J. New Scavenger Receptor-like Receptors for the Binding of Lipopolysaccharide to Liver Endothelial and Kupffer Cells. *Infect. Immun.* **1998**, *66* (11), 5107–5112. https://doi.org/10.1128/iai.66.11.5107-5112.1998.
(325) Yao, Z.; Mates, J. M.; Cheplowitz, A. M.; Hammer, L. P.; Maiseyeu, A.; Phillips, G. S.; Wewers, M. D.; Rajaram, M. V. S.; Robinson, J. M.; Anderson, C. L.; Ganesan, L. P. Blood-Borne Lipopolysaccharide Is Rapidly Eliminated by Liver Sinusoidal Endothelial Cells via High-Density Lipoprotein. *J. Immunol.* **2016**, *197* (6), 2390–2399. https://doi.org/10.4049/jimmunol.1600702.
(326) Limmer, A.; Ohl, J.; Kurts, C.; Ljunggren, H. G.; Reiss, Y.; Groettrup, M.; Momburg, F.; Arnold, B.; Knolle, P. A. Efficient Presentation of Exogenous Antigen by Liver Endothelial Cells to CD8+ T Cells Results in Antigen-Specific T-Cell Tolerance. *Nat. Med.* **2000**, *6* (12), 1348–1354. https://doi.org/10.1038/82161.
(327) Schwocho, L. R.; Moon, R. J. Clearance and Killing of Candida Albicans in the Perfused Mouse Liver. *Mycopathologia* **1981**, *76* (3), 175–183. https://doi.org/10.1007/BF00437198.
(328) Martens, J. H.; Kzhyshkowska, J.; Falkowski-Hansen, M.; Schledzewski, K.; Gratchev, A.; Mansmann, U.; Schmuttermaier, C.; Dippel, E.; Koenen, W.; Riedel, F.; Sankala, M.; Tryggvason, K.; Kobzik, L.; Moldenhauer, G.; Arnold, B.; Goerdt, S. Differential Expression of a Gene Signature for Scavenger/Lectin Receptors by Endothelial Cells and Macrophages in Human Lymph Node Sinuses, the Primary Sites of Regional Metastasis. *J. Pathol.* **2006**, *208* (4), 574–589. https://doi.org/10.1002/path.1921.
(329) Fadok, V. A.; Voelker, D. R.; Campbell, P. A.; Cohen, J. J.; Bratton, D. L.; Henson, P. M. Exposure of Phosphatidylserine on the Surface of Apoptotic Lymphocytes Triggers Specific Recognition and Removal by Macrophages. *J. Immunol.* **1992**, *148* (7), 2207–2216. https://doi.org/10.4049/jimmunol.148.7.2207.
(330) Lee, W. Y.; Moriarty, T. J.; Wong, C. H. Y.; Zhou, H.; Strieter, R. M.; Van Rooijen, N.; Chaconas, G.; Kubes, P. An Intravascular Immune Response to Borrelia Burgdorferi Involves Kupffer Cells and INKT Cells. *Nat. Immunol.* **2010**, *11* (4), 295–302. https://doi.org/10.1038/ni.1855.

(331) Park, S. Y.; Kim, I. S. Stabilin Receptors: Role as Phosphatidylserine Receptors. *Biomolecules* **2019**, *9* (8), 1–16. https://doi.org/10.3390/biom9080387.
(332) Tavassoli, M.; Kishimoto, T.; Kataoka, M. Liver Endothelium Mediates the Hepatocyte's Uptake of Ceruloplasmin. *J. Cell Biol.* **1986**, *102* (4), 1298–1303. https://doi.org/10.1083/jcb.102.4.1298.
(333) Tavassoli, M.; Kishimoto, T.; Soda, R.; Kataoka, M.; Harjes, K. Liver Endothelium Mediates the Uptake of Complex by Hepatocytes MEHDI TAVASSOLI ,* TAKUMI KISHIMO ' IQ RYO SODA , Liver Is a Major Organ in the Metabolism of Iron (Fe) Which Is Transported in the Circulation by the Glycoprotein Transfenin (TF). Using. *Exp. Cell Res.* **1986**, *165*, 369–379.
(334) Irie, S.; Kishimoto, T.; Tavassoli, M. Desialation of Transferrin by Rat Liver Endothelium. *J. Clin. Invest.* **1988**, *82* (2), 508–513. https://doi.org/10.1172/JCI113625.
(335) Eskild, W.; Kindberg, G. M.; Smedsræd, B.; Blomhoff, R.; Norum, K. R.; Berg, T. Intracellular Transport of Formaldehyde-Treated Serum Albumin in Liver Endothelial Cells after Uptake via Scavenger Receptors. *Biochem. J.* **1989**, *258*, 511–520.
(336) Hellevik, T.; Bondevik, A.; Smedsrød, B. Intracellular Fate of Endocytosed Collagen in Rat Liver Endothelial Cells. *Exp. Cell Res.* **1996**, *223* (1), 39–49. https://doi.org/10.1006/excr.1996.0056.
(337) Hellevik, T.; Martinez, I.; Olsen, R.; Toh, B.-H.; Webster, P.; Smedsrød, B. Transport of Residual Endocytosed Products into Terminal Lysosomes Occurs Slowly in Rat Liver Endothelial Cells. *Hepatology* **1998**, *28* (5), 1378–1389. https://doi.org/10.1002/hep.510280529.
(338) Simon-Santamaria, J.; Malovic, I.; Warren, A.; Oteiza, A.; Le Couteur, D.; Smedsrød, B.; McCourt, P.; Sørensen, K. K. Age-Related Changes in Scavenger Receptor-Mediated Endocytosis in Rat Liver Sinusoidal Endothelial Cells. *Journals Gerontol. - Ser. A Biol. Sci. Med. Sci.* **2010**, *65 A* (9), 951–960. https://doi.org/10.1093/gerona/glq108.
(339) Grosse, L.; Bulavin, D. V. LSEC Model of Ageing. *Aging (Albany. NY).* **2020**, *12* (11), 11152–11160.
(340) Alcaraz-Quiles, J.; Casulleras, M.; Oettl, K.; Titos, E.; Flores-Costa, R.; Duran-Güell, M.; López-Vicario, C.; Pavesi, M.; Stauber, R. E.; Arroyo, V.; Clària, J. Oxidized Albumin Triggers a Cytokine Storm in Leukocytes Through P38 Mitogen-Activated Protein Kinase: Role in Systemic Inflammation in Decompensated Cirrhosis. *Hepatology* **2018**, *68* (5), 1937–1952. https://doi.org/10.1002/hep.30135.
(341) Clària, J.; Stauber, R. E.; Coenraad, M. J.; Moreau, R.; Jalan, R.; Pavesi, M.; Amorós, À.; Titos, E.; Alcaraz-Quiles, J.; Oettl, K.; Morales-Ruiz, M.; Angeli, P.; Domenicali, M.; Alessandria, C.; Gerbes, A.; Wendon, J.; Nevens, F.; Trebicka, J.; Laleman, W.; Saliba, F.; Welzel, T. M.; Albillos, A.; Gustot, T.; Benten, D.; Durand, F.; Ginès, P.; Bernardi, M.; Arroyo, V.; Melero, P. A.; Bañares, R.; Bocci, M.; Caraceni, P.; Catalina, M. V.; Chin, J. L.; Concepción, M.; Coilly, A.; Deulofeu, C.; Elkrief, L.; Fernandez, J.; Gola, E.; de Gottardi, A.; Grøenbæk, H.; Hausen, A. K.; Lohse, A. W.; Maggioli, C.; Markwardt, D.; Martinez, J.; de la Mata, M.; McCormick, P. A.; Mesonero, F.; Álvarez, J. L. M.; Mookerjee, R. P.; Moreno, C.; Morrell, B.; Mortensen, C.; Peck-Radosavljevic, M.; Risso, A.; Samuel, D.; Simon-Talero, M.; Solà, E.; Solis-Muñoz, P.; Soriano, G.; Sperl, J.; Spindelboeck, W.; Valla, D.; Vargas, V.; Van Vlierberghe, H.; Vogel, W.; Wege, H.; Willars, C.; Zaccherini, G.; Zeuzem, S. Systemic Inflammation in Decompensated Cirrhosis: Characterization and Role in Acute-on-Chronic Liver Failure. *Hepatology* **2016**, *64* (4), 1249–1264. https://doi.org/10.1002/hep.28740.
(342) Noce, A.; Rovella, V.; Marrone, G.; Cattani, G.; Zingaretti, V.; Limongi, D.; D'Agostini, C.; Sorge, R.; Casasco, M.; Di Daniele, N.; Ricci, G.; Bocedi, A. Hemodialysis Biomarkers: Total Advanced Glycation End Products (AGEs) against Oxidized Human Serum Albumin (HSAox). *Acta Diabetol.* **2019**, *56* (12), 1323–1331. https://doi.org/10.1007/s00592-019-01413-7.
(343) Itabe, H.; Obama, T. The Oxidized Lipoproteins In Vivo: Its Diversity and Behavior in the Human Circulation. *Int. J. Mol. Sci.* **2023**, *24* (6), 5747. https://doi.org/10.3390/ijms24065747.
(344) Fujii, R.; Ueyama, J.; Aoi, A.; Ichino, N.; Osakabe, K.; Sugimoto, K.; Suzuki, K.; Hamajima, N.; Wakai, K.; Kondo, T. Oxidized Human Serum Albumin as a Possible Correlation Factor for Atherosclerosis in a Rural Japanese Population: The Results of the Yakumo Study. *Environ. Health Prev. Med.* **2018**, *23* (1), 1–7. https://doi.org/10.1186/s12199-017-0690-z.
(345) Oteiza, A.; Li, R.; McCuskey, R. S.; Smedsrød, B.; Sørensen, K. K. Effects of Oxidized Low-Density Lipoproteins on the Hepatic Microvasculature. *Am. J. Physiol. - Gastrointest. Liver Physiol.* **2011**, *301* (4), 684–693. https://doi.org/10.1152/ajpgi.00347.2010.
(346) Svistounov, D.; Oteiza, A.; Zykova, S. N.; Sørensen, K. K.; McCourt, P.; McLachlan, A. J.; McCuskey, R. S.; Smedsrød, B. Hepatic Disposal of Advanced Glycation End Products during Maturation and Aging. *Exp. Gerontol.* **2013**, *48* (6), 549–556. https://doi.org/10.1016/j.exger.2013.03.005.
(347) Li, R.; Bhandari, S.; Martinez-Zubiaurre, I.; Bruun, J. A.; Urbarova, I.; Smedsrød, B.; Simón-Santamaría, J.; Sørensen, K. K. *Changes in the Proteome and Secretome of Rat Liver Sinusoidal Endothelial Cells during Early Primary Culture and Effects of Dexamethasone*; 2022; Vol. 17. https://doi.org/10.1371/journal.pone.0273843.
(348) Namdari, R.; Jones, K.; Chuang, S. S.; Van Cruchten, S.; Dincer, Z.; Downes, N.; Mikkelsen, L. F.; Harding, J.; Jäckel, S.; Jacobsen, B.; Kinyamu-Akunda, J.; Lortie, A.; Mhedhbi, S.; Mohr, S.; Schmitt, M. W.; Prior, H. Species Selection for Nonclinical Safety Assessment of Drug Candidates: Examples of Current Industry Practice. *Regul. Toxicol. Pharmacol.* **2021**, *126* (August). https://doi.org/10.1016/j.yrtph.2021.105029.
(349) Tyshkovskiy, A.; Ma, S.; Shindyapina, A. V.; Tikhonov, S.; Lee, S. G.; Bozaykut, P.; Castro, J. P.; Seluanov, A.; Schork, N. J.; Gorbunova, V.; Dmitriev, S. E.; Miller, R. A.; Gladyshev, V. N. Distinct Longevity Mechanisms across and within Species and Their Association with Aging. *Cell* **2023**, *186* (13), 2929-2949.e20. https://doi.org/10.1016/j.cell.2023.05.002.
(350) F, B.; E, W. Structural and Functional Aspects of Liver Sinusoidal Endothelial Cell Fenestrae: A Review. *Comp. Hepatol.* **2002**, *1* (1), 1.
(351) Zapotoczny, B.; Braet, F.; Kus, E.; Ginda-Mäkelä, K.; Klejevskaja, B.; Campagna, R.; Chlopicki, S.; Szymonski, M.

Actin-Spectrin Scaffold Supports Open Fenestrae in Liver Sinusoidal Endothelial Cells. *Traffic* **2019**, No. April, 1–11. https://doi.org/10.1111/tra.12700.
(352) Zapotoczny, B.; Szafranska, K.; Lekka, M.; Ahluwalia, B. S.; McCourt, P. Tuning of Liver Sieve: The Interplay between Actin and Myosin Regulatory Light Chain Regulates Fenestration Size and Number in Murine Liver Sinusoidal Endothelial Cells. *Int. J. Mol. Sci.* **2022**, *23* (17). https://doi.org/10.3390/ijms23179850.
(353) Zhang, X.; Li, P.; Zhou, J.; Zhang, Z.; Wu, H.; Shu, X. Biomaterials FAK-P38 Signaling Serves as a Potential Target for Reverting Matrix Stiffness-Modulated Liver Sinusoidal Endothelial Cell Defenestration. **2024**, *305* (October 2023), 1–17. https://doi.org/10.1016/j.biomaterials.2023.122462.
(354) Jamieson, H. A.; Hilmer, S. N.; Cogger, V. C.; Warren, A.; Cheluvappa, R.; Abernethy, D. R.; Everitt, A. V.; Fraser, R.; de Cabo, R.; Le Couteur, D. G. Caloric Restriction Reduces Age-Related Pseudocapillarization of the Hepatic Sinusoid. *Exp. Gerontol.* **2007**, *42* (4), 374–378. https://doi.org/10.1016/j.exger.2006.11.004.
(355) Piotrowska, K.; Zgutka, K.; Tomasiak, P.; Tarnowski, M.; Pawlik, A. Every-Other Day (EOD) Feeding Regime Decreases Oxidative Stress and Inflammatory Cascade in Mouse Liver: The Immunohistochemical Study. *Tissue Cell* **2023**, *85* (August). https://doi.org/10.1016/j.tice.2023.102236.
(356) Cogger, V. C.; Mross, P. E.; Hosie, M. J.; Ansselin, a D.; McLean, a J.; Le Couteur, D. G. The Effect of Acute Oxidative Stress on the Ultrastructure of the Perfused Rat Liver. *Pharmacol. Toxicol.* **2001**, *89* (6), 306–311. https://doi.org/DOI 10.1034/j.1600-0773.2001.d01-165.x.
(357) Haimerl, M.; Verloh, N.; Fellner, C.; Zeman, F.; Teufel, A.; Fichtner-Feigl, S.; Schreyer, A. G.; Stroszczynski, C.; Wiggermann, P. MRI-Based Estimation of Liver Function: Gd-EOB-DTPA-Enhanced T1 Relaxometry of 3T vs. The MELD Score. *Sci. Rep.* **2014**, *4*, 1–7. https://doi.org/10.1038/srep05621.
(358) Peter, O.; Clemmesen, O.; Keiding, S. Interpretation of Simultaneous Measurements of Hepatic Extraction Fractions of Indocyanine Green and Sorbitol: Evidence of Hepatic Shunts and Capillarization? *Dig. Dis. Sci.* **2000**, *45* (2), 359–365. https://doi.org/10.1023/A:1005476913311.
(359) Ohtani, O.; Ohtani, Y. Lymph Circulation in the Liver. *Anat. Rec.* **2008**, *291* (6), 643–652. https://doi.org/10.1002/ar.20681.
(360) Bobe, S.; Beckmann, D.; Klump, D. M.; Dierkes, C.; Kirschnick, N.; Redder, E.; Bauer, N.; Schäfers, M.; Erapaneedi, R.; Risse, B.; van de Pavert, S. A.; Kiefer, F. Volumetric Imaging Reveals VEGF-C-Dependent Formation of Hepatic Lymph Vessels in Mice. *Front. Cell Dev. Biol.* **2022**, *10* (August), 1–14. https://doi.org/10.3389/fcell.2022.949896.
(361) Sørensen, K. K.; Simon-Santamaria, J.; McCuskey, R. S.; Smedsrød, B. Liver Sinusoidal Endothelial Cells. *Compr. Physiol.* **2015**, *5* (4), 1751–1774. https://doi.org/10.1002/cphy.c140078.
(362) Colombo, G.; Clerici, M.; Giustarini, D.; Rossi, R.; Milzani, A.; Dalle-Donne, I. Redox Albuminomics: Oxidized Albumin in Human Diseases. *Antioxidants Redox Signal.* **2012**, *17* (11), 1515–1527. https://doi.org/10.1089/ars.2012.4702.
(363) Kettle, A. J.; Winterbourn, C. C. Myeloperoxidase: A Key Regulator of Neutrophil Oxidant Product. *Redox Rep.* **1997**, *3* (1), 3–15. https://doi.org/10.1080/13510002.1997.11747085.
(364) Zhang, L.-F.; Wang, X.-H.; Zhang, C.-L.; Lee, J.; Duan, B.-W.; Xing, L.; Li, L.; Oh, Y.-K.; Jiang, H.-L. Sequential Nano-Penetrators of Capillarized Liver Sinusoids and Extracellular Matrix Barriers for Liver Fibrosis Therapy. *ACS Nano* **2022**. https://doi.org/10.1021/acsnano.2c03858.
(365) Liu, Q.; Wang, X.; Liao, Y. P.; Chang, C. H.; Li, J.; Xia, T.; Nel, A. E. Use of a Liver-Targeting Nanoparticle Platform to Intervene in Peanut-Induced Anaphylaxis through Delivery of an Ara H2 T-Cell Epitope. *Nano Today* **2022**, *42*, 101370. https://doi.org/10.1016/j.nantod.2021.101370.
(366) Kaps, L.; Limeres, M. J.; Schneider, P.; Svensson, M.; Zeyn, Y.; Fraude, S.; Cacicedo, M. L.; Galle, P. R.; Gehring, S.; Bros, M. Liver Cell Type-Specific Targeting by Nanoformulations for Therapeutic Applications. *Int. J. Mol. Sci.* **2023**, *24* (14). https://doi.org/10.3390/ijms241411869.
(367) Hide, D.; Raurell, I.; de So Rafael, D. F.; Andrade, F. D. S.; Schwartz, S.; Augustin, S.; Genesca, J.; Martell, M. Simvastatin-Loaded Polymeric Micelles Are a New, Safe and Effective Drug Delivery System Targeting Liver Sinusoidal Endothelial Cells. *J. Hepatol.* **2018**, *68*, S466. https://doi.org/10.1016/S0168-8278(18)31176-0.
(368) Hunt, N. J.; Lockwood, G. P.; Kang, S. W. S.; Westwood, L. J.; Limantoro, C.; Chrzanowski, W.; McCourt, P. A. G.; Kuncic, Z.; Le Couteur, D. G.; Cogger, V. C. Quantum Dot Nanomedicine Formulations Dramatically Improve Pharmacological Properties and Alter Uptake Pathways of Metformin and Nicotinamide Mononucleotide in Aging Mice. *ACS Nano* **2021**, *15* (3), 4710–4727. https://doi.org/10.1021/acsnano.0c09278.
(369) Carambia, A.; Freund, B.; Schwinge, D.; Bruns, O. T.; Salmen, S. C.; Ittrich, H.; Reimer, R.; Heine, M.; Huber, S.; Waurisch, C.; Eychmüller, A.; Wraith, D. C.; Korn, T.; Nielsen, P.; Weller, H.; Schramm, C.; Lüth, S.; Lohse, A. W.; Heeren, J.; Herkel, J. Nanoparticle-Based Autoantigen Delivery to Treg-Inducing Liver Sinusoidal Endothelial Cells Enables Control of Autoimmunity in Mice. *J. Hepatol.* **2015**, *62* (6), 1349–1356. https://doi.org/10.1016/j.jhep.2015.01.006.
(370) Praaning-Van Dalen, D. P.; Brouwer, A.; Knook, D. L. Clearance Capacity of Rat Liver Kupffer, Endothelial, and Parenchymal Cells. *Gastroenterology* **1981**, *81* (6), 1036–1044. https://doi.org/10.1016/S0016-5085(81)80009-1.
(371) Heil, M. F.; Dingman, A. D.; Garvey, J. S. Antigen Handling in Ageing. III. Age-Related Changes in Antigen Handling by Liver Parenchymal and Nonparenchymal Cells. *Mech. Ageing Dev.* **1984**, *26* (2–3), 327–340. https://doi.org/10.1016/0047-6374(84)90104-0.
(372) Yamano, T.; DeCicco, L. A.; Rikans, L. E. Attenuation of Cadmium-Induced Liver Injury in Senescent Male Fischer 344 Rats: Role of Kupffer Cells and Inflammatory Cytokines. *Toxicol. Appl. Pharmacol.* **2000**, *162* (1), 68–75. https://doi.org/10.1006/taap.1999.8833.
(373) Videla, L. A.; Tapia, G.; Fernández, V. Influence of Aging on Kupffer Cell Respiratory Activity in Relation to Particle Phagocytosis and Oxidative Stress Parameters in Mouse Liver. *Redox Rep.* **2001**, *6* (3), 155–159.

https://doi.org/10.1179/135100001101536265.
(374) Caperna, T. J.; Garvey, J. S. Antigen Handling in Aging II. The Role of Kupffer and Endothelial Cells in Antigen Processing in Fischer 344 Rats. *Mech. Ageing Dev.* **1982**, *20* (3), 205–221. https://doi.org/10.1016/0047-6374(82)90088-4.
(375) Maeso-Díaz, R.; Ortega-Ribera, M.; Fernández-Iglesias, A.; Hide, D.; Muñoz, L.; Hessheimer, A. J.; Vila, S.; Francés, R.; Fondevila, C.; Albillos, A.; Peralta, C.; Bosch, J.; Tacke, F.; Cogger, V. C.; Gracia-Sancho, J. Effects of Aging on Liver Microcirculatory Function and Sinusoidal Phenotype. *Aging Cell* **2018**, *17* (6), 1–14. https://doi.org/10.1111/acel.12829.
(376) Hunt, N. J.; McCourt, P. A. G.; Kuncic, Z.; Le Couteur, D. G.; Cogger, V. C. Opportunities and Challenges for Nanotherapeutics for the Aging Population. *Front. Nanotechnol.* **2022**, *4* (January), 1–15. https://doi.org/10.3389/fnano.2022.832524.
(377) Berg, T. J.; Dahl-Jørgensen, K.; Torjesen, P. A.; Hanssen, K. F. Increased Serum Levels of Advanced Glycation End Products (AGEs) in Children and Adolescents with IDDM. *Diabetes Care* **1997**, *20* (6), 1006–1008. https://doi.org/10.2337/diacare.20.6.1006.
(378) Hansen, B.; Svistounov, D.; Olsen, R.; Nagai, R.; Horiuchi, S.; Smedsrød, B. Advanced Glycation End Products (AGEs) Lower the Clearance Function of Hepatic Scavenger Endothelial Cells (SEC). *Int. Congr. Ser.* **2002**, *1245* (C), 125–128. https://doi.org/10.1016/S0531-5131(02)00993-7.
(379) Ashare, A.; Stanford, C.; Hancock, P.; Stark, D.; Lilli, K.; Birrer, E.; Nymon, A.; Doerschug, K. C.; Hunninghake, G. W. Chronic Liver Disease Impairs Bacterial Clearance in a Human Model of Induced Bacteremia. *Clin. Transl. Sci.* **2009**, *2* (3), 199–205. https://doi.org/10.1111/j.1752-8062.2009.00122.x.
(380) Vollmar, B.; Pradarutti, S.; Richter, S.; Menger, M. D. In Vivo Quantification of Ageing Changes in the Rat Liver from Early Juvenile to Senescent Life. *Liver* **2002**, *22* (4), 330–341. https://doi.org/10.1034/j.1600-0676.2001.01631.x.
(381) Connolly, M. K.; Bedrosian, A. S.; Malhotra, A.; Henning, J. R.; Ibrahim, J.; Vera, V.; Cieza-Rubio, N. E.; Hassan, B. U.; Pachter, H. L.; Cohen, S.; Frey, A. B.; Miller, G. In Hepatic Fibrosis, Liver Sinusoidal Endothelial Cells Acquire Enhanced Immunogenicity. *J. Immunol.* **2010**, *185* (4), 2200–2208. https://doi.org/10.4049/jimmunol.1000332.
(382) Martinez-Zubiaurre, I. Contribution of Inflammatory Agents to the Regulation of Receptor-Mediated Endocytosis in Hepatic Sinusoidal Endothelium, Universidad del País Vasco - (España), 1997.
(383) Kindberg, G. M.; Tolleshaug, H.; Gjøen, T.; Berg, T. Lysosomal and Endosomal Heterogeneity in the Liver: A Comparison of the Intracellular Pathways of Endocytosis in Rat Liver Cells. *Hepatology* **1991**, *13* (2), 254–259. https://doi.org/10.1002/hep.1840130209.
(384) Geerts, S. O.; Nys, M.; De Mol, P.; Charpentier, J.; Albert, A.; Legrand, V.; Rompen, E. H. Systemic Release of Endotoxins Induced by Gentle Mastication: Association With Periodontitis Severity. *J. Periodontol.* **2002**, *73* (1), 73–78. https://doi.org/10.1902/jop.2002.73.1.73.
(385) Violi, F.; Cammisotto, V.; Bartimoccia, S.; Pignatelli, P.; Carnevale, R.; Nocella, C. Gut-Derived Low-Grade Endotoxaemia, Atherothrombosis and Cardiovascular Disease. *Nat. Rev. Cardiol.* **2023**, *20* (1), 24–37. https://doi.org/10.1038/s41569-022-00737-2.
(386) Campbell, F.; Bos, F. L.; Sieber, S.; Arias-Alpizar, G.; Koch, B. E.; Huwyler, J.; Kros, A.; Bussmann, J. Directing Nanoparticle Biodistribution through Evasion and Exploitation of Stab2-Dependent Nanoparticle Uptake. *ACS Nano* **2018**, *12* (3), 2138–2150. https://doi.org/10.1021/acsnano.7b06995.
(387) Arias-Alpizar, G.; Koch, B.; Hamelmann, N. M.; Neustrup, M. A.; Paulusse, J. M. J.; Jiskoot, W.; Kros, A.; Bussmann, J. Stabilin-1 Is Required for the Endothelial Clearance of Small Anionic Nanoparticles. *Nanomedicine Nanotechnology, Biol. Med.* **2021**, *34*, 102395. https://doi.org/10.1016/j.nano.2021.102395.
(388) Tsoi, K. M.; MacParland, S. A.; Ma, X.-Z.; Spetzler, V. N.; Echeverri, J.; Ouyang, B.; Fadel, S. M.; Sykes, E. A.; Goldaracena, N.; Kaths, J. M.; Conneely, J. B.; Alman, B. A.; Selzner, M.; Ostrowski, M. A.; Adeyi, O. A.; Zilman, A.; McGilvray, I. D.; Chan, W. C. W. Mechanism of Hard-Nanomaterial Clearance by the Liver. *Nat. Mater.* **2016**, *15* (11), 1212–1221. https://doi.org/10.1038/nmat4718.
(389) Haute, D. Van; Berlin, J. M. Challenges in Realizing Selectivity for Nanoparticle Biodistribution and Clearance: Lessons from Gold Nanoparticles. *Ther. Deliv.* **2017**, *8* (9), 763–774. https://doi.org/10.4155/tde-2017-0057.
(390) Wei, Y.; Quan, L.; Zhou, C.; Zhan, Q. Factors Relating to the Biodistribution & Clearance of Nanoparticles & Their Effects on in Vivo Application. *Nanomedicine* **2018**, *13* (12), 1495–1512. https://doi.org/10.2217/nnm-2018-0040.
(391) Baijal, P.; Periyakoil, V. Understanding Frailty in Cancer Patients. *Cancer J. (United States)* **2014**, *20* (5), 358–366. https://doi.org/10.1097/PPO.0000000000000068.
(392) Balducci, L. Aging , Frailty , and Chemotherapy. **2007**, 7–12.
(393) Thakur, R. S.; Chatterjee, S.; Yadav, R. N.; Gupta, L. Image De-Noising with Machine Learning: A Review. *IEEE Access* **2021**, *9* (1), 93338–93363. https://doi.org/10.1109/ACCESS.2021.3092425.
(394) Cogger, V. C.; McNerney, G. P.; Nyunt, T.; DeLeve, L. D.; McCourt, P.; Smedsrød, B.; Le Couteur, D. G.; Huser, T. R. Three-Dimensional Structured Illumination Microscopy of Liver Sinusoidal Endothelial Cell Fenestrations. *J. Struct. Biol.* **2010**, *171* (3), 382–388. https://doi.org/10.1016/j.jsb.2010.06.001.
(395) Martino, J. Di; Mascalchi, P.; Legros, P.; Lacomme, S.; Gontier, E.; Bioulac-Sage, P.; Balabaud, C.; Moreau, V.; Saltel, F. STED Microscopy: A Simplified Method for Liver Sinusoidal Endothelial Fenestrae Analysis. *Biol. Cell* **2018**, *110* (7), 159–168. https://doi.org/10.1111/boc.201800016.
(396) Mönkemöller, V.; Øie, C.; Hübner, W.; Huser, T.; McCourt, P. Multimodal Super-Resolution Optical Microscopy Visualizes the Close Connection between Membrane and the Cytoskeleton in Liver Sinusoidal Endothelial Cell Fenestrations. *Sci. Rep.* **2015**, *5* (November), 1–10. https://doi.org/10.1038/srep16279.
(397) Bárcena, M.; Koster, A. J. Electron Tomography in Life Science. *Semin. Cell Dev. Biol.* **2009**, *20* (8), 920–930.

https://doi.org/10.1016/j.semcdb.2009.07.008.
(398) Saibil, H. R. Cryo-EM in Molecular and Cellular Biology. *Mol. Cell* **2022**, *82* (2), 274–284. https://doi.org/10.1016/j.molcel.2021.12.016.
(399) Li, P.; Zhou, J.; Li, W.; Wu, H.; Hu, J.; Ding, Q.; Lü, S.; Pan, J.; Zhang, C.; Li, N.; Long, M. Characterizing Liver Sinusoidal Endothelial Cell Fenestrae on Soft Substrates upon AFM Imaging and Deep Learning. *Biochim. Biophys. Acta - Gen. Subj.* **2020**, *1864* (12), 129702. https://doi.org/10.1016/j.bbagen.2020.129702.
(400) Kong, C.; Bobe, S.; Pilger, C.; Lachetta, M.; Øie, C. I.; Kirschnick, N.; Mönkemöller, V.; Hübner, W.; Förster, C.; Schüttpelz, M.; Kiefer, F.; Huser, T.; Schulte am Esch, J. Multiscale and Multimodal Optical Imaging of the Ultrastructure of Human Liver Biopsies. *Front. Physiol.* **2021**, *12* (February), 1–15. https://doi.org/10.3389/fphys.2021.637136.
(401) Julien-Schraermeyer, S.; Illing, B.; Tschulakow, A.; Taubitz, T.; Guezguez, J.; Burnet, M.; Schraermeyer, U. Penetration, Distribution, and Elimination of Remofuscin/Soraprazan in Stargardt Mouse Eyes Following a Single Intravitreal Injection Using Pharmacokinetics and Transmission Electron Microscopic Autoradiography: Implication for the Local Treatment of Star. *Pharmacol. Res. Perspect.* **2020**, *8* (6), 1–10. https://doi.org/10.1002/prp2.683.
(402) Hoyng, C. C. B.; Lotery, A.; Stingl, K.; Boon, C.; Parodi, M.; Dhooge, P.; Peters, T.; Klein, W.; Fsadni, M. G.; Müller, H.; Jungmann, O. Designing a Clinical Trial to Evaluate the Safety and Efficacy of Oral Soraprazan in Stargardt Disease. *Invest. Ophthalmol. Vis. Sci.* **2019**, *60* (9), 5704-undefined.
(403) Federspiel, C. A.; Bertelsen, M.; Kessel, L. Vitamin A in Stargardt Disease—an Evidence-Based Update. *Ophthalmic Genet.* **2018**, *39* (5), 555–559. https://doi.org/10.1080/13816810.2018.1488174.
(404) Senoo, H.; Mezaki, Y.; Fujiwara, M. The Stellate Cell System (Vitamin A-Storing Cell System). *Anat. Sci. Int.* **2017**, *92* (4), 387–455. https://doi.org/10.1007/s12565-017-0395-9.
(405) Larsen, A. K.; Simón-Santamaría, J.; Elvevold, K.; Ericzon, B. G.; Mortensen, K. E.; McCourt, P.; Smedsrød, B.; Sørensen, K. K. Autofluorescence in Freshly Isolated Adult Human Liver Sinusoidal Cells. *Eur. J. Histochem.* **2021**, *65* (4), 1–6. https://doi.org/10.4081/ejh.2021.3337.

Papers I-IV:

Paper I

"The wHole story about fenestrations in LSEC."

Karolina Szafranska, Larissa D. Kruse, **Christopher Florian Holte**, Peter McCourt, and Bartlomiej Zapotoczny.

Frontiers in physiology 12 (2021): 735573.

frontiers in Physiology

REVIEW
published: 13 September 2021
doi: 10.3389/fphys.2021.735573

The wHole Story About Fenestrations in LSEC

Karolina Szafranska[1†], Larissa D. Kruse[1†], Christopher Florian Holte[1†], Peter McCourt[1*] and Bartlomiej Zapotoczny[1,2]

[1] Vascular Biology Research Group, Department of Medical Biology, University of Tromsø – The Arctic University of Norway, Tromsø, Norway, [2] Department of Biophysical Microstructures, Institute of Nuclear Physics, Polish Academy of Sciences, Kraków, Poland

The porosity of liver sinusoidal endothelial cells (LSEC) ensures bidirectional passive transport of lipoproteins, drugs and solutes between the liver capillaries and the liver parenchyma. This porosity is realized via fenestrations – transcellular pores with diameters in the range of 50–300 nm – typically grouped together in sieve plates. Aging and several liver disorders severely reduce LSEC porosity, decreasing their filtration properties. Over the years, a variety of drugs, stimulants, and toxins have been investigated in the context of altered diameter or frequency of fenestrations. In fact, any change in the porosity, connected with the change in number and/or size of fenestrations is reflected in the overall liver-vascular system crosstalk. Recently, several commonly used medicines have been proposed to have a beneficial effect on LSEC re-fenestration in aging. These findings may be important for the aging populations of the world. In this review we collate the literature on medicines, recreational drugs, hormones and laboratory tools (including toxins) where the effect LSEC morphology was quantitatively analyzed. Moreover, different experimental models of liver pathology are discussed in the context of fenestrations. The second part of this review covers the cellular mechanisms of action to enable physicians and researchers to predict the effect of newly developed drugs on LSEC porosity. To achieve this, we discuss four existing hypotheses of regulation of fenestrations. Finally, we provide a summary of the cellular mechanisms which are demonstrated to tune the porosity of LSEC.

Keywords: fenestration, fenestra, nanopores, LSEC, liver sinusoidal endothelial cells, porosity, liver disease, drug response

OPEN ACCESS

Edited by:
Leo A. van Grunsven, Vrije Universiteit Brussel, Belgium

Reviewed by:
Savneet Kaur, The Institute of Liver and Biliary Sciences (ILBS), India
Edward N. Harris, University of Nebraska System, United States

****Correspondence:***
Peter McCourt
peter.mccourt@uit.no

†These authors have contributed equally to this work and share first authorship

Specialty section:
This article was submitted to Gastrointestinal Sciences, a section of the journal Frontiers in Physiology

Received: *02 July 2021*
Accepted: *16 August 2021*
Published: *13 September 2021*

Citation:
Szafranska K, Kruse LD, Holte CF, McCourt P and Zapotoczny B (2021) The wHole Story About Fenestrations in LSEC. Front. Physiol. 12:735573. doi: 10.3389/fphys.2021.735573

INTRODUCTION

Within the human body, the main blood-organ barrier is made up of a single layer of thin endothelial cells. In the liver, the microcirculation has a unique morphology that facilitates bi-directional exchange of substrates between hepatocytes and blood in the liver sinusoids (Cogger and Le Couteur, 2009; Fraser et al., 2012). Liver sinusoidal endothelial cells (LSEC) are very thin and perforated with transcellular pores (50–300 nm in diameter) that are also termed as fenestrae or fenestrations (**Figure 1**). These structures were first correctly identified as such with transmission electron microscopy (TEM) by Yamagishi (1959) and described in detail by Wisse (1970). Between 2 and 20% of the LSEC surface is covered by fenestrations which are either scattered individually across the surface or clustered into groups called sieve plates. As there are no diaphragms or underlying basement membrane, fenestrations make LSEC a highly efficient ultrafiltration system. LSEC thus retain blood cells inside the vessel lumen, whereas small molecules, such as drugs, proteins, lipoproteins, and small viruses can pass this endothelial barrier via fenestrations to reach the surrounding hepatocytes, and vice versa (Fraser et al., 1995a). Fenestrations are therefore a vital structure in liver physiology, providing the primary communication conduit between the liver and the rest of the body, via the circulation. LSEC fenestrations, and the effects of various agents upon them, have been studied extensively with electron microscopy. During the last decade new techniques have been developed and became available to investigate fenestrations in cultured LSEC. Super-resolution optical microscopy provided first detailed information about the composition of fenestration (Cogger et al., 2010, 2013; Mönkemöller et al., 2015; Zapotoczny et al., 2019a) while atomic force microscopy (AFM) provided first information about the dynamics of fenestrations *in vitro* (Zapotoczny et al., 2019b, 2020). Such tools will accelerate the development of therapies that can reverse the loss of fenestrations seen in aging and liver fibrosis (DeLeve, 2015; Hunt et al., 2019).

Fenestration loss during aging manifests as changes in the liver microcirculation, in particular within LSEC, which is a likely cause of dyslipidemia (Le Couteur et al., 2002) and insulin resistance in old age (Mohamad et al., 2016). At the morphological level, LSEC in old age have markedly reduced porosity (percent of the cell surface area covered in fenestrations) by about 50% – in other words, old LSEC become "defenestrated" (**Figure 2**). This defenestration results in hampered bi-directional traffic of substrates between the blood and the hepatocytes. Biomolecules such as lipoproteins, or hormones, or drugs (such as statins or insulin) pass less easily through aged LSEC to reach the hepatocytes to be processed and/or exert their effects. For example, older rats showed a significant reduction in the hepatic volume of insulin distribution (Mohamad et al., 2016), showing that fenestrations facilitate insulin transfer to hepatocytes. Another example is the transfer of lipoproteins across LSEC, which was almost totally abolished in livers from old animals, providing a novel mechanism for age-related dyslipidemia and postprandial hyperlipidemia (Hilmer et al., 2005) and is now accepted as a significant factor in age-related hyperlipidemia (Liu et al., 2015). The same applies in the reverse direction across LSEC – biomolecules produced by the hepatocytes need to pass through fenestrations for release into the plasma, and defenestration hinders this process. Age-related LSEC defenestration is also accompanied by altered expression of many vascular proteins including von Willebrand factor, ICAM-1, laminin, caveolin-1 and various collagens (Le Couteur et al., 2008). However, these changes occur without any age-related pathology of hepatocytes or activation of stellate cells (Warren et al., 2011). The sum of all these processes results in a state whereby liver sinusoidal vessels become more like continuous capillaries, but without the other manifestations seen in diseased livers during "capillarization." Age-related defenestration is therefore also termed "pseudocapillarization." Cellular senescence is one hallmark of aging (Robbins et al., 2021), and (Grosse et al., 2020) proposed that LSEC become senescent at 10–12 months of age in mice, as evidenced by the increased expression of the senescence marker p16. Senolytic drugs (which selectively kill senescent cells) have been proposed as a potential therapy to alleviate the effects of senescent cell mediated aging and disease (Robbins et al., 2021). However, p16^{high} LSEC are essential for mouse healthspan, as ablation of these cells results in disruption of the hepatic sinusoid and liver fibrosis (Grosse et al., 2020).

Defenestration of LSEC also occurs during chronic liver disease, liver fibrosis and consequently cirrhosis, which are an increasing worldwide problem, and are becoming a major cause of morbidity and death (Asrani et al., 2019). Currently, there is no therapy that can alleviate fibrosis progression or reverse fibrosis (Higashi et al., 2017). Fibrosis is characterized by excessive extracellular matrix production from activated stellate cells. In addition to LSEC defenestration, during chronic liver disease, a basement membrane develops in the Space of Disse, leading to the process of capillarization, and thereby further reducing the free passage of substrates to and from the hepatocytes (Poisson et al., 2017). Defenestration of LSEC occurs earlier than the formation of fibrous septa in liver diseases such as alcoholic liver injury and non-alcoholic fatty liver disease (Horn et al., 1987) which could indicate that LSEC can play an important role during the early stages of fibrosis. Restoration of differentiation to LSEC led to quiescence of hepatic stellate cells and regression of fibrosis in thioacetamide challenged rats (Xie et al., 2012b) potentially suggesting that therapies that revert LSEC from a diseased/defenestrated state to a normal state may also be of benefit for treatment of liver fibrosis (DeLeve, 2015).

As mentioned above, defenestration of the liver sinusoidal endothelium impairs the hepatic clearance of pharmacological agents (Mitchell et al., 2011). As for lipoproteins and insulin, fenestrations are conduits for pharmaceuticals, from the plasma to the hepatocytes. Reduction in LSEC porosity thus reduces the passage of drugs to the cells where they are processed and metabolized. This can result in elevated and potentially toxic concentrations of drugs in the elderly (and patients with liver disease), when administering drug doses appropriate for healthy young people. In addition, polypharmacy is becoming a major issue in the aging population, with over 42% of people over 65 years of age were reported being administrated five or more different medications per day (Midão et al., 2018). The majority of these medications need to cross the liver sinusoidal endothelium to be detoxified, and it is possible that some of the polypharmacy "cocktails" are detrimental for LSEC porosity. Another serious consequence of reduced porosity is that statins are less able to reach the hepatocytes and inhibit cholesterol production. Increased statin doses are then required to achieve therapeutic effects, sometimes resulting in side effects such as muscle pain and rhabdomyolysis, resulting in medication non-compliance in patients.

Given the vital role of LSEC fenestrations (and the bi-directional flow of substrates through them) in physiology and homeostasis, a better understanding of how these structures are regulated will enable us to design novel therapeutic approaches targeting biological changes of aging and liver diseases.

It needs to be highlighted, however, that many reports in the literature "suffer" from developing experimental methodologies.

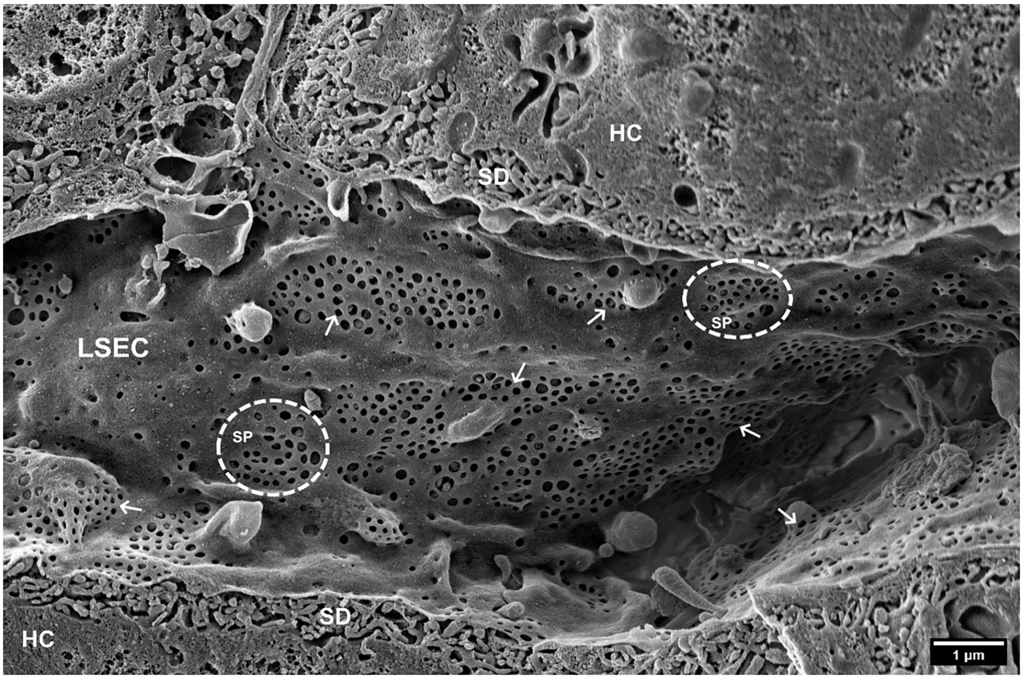

FIGURE 1 | SEM image of hepatic sinusoids of a C57BL6 mouse, approximately 4 months old. Liver Sinusoidal Endothelial Cells (LSECs) are covered in multiple fenestrations (arrows) arranged into sieve plates (SP, dotted line circles) distributed over the whole sinusoid. SD, space of Disse; HC, hepatocytes. (Courtesy of Karen K. Sørensen, UiT, Tromsø, Norway).

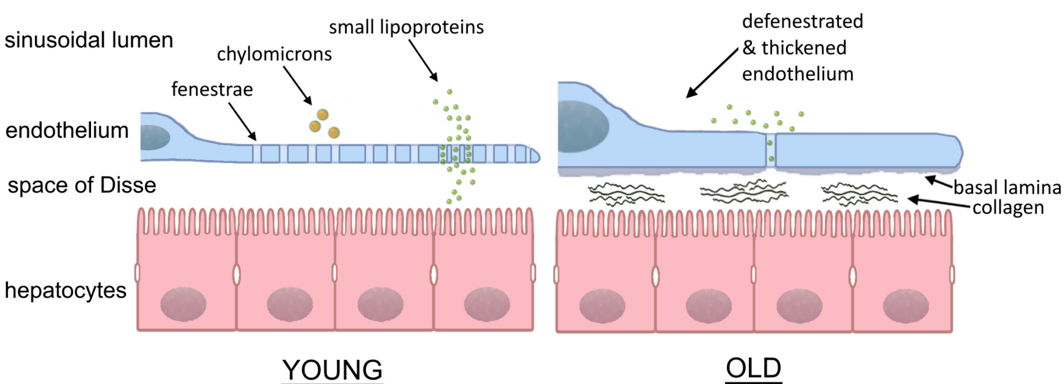

FIGURE 2 | Sinusoidal lumen in young and old liver. With age, the fenestrated morphology of the sinusoids is lost in the process of "pseudocapillarization." Additionally, the endothelium thickens and collagen deposits can be found within the space of Disse. The result is the inhibition of transfer between the blood and hepatocytes. (Courtesy of Eike Struck, UiT, Tromsø, Norway and David Le Couteur, ANZAC Research Institute, Sydney, Australia).

Errors during liver perfusion, cell isolation methodologies and sample preparations may lead to altered cell phenotypes. Also, it should be noted that studies from pre-super-resolution era where light microscopy was the only technique used for quantification of fenestrations may be imprecise. As reported, fenestrations in LSEC are in the range of 50–300 nm, gathered in sieve plates of several to tens of pores, with limited number of gaps (DeLeve and Maretti-Mira, 2017). These can be visualized only using non-diffraction limited methods such as electron microscopy, optical nanoscopy, or atomic force microscopy. The distribution of fenestration diameter in this range was presented for both LSEC in tissue (*in vivo*) and for isolated cells (*in vitro*). *In vivo* data are limited to fixed and dried material, while data for isolated LSEC covers fixed and dried, wet-fixed, and live cells. Recently, we summarized that the differences in mean fenestration diameter for fixed and dried, wet-fixed and live LSECs *in vitro* can be up to 30% (Supplementary Table 1 in Zapotoczny et al., 2019b). The differences between *in vivo* and *in vitro* data can be even larger *ibid*., (Wisse et al., 2010). The comparison between the groups in a single report provides information about the alterations as the same microscopy method is applied. The methodological details enabling avoiding errors in imaging and data analysis were described: SEM (Wisse et al., 2010; Cogger et al., 2015; Szafranska et al., 2021), AFM (Zapotoczny et al., 2017a, 2020; Szafranska et al., 2021), SIM (Kong et al., 2021; Szafranska et al., 2021). Moreover, the comparative measurements using different microscopies were reported in the past showing good correlation between the methods. However, the comparative analysis of newly developed techniques applied recently for LSECs, such as SIM, STED, and AFM, is lacking. Each method has its advantages and limitations. To enable easy tracking of the model (*in vivo/in vitro* and microscopy technique) we provide the relevant information in the presented tables.

The purpose of this review is to: (i) provide a medical and cell biology "tool-kit," for researchers and clinicians to design potential LSEC refenestration strategies and (ii) summarize the existing knowledge around fenestration biology which can help to find new ways to reveal how fenestrations actually work. The first part of this review fucuses on the reported influence of drugs on LSEC fenestration number and porosity, while the second part gives a deeper knowledge about fenestration biology and mechanisms behind structure, formation and maintenance of fenestration. This review does not cover a number of other aspects of LSEC biology, but these can be found in in the following excellent reviews about LSEC in: diseases (Gracia-Sancho et al., 2021; Wang and Peng, 2021), hepatic fibrosis (DeLeve, 2015), mechanotransduction (Shu et al., 2021), inflammation and cancer (Wilkinson et al., 2020; Yang and Zhang, 2021), receptor expression (Pandey et al., 2020), immunological functions (Shetty et al., 2018), aging (Hunt et al., 2019), scavenging (Sørensen et al., 2012), and overall biology of LSECs (Sørensen et al., 2015).

LSEC AND DRUG INTERACTIONS

Recreational and Medicinal Drugs, and Their Effects on LSEC Porosity

The human race already uses an extensive array of drugs for medical and recreational purposes. The majority of these compounds are safe, or at least relatively safe for normal human consumption if used appropriately. Reported negative side-effects of these drugs are typically well-documented at the systemic or organ level, but little is known about their direct effects on LSEC fenestration status. Additionally, some drugs with other intended targets may actually have positive side effects on LSEC fenestration, leading to increased LSEC porosity and improving bi-directional exchange of solutes between hepatocytes and plasma. This concept was first tested by Hunt et al. (2019, 2020) who found that a number of drugs for intended use for the treatment of high blood pressure, erectile dysfunction and diabetes improved LSEC porosity in young and old mice. **Table 1** lists the effects of some recreational and medicinal drugs on LSEC fenestrations.

Recreational Drugs

The effects of recreational drugs on LSEC porosity have not been studied extensively (**Table 1**). The few studies performed showed that the recreational drugs nicotine, ethanol, and cocaine reduce LSEC porosity (Fraser et al., 1988; McCuskey et al., 1993), while the psychedelic drug 2,5-Dimethoxy-4-iodoamphetamine (DOI) increases porosity in LSEC in young and old rodents (Cogger et al., 2014; Hunt et al., 2019). The effects on LSEC porosity of other recreational/non-medicinal drugs such as opioids, amphetamines, cannabis, and xanthines (such as caffeine and theobromine) have, to the best of our knowledge, not been studied. This would be an area of great interest, given the extensive use of all of these among the general population. This is exemplified by opioid use (which is also for medicinal purposes) leading to the current "opioid epidemic" in the US arising from the use of prescription oxycodone. Below is a summary of the reported interactions of ethanol, cocaine, DOI, and nicotine with LSEC.

Ethanol Given the wide use and general acceptance of alcohol, and the suggested health benefits from moderate consumption, it was discussed in the LSEC field whether moderate amounts of alcohol could improve LSEC porosity and thereby lipoprotein clearance. Of the studies (*in vitro* and *in vivo*) investigating the effects of ethanol on LSEC, the majority were performed in rats, but mice, baboons and human LSEC were studied as well, with electron and atomic force microscopy methods used as readout. Several studies reported that the fenestration number was reduced, while the average fenestration diameter was increased – this pattern was consistent in all the *in vitro* studies (Mak and Lieber, 1984; Charles et al., 1986; Van Der Smissen et al., 1986; Horn et al., 1987; Tanikawa et al., 1991; McCuskey et al., 1993; Braet et al., 1994, 1995a, 1996c; de Zanger et al., 1997) and with reduced porosity reported in one study (Takashimizu et al., 1999). Takashimizu et al. (1999) described reduction in fenestration diameter in rat during *in vivo* continuous administration of ethanol into the portal vein, and pre-treatment with **BQ123** [an endothelin (ET) receptor antagonist, see **Table 2**] reduced the effect of ethanol. One *in vivo* study reported no changes in in the liver sinusoids in mice after 9 weeks of ethanol feeding (McCuskey et al., 1993) but ethanol in combination with cocaine caused the sinusoids to become thickened and defenestrated. In other *in vivo* chronic ethanol challenge studies (ethanol given to rats in food, or human studies where biopsies were used), one rat study yielded results consistent with the *in vitro* findings (reduced fenestration number, increased diameter, reduced porosity) (Tanikawa et al., 1991) while the other study reported reduced fenestration diameter and number – this was the only study to find that the diameter became smaller after ethanol challenge (Takashimizu et al., 1999). In the human biopsy study, similar results were obtained - chronic alcohol consumption (defined as $>$ 60 g alcohol intake every day for more than 3 years) resulted in fewer fenestrations, diameters of between 50–300 nm and a "visible difference" for porosity between the two groups. A study in baboons showed that the duration of alcohol consumption does not seem to have any impact on fenestrations (diameter in second group (4–24 months alcohol consumption vs. 61–112 months) was larger than control but smaller than first group) (Mak and Lieber, 1984). In summary, ethanol at any dose does not appear to improve LSEC porosity but rather has the opposite effect.

TABLE 1 | Influence of medicinal drugs on LSEC fenestrations.

	Fenestration diameter	Porosity	Fenestration frequency	References	Methods
Recreational drugs					
Ethanol	+/-	-	-	Van Der Smissen et al., 1986; Braet et al., 1995a	SEM, TEM, *in vitro*
				Mak and Lieber, 1984; Charles et al., 1986; de Zanger et al., 1997	SEM, *in vivo*
				Tanikawa et al., 1991; McCuskey et al., 1993	TEM, *in vivo*
				Horn et al., 1987; Takashimizu et al., 1999	SEM, *in vivo*
				Braet et al., 1996c	SEM, AFM, *in vitro*
				Braet et al., 1994	SEM, *in vitro*
Ethanol +cocaine	nd	-	-	McCuskey et al., 1993	TEM, *in vivo*
Cocaine	nd	nd	nd	McCuskey et al., 1993	TEM, *in vivo*
2,5-Dimethoxy-4-iodoamphetamine (DOI)	+	+/-	+/-	Furrer et al., 2011; Cogger et al., 2014	SEM, *in vivo*
				Hunt et al., 2019	SEM *in vitro*
Nicotine	-	- -	-	Fraser et al., 1988	SEM, *in vivo*
Prescription drugs					
Acetaminophen/ paracetamol +ethanol	G	nd	nd	McCuskey et al., 2004	SEM, TEM, *in vivo*, *in vitro*
Acetaminophen/ paracetamol	G	-	-	Ito et al., 2006b	SEM, *in vivo*
				Walker et al., 1983	SEM, TEM, *in vivo*
				McCuskey et al., 2004; McCuskey, 2006	SEM, TEM, *in vivo*, *in vitro*
Amlodipine	-	+	+	Hunt et al., 2019	SEM, *in vitro*
Bosentan	0	+	+	Hunt et al., 2019	SEM, *in vitro*
Colchicine	nd	nd	0	Braet et al., 1996b	TEM, *in vitro*
Disulfiram	-	nd	+	Bernier et al., 2020	SEM, *in vivo*
Metformin	0	+	+	Hunt et al., 2020	SEM, *in vitro*, *in vivo*
				Alfaras et al., 2017	SEM, *in vivo*
Nicotinamide mononucleotide (NMN)	0	+	+	Hunt et al., 2019	SEM, *in vitro*
				Mao et al., 2019	dSTORM, *in vitro*
Cholesterol	0	0	0	Fraser et al., 1988, 1989	SEM, *in vivo*
Cholesterol +nicotine	-	-	-	Fraser et al., 1988	SEM, *in vivo*
Pantethine + cholesterol	+	+	+	Fraser et al., 1989	SEM, *in vivo*
Prostaglandin E1	+			Oda et al., 1997	SEM, TEM, *in vitro*
Sildenafil	0/+	++	+	Hunt et al., 2019	SEM, *in vitro*
				Mao et al., 2019	dSTORM, *in vitro*
Simvastatin	+	+	+	Hide et al., 2020	SEM, TEM, *in vivo*, SEM, *in vitro*
				Venkatraman and Tucker-Kellogg, 2013; Hunt et al., 2019	SEM, *in vitro*
Taxol	nd	nd	0	Braet et al., 1996b	TEM, *in vitro*
TNF-related apoptosis-inducing ligand (TRAIL)	+/0	+/0	+/0	Hunt et al., 2019	SEM, *in vitro*

"0," no change; G, gaps; increase: "+," <50%; "++," 50–100%; "+++," >100%; decrease: "-," <50%; "- -," >50%; "- - -," defenestration; "nd," no data.

Cocaine is a widely used recreational drug with vasoconstricting properties (Kim and Park, 2019), often consumed in combination with alcohol. In a study from McCuskey et al. (1993), mice challenged with cocaine alone developed basement membrane deposition in the space of Disse, some hepatocellular necrosis and slightly reduced centrilobular sinusoid blood flow after 5 weeks, worsening up to 9 weeks of challenge. In combination with ethanol these changes were significantly exacerbated, in addition the sinusoidal endothelium was thickened and defenestrated. Interestingly rats were more resistant to these challenges, only developing some of these changes at the end of the 15-week treatment regime. The

TABLE 2 | Influence of hormones and other agents acting on LSEC fenestrations.

	Fenestration diameter	Porosity	Fenestration frequency	References	Methods
Vasoactive stimuli					
Vasodilators					
Acetylcholine	+	nd	nd	Tsukada et al., 1986; Oda et al., 1990	SEM, *in vivo*, *in vitro*
Bethanechol	+	nd	nd	Oda et al., 1990	SEM, *in vivo*
Isoproterenol	+	nd	nd	Oda et al., 1990	SEM, *in vivo*, *in vitro*
Vasoactive intestinal peptide (VIP)	+	nd	nd	Oda et al., 1990	SEM, *in vivo*
BQ-123	++	nd	-	Watanabe et al., 2007	SEM, TEM, *in vivo*
Vasoconstrictors					
Endothelin (ET)	-	-	nd	Oda et al., 1997; Kamegaya et al., 2002	SEM, *in vitro*
Neuropeptide Y	-	nd	nd	Oda et al., 1990	SEM, *in vivo*
Norepinephrine/ noradrenaline	-	nd	nd	Tsukada et al., 1986; Oda et al., 1990	SEM, *in vivo*, *in vitro*
				Wisse et al., 1980	TEM, SEM, *in vivo*
Serotonin	-	nd	nd	Wisse et al., 1980; Braet et al., 1995a	SEM, TEM, *in vivo*
				Tanikawa et al., 1991	TEM, *in vivo*
				Braet et al., 1996c	SEM, AFM, *in vitro*
				Kalle et al., 1997	AFM, *in vitro*
Pilocarpin	-	nd	nd	Wisse et al., 1980	TEM, SEM, *in vivo*
Adrenaline/ epinephrine	-	nd	nd	Wisse et al., 1980	TEM, SEM, *in vivo*
Signaling/Maintenance					
Vascular endohelial growth factor (VEGF)	+	+++	++	Funyu et al., 2001; Yokomori et al., 2003	SEM, *in vitro*
				Carpenter et al., 2005	SEM, TEM, *in vivo*
				Xie et al., 2012b	SEM, *in vivo*, *in vitro*
Bone morphogenetic protein (BMP)	Strain specific	Strain specific	Strain specific	Desroches-Castan et al., 2019a,b	(a) SEM, *in vivo*, *in vitro* (b) SEM, *in vitro*
Platelet derived growth factor (PDGF-B) signaling	nd	-	nd	Raines et al., 2011	TEM, *in vivo*
Liver X receptor (LXR)	NA	NA	NA	Xing et al., 2016	SEM, TEM, *in vivo*
Hedgehog (Hh) signaling	nd	-	nd	Xie et al., 2012a	SEM, *in vitro*
Plasmalemma vesicle associated protein (PLVAP)	+/-	+/-	+/-	Herrnberger et al., 2014	SEM, TEM, *in vivo*
				Auvinen et al., 2019	SEM, *in vivo*

"0," no change; G, gaps; "nd," no data; "NA," not applicable. increase: "+," <50%; "++," 50–100%; "+++," >100%; decrease: "-," <50%; "- -," >50%; "- - -," defenestration.

mechanism(s) by which cocaine and cocaine/ethanol challenge elicit these changes remains to be elucidated, but in any case the combined abuse of these drugs raises particular concerns with regards to liver function.

Nicotine is the primary stimulant found in tobacco products and is also a known vasoconstrictor (Benowitz and Burbank, 2016). Rats fed nicotine (dose equivalent to 50–100 cigarettes per day in humans for 6 weeks) had LSEC porosity 40% of that of controls, primarily as a function of reduced average fenestration diameter and not of reduced fenestration number. The nicotine treated animals also had near 50% higher serum cholesterol than controls, probably as a consequence of reduced LSEC porosity and thereby filtration of low-density lipoprotein (LDL) out from the plasma of these animals (Fraser et al., 1988). Nicotine and cholesterol fed animals had similar porosity and diameter to nicotine-fed only animals. Together with results from cholesterol-only fed animals (no visible changes), it suggests that nicotine (but not cholesterol) has an effect on fenestrations (Fraser et al., 1988). Other studies have shown that oral nicotine induces an atherogenic lipoprotein profile (Cluette-Brown et al., 1986) (including increased plasma LDL) and impairs plasma LDL clearance (Hojnacki et al., 1986). The mechanism of action of nicotine in the LSEC context remains to be elucidated but given the continued consumption of nicotine by humans in various forms (e.g., tobacco products, e-cigarettes, and nicotine supplements) this field warrants further study.

2,5-Dimethoxy-4-iodoamphetamine (DOI) is a substituted amphetamine but is not a stimulant. It is a potent 5-HT_{2A} serotonin receptor agonist and is used recreationally as a hallucinogenic drug (Lapoint et al., 2013). DOI induces cutaneous vascular constriction in rabbits and rats, and this is the suggested cause of hyperthermia resulting from serotonin receptor stimulation (Blessing and Seaman, 2003). DOI has reported beneficial effects on survival, liver regeneration and LSEC morphology after partial hepatectomy (Tian et al., 2011). Furrer et al. (2011) showed that *in vivo* DOI challenge increased porosity in old but not young LSEC, and pre-treatment of old mice with DOI prior to partial hepatectomy resulted in LSEC with improved porosity (Furrer et al., 2011). However, the finding that DOI improved porosity in aged LSEC is at odds with the *in vivo* study of Cogger et al. (2014) who found that DOI improved LSEC porosity in young but not old animals. Both studies used SEM of tissue blocks to quantify fenestrations. Further complicating the DOI story, SEM *in vitro* studies by Hunt et al. (2019) on cultured LSEC from young and old mice revealed that DOI challenge increased porosity in old but not young LSEC, and this increase was most likely a function of increase in both fenestration diameter and frequency. LSEC respond to ligands for the 5-HT2 receptor, as they were reported to being inhibited by ketanserin (a selective 5-HT2 receptor antagonist) (Gatmaitan et al., 1996). The role of 5-HT2A and 2B receptors was proposed as being involved in liver regeneration after liver partial hepatectomy (Lesurtel et al., 2006). Similarly, the presence of the 5HT2 receptor was later highlighted (Braet and Wisse, 2002; Braet, 2004). However, newly reported data showed that known 5-HT receptor mRNAs were absent or at very low levels in mouse, rat and human LSEC (Bhandari et al., 2020). It would thus be of interest to resolve the question of DOI mediated effects, the downstream mechanisms, and whether there is/are age-related responses to DOI.

Medicinal Drugs

Pharmaceutical treatment and prevention of diseases is constantly evolving, with an increasing number of novel medicines entering the market every year. It was reported that the EU retail pharmaceutical bill was around EUR 190 billion in 2018 (OECD/European Union, 2020). Hepatic clearance and metabolism are the basic routes of removing drugs from the system. With decreased porosity prolonged circulation of drugs increases their side effects. Nitric oxide (NO)-based drug therapy was shown to have beneficial effects on the liver (Maslak et al., 2015) and detailed studies on isolated cells confirm the positive role of NO on fenestrated morphology in LSEC (Xie et al., 2012b). Medicinal drugs with other intended targets may also affect LSEC. A recent comparative study revealed the different drug effects on fenestrations in LSEC in an age-related manner (Hunt et al., 2019). Here we summarize the effects of various medicines where fenestration number and size were reported.

Amlodipine is a calcium channel blocker used to treat hypertension by dilating blood vessels to reduce blood pressure. Amlodipine is also reported to increase endothelial NO (Xu et al., 2002; Mason et al., 2014). Hunt et al. (2019) reported that amlodipine increased the porosity in cultured LSEC from both young and old animals and proposed that this increase was more likely mediated by NO production than by calcium transport blockage. This safe and commonly used blood pressure medicine may thus also represent a pharmacological means to counteract age-related defenestration.

Bosentan is a competitive antagonist of endothelin -A and -B receptors, and is used to treat moderate pulmonary hypertension, exerting its vasodilative effect via ET-A receptors (Bacon et al., 1996). Endothelin-1 (ET-1) constricts fenestrations pronouncedly and reduces porosity (Kamegaya et al., 2002), and an ET-B receptor antagonist (BQ788) blocked this effect while an ET-A receptor antagonist (BQ485) partially blocked the ET-1 effect (Kamegaya et al., 2002). The ET-A receptor antagonist **BQ123** increased fenestration diameters, but caused major gaps in sinusoidal cells and fusions of fenestrations within sieve plates (Watanabe et al., 2007). Hunt et al. (2019) demonstrated that lower doses of bosentan increased the porosity of LSEC from old mice, while LSEC from younger mice were non-responsive. Bosentan treatment of LSEC did not elicit an increase in NO production in this study.

Colchicine is used as a therapy for gout and familial Mediterranean fever. It decreases inflammation but its pharmacotherapeutic mechanism of action is not fully understood – its main mechanism of action is tubulin disruption (Leung et al., 2015). Treatment of cultured rat LSEC with 200 μM colchicine did not affect porosity while causing significant loss of microtubules. Interestingly, the microtubules surrounding sieve plates were still present (Braet et al., 1996b). Together with the effect of taxol, which completely disrupts microtubules and prevents cytochalasin-mediated induction of fenestrations, this would suggest that tubulin architecture may have a crucial role in LSEC porosity. **Taxol** (generic name paclitaxel) is a microtubule-stabilizing drug used for the treatment of ovarian, breast, and lung cancer, as well as Kaposi's sarcoma (Weaver, 2014). Braet et al. (1996b) challenged cultured rat LSEC with 10 μM taxol and saw no change in porosity but reported an overabundance of microtubules throughout the cytoplasm, and alongside sieve plates. Moreover, treatment with 10 μM taxol not only did not show a significant change in fenestration number but pretreatment with taxol and two hours later with cytochalasin B, inhibits the effect of the latter, i.e., the increase in fenestration number is reduced in comparison to treatment with cytochalasin B only.

Disulfiram (commercial name Antabuse) is a FDA approved treatment for chronic alcohol addiction. It is an inhibitor of acetaldehyde dehydrogenase and causes the feeling of a hangover immediately upon alcohol consumption (Suh et al., 2006). It is an inhibitor of the transcription factor NF-KB (Schreck et al., 1992) which contributes to its anti-inflammatory properties. In the experimental setting, the consumption of disulfiram was found to normalize body weight in mice. It was also found to increase the frequency of LSEC fenestrations *in vivo*, while decreasing their average diameter, resulting in no net increase in porosity in mice and rats (Bernier et al., 2020). The mechanism(s) by which disulfiram increases fenestration number remain to be elucidated.

Metformin is a first line treatment for type II diabetes for serum glucose reduction (Maruthur et al., 2016). The mechanism by which this drug exerts this effect remains to be elucidated, but its primary target appears to be hepatocyte mitochondria via inhibition of complex I of the respiratory chain. Inhibition of gluconeogenesis (Owen et al., 2000) results in the activation of the energy sensor AMP-activated protein kinase (AMPK) leading to increased beta-oxidation of fatty acids. Alfaras et al. (2017) tested 1% metformin administered every-other-week or 2-weeks-every-month to mice – these strategies being chosen to avoid metformin induced nephrotoxicity. They found numerous health benefits, particularly with the every-other-week regime, and that the every-other-week approach also increased porosity in LSEC in 2-year-old mice. Metformin (50 μM) increased LSEC porosity *in vitro* in both young and old mice by 25 and 50%, respectively (Hunt et al., 2020). This increase was due to increases in fenestration frequency (20 and 50%, respectively) since the fenestration diameter remained unchanged. *In vivo* studies in mice treated with 0.1% metformin in their diet increased LSEC porosity/fenestration frequency in young and old mice and reduced the age-related loss of porosity in older mice by 50% (Hunt et al., 2020). The mechanism of metformin action in LSEC, with regards to fenestration status, remains to be established.

Nicotinamide mononucleotide (NMN) is a key nicotinamide adenine dinucleotide (NAD+) intermediate. Long-term administration of NMN is reported to mitigate age-related physiological decline in mice (Mills et al., 2016), while short term *in vitro* treatment reverses endothelial dysfunction (Mateuszuk et al., 2020). NMN increased LSEC porosity in young and old mice, via increased fenestration frequency, while the average fenestration diameter was essentially unchanged (Hunt et al., 2019). NMN challenge had no apparent effects on NOS or cGMP levels in LSEC. Analysis of NMN challenged LSEC using direct stochastical optical reconstruction microscopy (dSTORM) revealed that the F-actin within LSEC was more condensed and that the actin rings delineating fenestrations became more pronounced (Mao et al., 2019). The mode of NMN action in LSEC remains to be elucidated – NAD + associates with sirtuins which play a critical role in multiple cellular functions (Imai and Yoshino, 2013) so the study of the role of sirtuins in fenestration biology is therefore warranted.

Pantethine is a derivative of vitamin B5 and has been suggested as a therapy for reducing LDL levels (Rumberger et al., 2011). Fraser et al. (1989) studied the effect of pantethine in cholesterol fed rabbits. The pantethine plus cholesterol fed animals had higher LSEC porosity, fenestration diameter and frequency and lower total cholesterol than the animals fed cholesterol alone. **Cholesterol** feeding had no effect on LSEC porosity. The same result had been found in another study (Fraser et al., 1988). Unfortunately, there was no group fed only pantethine, so it would be interesting to establish if pantethine alone increases LSEC porosity and if this can explain (in part) the reported pantethine-mediated reduction of plasma LDL seen in other studies (Fraser et al., 1989; Rumberger et al., 2011).

Paracetamol (also known as acetaminophen or commercially as APAP, Panadol) is one of the most widely used analgesic medicines. Acute overdoses of paracetamol can cause lethal liver damage, due to the toxic metabolite *N*-acetyl-*p*-benzoquinone imine (NAPQI) (Hodgman and Garrard, 2012). The consensus is that, *in vivo*, paracetamol reduces rodent LSEC porosity both via reduction of fenestration diameter and frequency at "clinical" doses (Walker et al., 1983; McCuskey et al., 2004; McCuskey, 2006; Ito et al., 2006b). The *in vitro* effect of paracetamol on LSEC was reported to be dependent on NAPQI induced depletion of glutathione levels. In C3H mice, acetaminophen is directly toxic to LSEC via P450 activation, while in Swiss Webster mice the toxic effect on LSEC was indirectly driven by hepatocytes (DeLeve et al., 1997). APAP-induced LSEC injury precedes hepatocellular injury, supporting the hypothesis that LSECs are an early and direct target for APAP toxicity. These findings also suggest that reduced sinusoidal perfusion and increased Kupffer cell activity contribute to the development of APAP-induced liver injury (Ito et al., 2003). Although it was presented that large gaps are formed and the porosity is reduced in LSEC *in vivo*, the effects of paracetamol challenge on LSEC porosity *in vitro* have not been reported.

Prostaglandin E1 (synthetic form: alprostadil) is a naturally occurring eicosanoid used as vasodilator for several different medical purposes (Kirtland, 1988). Applications include erectile dysfunction (ED) treatment in men who do not respond to PDE5 inhibitors (Hanchanale and Eardley, 2014) and the opening of ductus arteriosus in neonates requiring heart surgery (Singh and Mikrou, 2018). Prostaglandin E1 exerts its effect via the production of nitric oxide which stimulates soluble guanylyl cyclase to increase production of cyclic GMP (cGMP) and/or by the direct binding of prostaglandin to prostaglandin receptors, activating adenylyl cyclase to convert ATP to cyclic AMP (cAMP). The end result is the same in either pathway - decreased intracellular Ca^{2+} (Namkoong et al., 2005). Oda et al. (1997) showed that prostaglandin E1 significantly increased LSEC fenestration diameter in rat LSEC and also caused partial fusion of some fenestrations within sieve plates. They also reported increased Ca^{2+}-ATPase on fenestral plasma membrane after prostaglandin E1 challenge and postulated that cytoplasmic Ca^{2+} efflux caused relaxation (and thereby dilation) of LSEC fenestrations.

Sildenafil (also known as Viagra) is a vasoactive agent used for the treatment of ED. It is a potent and selective inhibitor of cGMP-specific phosphodiesterase (PDE) type 5, due to its structural similarity to cGMP (Bender and Beavo, 2006). Sildenafil increases cGMP levels by inactivating PDEs that metabolize cGMP to GMP as well as by blocking ABCC5 transport protein responsible for active efflux of cGMP from the cell (Aronsen et al., 2014). cGMP is an intracellular mediator of the NO pathway that can lead to relaxion of the vascular smooth muscle (vasodilation) and thereby increase blood flow (Denninger and Marletta, 1999). Hunt et al. (2019) challenged LSEC from young (3–4 months) and old (18–25 months) mice with sildenafil and found that porosity and fenestration frequency (but not diameter) increased in LSEC from young and old mice. Sildenafil also increased cGMP levels, NO synthesis and levels of phosphorylated nitric oxide synthase (pNOS). Mao et al. (2019) also challenged LSEC (from young mice) and found that the actin rings (which delineate fenestrations) and actin stress fibers became more pronounced. In contrast to Hunt et al. (2019) and Mao et al. (2019) found that sildenafil increased fenestration diameter on average by 30%. This inconsistency might be due to the methods used – the first study used SEM to score LSEC morphology after dehydration, while the second study used dSTORM on "wet" LSEC samples. Sildenafil (and other PDE and ABC transporters inhibitors) may be an interesting therapeutic option to increase LSEC porosity in the elderly.

Simvastatin is a cholesterol lowering agent. Its cholesterol reducing action is via inhibition of 3-hydroxy-3-methylglutaryl (HMG) coenzyme A reductase, the rate limiting enzyme in cholesterol synthesis. Simvastatin also upregulates NO levels suggesting vascular protective effects beyond cholesterol reduction (de Sotomayor et al., 2005; Rikitake and Liao, 2005). Hide et al. (2020) reported that simvastatin was somewhat protective against warm ischemia reperfusion induced LSEC defenestration in (male Wistar) rats, so simvastatin may be able to provide a protective role in maintenance of porosity. Venkatraman and Tucker-Kellogg (2013) showed that simvastatin can antagonize Rho/ROCK (Rho-associated protein kinase) signaling, protecting from the defenestration resulting from activation of this pathway. Moreover, simvastatin treatment led to increase on both porosity and fenestration frequency in (male Wistar) rats. Interestingly these results in rats were not replicated in mice. Findings of Hunt et al. (2019) in (male C57/BL6) mice showed no significant changes in porosity or fenestration frequency in young or old mice, and only a 20% increase in mean diameter in the aged group. These findings may suggest species dependent difference in the simvastatin mechanism of action.

TRAIL [tumor necrosis factor (TNF)-related apoptosis-inducing ligand] is a protein ligand reported to induce cell death in transformed cells by binding to "death receptors" (Wiley et al., 1995). It is also reported to induce NO production *via* eNOS (Bartolo et al., 2015). Hunt et al. (2019) reported that LSEC challenged with lower doses of TRAIL increased LSEC porosity and fenestration frequency in young but not old mice. The lack of TRAIL response of old mice LSEC could be explained by reduced expression of TRAIL receptors in older mouse LSEC, but the level of TRAIL receptor expression in young vs. old mice remains to be determined.

Hormones and Other Agents Acting on LSEC

LSEC and Vasoactive Agents

Vasoactive signaling molecules commonly act through a receptor induced relaxation in the smooth muscle surrounding the vasculature (Webb, 2003). Signaling is mostly mediated by the NO/cGMP pathway and via intracellular calcium concentrations (Chen et al., 2008). Crucially, whether a stimuli directs toward constriction or relaxation will depend on the tissue specific expression of certain receptors and the presence or absence of inhibition of parallel pathways.

Hepatic sinusoids lack smooth muscle cells but can dilate and contract responding to various vasoactive agents. Moreover, according to the two main studies addressing this issue (Oda et al., 1990; Gatmaitan et al., 1996), LSEC porosity and fenestration diameter seem to correlate with vasodilation or vasoconstriction (**Table 2**). These results suggest that vasodilators and vasoconstrictors have a direct effect upon the fenestrations of LSEC. The lack of super resolution techniques for living cells was one of the main drawbacks at the time of these studies of vasoactive agents' effects on LSEC. It will be therefore beneficial for the field investigate the role of vasoconstriction and dilation in fenestration regulation using live cell imaging techniques, such as AFM, SIM or stimulated emission depletion microscopy (STED).

Vasodilators

Acetylcholine is a vasodilator acting through the cholinergic/muscarinic receptor (Sakai, 1980). In LSEC acetylcholine dilates sinusoids increasing blood flow rate and increasing fenestration diameter (Oda et al., 1990), when administered intravenously. On the other hand, **cholinergic receptor agonists** were also noted to cause narrowing of the sinusoids: **bethanechol, carbachol,** and **pilocarpine** applied topically to the liver caused constriction of the liver microvasculature, but fenestrations were not quantified (Reilly et al., 1982; McCuskey and Reilly, 1993). To further complicate these findings, intravascular admission of pilocarpine decreased while bethanechol increased the fenestration diameter. These differences in the effects can be explained by the expression of certain receptors responding to the same stimuli but having contradictory effects, however, further studies are needed. **Bethanechol** is already used as a therapy for postoperative and postpartum non-obstructive urinary retention, it would therefore be of interest to further study its effects on LSEC porosity (Oda et al., 1990). **Vasoactive intestinal peptide (VIP)** is a class II G-protein coupled receptor ligand (Umetsu et al., 2011). It has multiple physiological effects including vasodilation and increased gut motility during digestion (Iwasaki et al., 2019). VIP was shown to dilate the sinusoids and fenestra, increasing blood flow through the sinusoids which would enhance the uptake of circulating nutrients after a meal (Oda et al., 1990). **Isoprenaline** (also known as isoproterenol) is another vasodilating agent acting as a β-adrenergic receptor agonist. This G-protein is essential for cardiac function (reviewed in Wachter and Gilbert, 2012) and is used to treat bradycardia and (rarely) asthma. The effect on LSEC follows that of other of vasodilating agents increasing in both sinusoidal blood flow and fenestration diameter (Oda et al., 1990).

Vasoconstrictors

Serotonin (also known as 5-HT) is a monoamine neurotransmitter with numerous physiological functions (Berger et al., 2009). Depending on the particular receptors expressed in each vessel wall and surrounding smooth muscle tissue, serotonin can cause vasoconstriction or vasodilation in different vascular beds (Kaumann and Levy, 2006). In the liver, serotonin constricts sinusoids and reduces fenestration size (Wisse et al., 1980; Oda et al., 1990). Gatmaitan et al. (1996)

showed that the effect is mediated by decreasing cAMP and increasing intracellular calcium levels in a matter of seconds. **Endothelin (ET)** is a vasoconstricting peptide that is produced in the endothelium and plays an important role in vascular homeostasis (Kawanabe and Nauli, 2011). In LSEC, it decreases both the number and the size of fenestrations (Kamegaya et al., 2002; Yokomori et al., 2006) and it reduces the blood-flow through the sinusoids (Zhang et al., 1994). Many ET receptor antagonists are used as an efficient treatment for hypertension. ET-A receptor antagonist (**BQ-123**) treatment (but not ET-B receptor antagonists) abolished ET induced defenestration and contraction of fenestrations (Yokomori et al., 2006). Blocking ET-1 activity *in vivo* by BQ-123 led to gap formation shown by SEM and TEM (Watanabe et al., 2007). The α-adrenergic receptor family mediates vasoconstriction and is coupled to guanine nucleotide regulatory proteins (G-proteins) (reviewed in Ruffolo and Hieble, 1994). α-**adrenergic receptor agonists** were found to have different effects on LSEC, **epinephrine** (adrenaline) decreased sinusoidal blood flow and contracted sinusoids and LSEC fenestrations (Oda et al., 1990), while in another study sinusoids were found slightly enlarged, and fenestrations unchanged (Wisse et al., 1980). **Norepinephrine** (noradrenaline) was found to contract sinusoids and fenestrations in both studies (Wisse et al., 1980; Oda et al., 1990). **Neuropeptide Y (NPY)**, another vasoconstrictor generally coupled to G-protein signaling, is involved in various physiological and homeostatic processes (White, 1993) but also inhibits gastrointestinal motility (Holzer et al., 2012). In LSEC, NPY constricts both sinusoid and fenestrations (Oda et al., 1990).

Signaling and Fenestration Maintenance

One of the most challenging aspects of studying LSEC is the dedifferentiation *in vitro* after cell extraction. LSEC lose their characteristic porous morphology after just few days in culture, significantly restricting time for experiments. There have been many attempts to slow down, stop or reverse that process (Bravo et al., 2019; Di Martino et al., 2019) but the main mechanism(s) behind the loss of fenestrations remain unknown.

Vascular Endothelial Growth Factor (VEGF) is a hormone that stimulates acetogenesis and angiogenesis (Apte et al., 2019). In LSEC, VEGF has been shown to increase LSEC porosity *in vitro* (Funyu et al., 2001; Yokomori et al., 2003) as well as to prolong the fenestrated phenotype of cultured LSEC *in vitro* (Xie et al., 2012b). Downregulation of VEGF signaling has been associated with LSEC defenestration, capillarization of sinusoids, and abnormal liver physiology (Carpenter et al., 2005; DeLeve, 2015). DeLeve (2015) showed that VEGF promotes fenestration formation/maintenance *via* NO-dependent and NO-independent pathways. Moreover, VEGF can induce fenestration like structures in other microvasculature, e.g., rat cremaster capillary (Roberts and Palade, 1995).

Bone Morphogenetic Protein 9 (BMP9, also known as GDF2) is a circulating endothelial quiescence factor (David et al., 2008). In LSEC it has been indicated as necessary for fenestration maintenance and treating cells with BMP9 prolonged fenestrated phenotype in cultured LSEC (Desroches-Castan et al., 2019a). BMP9 knockouts in 129/Ola mice showed very low fenestration frequency compared to WT, without changes to diameters (Desroches-Castan et al., 2019a). However, a follow up study using C57/Black mice did not confirm these results (Desroches-Castan et al., 2019b).

Platelet derived growth factor B (PDGF) is a member of the PDGF family of major mitogens for many cell types (Fredriksson et al., 2004). Hepatic vascular permeability was highly increased in PDGF-B retention deficient mice, with a three-fold increase in FITC-dextran absorption and a more fenestrated phenotype (Raines et al., 2011). PDGF-B signaling is involved in pericyte recruitment and function, and stellate cell activation (Raines et al., 2011).

Liver X receptor (LXR) is a nuclear receptor expressed in a number of tissues, but with highest expression in the liver (Willy et al., 1995). Oxysterols are natural ligands of LXR and LXR deletion exacerbates CCl_4 induced capillarization and basement membrane deposition (Xing et al., 2016). LXR also acts antagonistically on Hedgehog signaling (Hh) (Kim et al., 2009), while LSEC produce and respond to Hh ligands and use Hh signaling to regulate complex phenotypic changes that occur during capillarization. Moreover, inhibition of Hh using **cyclopamine** induced fenestration *in vitro* (Xie et al., 2012a).

Plasmalemma vesicle-associated protein (PLVAP) is associated with angiogenesis and vascular permeability, with less expression in barrier endothelium, and its expression is stimulated by VEGF (Bosma et al., 2018). PLVAP was found to be associated with a normally fenestrated phenotype, while PLVAP deficient mice present extremely low porosity and accumulation of collagen in the space of Disse (Herrnberger et al., 2014). Auvinen et al. (2019) found that there was no difference in number of fenestrations in PLVAP–/– mice, though their data shows greater variability in the knockouts. Both studies used SEM of tissue blocks for quantitative analysis of fenestrations. The difference may relate to the methods used to attain the knockouts raising the question of either knockouts being too broad/non-specific or insufficient. PLVAP mutations are associated with loss of fenestration diaphragms in other tissues (such as small intestine) (Elkadri et al., 2015).

Lab Tools and Experimental Models

Experimental Animal Models for the Study of LSEC Fenestrations

Liver sinusoidal endothelial cells are the first line of defense in the liver and alterations in LSEC play a crucial role in the development of many liver diseases such as fibrosis, cirrhosis, or cancer (Gracia-Sancho et al., 2021) as well as in the age-related conditions (Hunt et al., 2018). To better understand this role, many animal models have been used. Challenge with certain drugs can mimic the development of these diseases and reduce the time and/or costs compared to waiting for them to spontaneously occur in animals (**Table 3**). Although the exact mechanism of action of many of these drugs is not known, the outcome is similar enough to study and propose possible treatments.

Cirrhosis is a pathological liver state characterized by abnormalities in hepatic architecture such as loss of fenestrations

TABLE 3 | Experimental models and lab tools affecting LSEC fenestrations.

	Fenestration diameter	Porosity	Fenestration frequency	References	Methods
Cytoskeleton disruptors					
Cytochalasin B	0/+	+++	+++	Braet et al., 1996a,b,c	a/b AFM, SEM, *in vitro* c SEM, TEM, *in vitro*
				Steffan et al., 1987	SEM, TEM, *in vitro* SEM, *in vivo*
				Braet et al., 1995a	TEM, *in vitro*
				Zapotoczny et al., 2017b, 2019b	AFM, *in vitro* live
				Spector et al., 1999	FL, SEM, TEM, *in vitro*
				Oda et al., 1993	SEM, TEM, *in vitro*
				Van Der Smissen et al., 1986	TEM, *in vitro*, *in vivo*
				Steffan et al., 1986	SEM, *in vivo*
				Kalle et al., 1997	AFM, *in vitro*
Cytochalasin D	0/-	+	+	Svistounov et al., 2012; Hunt et al., 2019	SEM, *in vitro*
Dihydrohalichondramide	-	nd	++	Braet et al., 2002	SEM, *in vitro*
Halihondramide	-	nd	++	Braet et al., 2002	SEM, *in vitro*
Jasplakinolide	-	nd	+	Zapotoczny et al., 2019b	AFM, *in vitro* live
				Braet et al., 1998	SEM, TEM, *in vitro*
				Spector et al., 1999	FL, *in vitro*
Latrunculin A	0	nd	++	Braet et al., 1996a	SEM, TEM, *in vitro*
				Spector et al., 1999	FL, *in vitro*
				Braet et al., 1997	SEM, *in vitro*
Misakinolide	-	nd	++	Braet et al., 1998, 1999; Spector et al., 1999	SEM, TEM, *in vitro*
Swinholide A	- -	nd	+++	Braet et al., 1998, 1999; Spector et al., 1999	SEM, TEM, *in vitro*
Disease models					
Dimethyl nitrosamine (DMN)	-	- -	nd	Fraser et al., 1991, 1995b; Rogers et al., 1992; Tamba-Lebbie et al., 1993	SEM, *in vivo*
Endotoxin/LPS	-/G	- -/0	-	Dobbs et al., 1994; Fraser et al., 1995b	SEM, *in vivo*
				Frenzel et al., 1977; Ito et al., 2006a	SEM, TEM, *in vivo*
				Sasaoki et al., 1995	SEM, *in vitro*
Galactosamine + endotoxin	G	nd	-	Ito et al., 2006a	SEM, TEM, *in vivo*
Galactosamine + endotoxin + matrix metaloproteinase	0	nd	0	Ito et al., 2006a	SEM, TEM, *in vivo*
Monocrotaline	G	nd	- -	DeLeve et al., 1999	SEM, TEM, *in vivo*
				DeLeve et al., 2003a,b	SEM, *in vivo*
Monocrotaline + V-PYRRO/NO	0	0	nd	DeLeve et al., 2003b	SEM, *in vivo*
Poloxamer 407	nd	nd	- -	Cogger et al., 2006	SEM, TEM, *in vitro*, *in vivo*
Pyocyanin	nd	- -	nd	Cheluvappa et al., 2007	SEM, *in vitro*
Thioacetamide (TAA)	-	- -	nd	Mori et al., 1993a,b	SEM, TEM, *in vivo*
				Xie et al., 2012b	SEM, *in vivo*
Other					
Superoxide anion (SOA) and nitric oxide NO	G	nd	-	Deaciuc et al., 1999	SEM, TEM, *in vivo*
7 keto cholesterol (7KC)	+	+	+	Svistounov et al., 2012; Hunt et al., 2019	SEM, *in vitro*
Antimycin A	nd	-	- - -	Zapotoczny et al., 2017b	AFM, *in vitro* live
				Braet et al., 2003	SEM, TEM, *in vitro*
Arsenic	nd	- -	nd	Straub et al., 2008	SEM, TEM, *in vitro*, *in vivo*
C3 transferase	+	+	nd	Yokomori et al., 2004	SEM, TEM, *in vitro*

(Continued)

TABLE 3 | (Continued)

	Fenestration diameter	Porosity	Fenestration frequency	References	Methods
Calcium ionophore	-	nd	0	Zapotoczny et al., 2019a	AFM, *in vitro*
				Oda et al., 1993	SEM, TEM, *in vivo*
Calmodulin agonist w7	+	nd	nd	Oda et al., 1993	SEM, TEM, *in vitro*
Cyclopamine	nd	+	nd	Xie et al., 2012a	SEM, *in vitro*
Diamide	nd	nd	- - -	Zapotoczny et al., 2019a	AFM, *in vitro* live
Hydrogen peroxide	+/G	- -/+	-	Cogger et al., 2001	SEM, TEM, *in vivo*
				Straub et al., 2008	SEM, TEM, *in vitro*, *in vivo*
Iodoacetic acid	nd	nd	+	Zapotoczny et al., 2019a	AFM, *in vitro* live
Lysophosphatic acid (LPA)	-	nd	- -	Yokomori et al., 2004	SEM, TEM, *in vitro*
Phorbol myristate acetate (PMA)	0	nd	-	de Zanger et al., 1997	SEM, *in vitro*
S-nitroso-*N*-acetyl penicillamine (SNAP)	G	nd	0	Deaciuc et al., 1999	SEM, TEM, *in vivo*
Staurosporine	0	nd	-	de Zanger et al., 1997	SEM, *in vitro*
Tert-butyl hydroperoxide	G	+	0	Cogger et al., 2004	SEM, TEM, *in vitro*, *in vivo*
Triton x100	0	- -	nd	Svistounov et al., 2012	SEM, *in vitro*
Trombospondin 1	nd	- -	- -	Venkatraman and Tucker-Kellogg, 2013	SEM, *in vitro*

"0," no change; G, gaps; nd, no data; increase: "+," <50%; "++," 50–100%; "+++," >100%; decrease: "-," <50%; "- -," >50%; "- - -," defenestration.

(defenestration) and the build-up of basement membrane formed from collagen deposition in the space of Disse. Interestingly, the first stages of capillarization and defenestration was reported to be reversible prior to the deposition of collagen and formation of a basement membrane which indicates progression from fibrosis to cirrhosis (Xie et al., 2012b). Drugs such as **dimethyl nitrosamine (DMN)** or **thioacetamide (TAA)** are used to induce cirrhotic morphology in LSEC in animal models. Chronic admission of DMN (Fraser et al., 1991; Tamba-Lebbie et al., 1993) and TAA (Mori et al., 1993b; Xie et al., 2012b) was shown to lead to the loss of fenestrations, however the precise mechanism(s) behind this remains unknown. It was suggested that soluble guanine cyclase (sGC) is a crucial element of signaling necessary to maintain fenestrated LSEC morphology. sGC activation normalizes LSEC phenotype and completely prevents progression of fibrosis despite ongoing TAA exposure, so the limiting defect responsible for capillarization in this model of cirrhosis was in the NO/sGC/cGMP pathway (Xie et al., 2012b). Defenestration is an important step not only in cirrhosis and fibrosis but also with aging and its development and has an impact on the whole organism. Lack of filtration of chylomicrons and chylomicron remnants leads to hyperlipidemia (Rogers et al., 1992). Cogger et al. (2006) showed that **poloxamer 407**, a synthetic surfactant causes dramatic defenestration and massive hyperlipidemia. This finding suggests a direct role of LSEC porosity in the lipid clearance in the liver.

Monocrotaline has been used to a model hepatic veno-occlusive disease (DeLeve et al., 1999) and sinusoidal obstruction syndrome (SOS) (DeLeve et al., 2003a,b). Toxic effects were observed only in LSEC but not in hepatocytes nor in other parts of the endothelium. LSEC metabolize monocrotaline by conjugation to glutathione and detoxify to pyrrolic metabolite. It is believed to be a stable reproducible model resulting in a decreased number of fenestrations, gap formation and discontinuous sinusoid occurrence (DeLeve et al., 1999). It is an important reminder that LSEC also can metabolize drugs and it is not only the hepatocytes that have this function in the liver.

Galactosamine, together with **endotoxin** or **TNF**, causes gap formation in the sinusoids and can be used to study the neutrophil extravasation in the acute inflammatory tissue injury (Ito et al., 2006a). It was shown that inhibition of **matrix metalloproteinases**, which are involved in gap formation, reduces the neutrophil accumulation in the sinusoids. **Bacterial endotoxin** alone plays a role in the pathogenesis of cirrhosis, decreasing both number and diameter of fenestrations (Dobbs et al., 1994). Other bacterial toxins, such as **pyocyanin** or **LPS**, are used in studies of post-transplantation complications such as sepsis or ischemia-reperfusion injury. **Pyocyanin** treatment decreases porosity by its effects on the frequency of fenestrations and can be prevented by addition of catalase. This result suggests that the mechanism involves hydrogen peroxide–induced oxidative stress (Cheluvappa et al., 2007).

Another bacterial toxin, ***Clostridium botulinum* C3-like transferase (C3-transferase)**, together with **lysophosphatic acid (LPA)** was tested in a study from 2004. C3-transferase is a rho inhibitor, while LPA is a rho stimulator. Rho was found to be an important regulator of the actin cytoskeleton and was therefore tested for its influence on fenestration and LSEC in general. The *in vitro* experiments on rat LSEC showed dilation and fusion of fenestrations after treatment with C3-transferase, while contraction occurred when the cells were treated with LPA. Additionally LPA caused an increase in F-actin stress fiber and actin microfilaments, while C3-transferase treatment showed the opposite (Yokomori et al., 2004).

Several models of experimental liver injury show similar morphological alterations, including gaps and ruptured sinusoids. Deaciuc et al. (1999) showed that these early changes can be mediated by the free radical species. The *in vitro* treatment of rat LSEC with **superoxide anion** or **nitric oxide** resemble the observations from *in vivo* experiments with various hepatotoxins. Treatment with **hydrogen peroxide** also increased fenestration diameter and decreased fenestration number (Cogger et al., 2001). High porosity values can be misleading in the studies where gap formation is observed so measurement of all three morphology parameters should be considered. Straub et al. (2008) presented that effect of low doses of **arsenic**, mimicking water contamination levels, also act through reactive oxygen species (ROS) generated by NADPH oxidase (NOX). This mechanism was confirmed by the protective (against arsenite) results from NOX deficient mice and use of NOX inhibitors.

Cytoskeleton Disruptors

Numerous agents acting on the actin cytoskeleton have significant effects on fenestration (**Table 3**). Two main groups include marine sponge- and mushroom-derived toxins. Relatively well-known mechanisms of action of these toxins allowed the study of the link between actin cytoskeleton and fenestrae. An extensive chapter from Braet et al. (2008), provides an overview on the *in vitro* effects of actin binding agents such as **cytochalasin B, latrunculin A, jasplakinolide A, swinholide A, misakinolide A, halichondramide, and dihydrohalichondramide**. Despite different mechanisms of promoting/inhibiting actin polymerization or fiber stabilization, all drugs result in an increase of fenestration number. The most surprising finding is the effects of jasplakinolide which promotes polymerization and stabilization of actin in other cells, but in LSEC no such effect was shown. Instead, the loss of fibers and accumulation of actin in single spots occurs within minutes of jasplakinolide treatment (Spector et al., 1999). These structures, described as 'actin dots,' are not fully understood, but they resemble recently described actin asters which may be connected with lipid raft reorganization (Fritzsche et al., 2017). There is an ongoing discussion about the specificity of those agents for actin. For example, cytochalasin B (but not D) was shown to influence transport of glucose across cell membranes and its overall effect can be influenced by changes in glycolysis and metabolism (Kapoor et al., 2016). **Iodoacetic acid** acts on both actin and spectrin and was shown to decrease stress filament formation. Moreover, it caused an increase in porosity and rapid opening and closing of fenestrations (Zapotoczny et al., 2019a). Nevertheless, agents acting on the actin cytoskeleton remain the most important tools for studying fenestration structure and dynamics.

Other Agents Affecting Fenestrations

Svistounov et al. (2012) emphasized the importance of lipid membrane stability and lipid rafts on LSEC morphology. Surfactants such as **Triton X100** or **poloxamer** showed destabilization of the cell membrane and promotion of lipid raft formation which resulted in a decrease or even complete ablation of fenestrations. Moreover, the reduction of lipid raft formation by **7 keto-cholesterol (7KC)** increased the number of fenestrations showing the connection between fenestration structure, actin and cell membrane (Hunt et al., 2019).

Thrombospondin 1 (TSP) is a matrix glycoprotein with pro-fibrotic effects. In a study from 2013 (Venkatraman and Tucker-Kellogg, 2013) it was shown to cause dose-dependent defenestration in LSECs at 100 ng/mL. The authors additionally showed that the CD47-binding fragment of TSP1, p4N1 – which has anti-angiogenic effects in endothelial cells, also induces defenestration in LSECs.

The influence of **phorbol myristate acetate (PMA)**, a protein-kinase-C (PKC) activator and **staurosporine**, a PKC inhibitor, on LSEC have been examined by de Zanger et al. (1997). The *in vitro* treatment of rat cells for 2–7 days resulted in a decrease in porosity, due to the decrease in fenestration number without any observable change in fenestration diameter, when treated with PMA. However, despite the decrease in porosity, PMA improves LSEC cultures in terms of viability and purit, and fenestrated morphology was maintained after 7 days (de Zanger et al., 1997). Treatment with staurosporine or PMA and staurosporine showed enlarged fenestrations, gap formation and a decrease in porosity. The authors concluded that PMA acts on LSEC through PKC based on the staurosporine treatment neutralizing the PMA treatment effects.

Deaciuc et al. (1999) tested rat livers challenged with superoxide anion [***S*-nitroso-*N*-acetyl penicillamine (SNAP)**] and nitric oxide [xanthine oxidase plus hypoxanthine (XO + HX)] generating substances. They theorized that early morphological LSEC alterations associated with liver injury are influenced by free radical species. When they perfused the rat livers with SNAP, they found a suppression of hyaluronan uptake (a test of LSEC endocytosis capacity) and the formation/creation of large gaps in LSEC morphology, sometimes instead of sieve plates, and sometimes together with fenestrations present in sieve plates.

MECHANISMS

As discussed above, a variety of agents have been tested so far showing their effect on fenestrae. Some of the agents changed the number of fenestrations, while others alter their diameters or distribution (gathered in sieve plates or individual fenestrations), including the formation of gaps. However, the clear understanding of why individual drugs have their effects on LSEC is still lacking. The main reason is that many drugs have cross-effects at the cellular level, affecting more than one cellular mechanism/pathway, including the rearrangement of cytoskeleton. Therefore, it is challenging to predict how a drug will work on LSEC fenestrations.

A thorough analysis of the effects of a variety of agents changing porosity, fenestration frequency, and fenestration diameters (including gap formation) resulted in four different hypotheses. These independent but overlapping ideas describe the possible mechanisms behind fenestration structure and dynamics.

(I) *Actin (de)polymerization regulates the number of fenestrations* (Braet et al., 1996b; Spector et al., 1999; Braet and Wisse, 2002; Mönkemöller et al., 2015). The hypothesis was discussed in Braet et al. (1995a), Braet et al. (1996b) and has been developed over the years. It was presented that the cytoskeleton plays a crucial role in the porosity of LSEC. Fenestrae-associated cytoskeleton rings (FACR) surround each fenestration and sieve plate-associated cytoskeleton surround sieve plates (Braet et al., 1995b). The application of actin (de)polymerization targeting drugs revealed the direct connection between actin cytoskeleton and fenestration number in LSEC (Spector et al., 1999; Carpenter et al., 2005). However, the disruption of actin does not destroy fenestration structure, which indicated the complex structure of FACR. Later it was reported that actin filaments surround each fenestration within a sieve plate (Mönkemöller et al., 2015).

(II) *Calcium ions regulate the diameter of fenestrations*. This second hypothesis was summed up in 2002 (Braet and Wisse, 2002). It is mainly based on the research of Oda and Yokomori presenting the role of calcium/calmodulin/actomyosin in the contractility of fenestration diameters (Oda et al., 1990; Yokomori et al., 2004). The regulation of myosin light chain (MLC) phosphorylation occurs via calcium-calmodulin signaling. Further it was suggested that MLC kinase and phosphatase may exert different effects on cell morphology (Yokomori et al., 2004).

(III) *Regulation of fenestrations depends on lipid rafts*. The sieve-raft hypothesis assumes that fenestrations are formed in the flat areas of the cell periphery, in between lipid rafts, where the cell membrane is more flexible and more prone to shape changes (Svistounov et al., 2012). Also, other ways in which lipid rafts can be connected with fenestration were proposed, such as influence on signal transduction or indirect regulation of some signaling pathways.

(IV) *Spectrin is involved in the open versus closed state of fenestration*. The hypothesis decouples the direct actin regulation from the number of fenestrations. Instead, the interplay between the membrane scaffold and actin cytoskeleton is responsible for the opening of the fenestration within the actin ring (Zapotoczny et al., 2019a).

All the above hypotheses do not exclude each other and only emphasize how complicated the mechanisms regulating the number, shape, and size of fenestrations can be. In the following subsections we will focus on the physiological regulation of number and size of fenestrations, apart from the direct (often toxic) effect of actin disturbing drugs (described above). The analysis of different agents acting on LSEC fenestrations leads to the conclusion that the phosphorylation of myosin light chain (MLC) is the core of various pathways regulating actin (de)polymerization. Calcium dependent and independent activation (phosphorylation) of MLC and release of actin binding proteins (such as tropomodulin, tropomyosin, caldesmon) leads to contraction of fenestrations and decrease in the number of fenestrations, while MLC dephosphorylation leads to the relaxation of MLC and promotes more fenestrated morphology of LSEC. The local balances regulating the levels of calcium, ROS, or NO in different parts of the cell ensure active control over the dynamics of fenestrated LSEC. The regulation covers the (de)activation of membrane proteins which may affect actin association to the membrane. Finally, the oxidative state of membrane cytoskeleton and lipid rafts distribution are additionally (passively or actively) involved in this regulation.

Cytoskeleton

SEM and TEM allowed visualization of the fenestrae-associated cytoskeleton rings (FACR) in LSEC (Braet et al., 1996b). Preparations of "ghost" cells, after removing cell membrane with detergent, revealed a network of filaments associated with sieve plates surrounded by thicker filaments. Precise identification was not possible, but the high resolution of those techniques allowed diameter measurements suggesting a mesh of actin fibers surrounded by microtubules. The gap in the chemical information has been filled with super resolution fluorescence microscopy. Mönkemöller et al. (2015) showed the first direct correlation between the localization of cell membrane and actin around fenestration, using SIM. Recently, FACR structures could be also visualized in high resolution using AFM and dSTORM (Zapotoczny et al., 2017b, 2019a). It was also presented that the complete actin ring is necessary to form an open pore within a FACR (Zapotoczny et al., 2019a).

Cytoskeleton remodeling that influences the number of fenestrations was demonstrated for live LSEC. During the first hours after isolation LSEC spread on the substrate, opening and closing individual fenestrations and whole sieve plates. It indicated that fenestrations are not preserved from the *in vivo* to the *in vitro* state and their formation and closing is dynamic as previously suggested (Braet and Wisse, 2012). With time, the dynamics of fenestrations was shown to be slower (Zapotoczny et al., 2020). Still, fenestrations in isolated LSEC were shown to freely migrate several micrometers, and changing their diameter up to 200% during their ∼ 20 min lifespan.

Interesting labyrinth like structures have been observed *in vitro* in the proximity of the perinuclear area of LSEC (Braet et al., 2009). Some fenestrations form three dimensional multi-folded tunnels that are not always passing through the cell which contradicts the sieving role of LSEC. One possible explanation could be that these structures are caused by the cell isolation process because they have not been observed *in vivo* (in tissue samples). After digestion of the liver with Liberase/collagenase cells are detached from each other, perhaps disrupting parts of their cytoskeleton in a way that can be beyond repair after reattachment *in vitro*. Another explanation assumes that microfilament-disruption induces translocation of pre-existing three-dimensional organized fenestrae forming centers (FFCs) from the perinuclear area toward the peripheral cytoplasm (Braet et al., 1998, 2007). Recently, the formation of FFC was shown in live LSEC. It was confirmed that FFC are involved in the rapid increase in fenestration number, both in control and drug treated LSEC.

The importance of the actin cytoskeleton and the structure of FACR was confirmed by the dramatic effects of any agent directly affecting actin. Actin disruptors (see **Table 3** and **Figure 3**) were shown to rapidly induce the formation of new fenestrations (up to 300% porosity increase in 30 min by cytochalasin B) despite different mechanisms of actin depolymerization (Steffan et al., 1987; Zapotoczny et al., 2017b).

Other drugs that indirectly cause actin depolymerization, such as iodoacetic acid, metformin or sildenafil, also resulted in the increase in fenestration number (Hunt et al., 2019; Zapotoczny et al., 2019a). Altogether, agents acting on actin cytoskeleton remain the most important tools in studying fenestration structure and dynamics.

Understanding the mode of action of actin disturbing agents may help us reveal fenestration structure. Actin fibers are regulated by a set of proteins such as profilin, gelsolin, or cofilin that create the dynamic, out-of-equilibrium state. Every actin-binding protein, regardless of the location of its actin-binding site, influences the adenine nucleotide exchange rate of actin and the ratio of G (monomer/globular) and F (polymerized/filamentous) actin (**Figure 3**). Control over that process is maintained by many signaling pathways allowing LSEC to adjust the morphology according to internal and external stimuli. Actin disrupting agents act similarly to those controlling proteins. However, they lack control or feedback loop systems therefore result in rapid and dramatic changes. The importance of the controlled signaling is especially visible in prolonged *in vitro* LSEC culture where changes in cytoskeleton, such as stress fiber formation and fenestration disappearance, occur (Yokomori et al., 2004). However, the direct relationship between the actin polymerization into the thick stress fibers and the decrease in the number of fenestrations needs to be evaluated.

In fact, actin is the only demonstrated protein that was validated to have a direct impact on the number of fenestrations. Therefore, we discuss the various signaling pathways leading to actin and actin related proteins and the ways to affect them to observe the desired effect on fenestrations in the next section.

MLC Phosphorylation – The Core of the Fenestration's Regulation

Myosins convert ATP to create a mechanical force on actin. Created tension in actomyosin cytoskeleton is necessary for number of cellular processes, including cell motility, cytokinesis and intracellular trafficking (Brito and Sousa, 2020). The myosins contain a neck region allowing to bind myosin light chain (MLC) domains, which are regulated by the phosphorylation and dephosphorylation via MLCK and MLCP respectively. In its phosphorylated/active form, MLC results in activation of ATP dependent myosin heavy chain binding to f-actin, which creates an active contractile force. With 30 classes of molecular motors in myosin superfamily regulating variety of cellular processes (Brito and Sousa, 2020) several reports have been dedicated to the role of MLC in the regulation of fenestration diameters. In the following subsections we focused on the cellular machinery involved in the regulation of MLC phosphorylation via calcium, NO, and ROS pathways.

Lipid Rafts

The existence and role of lipid rafts has caused divisions in the scientific community in recent years and during The Keystone Symposium on Lipid Rafts and Cell Function (2006) the following definition was adopted: "Membrane rafts are small (10–200 nm), heterogeneous, highly dynamic, sterol- and sphingolipid-enriched domains that compartmentalize cellular processes. Small rafts can sometimes be stabilized to form larger platforms through protein-protein and protein–lipid interactions." The role of lipid rafts in fenestrations structure and dynamics was studied only recently (Svistounov et al., 2012) and then the hypothesis of sieve-raft regulation of fenestrations was proposed by Cogger et al. (2013). Visualization with SIM revealed that rafts are not present inside sieve plates but rather surround them in an inverse distribution (Svistounov et al., 2012). Fenestrations are formed in the flat, non-raft lipid-disordered regions and are prone to changes in raft organization. 7 keto cholesterol (7KC) increases lipid ordered, non-raft regions and thus promotes fenestration formation while detergent Triton X-100 increases the relative area of raft rich regions and decreases fenestration number (Svistounov et al., 2012; Hunt et al., 2018) (causing complete defenestration at high Triton X-100 concentrations). High doses of 7KC caused gap formation and retraction of cell membrane, which can be explained by deficits in cell membranes after depletion of rafts. Another detergent, poloxamer 407, was also reported to elicit massive defenestration of LSEC (Cogger et al., 2006). Interestingly, pre-treatment with Triton X-100 (increases rafts) abrogated the effect of cytochalasin D and no increase in porosity was observed (Svistounov et al., 2012). This result elucidates the tight connection between rafts and actin cytoskeleton in fenestration structure and/or dynamics. However, it was reported that the lipid rafts in biological membranes induced by detergents may not fully resemble the normal functional rafts (Heerklotz, 2002).

Rafts are enriched in sphingolipids and cholesterol which engenders membrane stability and provides a platform for many membrane proteins that may contribute to their connection to the actin cytoskeleton (Viola and Gupta, 2007). The anchoring of actin to the lipid rafts was suggested to be realized through the FERM domain of ERM proteins and talin (Chichili and Rodgers, 2009), as well as adducin (Yang et al., 2018) and spectrin (Ciana et al., 2011). Functional rafts may not be steady-state phenomena; they might form, grow, cluster or break up, shrink, and vanish according to functional requirements, regulated by rather subtle changes in the activity (disordering or ordering) of membrane compounds (Heerklotz, 2002). These properties might be connected with the dynamic nature of fenestrations and LSEC's ability to rapidly respond via morphology changes. The amount of lipid rafts may also have an indirect effect on fenestrations, through interactions independent of actin. It has been reported that ABC transporters, which decrease intracellular cGMP levels by its efflux, work less efficiently out of raft regions (Klappe et al., 2009). cGMP is an important signaling molecule that acts on fenestrations through PKG, decreasing intracellular calcium and promoting relaxation, both of which are connected with growing fenestration number. Lipid rafts may also affect many signal transduction pathways in the cell by serving as platforms to bring receptors into proximity with activating kinases, scaffolding proteins, and adaptor molecules that are constituent residents of lipid rafts (Rauch and Fackler, 2007).

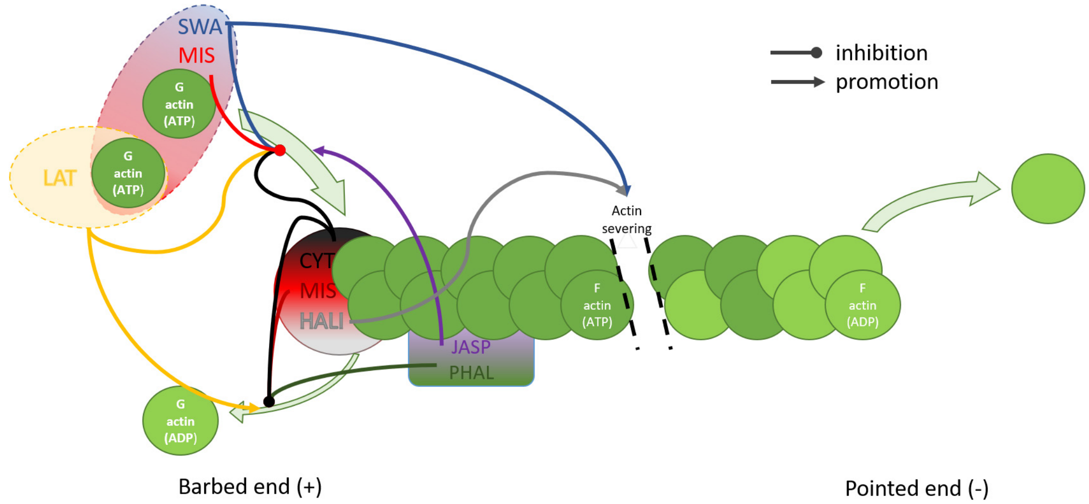

FIGURE 3 | Schematic representation of the effects of actin disrupting drugs on actin filaments. Depolymerization of the barbed end of the actin filament is inhibited by CYT, MIS, and HALI which cap the barbed end, and by PHAL and JASP which attach from the side, additionally stabilizing the fiber. Latrunculin promotes depolymerization by specific sequestration of monomeric actin. Polymerization is stimulated by JASP which also binds competitively to PHAL. Barbed end polymerization is inhibited by CYT, LAT, SWA, and MIS. Both MIS and SWA bind two actin monomers, however only MIS caps the barbed end. HALI and SWA stimulate severing of the actin filament. CYT, cytochalasin; HALI, halihondramide; JASP, jasplakinolide; LAT, latrunculin; MIS, misakinolide; PHAL, phalloidin; SWA, swinholide.

Spectrin

It was reported that only completely closed FACR structures contained fenestrations in the open state (Zapotoczny et al., 2019a). It was proposed that spectrin arranges actin to form a ring-like structure. Although the actin cytoskeleton is important part of fenestration structure, the membrane scaffold has a role in the regulation of opening of fenestration within FACR. In the spectrin-actin hypothesis, fenestrations can be opened if the cell height does not exceed 300–400 nm, which is double the length of the spectrin unit (Zapotoczny et al., 2019a). The proposed mechanism is based on the observation of both open and closed fenestrations within actin rings in live LSEC *in vitro*. The switch between the open and closed state was pharmacologically induced. The actin-spectrin complexes are strong enough to allow migration of the individual fenestrations across the cell membrane. Moreover, it can explain, why actin depolymerizing agents induce new fenestrations: spectrin can arrange short actin fibers to form ring like structures, and decreased cell height allows spectrin units to bind, forming new FACRs. In 2020, the role of actin/fodrin (non-erythroidal spectrin) was reported to be required in fenestration biogenesis in the endothelioma cell line bEND5, in which fenestrations can be induced pharmacologically (Ju et al., 2020). Authors showed a close association between beta actin and spectrin. Moreover, they reported that knockout of alpha spectrin resulted in 10-fold decrease in the number of fenestrations. Nevertheless, despite the increasing interest in this membrane cytoskeletal protein the knowledge of membrane skeleton regulation in endothelial cells is poorly understood.

Regulation *via* Ca^{2+}

The role of calcium in the regulation of fenestration diameters was discussed by Braet and Wisse (2002). The serotonin induced influx of calcium was described to cause calcium-calmodulin dependent phosphorylation of MLCK decreasing the size of fenestrae, denoted as contraction. The reverse effect remained as speculation. Later, Yokomori et al. (2004) summarized that calcium influx affected not only MLCK, but also Rho activity. Thus, calcium can affect both MLCK and ROCK dependent phosphorylation of MLC. The authors presented results of LPA and C3 transferase, causing fenestration closing and dilating respectively, indicating that they act through MLC phosphorylation. In the **Figure 4** we extended the possible regulation of MLC phosphorylation, based on the current state of knowledge. MLC is activated by the calcium mediated phosphorylation via myosin light chain kinase (MLCK) (Rigor et al., 2013). The activity of MLCK is increased by Ca^{2+}-calmodulin binding and by phosphorylation by protein kinase C (PKC). PKC can also further promote MLC phosphorylation by inhibition of MLCP, however, this pathway was not confirmed in endothelium (Somlyo and Somlyo, 2000). The activation of MLCK can be hampered by the cAMP dependent kinase – protein kinase A (PKA). PKA binds to the similar region of MLCK to the Ca^{2+}-calmodulin complex binding domain, hampering calcium dependent MLC phosphorylation. However, the activation of MLC is not sufficient to create a contractile force of the actomyosin complex. The actin binding proteins ensure additional control. Actin is stabilized by e.g., tropomyosin, tropomodulin, caldesmon, or calpain. The release of these proteins from actin is controlled in a calcium-concentration-dependent manner, allowing myosin to reach actin (Hepler, 2016). Moreover, the activation of actin polymerization processes, e.g., by gelsolin, profilin or cofilin is also calcium dependent and results in an increase in actin polymerization. The calcium level, regulated by calcium membrane channels and pumps or

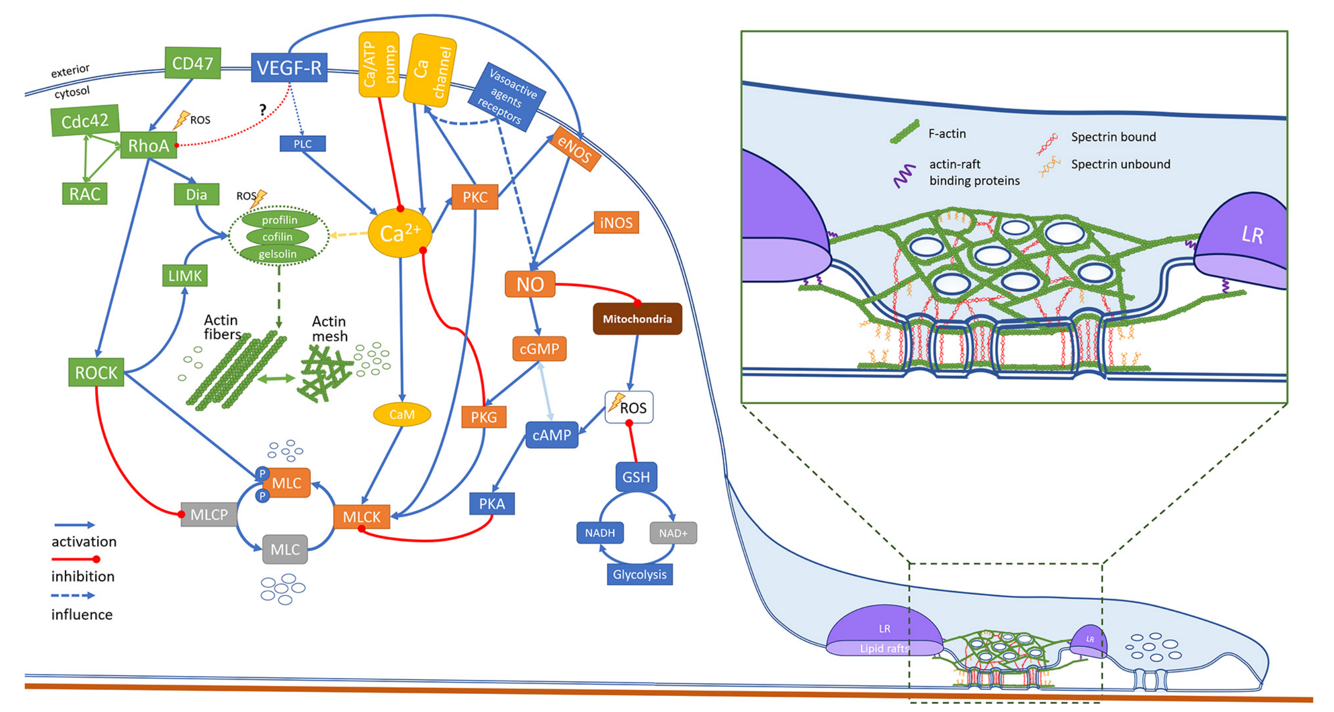

FIGURE 4 | This scheme represents an attempt in unifying the proposed hypotheses of mechanisms behind the structure and dynamics of fenestrations. Various signaling pathways involved in the regulation of fenestrations in LSEC are based on the studies of LSEC (or other endothelial cells). The drugs with known mechanisms of action and reported to affect fenestrations are summarized in **Table 4**.

by endoplasmic reticulum release, causes a cascade of cellular mechanisms driving local changes in the cytoskeleton. These changes vary in different cells and the details of these processes is beyond the scope of this review. The contraction of actomyosin is permanent. It means that it must be actively undone to ensure actomyosin relaxation. The balance of (de)phosphorylation of MLC is maintained by MLC phosphatase (MLCP). The enzyme activity is independent of the calcium plasma concentration (Álvarez-Santos et al., 2020). In addition to the role in the dephosphorylation of MLC, it exhibits phosphatase activity toward other proteins, such as ankyrin, adducin, Tau, merlin, calcineurin-A, interleukin-16, Rb, moezin, and ezrin (Kiss et al., 2019). Inhibition of MLCP (MYPT1 complex) by activation of the RhoA/ROCK pathway, results in indirect increase in the level of phosphorylated MLC and an increase in/of the contractile forces. PKA, PKG, and PKC also cause phosphorylation of MLCP. However, a recent study showed that in contrast to the RhoA/ROCK pathway, PKG- induced phosphorylation has no effect on MLCP activity (MacDonald and Walsh, 2018). It needs to be emphasized that the phosphorylation of MLC is connected to the formation of fibrous actin (via activation of actin nucleation proteins – e.g., gelsolin, profilin, cofilin, as mentioned) and vice versa. It was suggested that actin polymerization is necessary for force development (Mehta and Gunst, 1999). Therefore, the actin relaxation/contraction state is to some extent connected with the (de)polymerization of actin. The effects of certain drugs on fenestrations may be a sum of both.

Regulation *via* NO

Nitric oxide is one of the most important signaling molecules in endothelial cells and plays a crucial role in the maintenance of fenestrations in LSEC (DeLeve, 2015). NO stimulates sGC synthase and thus increases the cGMP level which then starts a cascade of signaling. cGMP stimulates the efflux of intracellular calcium into endoplasmic reticulum storage which reduces activation of MLCK through calmodulin. There are also suggestions that cGMP in microvascular endothelium can act through PKG to activate MLCP leading to further dephosphorylation of MLC (Rigor et al., 2013), but this mechanism was shown only in vascular smooth muscle cells. As described above, we propose that inactivation of MLCK together with a decrease in Ca^{2+} leads to actin relaxation, which results in the increase in fenestration diameter and/or number. There is also evidence of crosstalk between cGMP and cAMP levels which could further affect the MLC phosphorylation state (Chong et al., 2005). The exact mechanisms of action of NO on LSEC fenestration have not been described yet, however the cGMP/Ca pathway has been shown to be a part of VEGF induced NO production (Xie et al., 2012b; DeLeve, 2015). Two main sources of intracellular NO are synthases eNOS (activated among others by VEGF, endothelin, or estrogen) and iNOS (activated by cytokines during liver injuries). Both are responsible for LSEC phenotype maintenance as well as cell response to pathophysiological conditions (DeLeve et al., 2003b). The results of treatment with PMA — which activates PKC and can lead to increased NO production by eNOS — show a positive

TABLE 4 | Agents with known mechanism of action and their effects on LSEC fenestrations.

Inhibitor	Target	Effect	References
C3 transferase	RhoA	FN ↑, D ↑	Yokomori et al., 2004
Simvastatin	CD47	FN ↑, D ↑	Hunt et al., 2019
Y27635	ROCK	FN ↑	Venkatraman and Tucker-Kellogg, 2013
W7	Calmodulin	D ↑	Oda et al., 1993
7 keto cholesterol	Lipid rafts	FN ↑, D ↑	Svistounov et al., 2012
Amlodipine	Ca channel	FN ↑	Hunt et al., 2019
Promotor/activator	**Target**	**Effect**	**References**
LPA	RhoA	D↓	Yokomori et al., 2004
Sildenafil Amlodipine TRAIL	cGMP	FN↑	Hunt et al., 2019
Phorbol myristate	PKC	FN↓	de Zanger et al., 1997
Thrombospondin	CD47	Defenestration	Venkatraman and Tucker-Kellogg, 2013
Simvastatin	NO	FN ↑, D ↓	Venkatraman and Tucker-Kellogg, 2013; Hunt et al., 2019
Serotonin	Ca channel	D↓	Gatmaitan and Arias, 1993; Braet et al., 1995a

FN, fenestration number; D, fenestration diameter; ↑/↓, increase/decrease.

effect on maintenance of LSEC morphology *in vitro* (de Zanger et al., 1997). The effect was confirmed by co-administration of staurosporine, which inhibits PKC.

The effect of NO is complex and involves many different pathways. Besides cGMP signaling, NO can (competitively to O2) bind to complex IV in mitochondria, blocking the electron transport chain which results in an increased ROS production (Moncada and Erusalimsky, 2002). NO can then combine with ROS creating highly reactive peroxynitrate $ONOO^-$. NO production by NOS is calcium dependent but at the same time NO contributes to changes in intracellular calcium. Those mechanisms seem to work as a feedback loop gently steering the cell response, especially since NO is not a stable molecule so its influence is restricted to areas local to its synthesis. In LSEC, NO is required for fenestration maintenance. However, it is not sufficient alone, and other NO independent pathways are necessary. It has been shown that, besides NO production stimulated by VEGF, NO-independent VEGF signaling is needed also (Xie et al., 2012b). We propose two possible mechanisms: in endothelial cells VEGF can act through its membrane receptor on PLC, followed release of the Ca^{2+} from the endoplasmic reticulum (Rigor et al., 2013). Then, PKC enters a feedback loop of NO production leading to a decrease in Ca^{2+}. This would even further increase the NO production, but also would act as a balancing effect for calcium ions. NO can also induce protein *S*-nitrosilation, however it has been found not to affect fenestrations (Xie et al., 2012b). The other possibility is, reported in HUVEC, inhibition of Rho/ROCK pathway by VEGF receptors (Tagashira et al., 2018) which has been shown to play an important role in fenestration maintenance.

The cGMP pathway is a promising target for novel therapeutics for liver diseases and aging as restoration of cGMP levels can restore fenestrations in LSEC (Xie et al., 2012b). Drugs such as sildenafil influence cGMP by blocking its efflux by ABC transporters and degradation by phosphodiesterases (PDE) (Toque et al., 2008; Sager et al., 2012). Amlodipine, a blood pressure medication also affects fenestrations by acting through both cGMP and inhibition of Ca^{2+} channels (Berkels et al., 2004). Another drug used for lowering blood lipid levels – simvastatin, promotes NO production directly via the Akt pathway and through inhibition of Rho GTPases (de Sotomayor and Andriantsitohaina, 2001).

Regulation *via* ROS

There are many sources of ROS within the cell, such as the mitochondrial electron transport chain, NADPH and xanthine oxidase and, highly expressed in endothelium, eNOS when uncoupled (Widlansky and Gutterman, 2011; Jerkic and Letarte, 2015). ROS were initially considered mostly as cytotoxic, but recent reports summarize their positive regulatory roles both in physiological and pathological endothelium, reviewed in Widlansky and Gutterman (2011).

Recently the cytoprotective role of ROS through activation of autophagy signaling was shown in early ischemia injury (Bhogal et al., 2018). LSEC morphology is sensitive to ROS levels and many agents act through this mechanism, such as e.g., ethanol and acetaminophen causing the disappearance of fenestrations (Deaciuc et al., 1999). *In vivo* studies showed large gaps in LSEC caused by ROS, generated by xanthine oxidase and hypoxanthine suggesting destabilization of fenestrations which also prevent cells from closing those gaps (Deaciuc et al., 1999). Glutathione (GSH) is the main physiological countermeasure to free radicals such as ROS. Reducing agents such as NAC can reduce the depletion of GSH due to the presence of oxidative stress (Sun et al., 2014). The effect of ROS on fenestrations may come from different mechanisms based on the disturbance of the redox balance in the cell. Intracellularly, mitochondria are the main source of ROS while glycolysis is the main source of reducing agents such as GSH and NADH. Scavenging of ROS directly activates the Rho/ROCK signaling pathways (Popova et al., 2010) which may lead to promotion of stress fibers. By analogy, the reduction of ROS by antioxidants should lead to reduction of Rho/ROCK signaling, therefore promoting fenestration formation. This mechanism would explain the age-related defenestration associated with higher levels of ROS and reduced redox capabilities in the cells (Herrera et al., 2010).

In endothelial cells, ROS can act as a messenger molecule activating various signaling pathways. Besides the mitochondria, a second main ROS source are NAD(P)H oxidases which can be stimulated by various vasoactive agents (Griendling et al., 2000). It has been shown that LSEC morphology is sensitive to both vasodilators and vasoconstrictors, which was shown to increase and decrease the fenestration diameter respectively (**Table 2**). Moreover, LSEC lack underlying smooth muscles cells to emphasize the response to vasoconstrictors/dilators. There might exist more complicated cellular mechanisms in LSEC to compensate for this. Altogether, those findings suggest that ROS may be part of signaling cascades activating redox-sensitive proteins.

CONCLUSION

Drug clearance mediated by the liver is heavily dependent on the proper phenotype of LSEC, including the transport through fenestrations. Individual drugs and stimulants have been reported to influence the porosity of LSEC. Some drugs show beneficial effects on LSEC phenotype, potentially allowing re-opening fenestration ("re-fenestration") which could be of benefit in the elderly. The role of LSEC senescence and "anti-aging" senolytic drugs, with regard to porosity, warrants further study. However, the background of polypharmacy (regular daily consumption of 4 or more medicines) in much of the elderly population needs to be considered in the refenestration context. Within this review we highlighted the areas of research which will be particularly beneficial for both physicians and researchers. LSEC research is growing in recent years and the latest stage of our knowledge about fenestrations is now facilitated with novel microscopic techniques. These super-resolution methods will continue to improve, so it is appropriate for the field to simultaneously improve sample status, for example to examine living LSEC, or "wet" fixed preparations of LSEC or whole liver mounts instead of dehydrated cells. The substrate upon which LSEC are typically cultured also likely needs to be re-worked – tissue culture plastic is considerably stiffer than the LSEC's natural surroundings, so other softer gel-based substrates should be considered, such as those described by Guixé-Muntet et al. (2020). Ultimately, *in vivo* imaging of LSEC fenestrations *in situ* would be the ideal real-time test of refenestration therapies, but the challenges (e.g., movement due breathing and heart beat) for this type of technology are rather significant. That said, existing technologies should allow for comprehensive studies and better understanding of these unique structures, and how they work, in the coming years.

AUTHOR CONTRIBUTIONS

KS, LK, and CH prepared the figures and tables. PM and BZ acquired the funding. All authors took part in conceptualization, analysis and writing of the manuscript, are responsible for all aspects of the manuscript and read and agreed to the submitted version of the manuscript.

FUNDING

This work received funding from the European Union's Horizon 2020 Research and Innovation Program under the Marie Skłodowska-Curie Grant Agreement No. 766181, project "DeLIVER," the Research Council of Norway Nano2021 program grant to "NanoChip" Grant No. 288565, and the Polish National Science Centre under the "SONATA 15" Project, Grant Agreement No.: UMO-2019/35/D/NZ3/01804.

ACKNOWLEDGMENTS

We would like to thank Professor Karen Kristine Sørensen from the University of Tromsø for sharing her SEM image of a liver sinusoid, and Mr. Eike Struck from University of Tromsø and Professor David Le Couteur from the ANZAC Research Institute in Sydney for the artwork in **Figure 2**. We would also like to thank Professor Bård Smedsrød from University of Tromsø for sharing his experience and knowledge about the history of LSEC.

REFERENCES

Alfaras, I., Mitchell, S. J., Mora, H., Lugo, D. R., Warren, A., Navas-Enamorado, I., et al. (2017). Health benefits of late-onset metformin treatment every other week in mice. *NPJ Aging Mechan. Dis.* 3:16. doi: 10.1038/s41514-017-0018-7

Álvarez-Santos, M. D., Álvarez-González, M., Estrada-Soto, S., and Bazán-Perkins, B. (2020). Regulation of myosin light-chain phosphatase activity to generate airway smooth muscle hypercontractility. *Front. Physiol.* 11:701. doi: 10.3389/fphys.2020.00701

Apte, R. S., Chen, D. S., and Ferrara, N. (2019). VEGF in signaling and disease: beyond discovery and development. *Cell* 176, 1248–1264. doi: 10.1016/j.cell.2019.01.021

Aronsen, L., Orvoll, E., Lysaa, R., Ravna, A. W., and Sager, G. (2014). Modulation of high affinity ATP-dependent cyclic nucleotide transporters by specific and non-specific cyclic nucleotide phosphodiesterase inhibitors. *Eur. J. Pharmacol.* 745, 249–253. doi: 10.1016/j.ejphar.2014.10.051

Asrani, S. K., Devarbhavi, H., Eaton, J., and Kamath, P. S. (2019). Burden of liver diseases in the world. *J. Hepatol.* 70, 151–171. doi: 10.1016/j.jhep.2018.09.014

Auvinen, K., Lokka, E., Mokkala, E., Jäppinen, N., Tyystjärvi, S., Saine, H., et al. (2019). Fenestral diaphragms and PLVAP associations in liver sinusoidal endothelial cells are developmentally regulated. *Sci. Rep.* 9:15698. doi: 10.1038/s41598-019-52068-x

Bacon, C. R., Cary, N., and Davenport, A. P. (1996). Endothelin peptide and receptors in human atherosclerotic coronary artery and aorta. *Circulation Res.* 79, 794–801. doi: 10.1161/01.RES.79.4.794

Bartolo, B. A. D., Cartland, S. P., Prado-Lourenco, L., Griffith, T. S., Gentile, C., Ravindran, J., et al. (2015). Tumor necrosis factor-related apoptosis-inducing ligand (TRAIL) promotes angiogenesis and ischemia-induced neovascularization via NADPH Oxidase 4 (NOX4) and Nitric Oxide-dependent mechanisms. *J. Am. Heart Assoc.* 4, 1–16. doi: 10.1161/JAHA.115.002527

Bender, A., and Beavo, J. A. (2006). Cyclic nucleotide phosphodiesterases: molecular regulation to clinical use. *Pharmacol. Rev.* 58, 488–520. doi: 10.1124/pr.58.3.5

Benowitz, N. L., and Burbank, A. (2016). Cardiovascular toxicity of nicotine: implications for electronic cigarette use neal. *Trends Cardiovasc. Med.* 26, 515–523. doi: 10.1016/j.tcm.2016.03.001

Berger, M., Gray, J. A., and Roth, B. L. (2009). The expanded biology of serotonin. *Annu. Rev. Med.* 60, 355–366. doi: 10.1146/annurev.med.60.042307.110802

Berkels, R., Taubert, D., Bartels, H., Breitenbach, T., Klaus, W., and Roesen, R. (2004). Amlodipine increases endothelial nitric oxide by dual mechanisms. *Pharmacology* 70, 39–45. doi: 10.1159/000074241

Bernier, M., Mitchell, S. J., Wahl, D., Diaz, A., Singh, A., Seo, W., et al. (2020). Disulfiram treatment normalizes body weight in obese mice. *Cell Metabolism* 32, 203.e4–214.e4. doi: 10.1016/j.cmet.2020.04.019

Bhandari, S., Li, R., Simón-Santamaría, J., McCourt, P., Johansen, S. D., Smedsrød, B., et al. (2020). Transcriptome and proteome profiling reveal complementary scavenger and immune features of rat liver sinusoidal endothelial cells and liver macrophages. *BMC Mol. Cell Biol.* 21:85. doi: 10.1186/s12860-020-00331-9

Bhogal, R. H., Weston, C. J., Velduis, S., Leuvenink, H. G. D., Reynolds, G. M., Davies, S., et al. (2018). The reactive oxygen species-mitophagy signalling pathway regulates liver endothelial cell survival during Ischaemia/Reperfusion injury. *Liver Transplantation* 24, 1437–1452. doi: 10.1002/lt.25313

Blessing, W. W., and Seaman, B. (2003). 5-Hydroxytryptamine2A receptors regulate sympathetic nerves constricting the cutaneous vascular bed in rabbits and rats. *Neuroscience* 117, 939–948. doi: 10.1016/S0306-4522(02)00810-2

Bosma, E. K., Van Noorden, C. J. F., Schlingemann, R. O., and Klaassen, I. (2018). The role of plasmalemma vesicle-associated protein in pathological breakdown of blood-brain and blood-retinal barriers: potential novel therapeutic target for cerebral edema and diabetic macular edema. *Fluids Barriers CNS* 15:24. doi: 10.1186/s12987-018-0109-2

Braet, F. (2004). How molecular microscopy revealed new insights into the dynamics of hepatic endothelial fenestrae in the past decade. *Liver Int.* 24, 532–539. doi: 10.1111/j.1478-3231.2004.0974.x

Braet, F., De Zanger, R., Baekeland, M., Crabbé, E., Van Der Smissen, P., and Wisse, E. (1995a). Structure and dynamics of the fenestrae-associated cytoskeleton of rat liver sinusoidal endothelial cells. *Hepatology (Baltimore, Md.)* 21, 180–189.

Braet, F., De Zanger, R., Crabbe, E., and Wisse, E. (1995b). New observations on cytoskeleton and fenestrae in isolated rat-liver sinusoidal endothelial-cells. *J. Gastroenterol. Hepatol.* 10(Suppl. 1), S3–S7. doi: 10.1111/j.1440-1746.1995.tb01792.x

Braet, F., De Zanger, R., Jans, D., Spector, I., and Wisse, E. (1996a). Microfilament-disrupting agent latrunculin a induces an increased number of fenestrae in rat liver sinusoidal endothelial cells: comparison with cytochalasin B. *Hepatology* 24, 627–635. doi: 10.1053/jhep.1996.v24.pm0008781335

Braet, F., de Zanger, R., Sasaoki, T., Baekeland, M., Janssens, P., Smedsrød, B., et al. (1994). Assessment of a method of isolation, purification, and cultivation of rat liver sinusoidal endothelial cells. *Lab. Invest.* 70, 944–952.

Braet, F., de Zanger, R. B., Kalle, W., Raap, A. K., Tanke, H. J., and Wisse, E. (1996b). Comparative scanning, transmission and atomic force microscopy of the microtubular cytoskeleton in fenestrated liver endothelial cells. *Scanning Microscopy Suppl.* 10, 225–236.

Braet, F., de Zanger, R. B., Spector, I., and Wisse, E. (1997). The actin disrupting marine toxin latrunculin a induces an increased number of fenestrae in rat liver sinusoidal endothelial cells. *Kupffer Cell Foundation, Cells Hepatic Sinusoid* 6:82.

Braet, F., Kalle, W. H., De Zanger, R. B., De Grooth, B. G., Raap, A. K., Tanke, H. J., et al. (1996c). Comparative atomic force and scanning electron microscopy: an investigation on fenestrated endothelial cells in vitro. *J. Microscopy* 181(Pt 1), 10–17.

Braet, F., Muller, M., Vekemans, K., Wisse, E., and Le Couteur, D. G. (2003). Antimycin A-Induced defenestration in rat hepatic sinusoidal endothelial cells. *Hepatology* 38, 394–402. doi: 10.1053/jhep.2003.50347

Braet, F., Riches, J., Geerts, W., Jahn, K. A., Wisse, E., and Frederik, P. (2009). Three-dimensional organization of fenestrae labyrinths in liver sinusoidal endothelial cells. *Liver Int.* 29, 603–613. doi: 10.1111/j.1478-3231.2008.01836.x

Braet, F., Soon, L., Vekemans, K., Thordarson, P., and Spector, I. (2008). "Actin-Binding drugs: an elegant tool to dissect subcellular processes in endothelial and cancer cells," in *Actin-Binding Proteins and Disease. Protein Reviews*, Vol. 8, eds C. G. dos Remedios and D. Chhabra (New York, NY: Springer).

Braet, F., Spector, I., De Zanger, R., and Wisse, E. (1998). A novel structure involved in the formation of liver endothelial cell fenestrae revealed by using the actin inhibitor misakinolide. *Proc. Natl. Acad. Sci. U.S.A.* 95, 13635–13640. doi: 10.1073/pnas.95.23.13635

Braet, F., Spector, I., de Zanger, R. B., and Wisse, E. (1999). Fenestrae-Forming Center (FFC): a novel structure involved in the formation of liver sinusoidal endothelial cell fenestrae. *Kupffer Cell Foundation, Cells Hepatic Sinusoid.* 7:144.

Braet, F., Spector, I., Shochet, N., Crews, P., Higa, T., Menu, E., et al. (2002). The new anti-actin agent dihydrohalichondramide reveals fenestrae-forming centers in hepatic endothelial cells. *BMC Cell Biol.* 3:7. doi: 10.1186/1471-2121-3-7

Braet, F., and Wisse, E. (2002). Structural and functional aspects of liver sinusoidal endothelial cell fenestrae: a review. *Comparat. Hepatol.* 1:1. doi: 10.1186/1476-5926-1-1

Braet, F., and Wisse, E. (2012). AFM imaging of fenestrated liver sinusoidal endothelial cells. *Micron* 43, 1252–1258. doi: 10.1016/j.micron.2012.02.010

Braet, F., Wisse, E., Bomans, P., Frederik, P., Geerts, W., Koster, A., et al. (2007). Contribution of high-resolution correlative imaging techniques in the study of the liver sieve in three-dimensions. *Microscopy Res. Technique* 70, 230–242. doi: 10.1002/jemt.20408

Bravo, M., Raurell, I., Hide, D., Fernández-Iglesias, A., Gil, M., Barberá, A., et al. (2019). Restoration of liver sinusoidal cell phenotypes by statins improves portal hypertension and histology in rats with NASH. *Sci. Rep.* 9:20183. doi: 10.1038/s41598-019-56366-2

Brito, C., and Sousa, S. (2020). Non-muscle myosin 2A (NM2A): structure, regulation and function. *Cells* 9, 12–16. doi: 10.3390/cells9071590

Carpenter, B., Lin, Y., Stoll, S., Raffai, R. L., McCuskey, R., and Wang, R. (2005). VEGF is crucial for the hepatic vascular development required for lipoprotein uptake. *Development* 132, 3293–3303. doi: 10.1242/dev.01902

Charles, K., de Zanger, R. B., Van Bossuyt, H., Van Der Smissen, P., and Wisse, E. (1986). Influence of acute alcohol administration on endothelial fenestrae of rat livers: an invivo and in vitro scanning electron microscopic study. *Kupffer Cell Foundation, Cells Hepatic Sinusoid.* 1:497.

Cheluvappa, R., Jamieson, H. A., Hilmer, S. N., Muller, M., and Le Couteur, D. G. (2007). The effect of *pseudomonas aeruginosa* virulence factor, pyocyanin, on the liver sinusoidal endothelial cell. *J. Gastroenterol. Hepatol.* 22, 1350–1351. doi: 10.1111/j.1440-1746.2007.05016.x

Chen, K., Pittman, R. N., and Popel, A. S. (2008). Nitric oxide in the vasculature: where does it come from and where does it go? a quantitative perspective. *Antioxidants Redox Signal.* 10, 1185–1198. doi: 10.1089/ars.2007.1959

Chichili, G. R., and Rodgers, W. (2009). Cytoskeleton-membrane interactions in membrane raft structure. *Cell Mol. Life Sci.* 66, 2319–2328. doi: 10.1007/s00018-009-0022-6.Cytoskeleton-Membrane

Chong, T. J., Victorino, G. P., Schinco, M. A., and Coimbra, R. (2005). Cyclic nucleotide second messengers (CAMP and CGMP) play a central role in signal transduction and regulation of mesenteric postcapillary fluid leak. *J. Trauma - Injury, Infect. Crit. Care* 59, 302–307. doi: 10.1097/01.ta.0000180385.23675.98

Ciana, A., Achilli, C., Balduini, C., and Minetti, G. (2011). On the association of lipid rafts to the spectrin skeleton in human erythrocytes. *Biochim. Biophys. Acta - Biomembranes* 1808, 183–190. doi: 10.1016/j.bbamem.2010.08.019

Cluette-Brown, J., Mulligan, J., Doyle, K., Hagan, S., Osmolski, T., and Hojnacki, J. (1986). Oral nicotine induces an atherogenic lipoprotein profile. *Proc. Soc. Exp. Biol. Med.* 182, 409–413. doi: 10.3181/00379727-182-3-RC1

Cogger, V. C., Hilmer, S. N., Sullivan, D., Muller, M., Fraser, R., and Le Couteur, D. G. (2006). Hyperlipidemia and surfactants: the liver sieve is a link. *Atherosclerosis* 189, 273–281. doi: 10.1016/j.atherosclerosis.2005.12.025

Cogger, V. C., and Le Couteur, D. G. (2009). "Fenestrations in the liver sinusoidal endothelial cell," in *The Liver: Biology and Pathobiology*, 5th Edn, ed. I. M. Arias (Hoboken, NJ: Wiley Online Library), 389–406.

Cogger, V. C., McNerney, G. P., Nyunt, T., DeLeve, L. D., McCourt, P., Smedsrod, B., et al. (2010). Three-dimensional structured illumination microscopy of liver sinusoidal endothelial cell fenestrations. *J. Struct. Biol.* 171, 382–388. doi: 10.1016/j.jsb.2010.06.001

Cogger, V. C., Mitchell, S. J., Warren, A., De Cabo, R., and Le Couteur, D. G. (2014). Age-related loss of responsiveness to 2, 5-Dimethoxy-4-Iodoamphetamine in liver sinusoidal endothelial cells. *J. Gerontol. - Series A* 69, 514–518. doi: 10.1093/gerona/glt124

Cogger, V. C., Mross, P. E., Hosie, M. J., Ansselin, A. D., McLean, A. J., and Le Couteur, D. G. (2001). The effect of acute oxidative stress on the ultrastructure of the perfused rat liver. *Pharmacol. Toxicol.* 89, 306–311. doi: 10.1034/j.1600-0773.2001.d01-165.x

Cogger, V. C., Muller, M., Fraser, R., McLean, A. J., Khan, J., and Le Couteur, D. G. (2004). The effects of oxidative stress on the liver sieve. *J. Hepatol.* 41, 370–376. doi: 10.1016/j.jhep.2004.04.034

Cogger, V. C., O'Reilly, J. N., Warren, A., and Le Couteur, D. G. (2015). A standardized method for the analysis of liver sinusoidal endothelial cells and their fenestrations by scanning electron microscopy. *J. Visualized Exp.* 98:e52698. doi: 10.3791/52698

Cogger, V. C., Roessner, U., Warren, A., Fraser, R., and Le Couteur, D. G. (2013). A sieve-raft hypothesis for the regulation of endothelial fenestrations. *Computational Struct. Biotechnol. J.* 8, 1–9. doi: 10.5936/csbj.201308003

David, L., Mallet, C., Keramidas, M., Lamandé, N., Gasc, J. M., Dupuis-Girod, S., et al. (2008). Bone morphogenetic protein-9 is a circulating vascular quiescence factor. *Circulat. Res.* 102, 914–922. doi: 10.1161/CIRCRESAHA.107.165530 de Sotomayor, M. A., and Andriantsitohaina, R. (2001). Simvastatin and Ca2+ signaling in endothelial cells: involvement of Rho protein. *Biochem. Biophys. Res. Commun.* 280, 486–490. doi: 10.1006/bbrc.2000.4144

de Sotomayor, M. A., Pérez-Guerrero, C., Herrrera, M. D., Jimenez, L., Marín, R., Marhuenda, E., et al. (2005). Improvement of age-related endothelial dysfunction by simvastatin: effect on NO and COX pathways. *Br. J. Pharmacol.* 146, 1130–1138. doi: 10.1038/sj.bjp.0706420

de Zanger, R. B., Braet, F., Arnez Camacho, M. R., and Wisse, E. (1997). Prolongation of hepatic endothelial cell cultures by phorbol myristate acetate. *Kupffer Cell Foundation, Cells Hepatic Sinusoid.* 6:97.

Deaciuc, I. V., D'Souza, N. B., Sarphie, T. G., Schmidt, J., Hill, D. B., and McClain, C. J. (1999). Effects of exogenous superoxide anion and nitric oxide on the scavenging function and electron microscopic appearance of the sinusoidal endothelium in the isolated, perfused rat liver. *J. Hepatol.* 30, 213–221. doi: 10.1016/S0168-8278(99)80064-6

DeLeve, L. D. (2015). Liver sinusoidal endothelial cells in hepatic fibrosis. *Hepatology* 61, 1740–1746. doi: 10.1002/hep.27376

DeLeve, L. D., Ito, Y., Bethea, N. W., McCuskey, M. K., Wang, X., and McCuskey, R. S. (2003a). Embolization by sinusoidal lining cells obstructs the microcirculation in rat sinusoidal obstruction syndrome. *Am. J. Physiol. - Gastrointestinal Liver Physiol.* 284, 1045–1052. doi: 10.1152/ajpgi.00526.2002

DeLeve, L. D., and Maretti-Mira, A. C. (2017). Liver sinusoidal endothelial cell: an update. *Sem. Liver Dis.* 37, 377–387. doi: 10.1055/s-0037-1617455

DeLeve, L. D., McCuskey, R. S., Wang, X., Hu, L., McCuskey, M. K., Epstein, R. B., et al. (1999). Characterization of a reproducible rat model of hepatic veno-occlusive disease. *Hepatology* 29, 1779–1791. doi: 10.1002/hep.510290615

DeLeve, L. D., Wang, X., Kanel, G. C., Ito, Y., Bethea, N. W., McCuskey, M. K., et al. (2003b). Decreased hepatic nitric oxide production contributes to the development of rat sinusoidal obstruction syndrome. *Hepatology* 38, 900–908. doi: 10.1053/jhep.2003.50383

DeLeve, L. D., Wang, X., Kaplowitz, N., Shulman, H. M., Bart, J. A., and Van Der Hoek, A. (1997). Sinusoidal endothelial cells as a target for acetaminophen toxicity: direct action versus requirement for hepatocyte activation in different mouse strains. *Biochem. Pharmacol.* 53, 1339–1345. doi: 10.1016/S0006-2952(97)00048-8

Denninger, J. W., and Marletta, M. A. (1999). Guanylate cyclase and the .NO/CGMP signaling pathway. *Biochim. Biophys. Acta - Bioenerget.* 1411, 334–350. doi: 10.1016/S0005-2728(99)00024-9

Desroches-Castan, A., Tillet, E., Ricard, N., Ouarné, M., Mallet, C., Belmudes, L., et al. (2019a). Bone morphogenetic protein 9 is a paracrine factor controlling liver sinusoidal endothelial cell fenestration and protecting against hepatic fibrosis. *Hepatology* 70, 1392–1408. doi: 10.1002/hep.30655

Desroches-Castan, A., Tillet, E., Ricard, N., Ouarné, M., Mallet, C., Feige, J. J., et al. (2019b). Differential consequences of Bmp9 deletion on sinusoidal endothelial cell differentiation and liver fibrosis in 129/Ola and C57BL/6 Mice. *Cells* 8:1079. doi: 10.3390/cells8091079

Di Martino, J., Mascalchi, P., Legros, P., Lacomme, S., Gontier, E., Bioulac-Sage, P., et al. (2019). Actin depolymerization in dedifferentiated liver sinusoidal endothelial cells promotes fenestrae re-formation. *Hepatol. Commun.* 3, 213–219. doi: 10.1002/hep4.1301

Dobbs, B. R., Rogers, G. W. T., Xing, H. Y., and Fraser, R. (1994). Endotoxin-induced defenestration of the hepatic sinusoidal endothelium: a factor in the pathogenesis of cirrhosis? *Liver* 14, 230–233. doi: 10.1111/j.1600-0676.1994.tb00080.x

Elkadri, A., Thoeni, C., Deharvengt, S. J., Murchie, R., Guo, C., Stavropoulos, J. D., et al. (2015). Mutations in plasmalemma vesicle associated protein result in sieving protein-losing enteropathy characterized by hypoproteinemia, hypoalbuminemia, and hypertriglyceridemia. *Cellular Mol. Gastroenterol. Hepatol.* 1, 381–394. doi: 10.1016/j.jcmgh.2015.05.001

Fraser, R., Clark, S. A., Bowler, L. M., Murray, F. E. M., Wakasugi, J., Ishihara, M., et al. (1989). The opposite effects of nicotine and pantethine on the porosity of the liver sieve and lipoprotein metabolism. *Kupffer Cell Foundation, Cells Hepatic Sinusoid.* 2:335.

Fraser, R., Clark, S. A., Day, W. A., and Murray, F. E. (1988). Nicotine decreases the porosity of the rat liver sieve: a possible mechanism for hypercholesterolaemia. *Br. J. Exp. Pathol.* 69, 345–350.

Fraser, R., Cogger, V. C., Dobbs, B., Jamieson, H., Warren, A., Hilmer, S. N., et al. (2012). The liver sieve and atherosclerosis. *Pathology* 44, 181–186. doi: 10.1097/PAT.0b013e328351bcc8

Fraser, R., Dobbs, B. R., and Rogers, G. W. T. (1995a). Lipoproteins and the liver sieve: the role of the fenestrated sinusoidal endothelium in lipoprotein metabolism, atherosclerosis, and cirrhosis. *Hepatology* 21, 863–874. doi: 10.1016/0270-9139(95)90542-1

Fraser, R., Rogers, G. W. T., Bowler, L. M., Day, W. A., and Dobbs, B. R. (1991). Defenestration and vitamin a status in a rat model of cirrhosis. *Kupffer Cell Foundation, Cells Hepatic Sinusoid* 3:195.

Fraser, R., Rogers, G. W. T., Sutton, L. E., and Dobbs, B. R. (1995b). Single dose models of defenestration: tool to explore mechanisms, modulation and measurement of hepatic sinusoidal porosity. *Kupffer Cell Foundation, Cells Hepatic Sinusoid* 5:263.

Fredriksson, L., Li, H., and Eriksson, U. (2004). The PDGF family: four gene products form five dimeric isoforms. *Cytokine Growth Factor Rev.* 15, 197–204. doi: 10.1016/j.cytogfr.2004.03.007

Frenzel, H., Kremer, B., and Hucker, H. (1977). The liver sinusoids under various pathological conditions. A TEM and SEM study of rat liver after respiratory hypoxia, telecobalt-irradiation and endotoxin application. *Kupffer Other Liver Sinusoidal Cells* 213–222.

Fritzsche, M., Li, D., Colin-York, H., Chang, V. T., Moeendarbary, E., Felce, J. H., et al. (2017). Self-organizing actin patterns shape membrane architecture but not cell mechanics. *Nat. Commun.* 8:14347. doi: 10.1038/ncomms14347

Funyu, J., Mochida, S., Inao, M., Matsui, A., and Fujiwara, K. (2001). VEGF can act as vascular permeability factor in the hepatic sinusoids through upregulation of porosity of endothelial cells. *Biochem. Biophys. Res. Commun.* 280, 481–485. doi: 10.1006/bbrc.2000.4148

Furrer, K., Rickenbacher, A., Tian, Y., Jochum, W., Bittermann, A. G., Käch, A., et al. (2011). Serotonin reverts age-related capillarization and failure of regeneration in the liver through a VEGF-Dependent pathway. *Proc. Natl. Acad. Sci. U.S.A.* 108, 2945–2950. doi: 10.1073/pnas.1012531108

Gatmaitan, Z., and Arias, I. M. (1993). Hepatic endothelial cell fenestrae. *Kupffer Cell Foundation, Cells Hepatic Sinusoid* 4:3.

Gatmaitan, Z., Varticovski, L., Ling, L., Mikkelsen, R., Steffan, A. M., and Arias, I. M. (1996). Studies on fenestral contraction in rat liver endothelial cells in culture. *Am. J. Pathol.* 148, 2027–2041.

Gracia-Sancho, J., Caparrós, E., Fernández-Iglesias, A., and Francés, R. (2021). Role of liver sinusoidal endothelial cells in liver diseases. *Nat. Rev. Gastroenterol. Hepatol.* 18, 411–431. doi: 10.1038/s41575-020-00411-3

Griendling, K. K., Sorescu, D., Lassègue, B., and Ushio-Fukai, M. (2000). Modulation of protein kinase activity and gene expression by reactive oxygen species and their role in vascular physiology and pathophysiology. *Arteriosclerosis, Thrombosis, Vasc. Biol.* 20, 2175–2183. doi: 10.1161/01.ATV.20.10.2175

Grosse, L., Wagner, N., Emelyanov, A., Molina, C., Lacas-Gervais, S., Wagner, K. D., et al. (2020). Defined P16High senescent cell types are indispensable for mouse healthspan. *Cell Metabolism* 32, 87.e6–99.e6. doi: 10.1016/j.cmet.2020.05.002

Guixé-Muntet, S., Ortega-Ribera, M., Wang, C., Selicean, S., Andreu, I., Kechagia, J. Z., et al. (2020). Nuclear deformation mediates liver cell mechanosensing in cirrhosis. *JHEP Rep.* 2:100145. doi: 10.1016/j.jhepr.2020.100145

Hanchanale, V., and Eardley, I. (2014). Alprostadil for the treatment of impotence. *Exp. Opin. Pharmacother.* 15, 421–428. doi: 10.1517/14656566.2014.873789

Heerklotz, H. (2002). Triton promotes domain formation in lipid raft mixtures. *Biophys. J.* 83, 2693–2701. doi: 10.1016/S0006-3495(02)75278-8

Hepler, P. K. (2016). The cytoskeleton and its regulation by calcium and protons. *Plant Physiol.* 170, 3–22. doi: 10.1104/pp.15.01506

Herrera, M. D., Mingorance, C., Rodríguez-Rodríguez, R., and Alvarez de Sotomayor, M. (2010). Endothelial dysfunction and aging: an update. *Ageing Res. Rev.* 9, 142–152. doi: 10.1016/j.arr.2009.07.002

Herrnberger, L., Hennig, R., Kremer, W., Hellerbrand, C., Goepferich, A., Kalbitzer, H. R., et al. (2014). Formation of fenestrae in murine liver sinusoids depends on plasmalemma vesicle-associated protein and is required for lipoprotein passage. *PLoS One* 9:e115005. doi: 10.1371/journal.pone.0115005

Hide, D., Warren, A., Fernández-Iglesias, A., Maeso-Díaz, R., Peralta, C., Le Couteur, D. G., et al. (2020). Ischemia/Reperfusion injury in the aged liver: the importance of the sinusoidal endothelium in developing therapeutic strategies for the elderly. *J. Gerontol. - Series A Biol. Sci. Med. Sci.* 75, 268–277. doi: 10.1093/gerona/glz012

Higashi, T., Friedman, S. L., and Hoshida, Y. (2017). Hepatic stellate cells as key target in liver fibrosis. *Adv. Drug Delivery Rev.* 121, 27–42. doi: 10.1016/j.addr.2017.05.007

Hilmer, S. N., Cogger, V. C., Fraser, R., McLean, A. J., Sullivan, D., and Le Couteur, D. G. (2005). Age-Related changes in the hepatic sinusoidal endothelium impede lipoprotein transfer in the rat. *Hepatology* 42, 1349–1354. doi: 10.1002/hep.20937

Hodgman, M., and Garrard, A. (2012). A review of acetaminophen poisoning. *Crit. Care Clin.* 28, 499–516.

Hojnacki, J., Mulligan, J., and Cluette-Brown, J. (1986). Oral nicotine impairs clearance of plasma low density lipoproteins. *Proc. Soc. Exp. Biol. Med.* 182, 414–418. doi: 10.3181/00379727-182-3-RC2

Holzer, P., Reichmann, F., and Farzi, A. (2012). Neuropeptide Y, Peptide YY and pancreatic polypeptide in the gut-brain axis. *Neuropeptides* 46, 261–274. doi: 10.1016/j.npep.2012.08.005

Horn, T., Christoffersen, P., and Henriksen, J. H. (1987). Alcoholic liver injury: defenestration in noncirrhotic livers-a scanning electron microscopic study. *Hepatology* 7, 77–82. doi: 10.1002/hep.1840070117

Hunt, N. J., Lockwood, G. P., Kang, S. W., Pulpitel, T., Clark, X., Mao, H., et al. (2020). The effects of metformin on age-related changes in the liver sinusoidal endothelial cell. *J. Gerontol. - Series A Biol. Sci. Med. Sci.* 75, 278–285. doi: 10.1093/gerona/glz153

Hunt, N. J., Lockwood, G. P., Warren, A., Mao, H., McCourt, P. A. G., Le Couteur, D. G., et al. (2019). Manipulating fenestrations in young and old liver sinusoidal endothelial cells. *Am. J. Phys. - Gastrointestinal Liver Physiol.* 316, G144–G154. doi: 10.1152/ajpgi.00179.2018

Hunt, N. J., McCourt, P. A. G., Le, D. G., and Cogger, V. C. (2018). Novel targets for delaying aging: the importance of the liver and advances in drug delivery. *Adv. Drug Delivery Rev.* 135, 39–49. doi: 10.1016/j.addr.2018.09.006

Imai, S., and Yoshino, J. (2013). The importance of NAMPT/NAD/SIRT1 in the systemic regulation of metabolism and ageing. *Diabetes, Obesity Metabolism* 15(Suppl. 3), 26–33. doi: 10.1111/dom.12171

Ito, Y., Abril, E. R., Bethea, N. W., McCuskey, M. K., Cover, C., Jaeschke, H., et al. (2006a). Mechanisms and pathophysiological implications of sinusoidal endothelial cell gap formation following treatment with Galactosamine/Endotoxin in mice. *Am. J. Physiol. - Gastrointestinal Liver Physiol.* 291, 211–218. doi: 10.1152/ajpgi.00312.2005

Ito, Y., Abril, E. R., Bethea, N. W., McCuskey, M. K., and McCuskey, R. S. (2006b). Dietary steatotic liver attenuates acetaminophen hepatotoxicity in mice. *Microcirculation* 13, 19–27. doi: 10.1080/10739680500383423

Ito, Y., Bethea, N. W., Abril, E. R., and McCuskey, R. S. (2003). Early hepatic microvascular injury in response to acetaminophen toxicity. *Microcirculation* 10, 391–400. doi: 10.1038/sj.mn.7800204

Iwasaki, M., Akiba, Y., and Kaunitz, J. D. (2019). Recent advances in vasoactive intestinal peptide physiology and pathophysiology: focus on the gastrointestinal system. *F1000Research* 8, 1–13. doi: 10.12688/f1000research.18039.1

Jerkic, M., and Letarte, M. (2015). Contribution of oxidative stress to endothelial dysfunction in hereditary hemorrhagic telangiectasia. *Front. Genet.* 5:34. doi: 10.3389/fgene.2015.00034

Ju, M., Ioannidou, S., and Munro, P. (2020). A Na,K-ATPase–Fodrin–Actin membrane cytoskeleton complex is required for endothelial fenestra biogenesis. *Cells* 9:1387. doi: 10.3390/cells9061387

Kalle, W. H. J., Braet, F., Raap, A. K., De Grooth, B. G., Tanket, H. J., and Wisse, E. (1997). Imaging of the membrane surface of sinusoidal rat liver endothelial cells by atomic force microscopy. *Kupffer Cell Foundation, Cells Hepatic Sinusoid* 6:94.

Kamegaya, Y., Oda, M., Yokomori, H., and Ishii, H. (2002). Role of endothelin receptors in endothelin-1-induced morphological changes of hepatic sinusoidal endothelial fenestrae: morphometric evaluation with scanning electron microscopy. *Hepatol. Res.* 22, 89–101. doi: 10.1016/S1386-6346(01)00147-4

Kapoor, K., Finer-Moore, J. S., Pedersen, B. P., Caboni, L., Waight, A., Hillig, R. C., et al. (2016). Mechanism of inhibition of human glucose transporter GLUT1 is conserved between cytochalasin B and Phenylalanine amides. *Proc. Natl. Acad. Sci. U.S.A.* 113, 4711–4716. doi: 10.1073/pnas.1603735113

Kaumann, A. J., and Levy, F. O. (2006). 5-Hydroxytryptamine receptors in the human cardiovascular system. *Pharmacol. Therapeutics* 111, 674–706. doi: 10.1016/j.pharmthera.2005.12.004

Kawanabe, Y., and Nauli, S. M. (2011). Endothelin. *Cellular Mol. Life Sci.* 68, 195–203. doi: 10.1007/s00018-010-0518-0

Kim, S. T., and Park, T. (2019). Acute and chronic effects of cocaine on cardiovascular health. *Int. J. Mol. Sci.* 20:584. doi: 10.3390/ijms20030584

Kim, W. K., Meliton, V., Kye, W. P., Hong, C., Tontonoz, P., Niewiadomski, P., et al. (2009). Negative regulation of hedgehog signaling by liver X receptors. *Mol. Endocrinol.* 23, 1532–1543. doi: 10.1210/me.2008-0453

Kirtland, S. J. (1988). Prostaglandin E1: a review. *Prostaglandins, Leukotrienes Essential Fatty Acids* 32, 165–174. doi: 10.1016/0952-3278(88)90168-8

Kiss, A., Erdődi, F., and Lontay, B. (2019). Myosin phosphatase: unexpected functions of a long-known enzyme. *Biochim. Biophys. Acta - Mol. Cell Res.* 1866, 2–15. doi: 10.1016/j.bbamcr.2018.07.023

Klappe, K., Hummel, I., Hoekstra, D., and Kok, J. W. (2009). "Lipid dependence of ABC transporter localization and function. *Chem. Phys. Lipids* 161, 57–64. doi: 10.1016/j.chemphyslip.2009.07.004

Kong, C., Bobe, S., Pilger, C., Lachetta, M., Øie, C. I., Kirschnick, N., et al. (2021). Multiscale and multimodal optical imaging of the ultrastructure of human liver biopsies. *Front. Physiol.* 12:637136. doi: 10.3389/fphys.2021.637136

Lapoint, J., Dargan, P. I., and Hoffman, R. S. (2013). "Chapter 7 - Synthetic amphetamine derivatives", in *Novel Psychoactive Substances* eds Paul I. Dargan and David M. Wood (Boston: Academic Press), 161–178. doi: 10.1016/B978-0-12-415816-0.00007-9

Le Couteur, D. G., Fraser, R., Cogger, V. C., and McLean, A. J. (2002). Hepatic pseudocapillarisation and atherosclerosis in ageing. *Lancet* 359, 1612–1615. doi: 10.1016/S0140-6736(02)08524-0

Le Couteur, D. G., Warren, A., Cogger, V. C., Smedsrød, B., Sørensen, K. K., De Cabo, R., et al. (2008). Old age and the hepatic sinusoid. *Anatomical Rec.* 291, 672–683. doi: 10.1002/ar.20661

Lesurtel, M., Graf, R., Aleil, B., Walther, D. J., Tian, Y., Jochum, W., et al. (2006). Platelet-derived serotonin mediates liver regeneration. *Science* 312, 104–107. doi: 10.1126/science.1123842

Leung, Y. Y., Hui, L. L. Y., and Kraus, V. B. (2015). Colchicine-update on mechanisms of action and therapeutic uses. *Semin. Arthritis Rheumatism* 45, 341–350.

Liu, D., Yovchev, M. I., Zhang, J., Alfieri, A. A., Tchaikovskaya, T., Laconi, E., et al. (2015). Identification and characterization of mesenchymal-epithelial progenitor-like cells in normal and injured rat liver. *Am. J. Pathol.* 185, 110–128. doi: 10.1016/j.ajpath.2014.08.029

MacDonald, J. A., and Walsh, M. P. (2018). Regulation of smooth muscle myosin light chain phosphatase by multisite phosphorylation of the myosin targeting subunit, MYPT1. *Cardiovasc. Hematol. Disord.-Drug Targets* 18, 4–13. doi: 10.2174/1871529x18666180326120638

Mak, K. M., and Lieber, C. S. (1984). Alterations in endothelial fenestrations in liver sinusoids of baboons fed alcohol: a scanning electron microscopic study. *Hepatology* 4, 386–391. doi: 10.1002/hep.1840040306

Mao, H., Diekmann, R., Liang, H. P. H., Cogger, V. C., Le Couteur, D. G., Lockwood, G. P., et al. (2019). Cost-efficient nanoscopy reveals nanoscale architecture of liver cells and platelets. *Nanophotonics* 8, 1299–1313. doi: 10.1515/nanoph-2019-0066

Maruthur, N. M., Tseng, E., Hutfless, S., Wilson, L. M., Suarez-Cuervo, C., Berger, Z., et al. (2016). Diabetes medications as monotherapy or metformin-based combination therapy for Type 2 diabetes: a systematic review and meta-analysis. *Ann. Int. Med.* 164, 740–751. doi: 10.7326/M15-2650

Maslak, E., Gregorius, A., and Chlopicki, S. (2015). Liver Sinusoidal Endothelial Cells (LSECs) function and NAFLD; NO-Based therapy targeted to the liver. *Pharmacol. Rep.* 67, 689–694. doi: 10.1016/j.pharep.2015.04.010

Mason, R. P., Jacob, R. F., Corbalan, J. J., Kaliszan, R., and Malinski, T. (2014). Amlodipine increased endothelial nitric oxide and decreased nitroxidative stress disproportionately to blood pressure changes. *Am. J. Hypertens.* 27, 482–488. doi: 10.1093/ajh/hpt202

Mateuszuk, L., Campagna, R., Kutryb-Zając, B., Kuś, K., Słominska, E. M., Smolenski, R. T., et al. (2020). Reversal of endothelial dysfunction by nicotinamide mononucleotide via extracellular conversion to nicotinamide riboside. *Biochem. Pharmacol.* 178:114019. doi: 10.1016/j.bcp.2020.114019

McCuskey, R., and Reilly, F. (1993). Hepatic microvasculature: dynamic structure and its regulation. *Semin. Liver Dis.* 13, 1–12. doi: 10.1055/s-2007-1007333

McCuskey, R. S. (2006). Sinusoidal endothelial cells as an early target for hepatic toxicants. *Clin. Hemorheol. Microcirculation* 34, 5–10.

McCuskey, R. S., Bethea, N. W., Wong, J., McCuskey, M. K., Abril, E. R., Wang, X., et al. (2004). Ethanol binging exacerbates sinusoidal endothelial and parenchymal injury elicited by acetaminophen. *J. Hepatol.* 42, 371–377. doi: 10.1016/j.jhep.2004.11.033

McCuskey, R. S., Eguchi, H., Nishida, J., Krasovich, M. A., McDonell, D., Jolley, C. S., et al. (1993). Effects of ethanol and cocaine alone or in combination on the hepatic sinusoids of mice and rats. *Kupffer Cell Foundation, Cells Hepatic Sinusoid* 4:376.

Mehta, D., and Gunst, S. J. (1999). Actin polymerization stimulated by contractile activation regulates force development in canine tracheal smooth muscle. *J. Physiol.* 519, 829–840. doi: 10.1111/j.1469-7793.1999.0829n.x

Midão, L., Giardini, A., Menditto, E., Kardas, P., and Costa, E. (2018). Polypharmacy prevalence among older adults based on the survey of health, ageing and retirement in Europe. *Arch. Gerontol. Geriatrics* 78, 213–220. doi: 10.1016/j.archger.2018.06.018

Mills, K. F., Yoshida, S., Stein, L. R., Grozio, A., Kubota, S., Sasaki, Y., et al. (2016). Long-Term administration of nicotinamide mononucleotide mitigates age-associated physiological decline in mice. *Cell Metabolism* 24, 795–806. doi: 10.1016/j.cmet.2016.09.013

Mitchell, S. J., Huizer-Pajkos, A., Cogger, V. C., Mclachlan, A. J., Le Couteur, D. G., Jones, B., et al. (2011). Age-Related pseudocapillarization of the liver sinusoidal endothelium impairs the hepatic clearance of acetaminophen in rats. *J. Gerontol A Biol. Sci. Med. Sci.* 66, 400–408. doi: 10.1093/gerona/glq221

Mohamad, M., Mitchell, S. J., Wu, L. E., White, M. Y., Cordwell, S. J., Mach, J., et al. (2016). Ultrastructure of the liver microcirculation influences hepatic and systemic insulin activity and provides a mechanism for age-related insulin resistance. *Aging Cell* 15, 706–715. doi: 10.1111/acel.12481

Moncada, S., and Erusalimsky, J. D. (2002). Does nitric oxide modulate mitochondrial energy generation and apoptosis? *Nat. Rev. Mol. Cell Biol.* 3, 214–220. doi: 10.1038/nrm762

Mönkemöller, V., Øie, C., Hübner, W., Huser, T., and McCourt, P. (2015). Multimodal super-resolution optical microscopy visualizes the close connection between membrane and the cytoskeleton in liver sinusoidal endothelial cell fenestrations. *Sci. Rep.* 5:16279. doi: 10.1038/srep16279

Mori, T., Okanoue, T., Sawa, Y., Hori, N., Kanaoka, H., Itoh, Y., et al. (1993a). The change of sinusoidal endothelial cells in experimental liver cirrhosis - in vivo and in vitro study-. *Kupffer Cell Foundation, Cells Hepatic Sinusoid.* 4:280.

Mori, T., Okanoue, T., Sawa, Y., Hori, N., Ohta, M., and Kagawa, K. (1993b). Defenestration of the sinusoidal endothelial-cell in a rat model of cirrhosis. *Hepatology* 17, 891–897.

Namkoong, S., Lee, S. J., Kim, C. K., Kim, Y. M., Chung, H. T., Lee, H., et al. (2005). Prostaglandin E2 stimulates angiogenesis by activating the nitric Oxide/CGMP pathway in human umbilical vein endothelial cells. *Exp. Mol. Med.* 37, 588–600. doi: 10.1038/emm.2005.72

Oda, M., Azuma, T., Watanabe, N., Nishizaki, Y., Nishida, J., Ishii, K., et al. (1990). "Regulatory mechanism of hepatic microcirculation: involvement of the contraction and dilatation of sinusoids and sinusoidal endothelial fenestrae1," in *Proceeding of the Gastrointestinal Microcirculation. 9th Bodensee Symposium on Microcirculation, Bad Schachen/Konstanz, June/July 1989. Prog Appl Microcirc*, Vol. 17, eds K. Messmer and F. Hammersen (Basel: Karger), 103–128.

Oda, M., Kamegaya, Y., Yokomori, H., Han, J.-Y., Akiba, Y., Nakamura, M., et al. (1997). Roles of plasma membrane Ca2+-ATPase in the relaxation and contraction of hepatic sinusoidal endothelial fenestrae - effects of prostagrandin E1 and Endothelin1. *Kupffer Cell Foundation, Cells Hepatic Sinusoid* 6:313.

Oda, M., Kazemoto, S., Kaneko, H., Yokomori, H., Ishii, K., Tsukada, N., et al. (1993). Involvment of Ca2+-Calmodulin-Actomyosin system in contractility of hepatic sinusoidal endothelial fenestrae. *Kupffer Cell Foundation, Cells Hepatic Sinusoid* 4:174.

OECD/European Union (2020). *Health at a Glance: Europe 2020: State of Health in the EU Cycle*. Paris: OECD Publishing.

Owen, M. R., Doran, E., and Halestrap, A. P. (2000). Evidence that metformin exerts its anti-diabetic effects through inhibition of complex 1 of the mitochondrial respiratory chain. *Biochem. J.* 348(Pt 3), 607–614.

Pandey, E., Nour, A. S., and Harris, E. N. (2020). Prominent receptors of liver sinusoidal endothelial cells in liver homeostasis and disease. *Front. Physiol.* 11:873. doi: 10.3389/fphys.2020.00873

Poisson, J., Lemoinne, S., Boulanger, C., Durand, F., Moreau, R., Valla, D., et al. (2017). Liver sinusoidal endothelial cells: physiology and role in liver diseases. *J. Hepatol.* 66, 212–227. doi: 10.1016/j.jhep.2016.07.009

Popova, E. N., Pletjushkina, O. Y., Dugina, V. B., Domnina, L. V., Ivanova, O. Y., Izyumov, D. S., et al. (2010). Scavenging of reactive oxygen species in mitochondria induces myofibroblast differentiation. *Antioxidants Redox Signal.* 13, 1297–1307. doi: 10.1089/ars.2009.2949

Raines, S. M., Richards, O. C., Schneider, L. R., Schueler, K. L., Rabaglia, M. E., Oler, A. T., et al. (2011). Loss of PDGF-B activity increases hepatic vascular permeability and enhances insulin sensitivity. *Am. J. Physiol. - Endocrinol. Metabolism* 301, 517–526. doi: 10.1152/ajpendo.00241.2011

Rauch, S., and Fackler, O. T. (2007). Viruses, lipid rafts and signal transduction. *Signal Transduction* 7, 53–63. doi: 10.1002/sita.200600113

Reilly, F. D., Dimlich, R. V. W., Cilento, E. V., and McCuskey, R. S. (1982). Hepatic microvascular regulatory mechanisms. II. Cholinergic mechanisms. *Hepatology* 2, 230S–235S. doi: 10.1002/hep.1840020207

Rigor, R. R., Shen, Q., Pivetti, C. D., Wu, M. H., and Yuan, S. Y. (2013). Myosin light chain kinase signaling in endothelial barrier dysfunction. *Med. Res. Rev.* 33, 911–933. doi: 10.1002/med.21270

Rikitake, Y., and Liao, J. K. (2005). Rho GTPases, statins, and nitric oxide. *Circulat. Res.* 97, 1232–1235. doi: 10.1161/01.RES.0000196564.18314.23

Robbins, P. D., Jurk, D., Khosla, S., Kirkland, J. L., Lebrasseur, N. K., Miller, J. D., et al. (2021). Senolytic drugs: reducing senescent cell viability to extend health span. *Annu. Rev. Pharmacol. Toxicol.* 61, 779–803. doi: 10.1146/annurev-pharmtox-050120-105018

Roberts, W. G., and Palade, G. E. (1995). Increased microvascular permeability and endothelial fenestration induced by vascular endothelial growth factor. *J. Cell Sci.* 108, 2369–2379.

Rogers, G. W. T., Dobbs, B. R., and Fraser, R. (1992). Decreased hepatic uptake of cholesterol and retinol in the dimethylnitrosamine rat model of cirrhosis. *Liver* 12, 326–329. doi: 10.1111/j.1600-0676.1992.tb00581.x

Ruffolo, R. R., and Hieble, J. P. (1994). α-Adrenoceptors. *Pharmacol. Therapeutics* 61, 1–64. doi: 10.1016/0163-7258(94)90058-2

Rumberger, J. A., Napolitano, J., Azumano, I., Kamiya, T., and Evans, M. (2011). Pantethine, a derivative of vitamin B5 used as a nutritional supplement, favorably alters low-density lipoprotein cholesterol metabolism in low- to moderate-cardiovascular risk north American subjects: a triple-blinded placebo and diet-controlled investigation. *Nutr. Res.* 31, 608–615. doi: 10.1016/j.nutres.2011.08.001

Sager, G., Ørvoll, E. O., Lysaa, R. A., Kufareva, I., Abagyan, R., and Ravna, A. W. (2012). Novel CGMP efflux inhibitors identified by virtual ligand screening (VLS) and confirmed by experimental studies. *J. Med. Chem.* 55, 3049–3057. doi: 10.1021/jm2014666

Sakai, K. (1980). Coronary vasoconstriction by locally administered acetylcholine, carbachol and bethanechol in isolated, donor-perfused, rat hearts. *Br. J. Pharmacol.* 68, 625–632. doi: 10.1111/j.1476-5381.1980.tb10853.x

Sasaoki, T., Braet, F., de Zanger, R. B., Wisse, E., and Arii, S. (1995). The effect of endotoxin on liver sinusoidal endothelial cells. *Kupffer Cell Foundation, Cells Hepatic Sinusoid* 5:366.

Schreck, R., Meier, B., Mannel, D. N., Droge, W., and Baeuerle, P. A. (1992). Dithiocarbamates as potent inhibitors of nuclear factor Kb activation in intact cells. *J. Exp. Med.* 175, 1181–1194. doi: 10.1084/jem.175.5.1181

Shetty, S., Lalor, P. F., and Adams, D. H. (2018). Liver sinusoidal endothelial cells — gatekeepers of hepatic immunity. *Nat. Rev. Gastroenterol. Hepatol.* 15, 555–567. doi: 10.1038/s41575-018-0020-y

Shu, X., Li, N., Wu, Y., Li, W., Zhang, X., Li, P., et al. (2021). Mechanotransduction of liver sinusoidal endothelial cells under varied mechanical stimuli. *Acta Mechanica Sinica* 37, 201–217. doi: 10.1007/s10409-021-01057-3

Singh, Y., and Mikrou, P. (2018). Use of prostaglandins in duct-dependent congenital heart conditions. *Arch. Dis. Childhood: Educ. Practice Edn.* 103, 137–140. doi: 10.1136/archdischild-2017-313654

Somlyo, A. P., and Somlyo, A. V. (2000). Signal transduction by G-Proteins, Rho-Kinase and protein phosphatase to smooth muscle and non-muscle myosin II. *J. Physiol.* 522, 177–185. doi: 10.1111/j.1469-7793.2000.t01-2-00177.x

Sørensen, K. K., McCourt, P., Berg, T., Crossley, C., Le Couteur, D., Wake, K., et al. (2012). The scavenger endothelial cell: a new player in homeostasis and immunity. *Am. J. Physiol. - Regulat. Integrat. Comparat. Physiol.* 303, R1217–R1230. doi: 10.1152/ajpregu.00686.2011

Sørensen, K. K., Simon-Santamaria, J., McCuskey, R. S., and Smedsrød, B. (2015). Liver sinusoidal endothelial cells. *Comprehensive Physiol.* 5, 1751–1774. doi: 10.1002/cphy.c140078

Spector, I., Braet, F., Shochet, N. R., and Bubb, M. R. (1999). New anti-actin drugs in the study of the organization and function of the actin cytoskeleton. *Microscopy Res. Technique* 47, 18–37. doi: 10.1002/(SICI)1097-0029(19991001)47:1<18::AID-JEMT3>3.0.CO;2-E

Steffan, A. M., Gendrault, J. L., and Kirn, A. (1986). Phagocytosis and surface modulation of fenestrated areas - two properties of murine endothelial liver cells (EC) involving microfilaments. *Kupffer Cell Foundation, Cells Hepatic Sinusoid* 1:483.

Steffan, A. M., Gendrault, J. L., and Kirn, A. (1987). Increase in the number of fenestrae in mouse endothelial liver cells by altering the cytoskeleton with cytochalasin B. *Hepatology* 7, 1230–1238. doi: 10.1002/hep.1840070610

Straub, A. C., Clark, K. A., Ross, M. A., Chandra, A. G., Li, S., Gao, X., et al. (2008). Arsenic-Stimulated liver sinusoidal capillarization in mice requires NADPH oxidase-generated superoxide. *J. Clin. Investigat.* 118, 3980–3989. doi: 10.1172/JCI35092

Suh, J. J., Pettinati, H. M., Kampman, K. M., and O'Brien, C. P. (2006). The status of Disulfiram: a half of a century later. *J. Clin. Psychopharmacol.* 26, 290–302. doi: 10.1097/01.jcp.0000222512.25649.08

Sun, Y., Pu, L.-Y., Lu, L., Wang, X.-H., Zhang, F., and Rao, J.-H. (2014). N-Acetylcysteine attenuates reactive-oxygen-species- mediated endoplasmic reticulum stress during liver ischemia-reperfusion injury. *World J. Gastroenterol.* 20, 15289–15298. doi: 10.3748/wjg.v20.i41.15289

Svistounov, D., Warren, A., McNerney, G. P., Owen, D. M., Zencak, D., Zykova, S. N., et al. (2012). The relationship between fenestrations, sieve plates and rafts in liver sinusoidal endothelial cells. *PLoS One* 7:e46134. doi: 10.1371/journal.pone.0046134

Szafranska, K., Holte, C. F., Kruse, L. D., Mao, H., Øie, C. I., Szymonski, M., et al. (2021). Quantitative analysis methods for studying fenestrations in liver sinusoidal endothelial cells. A comparative study. *Micron* doi: 10.1016/j.micron.2021.103121

Tagashira, T., Fukuda, T., Miyata, M., Nakamura, K., Fujita, H., Takai, Y., et al. (2018). Afadin facilitates vascular endothelial growth factor-induced network formation and migration of vascular endothelial cells by inactivating Rho-Associated kinase through ARHGAP29. *Arteriosclerosis, Thrombosis, Vasc. Biol.* 38, 1159–1169. doi: 10.1161/ATVBAHA.118.310991

Takashimizu, S., Watanabe, N., Nishizaki, Y., Kawazoe, K., and Matsuzaki, S. (1999). Mechanisms of hepatic microcirculatory disturbances induced by acute ethanol administration in rats, with special reference to alterations of sinusoidal endothelial fenestrae. *Alcohol.: Clin. Exp. Res.* 23(Suppl. 4), 39S–46S. doi: 10.1111/j.1530-0277.1999.tb04532.x

Tamba-Lebbie, B., Rogers, G. W. T., Dobbs, B. R., and Fraser, R. (1993). Defenestration of the hepatic sinusoidal endothelium in the dimethylnitrosamine fed rat: is this process reversible? *Kupffer Cell Foundation, Cells Hepatic Sinusoid* 4:179.

Tanikawa, K., Noguchi, K., and Sata, M. (1991). Ultrastructural features of kupffer cells and sinusoidal endothelial cells in chronic ethanol-fed rats. *Kupffer Cell Foundation, Cells Hepatic Sinusoid* 3:445.

Tian, Y., Graf, R., El-Badry, A. M., Lesurtel, M., Furrer, K., Moritz, W., et al. (2011). Activation of serotonin Receptor-2B rescues small-for-size liver graft failure in mice. *Hepatology* 53, 253–262. doi: 10.1002/hep.23960

Toque, H. A., Teixeira, C. E., Priviero, F. B. M., Morganti, R. P., Antunes, E., and De Nucci, G. (2008). Vardenafil, but not sildenafil or tadalafil, has calcium-channel blocking activity in rabbit isolated pulmonary artery and human washed platelets. *Br. J. Pharmacol.* 154, 787–796. doi: 10.1038/bjp.2008.141

Tsukada, N., Oda, M., Yonei, Y., Honda, K., Aikawa, Y., Kiryu, Y., et al. (1986). Alterations of the hepatic sinusoidal endothelial fenestrae in response to vasoactive substances in the rat -in vivo and in vitro studies-. *Kupffer Cell Foundation, Cells Hepatic Sinusoid* 1:515.

Umetsu, Y., Tenno, T., Goda, N., Shirakawa, M., Ikegami, T., and Hiroaki, H. (2011). Structural difference of vasoactive intestinal peptide in two distinct membrane-mimicking environments. *Biochim. Biophys. Acta - Proteins Proteomics* 1814, 724–730. doi: 10.1016/j.bbapap.2011.03.009

Van Der Smissen, P., Van Bossuyt, H., Charles, K., and Wisse, E. (1986). The structure and function of the cytoskeleton in sinusoidal endothelial cells in the rat liver. *Kupffer Cell Foundation, Cells Hepatic Sinusoid* 1:517.

Venkatraman, L., and Tucker-Kellogg, L. (2013). The CD47-Binding peptide of thrombospondin-1 induces defenestration of liver sinusoidal endothelial cells. *Liver Int.* 33, 1386–1397. doi: 10.1111/liv.12231

Viola, A., and Gupta, N. (2007). Tether and trap: regulation of membrane-raft dynamics by actin-binding proteins. *Nat. Rev. Immunol.* 7, 889–896. doi: 10.1038/nri2193

Wachter, S. B., and Gilbert, E. M. (2012). Beta-Adrenergic receptors, from their discovery and characterization through their manipulation to beneficial clinical application. *Cardiology (Switzerland)* 122, 104–112. doi: 10.1159/000339271

Walker, R. M., Racz, W. J., and McElligott, T. F. (1983). Scanning electron microscopic examination of acetaminophen-induced hepatotoxicity and congestion in mice. *Am. J. Pathol.* 113, 321–330.

Wang, X.-K., and Peng, Z.-G. (2021). Targeting liver sinusoidal endothelial cells: an attractive therapeutic strategy to control inflammation in nonalcoholic fatty liver disease. *Front. Pharmacol.* 12:655557. doi: 10.3389/fphar.2021.655557

Warren, A., Cogger, V. C., Fraser, R., Deleve, L. D., McCuskey, R. S., and Le Couteur, D. G. (2011). The effects of old age on hepatic stellate cells. *Curr. Gerontol. Geriatrics Res.* 2011, 1–8. doi: 10.1155/2011/439835

Watanabe, N., Takashimizu, S., Nishizaki, Y., Kojima, S., Kagawa, T., and Matsuzaki, S. (2007). An endothelin a receptor antagonist induces dilatation of sinusoidal endothelial fenestrae: implications for endothelin-1 in hepatic microcirculation. *J. Gastroenterol.* 42, 775–782. doi: 10.1007/s00535-007-2093-1

Weaver, B. A. (2014). How Taxol/Paclitaxel kills cancer cells. *Mol. Biol. Cell* 25, 2677–2681. doi: 10.1091/mbc.E14-04-0916

Webb, R. C. (2003). Smooth muscle contraction and relaxation. *Am. J. Physiol. - Adv. Physiol. Educ.* 27, 201–206. doi: 10.1152/advan.00025.2003

White, J. D. (1993). Neuropeptide Y: a central regulator of energy homeostasis. *Regulat. Peptides* 49, 93–107. doi: 10.1016/0167-0115(93)90431-7

Widlansky, M. E., and Gutterman, D. D. (2011). Regulation of endothelial function by mitochondrial reactive oxygen species. *Antioxidants Redox Signal.* 15, 1517–1530. doi: 10.1089/ars.2010.3642

Wiley, S. R., Schooley, K., Smolak, P. J., Din, W. S., Huang, C. P., Nicholl, J. K., et al. (1995). Identification and characterization of a new member of the TNF family that induces apoptosis. *Immunity* 3, 673–682. doi: 10.1016/1074-7613(95)90057-8

Wilkinson, A. L., Qurashi, M., and Shetty, S. (2020). The role of sinusoidal endothelial cells in the axis of inflammation and cancer within the liver. *Front. Physiol.* 11:990. doi: 10.3389/fphys.2020.00990

Willy, P. J., Umesono, K., Ong, E. S., Evans, R. M., Heyman, R. A., and Mangelsdorf, D. J. (1995). LXR, a nuclear receptor that defines a distinct retinoid response pathway. *Genes Dev.* 9, 1033–1045. doi: 10.1101/gad.9.9.1033

Wisse, E. (1970). An electron microscopic study of the fenestrated endothelial lining of rat liver sinusoids. *J. Ultrasruct. Res.* 31, 125–150. doi: 10.1016/S0022-5320(70)90150-4

Wisse, E., Braet, F., Duimel, H., Vreuls, C., Koek, G., Damink, S. W. M. O., et al. (2010). Fixation methods for electron microscopy of human and other liver. *World J. Gastroenterol.* 16, 2851–2866. doi: 10.3748/wjg.v16.i23.2851

Wisse, E., Van Dierendonck, J. H., De Zanger, R. B., Fraser, R., and McCuskey, R. S. (1980). "On the role of the liver endothelial filter in the transport of particulate fat (Chylomicrons and Their Remnants) to parenchymal cells and the influence of certain hormones on the endothelial fenestrae," in *Proceeding of the Conference: Communications of Liver Cells*, eds H. Popper, L. Bianchi, F. Gudat, and W. Reutter (Lancaster: MTP Press Ltd), 195–200.

Xie, G., Choi, S. S., Syn, W.-K., Michelotti, G. A., Swiderska-Syn, M., Karaca, G., et al. (2012a). Hedgehog signaling regulates liver sinusoidal endothelial cell capillarisation. *Hepatol. Gut* 62, 299–309. doi: 10.1136/gutjnl-2011-301494

Xie, G., Wang, X., Wang, L., Wang, L., Atkinson, R. D., Kanel, G. C., et al. (2012b). Role of differentiation of liver sinusoidal endothelial cells in progression and regression of hepatic fibrosis in rats. *Gastroenterology* 142, 918.e6–927.e6. doi: 10.1053/j.gastro.2011.12.017

Xing, Y., Zhao, T., Gao, X., and Wu, Y. (2016). Liver X receptor α is essential for the capillarization of liver sinusoidal endothelial cells in liver injury. *Sci. Rep.* 6:21309. doi: 10.1038/srep21309

Xu, B., Xiao-hong, L., Lin, G., Queen, L., and Ferro, A. (2002). Amlodipine, but not verapamil or nifedipine, dilates rabbit femoral artery largely through a nitric oxide- and kinin-dependent mechanism. *Br. J. Pharmacol.* 136, 375–382. doi: 10.1038/sj.bjp.0704753

Yamagishi, M. (1959). Electron microscope studies on the fine structure of the sinusoidal wall and fat-storing cells of rabbit livers. *Arch. Histol. Jpn.* 18, 223–261. doi: 10.1679/aohc1950.18.223

Yang, C., Sui, Z., Xu, T., Liu, W., Wang, X., and Zeng, X. (2018). Lipid raft-associated ß-Adducin participates in neutrophil migration. *Mol. Med. Rep.* 18, 1353–1360. doi: 10.3892/mmr.2018.9113

Yang, M., and Zhang, C. (2021). The role of liver sinusoidal endothelial cells in cancer liver metastasis ming. *Am. J. Cancer Res.* 11, 1845–1860.

Yokomori, H., Oda, M., Yoshimura, K., Nagai, T., Ogi, M., Nomura, M., et al. (2003). Vascular endothelial growth factor increases fenestral permeability in hepatic sinusoidal endothelial cells. *Liver Int.* 23, 467–475. doi: 10.1111/j.1478-3231.2003.00880.x

Yokomori, H., Yoshimura, K., Funakoshi, F., Nagai, T., Fujimaki, K., Nomura, M., et al. (2004). Rho modulates hepatic sinusoidal endothelial fenestrae via regulation of the actin cytoskeleton in rat endothelial cells. *Lab. Investigat.* 84, 857–864. doi: 10.1038/labinvest.3700114

Yokomori, H., Yoshimura, K., Ohshima, S., Nagai, T., Fujimaki, K., Nomura, M., et al. (2006). The Endothelin-1 receptor-mediated pathway is not involved in the endothelin-1-induced defenestration of liver sinusoidal endothelial cells. *Liver Int.* 26, 1268–1276. doi: 10.1111/j.1478-3231.2006.01365.x

Zapotoczny, B., Braet, F., Kus, E., Ginda-Mäkelä, K., Klejevskaja, B., Campagna, R., et al. (2019a). Actin-spectrin scaffold supports open fenestrae in liver sinusoidal endothelial cells. *Traffic* 20, 932–942. doi: 10.1111/tra.12700

Zapotoczny, B., Braet, F., Wisse, E., Lekka, M., and Szymonski, M. (2020). Biophysical nanocharacterization of liver sinusoidal endothelial cells through atomic force microscopy. *Biophys. Rev.* 12, 625–636. doi: 10.1007/s12551-020-00699-0

Zapotoczny, B., Szafranska, K., Kus, E., Braet, F., Wisse, E., Chlopicki, S., et al. (2019b). Tracking fenestrae dynamics in live murine liver sinusoidal endothelial cells. *Hepatology* 69, 876–888. doi: 10.1002/hep.30232

Zapotoczny, B., Szafranska, K., Kus, E., Chlopicki, S., and Szymonski, M. (2017a). Quantification of fenestrations in liver sinusoidal endothelial cells by atomic force microscopy. *Micron* 101, 48–53. doi: 10.1016/j.micron.2017.06.005

Zapotoczny, B., Szafranska, K., Owczarczyk, K., Kus, E., Chlopicki, S., and Szymonski, M. (2017b). Atomic force microscopy reveals the dynamic morphology of fenestrations in live liver sinusoidal endothelial cells. *Sci. Rep.* 7:7994. doi: 10.1038/s41598-017-08555-0

Zhang, J. X., Pegoli, W., and Clemens, M. G. (1994). Endothelin-1 induces direct constriction of hepatic sinusoids. *Am. J. Physiol. - Gastrointestinal Liver Physiol.* 266, 624–632. doi: 10.1152/ajpgi.1994.266.4.g624

Conflict of Interest: The authors declare that the research was conducted in the absence of any commercial or financial relationships that could be construed as a potential conflict of interest.

Publisher's Note: All claims expressed in this article are solely those of the authors and do not necessarily represent those of their affiliated organizations, or those of the publisher, the editors and the reviewers. Any product that may be evaluated in this article, or claim that may be made by its manufacturer, is not guaranteed or endorsed by the publisher.

Paper II

"The Computed Sinusoid."

Matteo Boninsegna, Peter AG McCourt, and **Christopher Florian Holte**.

Livers 3, no. 4 (2023): 657-673.

livers

Article

The Computed Sinusoid

Matteo Boninsegna [1], Peter A. G. McCourt [2] and Christopher Florian Holte [2,*]

[1] Department of Physics, Bielefeld University, D-33501 Bielefeld, Germany; matteo.boninsegna@uni-bielefeld.de
[2] Faculty of Health Sciences, Institute for Medical Biology, UiT The Arctic University of Norway, 9010 Tromsø, Norway; peter.mccourt@uit.no
* Correspondence: christopher.holte@uit.no

Abstract: Hepatic sinusoids are lined with thin endothelial cells with transcellular pores, termed fenestrations. These fenestrations are open channels that connect the sinusoidal lumen to the underlying Space of Disse (SoD) and the hepatocytes of the liver parenchyma. Fenestrations range from 0.05 to 0.35 µm in diameter and cover 5–15% of the sinusoidal endothelial surface area, depending on their location along the sinusoids. The direct measurement of hemodynamic parameters, such as pressure and flow velocity, remains challenging within the narrow sinusoids. Such knowledge would increase our understanding of the physiology of the hepatic niche and possible implications in aging or diseases in which fenestrations are reduced or lost. Few simulations of liver blood flow focus on the level of the individual sinusoid, and fewer still include the transcellular pores (fenestrations) of the sinusoidal endothelium. Furthermore, none have included (i) a porosity gradient along the sinusoid wall, modeled using through-all pores rather than a porous medium, (ii) the presence of the SoD, or (iii) lymphatic drainage. Herein, computed fluid dynamics (CFD) simulations were performed using a numerical model with relevant anatomical characteristics (length, diameter, porosity, inlet/outlet pressure, and lymphatic outflow from the portal region of the SoD). The greatest contribution to luminal velocity magnitude and pressure was the overall shape of the vessel. Divergent-radius models yielded velocity magnitudes 1.5–2 times higher than constant-radius models, and pressures were 5–8% lower in the divergent-radius models compared to the constant-radius models. Porosity only modestly contributed to luminal pressure. The luminal velocity magnitude was largely unaffected by the presence or absence of lymphatic drainage. Velocity magnitudes through fenestrations were lower in higher-porosity models (20%) vs. lower-porosity models (5%) across all models (0.4–0.55-fold lower). Velocity magnitudes through the space of Disse were increased 3–4 times via the addition of lymphatic drainage to the models, while pressures were decreased by 6–12%. The flow velocity in the SoD was modified via differences in porosity, while the flow velocity in the lumens of the sinusoids was largely unaffected. The overall shape of the vessel is the single most important factor in the pressure flow behavior of the sinusoidal lumen. The flow rate over hepatocytes and the SoD is modestly affected by the distribution of porosity along the sinusoid and greatly affected by the lymphatic drainage, parameters that would be of interest for modeling the exchange of blood with the hepatic parenchyma.

Keywords: liver sinusoid; fenestrations; fenestrae; liver hemodynamic; CFD; liver fluid dynamic model; computational liver model

check for updates

Citation: Boninsegna, M.; McCourt, P.A.G.; Holte, C.F. The Computed Sinusoid. *Livers* **2023**, *3*, 657–673. https://doi.org/10.3390/livers3040043

Academic Editor: John N. Plevris

Received: 19 July 2023
Revised: 17 October 2023
Accepted: 26 October 2023
Published: 11 November 2023

1. Introduction

1.1. The Hepatic Sinusoid

In liver lobules, blood enters the sinusoids from the portal triad (PT) and flows toward the central vein (CV). Sinusoids are approximately 275 µm long and 5–15 µm wide [1,2]. Particularly, the periportal zone (zone 1) of the sinusoid has a lumen with a narrower diameter with respect to the perivenous zone (zone 3), while an intermediate width characterizes the zone in between (zone 2) (Figure 1) [3–5].

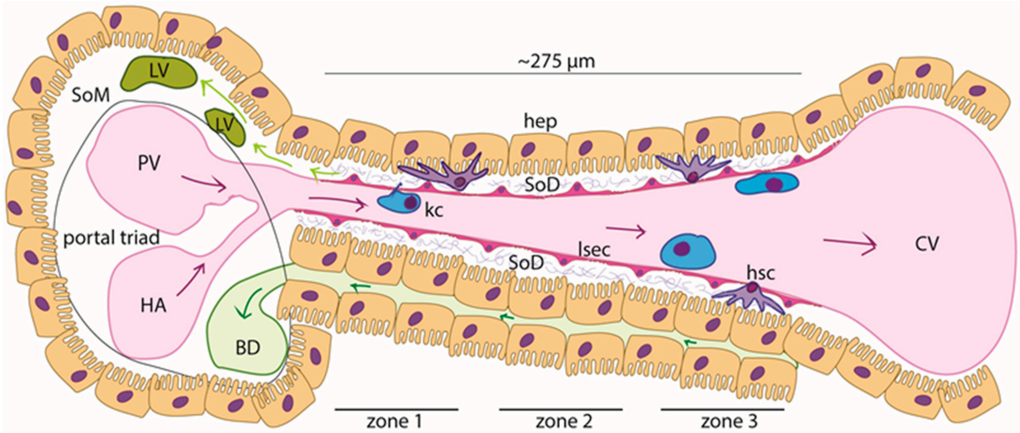

Figure 1. Schematic of the liver sinusoid: liver sinusoid endothelial cells (LSECs) form the highly specialized and fenestrated endothelium of the sinusoid. Resident macrophages (Kupffer cells (KCs)) populate the sinusoidal lumen, while hepatic stellate cells can be found within the Space of Disse (SoD), an approximately 1 µm thick region with a sparse extracellular matrix (grey bundles—proteoglycans and collagen type III) that separates the LSECs from the hepatocytes (hep). Blood rich in nutrients and oxygen flows from the portal vein (PV) and the hepatic artery (HA) toward the central vein (CV) (purple arrows). Bile is formed in the hepatocytes and flows through the bile canaliculi, which are situated between hepatic cords (dark green arrows). Lymph is largely (ca. 80%) formed from the filtrate in the SoD and flows into the lymphatic vasculature (LV), which is in the Space of Mall (SoM) (light green arrows).

In rats, the mean linear flow rate of blood within the hepatic microvasculature is roughly 144 µm/s. Flow speed and fluidic resistance increase from the periportal zone to the perivenous zone [1,5,6]. Conversely, the pressure along the sinusoid decreases from 70 mmHg (9333 Pa) in zone 1 to 30 mmHg (2666 Pa) in zone 3 [5]. While velocities can be measured directly by tracking leukocytes or other particles in the sinusoids via in vivo microscopy, pressures across the sinusoids must be estimated from measurements of terminal portal venules and terminal hepatic venules [5]. Endothelial porosity (the area of the endothelium covered with fenestrations) also varies across hepatic zones, with fewer and narrower fenestrations in the periportal zone relative to the pericentral zone (Table 1) [2,7–10].

Table 1. Partial summary of the literature concerning sinusoidal dimensions and flow parameters.

Reference	**(i) Model; (ii) Method; (iii) Sinusoid Dimensions; (iv) Flow; (v) Pressure; (vi) Fenestrations**
Wisse, 1983 [10]	(i) Rat; (ii) SEM; (vi) porosity is higher and fenestrations have wider diameters in zone 3 than in zone 1 (97.92 vs. 76.57 nm and 11.63 vs. 6.81%)
Vidal-Vanaclocha and Barbera-Guillem, 1985 [8]	(i) Rat; (ii) SEM; (vi) zone 3 has wider fenestrations (94–121 nm vs. 73–101 nm) and a higher frequency (10.21–10.68 fenestrations/µm^2 vs. 5.74–6.26 fenestrations/µm^2) than zone 1 and a greater number of sieve plates (1.73-fold greater)
Horn, 1986 [7]	(i) Human; (ii) SEM; (vi) in zone 3, fenestrations are more numerous (23.5 vs. 19.2%) than in zone 1, and porosity is higher in zone 3 than in zone 1 (9.1 vs. 7.6%)
Wake, 1988 [3]	(i) Rat; (ii) light and electron microscopy; (iii) centrilobular LSECs are larger (longer and wider) than periportal LSECs
Henriksen and Lassen, 1988 [11]	(i) Theoretical model; (iv) the shape of the sinusoid does not affect the flow profile, which is characterized by an increasing speed moving from zone 1 to zone 3; (v) in humans, the pressure drop between the portal and central veins is between 3 and 5 mmHg (450 Pa)

Table 1. *Cont.*

Reference	(i) Model; (ii) Method; (iii) Sinusoid Dimensions; (iv) Flow; (v) Pressure; (vi) Fenestrations
Komatsu, 1990 [5]	(i) Rat; (ii) in vivo fluorescence microscopy; (iii) the diameter of the sinusoid increases from zone 1 to zone 2 to zone 3; 6.4 μm–7 μm–8.3 μm; (iv) the flow rate increases along the sinusoid, 143–221–331 μm/s; (v) the interpolated values of pressure within sinusoids are as follows: zone 1, 68–50; zone 2, 50–40; and zone 3, 40–28 mmHg
MacPhee, 1995 [4]	(i) Mouse and rat; (ii) high resolution in vivo microscopy; (iv) the flow speed is highly variable due to interactions between blood cells and the cells of the sinusoid; generally, the velocity in zone 3 is greater than in zone 1
Yoon, 2013 [12]	(i) Mouse; (ii) computed tomography; (iii) zone 1 features a smaller diameter (8.8 vs. 13.7 μm) than zone 3; (vi) zone 1 has a lower porosity than zone 3
Ryou, 2020 [13]	(v) Clinical portal hypertension has pressure above 5 mmHg (666 Pa), while normal pressure is around 3.4 mmHg (450 Pa)

The liver is the largest site of lymph production in the body, with up to 50% of the lymph that drains into the thoracic duct formed here [14]. Hepatic lymph generation begins with the filtration of blood through the fenestrations of the sinusoidal lining, followed by drainage through the lymphatic vasculature beginning in the Space of Mall (SoM), a region of the portal tract situated between the outermost hepatocytes and the hepatic stroma [15–17]). Lymph production is correlated with hydrostatic pressure within the sinusoids, with even slight pressure changes increasing lymph production and flow [14,15]. This physiological consequence, which is particularly evident in pathological conditions such as portal hypertension, is due to the high permeability of the sinusoids [18].

1.2. Models of the Hepatic Sinusoids

Given the inaccessibility of the liver sinusoids to sensors for direct measurements of hemodynamic variables, computed fluid dynamics (CFD) simulations were used to model the flow field here (Table 2).

Table 2. The most significant studies on numerical models of the liver's microvasculature. Ref. = Reference, Mod. Obj. = models of a liver sinusoid or lobule, Dim. = dimensions, Bound. Cond. = boundary conditions, Eval. Param. = evaluation parameter, v = velocity; *FR* = flow rate; *WSS* = wall shear stress; *P* = pressure; 2D = two-dimensional; 3D = three-dimensional.

Ref.	Mod. Obj.	Dim.	Origin	Bound. Cond.	Eval. Param.	Highlights
Bonfiglio (2010) [19]; Siggers (2014) [20]	Lobule	2D	Numerical	Phys., post-resection, and lymph production	*P*, blood flow distribution (v), and lymph flow	An infinite lattice of hexagonal lobules, the sinusoid space as a porous medium, the resection effect, anisotropy and shear-dependent tissue deformation, and lymph production
Debbaut (2012) [21]	Three lobules	3D	Three human lobule casts digitized using a micro-CT scanner	Phys.	*P*, permeability, preferential flow pathways, and *WSS*	A liver circulation anisotropy estimation
Piergiovanni (2017) [22]	Sinusoidal network	3D	In vivo images; mouse model	Phys.	v_{mean}, FR_{mass}, and *WSS*	Local hemodynamics; an investigation into different degrees of occlusion
Hu (2017) [23]	Lobule	3D	Numerical	Phys.; path. (fibrosis; cirrhosis)	P, v_{mean}, and FR_{vol}	Porous media approach; fibrotic–cirrhotic lobule

There are few models of the fluid dynamics of the liver or hepatic sinusoids that account for the presence of fenestrations [24], with most studies simulating whole lobules or larger areas of the liver [19–23,25–33] and, as such, accounting for porosity in a more general way (as porous medium) in their models. No one has, to our knowledge, added variable porosity to their models as such. Furthermore, the porosity of the liver sinusoid is reduced in several pathologies/conditions, such as cirrhosis [34], alcoholic liver disease [35], and in aging [36]. We therefore believe there is value added in a model that examines the single-sinusoid level, investigating the contributions made by the overall shape and the distribution of fenestrations (the porosity) in a computational fluid dynamics model of a single sinusoid. This is especially due to the effects found in microfluidics of an increasing versus constant porosity on the fluid flow velocity through a microchannel [37]. Brainerd et al. found that in a micro-channel lined with pores, the magnitude of the outflow velocity dropped significantly along its length if the porosity (% area fraction covered by open pores) was even along the length, while to achieve an even outflow from the channel, the porosity needed to increase along the length. Taken together with electron microscopic observations made on liver tissue samples, porosity was expected to contribute to fluid dynamics in the liver sinusoid.

Here, we seek to model the hemodynamics of a single liver sinusoid with a computationally inexpensive model that contains the most important ultrastructural details of the sinusoid. We aim to decipher the relative contributions of (i) the radius of the sinusoid (either as constant or expanding), (ii) the presence or absence of a periportal lymphatic drainage outlet in the space of Disse, and (iii) the distribution of fenestrations to pressure profiles and flow behavior.

2. Materials and Methods

2.1. Computational Fluid Dynamics (CFD) Simulations

CFD simulations were performed using Ansys® 2021 R1 Academic software and a laptop with the features listed below (Table 3).

Table 3. Hardware specifications.

Processor	**Intel i5-10300H**
Clock Freq. [GHz]	2.50
Core #	8
Ram [GB]	8

The numerical 2D models utilized in the simulations were two half-sections of a simplified sinusoid with either a constant luminal radius (named C = constant-radius sinusoid) or a diverging luminal radius (named D = diverging sinusoid).

Each model was tested with different porosity and inlet pressure configurations (physiological vs. pathological pressure).

The effect of a lymphatic outflow in the portal tract of the SoD was explored for each model.

Linear porosity was defined as the ratio between the length given by the sum of the fenestrations and the length of the sinusoid.

Zonal linear porosity was defined as the ratio between the length given by the sum of the fenestrations in a certain zone and the length of the zone itself.

All three zones (periportal (1), perivenous (3), and intermediate (2)) were set to the same length (275/3 = 91.667 µm).

Numerical models with constant porosity were obtained by arranging fenestrations of a constant pitch along the whole length of the sinusoid. When variable porosity was applied, the fenestration pitch varied zone by zone (but the fenestrations were evenly spaced inside the zone itself). Zones 1, 2, and 3 of the sinusoid had porosities of 5%, 6%, and 20%, respectively. Thus, changes in porosity were applied by increasing the number of fenestrations rather than enlarging their diameter (Figure 2).

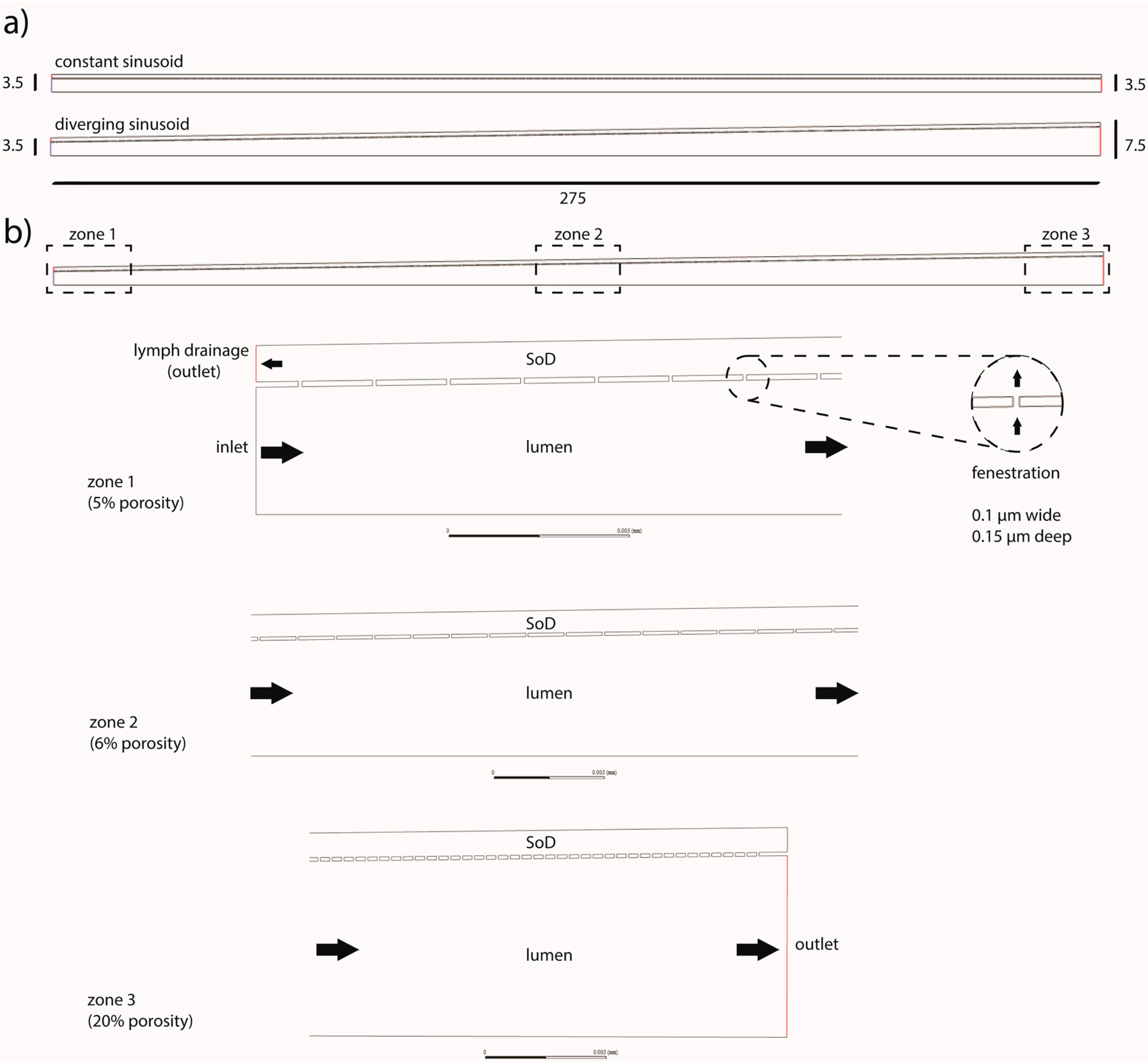

Figure 2. Schematics of the numerical models of the sinusoid. The model was designed as a half-section. Two main versions were adopted: constant-radius and diverging sinusoids (**a**). Sizes are in microns. An example of the more complete model adopted in the simulations (**b**) a diverging section, including a variable porosity (5%, 6%, and 20%) and an extra outlet at the portal side of the SoD to mimic lymphatic drainage (dark arrows indicate the direction of the flow).

2.2. Geometry and Mesh

The numerical 2D models of the sinusoid were designed to comply with both the computational capabilities of the hardware and anatomical likelihood.

- The sinusoid was designed as a half-section measuring 275 μm long. Two half-sections were evaluated, one with a constant radius (3.5 μm) and one with a linearly increasing radius (the inlet/outlet radii were, respectively, set to 3.5 μm and 7.5 μm).
- The SoD was modeled as a 1 μm thick 2D chamber surrounding the sinusoid lumen and communicating with it via fenestrations.
- The fenestrations were modeled as 100 nm long and 150 nm high channels connecting the sinusoidal lumen with the SoD (Figure 3).

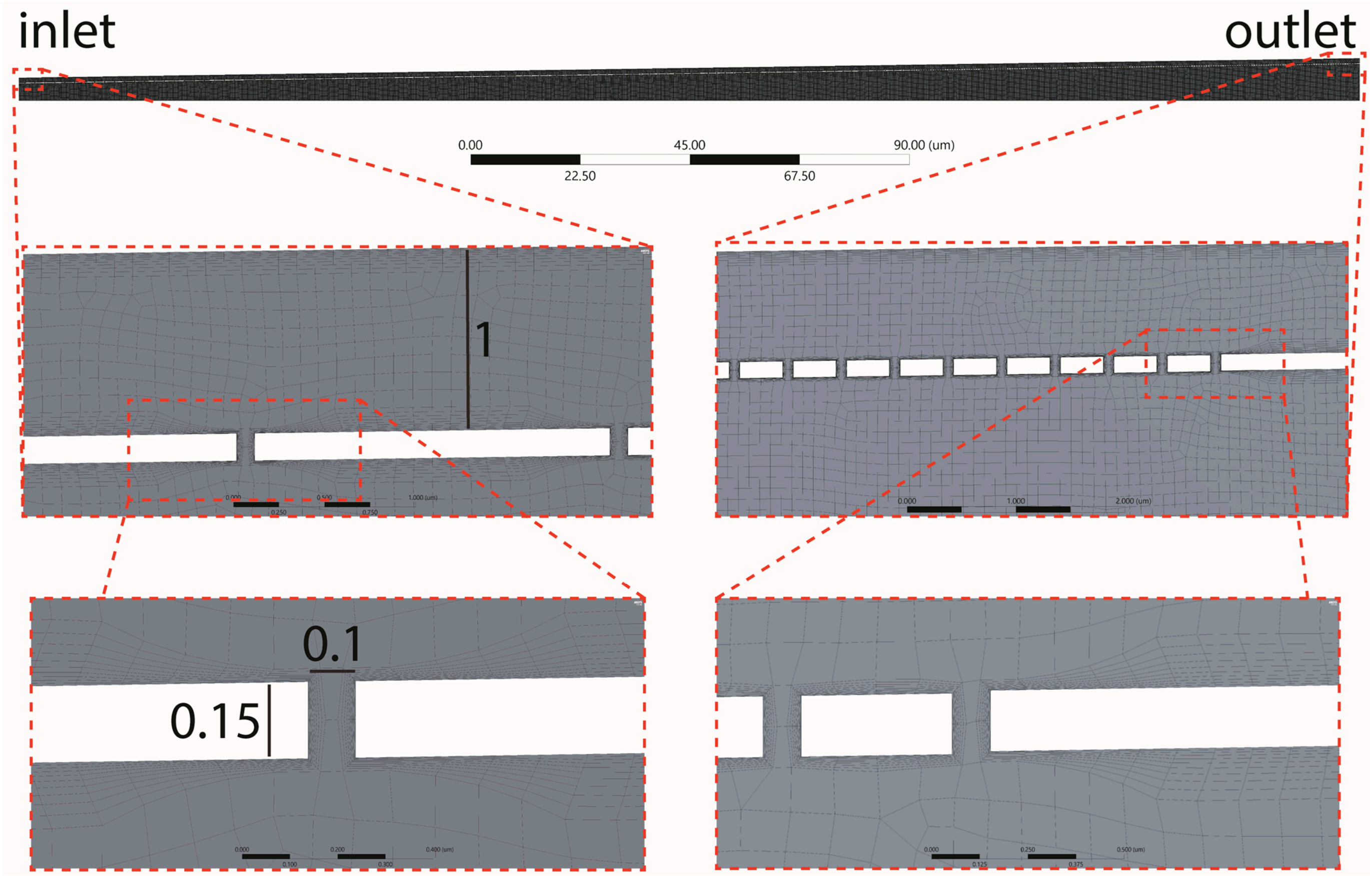

Figure 3. Mesh highlights shown for the diverging sinusoid model. The side of each element of the mesh was set to a max size of 0.1 µm. Further, in the bottom panel, the quality spectrum for the orthogonality metric is reported.

Proper geometry is essential to facilitating the meshing process (the discretization of the whole surface into tiny sub-surfaces defined by nodes for which the solver computes the solutions of the fluid dynamics equations). The main design strategies used to obtain the geometry of the sinusoid were as follows:

- The main walls (of the sinusoidal lumen and the Space of Disse lumen) were formed as two coaxial rectangles (or trapezoids when the sinusoid had a diverging section).
- Fenestrations were modeled as a linear pattern.
- The sketch was converted into a surface, and a symmetry axis was introduced (halving the model).

The finite element method (FEM) facilitates a complex system's numerical simulation. This involves the discretization of a continuous system into small elements (named cells, which are defined by nodes) over which to solve the equations. The obtained local solutions are ultimately integrated over entire domains and bodies to produce a global solution. Thus, the quality of the solutions generated by the solver strictly depend on the quality of the mesh, which defines the size, distribution, and shape of the finite elements. A reduced number of elements lead to a coarse solution with low computational costs. A high number of elements gives an accurate solution which requires time-consuming calculations. The mesh obtained had a good quality (Figure 3), thus ensuring accurate solutions. However, the mesh can be further improved by reducing the size of the elements (set here to 0.1 µm).

The laminar flow module of a pressure-based solver, which couples mass and momentum conservation with no-slip boundary conditions, was applied to disclose the pressure and linear speed profiles of a steady flow for an incompressible fluid (blood).

2.3. Solver Configuration

A Fluent solver (by Ansys) was utilized, setting a laminar-flow module with a no-slip condition at the boundaries (v = 0 at the walls). Blood at 37 °C was selected as the material (η = 0.0035 kg·m^{-1}·s^{-1}, ρ = 1060 kg/m^3). Since the computational model was based on a pressure-driven flow, the physiological pressures were set to 1067 and 800 Pa, respectively, at the inlet/outlet [13]. Pathological conditions (e.g., portal hypertension) were introduced, elevating inlet pressure up to 2400 Pa [13]. To simulate lymphatic drainage, a pressure outlet was added at the portal region (zone 1) of the SoD, and the selected exit pressure was set to 100 Pa [38]. The equations were solved using the COUPLED algorithm (keeping default under-relaxation factors). The solutions converged after 105 iterations (which were initially set to 2000 iterations).

The physics of the numerical model can be explained with the following partial differential equations (PDEs):

$$\nabla \cdot (\rho u) = 0 \tag{1}$$

That is, the mass conservation equation for an incompressible fluid where ρ is the density (kg/m^{-3}) and u is the 3D velocity vector (m/s)

$$\rho(u \cdot \nabla u) = -\nabla P + \mu \nabla 2u \tag{2}$$

which is the equation of momentum for Newtonian fluids (constant μ) where P is the pressure (Pa) and μ is the dynamic viscosity (Pa·s).

3. Results

The overall shape of the vessel had the greatest effect on the measured parameters, with the velocity magnitude greater in the divergent models compared with the constant-radii models. Velocity modules through the lumen were approximately 1.5–2-fold higher in the divergent models vs. the cylindrical models (Figures 4–6 and Tables 4–6), and the average pressure in the lumen was about 5–8% lower in the divergent models vs. the cylindrical models (Figures 7–9 and Tables 4, 7 and 8).

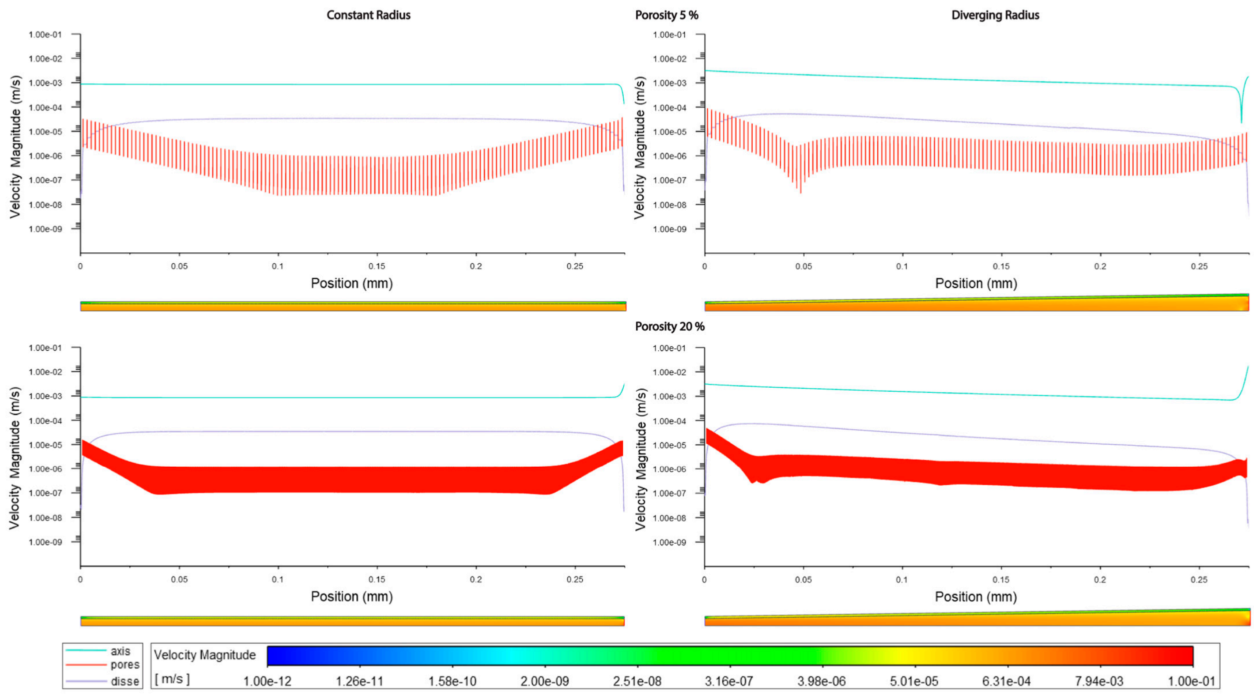

Figure 4. Velocity magnitudes along sinusoids modeled without lymphatic drainage. Models are with a constant radius (cylinder) or with a diverging radius (conical) and low (5%) porosity or high (20%) porosity.

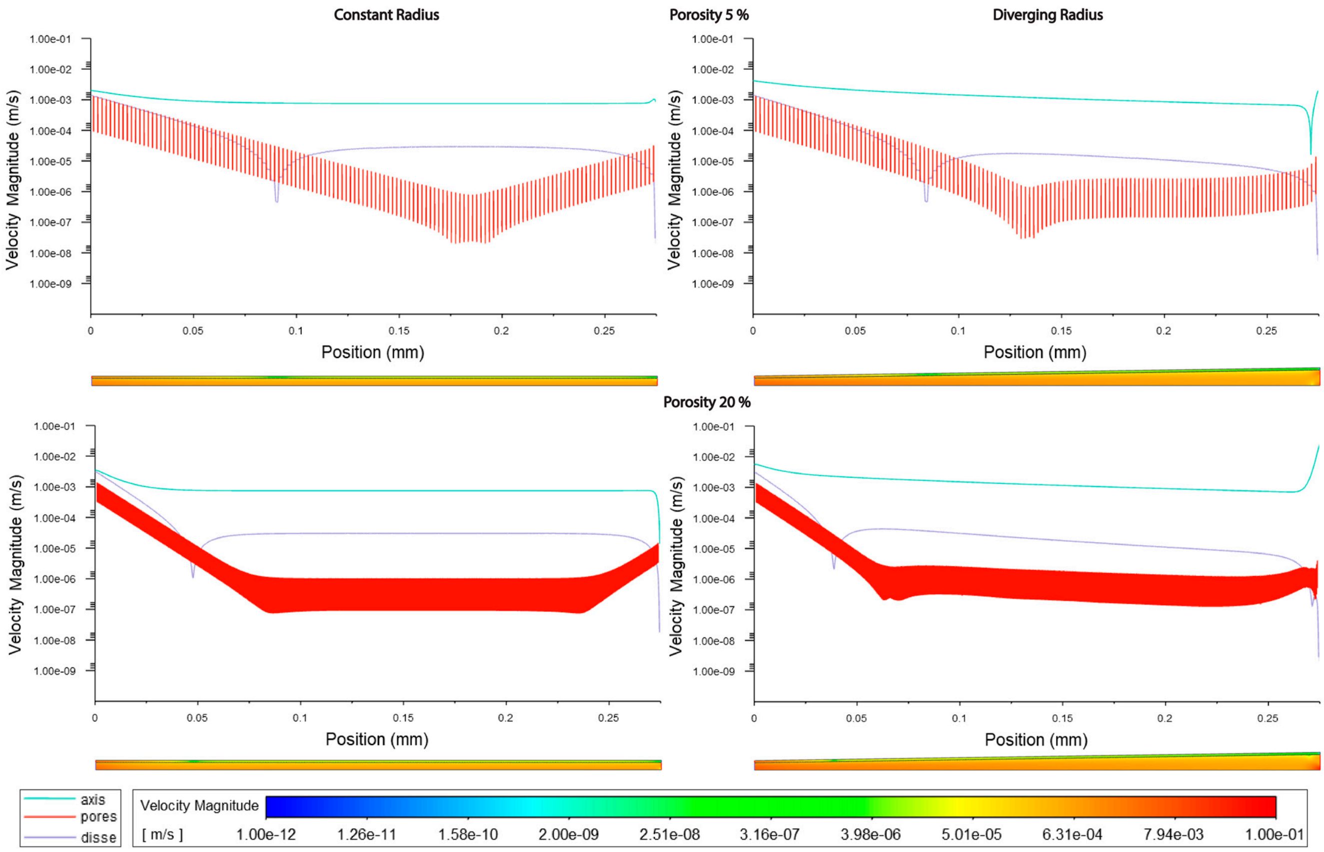

Figure 5. Velocity magnitudes along sinusoids modeled with lymphatic drainage. Models are with a constant radius (cylinder) or with a diverging radius (conical) and low (5%) porosity or high (20%) porosity.

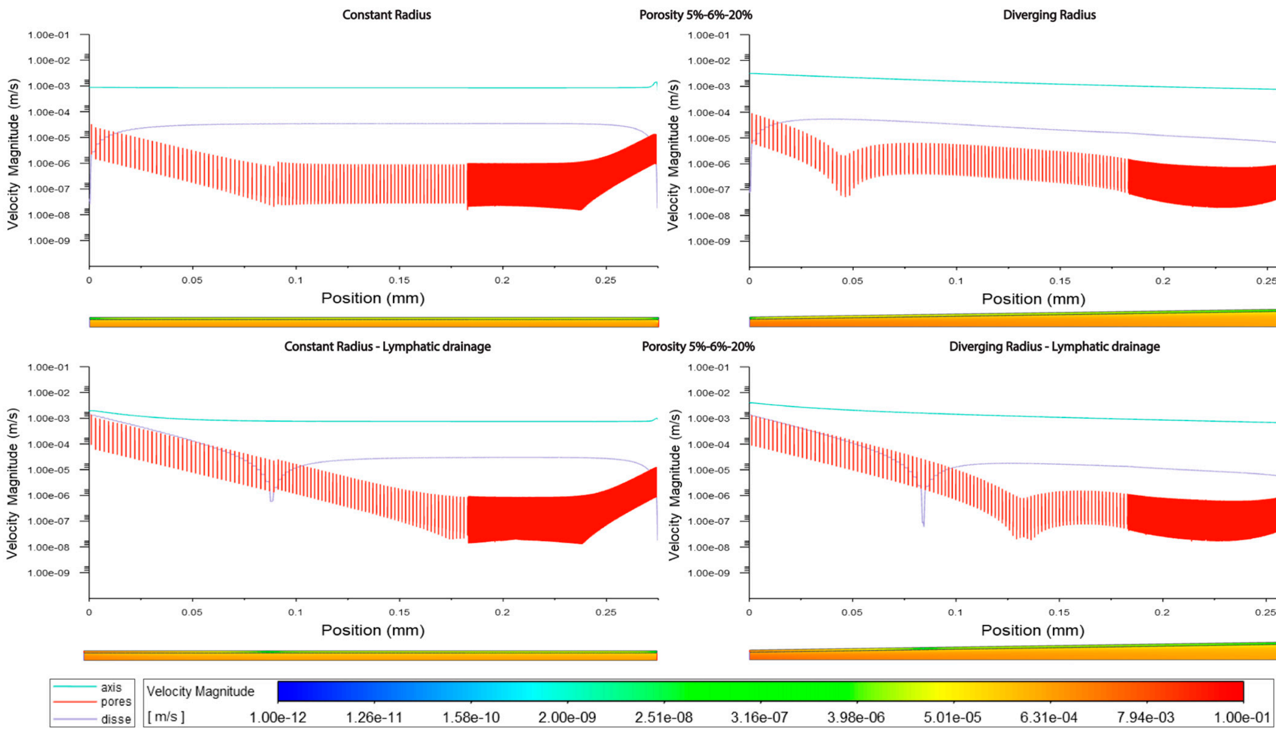

Figure 6. Velocity along sinusoids modeled with variable porosity (5, 6, 20%). Models are with a constant radius (cylinder) or with a diverging radius (conical) and with or without lymphatic drainage.

Table 4. Quantitative evaluation of pressure (P) and velocity (V) at the axis of the simplified models of the sinusoid without fenestrations or lymphatic drainage (constant-radius and diverging-radius microchannels).

	Constant Radius		**Divergent Radius**	
	P [Pa]	**V [m/s]**	**P [Pa]**	**V [m/s]**
max	1067.69	0.001	1066.95	0.0032
min	800.146	0.0008	799.876	0.0007
avg	933.5973	0.00085	871.9508	0.0015
Std.dev	77.1903	1.00×10^{-5}	69.201	0.0007

Table 5. Velocity magnitudes in sinusoids modeled without lymphatic drainage. Const. rad. = constant radius; Div. rad. = diverging radius; porosity given as %; Var = variable increasing porosity 5–20%; l = lumen centre line; f = fenestrations; D = Space of Disse.

	Const. rad. 5%			**Const. rad. Var**			**Const. rad 20%**		
	l	**f**	**D**	**l**	**f**	**D**	**l**	**f**	**D**
max	0.00087	0.000038	0.000034	0.0015	0.000033	0.000035	0.0033	0.000016	0.000035
min	0.00013	0	0	0.00054	0	0	0.00085	0	0
avg	0.00084	2.8×10^{-6}	0.000029	0.00086	1.2×10^{-6}	0.00003	0.00086	0.000001	0.000032
Std.dev	0.000047	0.000005	0.000008	0.000044	2.5×10^{-6}	7.7×10^{-6}	0.00013	1.9×10^{-6}	6.7×10^{-6}
	Div. rad. 5%			**Div. rad. Var**			**Div. rad. 20%**		
	l	**f**	**D**	**l**	**f**	**D**	**l**	**f**	**D**
max	0.0031	0.00009	0.000053	0.0032	0.00009	0.000054	0.019	0.000049	0.000075
min	0.000022	0	0	0.000019	0	0	0.0007	0	0
avg	0.0015	0.000004	0.000025	0.0015	0.000002	0.000026	0.0015	1.8×10^{-6}	0.000028
Std.dev	0.00066	8.5×10^{-6}	0.000016	0.00067	6.63×10^{-6}	0.000016	0.0011	4.3×10^{-6}	0.000022

Table 6. Velocity magnitudes in sinusoids modeled with lymphatic drainage. Const. rad. = constant radius; Div. rad. = diverging radius; porosity given as %; Var = variable increasing porosity 5–20%; l = lumen centre line; f = fenestrations; D = Space of Disse.

	Const. rad. 5%			**Const. rad. Var**			**Const rad. 20%**		
	l	**f**	**D**	**l**	**f**	**D**	**l**	**f**	**D**
max	0.002	0.0013	0.0014	0.002	0.0014	0.0014	0.0035	0.0014	0.003
min	0.00075	0	0	0.00065	0	0	0.000014	0	0
avg	0.00086	0.000057	0.00012	0.00086	0.000019	0.00012	0.00085	0.000029	0.00014
Std.dev	0.00024	0.00016	5.25×10^{-5}	0.00025	0.00085	0.00026	0.0004	0.00012	0.00042
	Div. rad. 5%			**Div. rad. Var**			**Div. rad. 20%**		
	l	**f**	**D**	**l**	**f**	**D**	**l**	**f**	**D**
max	0.0041	0.0013	0.0014	0.004	0.0013	0.0014	0.025	0.0014	0.003
min	0.000016	0	0	0.000016	0	0	0.0007	0	0
avg	0.0014	0.000051	0.00011	0.0014	0.000025	0.00011	0.0017	0.000031	0.00012
Std.dev	0.0008	0.00015	0.00026	0.0008	0.00011	0.00025	0.0016	0.00013	0.00041

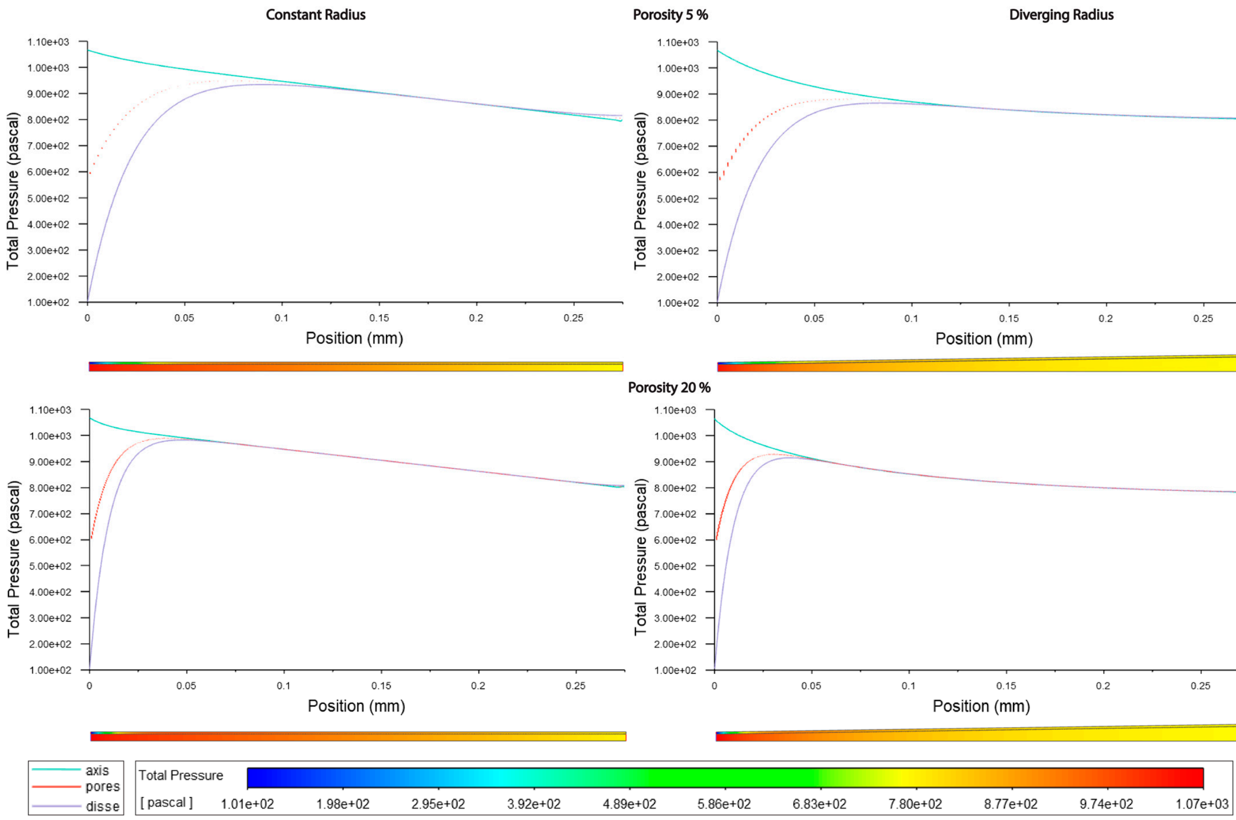

Figure 7. Pressure along sinusoids modeled with lymphatic drainage. Models are with a constant radius (cylinder) or with a diverging radius (conical) and low (5%) porosity or high (20%) porosity (top/bottom).

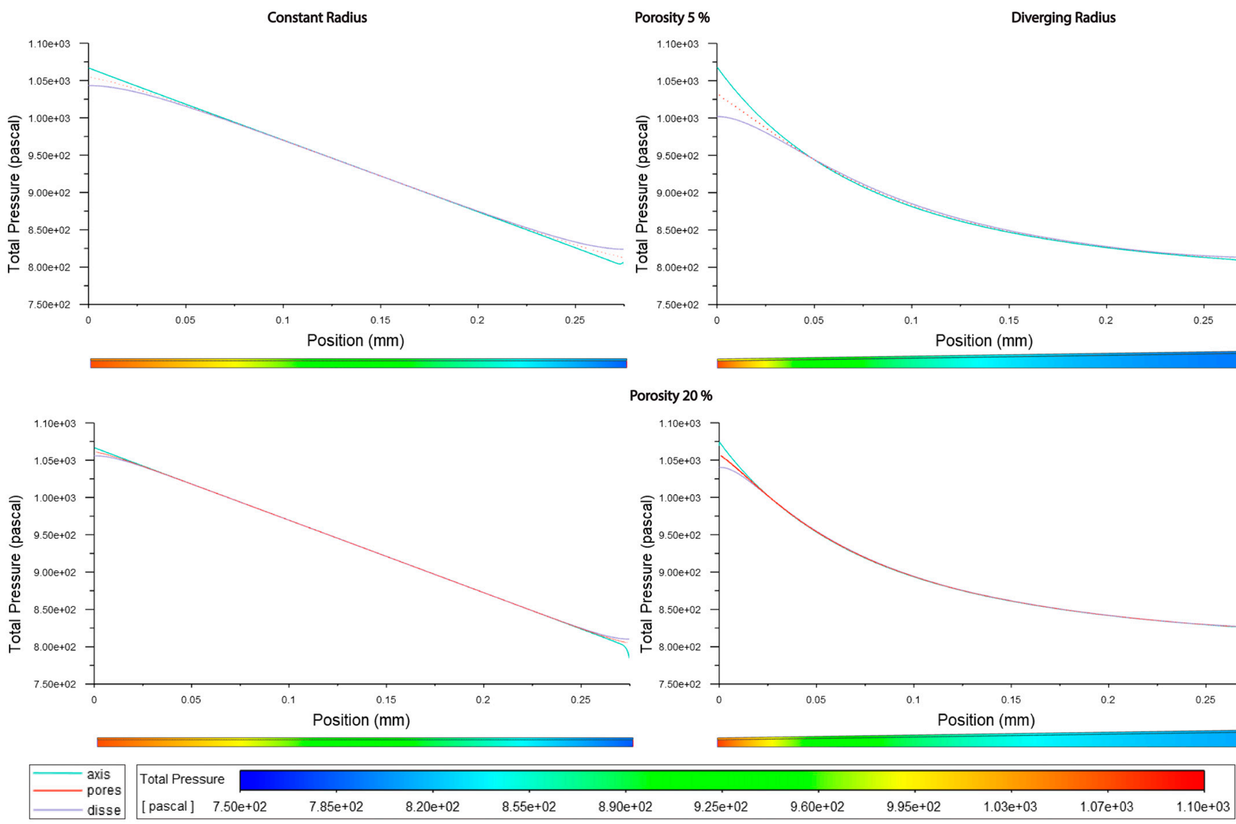

Figure 8. Pressure along sinusoids modeled without lymphatic drainage. Models are with a constant radius (cylinder) or with a diverging radius (conical) and low (5%) porosity or high (20%) porosity.

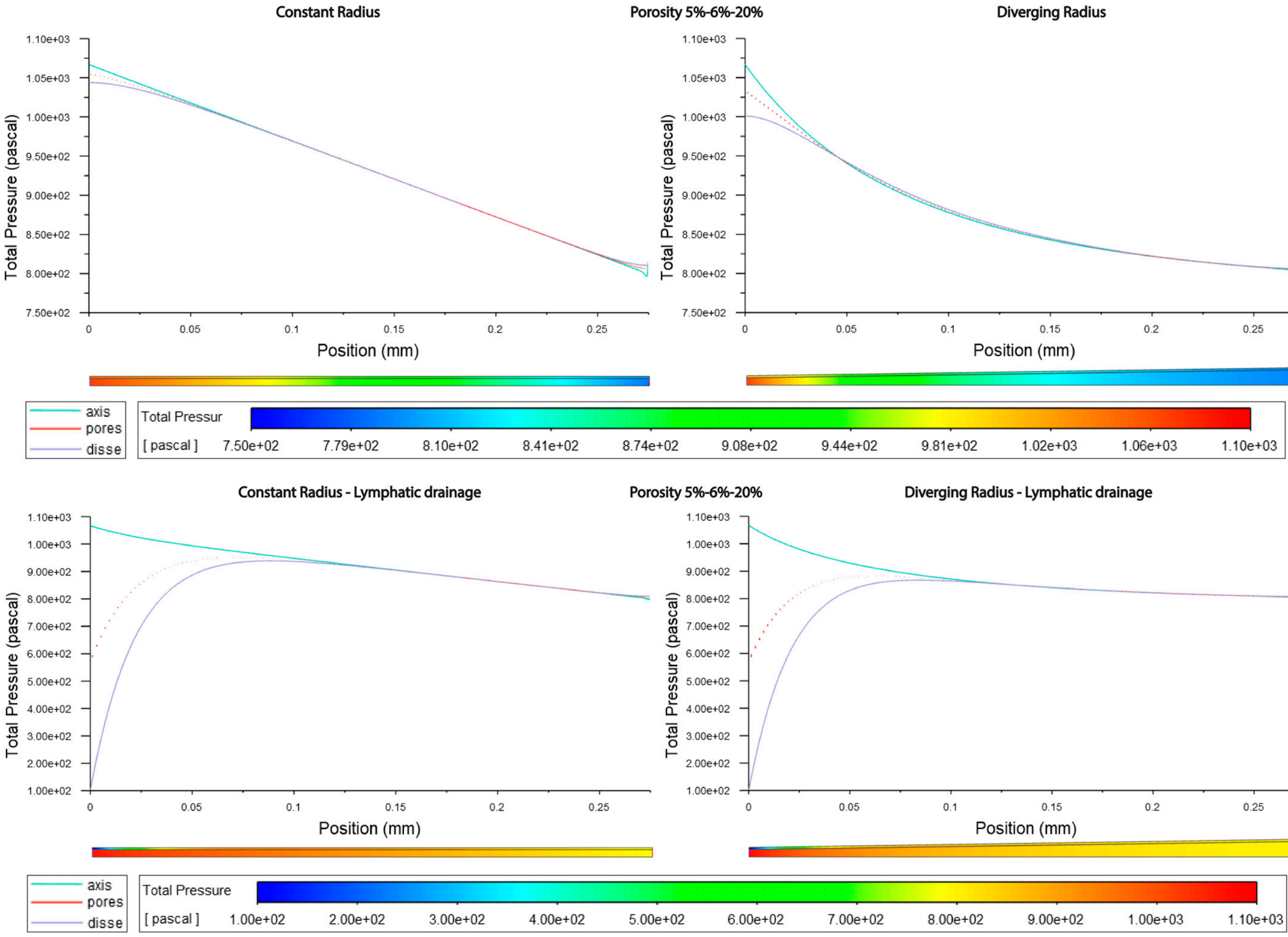

Figure 9. Pressure along sinusoids modeled with variable porosity (5, 6, 20%). Models are with a constant radius (cylinder) or with a diverging radius (conical) and with or without lymphatic drainage.

Table 7. Pressure in sinusoids modeled without lymphatic drainage. Const. rad. = constant radius; Div. rad. = diverging radius; porosity given as %; Var = variable increasing porosity 5–20%; l = lumen centreline; f = fenestrations; D = Space of Disse.

	Const. rad. 5%			**Const. rad. Var**			**Const rad. 20%**		
	l	**f**	**D**	**l**	**f**	**D**	**l**	**f**	**D**
max	1067	1054	1043	1067	1055	1044	1067	1061	1056
min	802	813	824	796	806	811	785	806	810
avg	934	934	934	933	883	931	933	933	933
Std.dev	76	73	73	77	67	74	77	76	76
	Div. rad. 5%			**Div. rad. Var**			**Div. rad. 20%**		
	l	**f**	**D**	**l**	**f**	**D**	**l**	**f**	**D**
max	1068	1031	1002	1067	1031	1001	1074	1056	1040
min	809	8110	813	805	802	806	748	826	827
avg	878	877	878	874	844	873	891	891	891
Std.dev	67	62	59	68	53	61	65	63	62

Table 8. Pressure in sinusoids modeled with lymphatic drainage. Const. rad. = constant radius; Div. rad. = diverging radius; porosity given as %; Var = variable increasing porosity 5–20%; l = lumen centreline; f=fenestrations; D = Space of Disse.

	Const. rad. 5%			Const. rad. Var			Const rad. 20%		
	l	f	D	l	f	D	l	f	D
max	1067	949	934	1067	952	939	1067	989	983
min	794	592	102	798	588	102	800	604	103
avg	917	876	836	919	857	840	917	900	881
Std.dev	73	65	140	71	50	140	69	65	110
	Div. rad. 5%			**Div. rad. Var**			**Div. rad. 20%**		
	l	f	D	l	f	D	l	f	D
max	1067	880	865	1067	883	868	1066	929	915
min	805	570	102	806	586	102	656	600	105
avg	869	828	791	870	823	792	850	834	816
Std.dev	65	50	129	65	34	128	68	50	93

The increment of zonal porosity increased the velocity in the SoD by 9–16% while decreasing the velocity through fenestrations by 40–55%; there was a modest decrease in luminal velocity in the cylindrical models, while there was a slight increase in the divergent models. Velocity magnitudes through the SoD were 3–4-fold higher in models with lymphatic drainage than in those without (Figures 4–6; Tables 5 and 6).

Velocity magnitudes through fenestrations were lower in high-porosity models (high = 20%) without lymphatic drainage, while in models with lymphatic drainage, the velocities were higher when the porosity was low (low = 5%) than when the porosity was high; additionally, velocities were lower in variable-porosity models (variable = 5, 6, 20%) than in either low- or high-porosity models (Figures 4–6; Tables 5 and 6).

The luminal velocity magnitude was slightly higher in constant-radius models without lymphatic drainage (with high and variable levels of porosity) and unchanged in divergent-radius models. In constant-radius models with lymphatic drainage, the luminal velocity was higher in low- and variable-porosity models. The luminal velocity in divergent-radius models was higher when models had high levels of porosity and lymphatic drainage and were equal in all others (Figures 4–6; Tables 5 and 6).

For models without lymphatic drainage and with a divergent radius, the luminal pressure was the lowest in variable-porosity models, while for constant-radius models with lymphatic drainage, variable-porosity models had slightly higher luminal pressure values. In divergent models with lymphatic drainage, variable-porosity models had the highest average pressure, with lower pressures observed in low-porosity models. The pressure was even lower in high-porosity models (Figures 7 and 8; Tables 7 and 8).

The pressure across fenestrations was the lowest in the variable-porosity models compared to those with uniform porosity. In the latter, pressure across fenestrations was greatest in the high-porosity models compared to the low-porosity models (Figures 7–9; Tables 7 and 8).

In models without lymphatic drainage, the pressure in the SoD was always lower in the variable-porosity models, whereas in models with lymphatic drainage, the pressure increased from low to variable to high (Figures 7–9; Tables 7 and 8).

In general, the variable porosity model had velocity and pressure curves between low constant porosity and high constant porosity, being somewhat closer to low constant porosity (Figures 4–9).

In total, the overall shape of the vessel (Figures 4–9, Tables 4–8) and the presence or absence of lymphatic drainage in the periportal zone had the largest effects on the flow parameters, while porosity had some less-pronounced effects.

Modeling with a pathological (elevated) pressure regimen did not show any changes in pressure or flow behavior. Increasing the input/output pressures to 2400/800 Pa, as per Ryou 2020 [13], only rescaled proportionally to increases in pressure, with the same patterns as those found for physiological pressures, i.e., the differences between them were merely rescaled.

Admixing: Regarding flowlines, the addition of lymphatic drainage in the periportal zone leads to more fluid moving through the SoD and more admixing relative to models without, whereas porosity only has a modest effect when comparing models with low, high, or variable porosity (Figures S1–S3). Divergent models show the formation of stronger vortexes at the outlet compared with constant-radius models.

4. Discussion

Four physiologically relevant 2D models of hepatic sinusoids were generated for CFD simulations to provide hemodynamics insights. Simulations were carried out using a laminar and steady flow of blood (constant dynamic viscosity) generated via a differential pressure between the sinusoid's inlet and outlet. Velocity and pressure trends were collected for all models for physiological and pathophysiological (elevated) pressure conditions. Also, an extra outlet was added to the model to reproduce the lymphatic drainage in the portal zone of the SoD.

4.1. Major Insights about Sinusoidal Pressure (P)

Pressure decreases linearly in constant-radius models (Cmods) and exponentially in diverging-radius models (Dmods). Dmods generally have lower pressure throughout when compared with Cmods. Increased porosity in the pericentral zone implies a generalized pressure reduction, mostly borne by the SoD. Lymphatic drainage reduces with the pressure within the sinusoid, especially inside the SoD. This effect might be exaggerated by the model (see below in general considerations).

Pathological conditions, (PatCs), elevated pressures, merely re-scale the same pressure behavior obtained for physiological conditions (PhyCs). In terms of average pressure, the sinusoidal lumen and SoD have comparable pressure, while through fenestrations, pressure is generally lower.

4.2. Major Insights Regarding Flow Velocity (V)

In general, Cmods have constant luminal velocity and an almost constant velocity within the SoD. Velocity through the fenestration develops along the sinusoid with a parabolic trend, with higher values at the inlet/outlet (where the flow enters/exits the SoD). In general, Dmods demonstrate a slowly decreasing velocity along the sinusoidal lumen and along the SoD. Through the fenestrations, velocity decreases within the first 50-100µm and then follows a sinusoidal trend, with values increasing in the proximity of the outlet. Globally, Dmods produced greater velocities in all compartments of the sinusoid when compared with Cmods. Some of the models (especially but not only the Dmods) present a reverse flow at the outlet. Porosity augmentation in the perivenous zone mostly affects velocity of the SoD and through fenestrations (with no effect on the luminal speed—the flow through fenestrations and the SoD seeks to compensate for the changes in porosity). Generally, velocity increases within the SoD, while it decreases through fenestrations. Adding lymphatic drainage to the perivenous zone generated a shift in the velocity trend toward the outlet. The average flow speed through fenestrations reaches higher values and decreases more slowly within the first half of the sinusoid (an increased flow exchange between the lumen and SoD). Similarly, the flow along the SoD is characterized by a higher average speed. PatCs merely re-scale the same velocity behavior obtained for PhyCs.

4.3. General Considerations and Limitations

The overall shape of the sinusoids had the greatest influence on the luminal pressure and velocities; this is a parameter that may be altered in disease states [12,34]. When implementing a larger-scale model, this is likely the single most important parameter investigated here. Intuitively, we would have expected that porosity would have far greater effects on these luminal parameters, but this was not the case except at an extremely high porosity.

The addition of lymphatic drainage affected the flow through the fenestrations and SoD. It is therefore an important parameter to consider when modeling liver sinusoids. Lymphatic drainage in the SoD was modeled as a depressurization affecting the flow within the entire sinusoid. Since the lymphatic flow rate is estimated to be 100–500 times lower than the flow rate of blood [39], it may be necessary to adjust the pressure value at the drainage outlet. Also, lymphatic drainage is expected to be much higher under pathological conditions [14,16]; this aspect was not taken into account in our simulations.

With the current boundary conditions (PhyCs and PatCs), porosity variations seem to be fully compensated for through an exchange of flow between the lumen and SoD via fenestrations without affecting the flow velocity inside the lumen. If this model translates to the liver, then, in theory, the liver can change the flow in the SoD by changing the porosity without altering the luminal flow velocity. In the model, the elevated pressure seen in pathologies does not cause alterations to the flow pattern with unchanged geometries. While the model does not account for cellular responses to elevated pressure and flow velocity, it shows that the sinusoidal geometry must be altered for flow patterns to change.

The model employs a homogeneous variation of porosity, with evenly spaced and sized fenestrations. We believe this simplification in our model is justified for our application, but others will need to evaluate the complexity required by their inquiry. The model simplifies the sinusoid into a straight line, whereas the real case would be curved and branching. In addition, liver sinusoids are flexible and dynamic structures due to the fact they are in a soft tissue and are exposed to pulsatile flow. Our simplifications were necessary to home in on the focus of this article, namely the variable porosity and diameter in and of the sinusoid.

Luminal flow and pressure are mainly affected by the overall shape, i.e., the evolution of the vessel's diameter, with porosity mostly affecting flow within the SoD. Variable porosity, with higher porosity toward the pericentral/zone 3, modestly increases flow velocity through the SoD relative to a constant-porosity model but also decreases velocity through fenestrations significantly. In the variable-porosity models, pressures through fenestrations were lower than for models with either high or low constant porosity. Similarly, the pressure in the SoD was lower for models without lymphatic drainage, or similar (less than 1% increase) for models with lymphatic drainage, in the variable-porosity models compared with the constant-low-porosity models and always lower than in the constant-high-porosity models.

We simulated lymphatic drainage by adding an outlet in the periportal area of the SoD; this inclusion increased flow velocity and the exchange between the lumen and SoD. However, more detailed studies of how this parameter evolves are required as it is poorly understood and it is currently not feasible to measure it directly. This is beyond the scope of the current study.

Some effects may be underestimated in the model due to parameter reductions as pulsatile flow, curved geometry, tissue compressibility, and the obstruction of flow by migrating blood cells [4,40] were not incorporated. The addition of these may be feasible with better computational hardware. Adding fenestrations with realistic porosity to a larger, more detailed model, such as the one used by Piergiovanni (2017) [22], would perhaps help elucidate the distribution patterns of various solutes and colloids at the sinusoid level but would have greater requirements in terms of both time and hardware.

The model did not account for the pulsatility of the flow, as is the case for blood flow, or the elasticity of the tissue itself, which can compress in response to pressure. Lymphatic outflow was simplified to a constant, and more accurate modeling would require an independent investigation in conjunction with experimental work. However, we showed that lymphatic drainage has the potential to affect relevant flow parameters within the sinusoid. The model reveals differences in the fluid flow velocity through the SoD between constant- and variable-porosity models, and this may have implications for solute exchange between the blood stream and the hepatocytes. Blood flow is crucial in liver function [41], and our model sought to elucidate how the ultra-structure of the liver affects this flow. Additional aspects we chose to simplify for the model were the shapes and sizes of the fenestrations. In reality, their diameters vary, and the distribution of their sizes has implications for the access of colloids and nanoparticles to the Space of Disse. It was not crucial to address this factor in the context of our fluid model, but for studies on nanoparticles or lipoproteins, this may be important to consider. There would be considerable benefit in generating more accurate and detailed models of the sinusoid. In addition to the parameters studied herein, these should also account for the branching (ideally in three dimensions) and elasticity of the tissue itself, a double inlet (arterial and venous contributions), pulsatile flow, lymphatic drainage (which is probably related to the pulsatility of the flow and probably has an intermittent outflow into the lymphatics based on pressure maxima in the sinusoid; however, this requires further dedicated studies for clarification), with mixing and flow-paths described in the case of pulsatile flow with lightly adherent blood cells (such as leukocytes) in the sinusoid (the contributions these make were theorized by Wisse [40]) and with fenestration diameters based on observed distributions. Nonetheless, this model represents a useful first approximation of the liver sinusoid which can be built upon with extra parameters and computing power.

Supplementary Materials: The following supporting information can be downloaded at: https://www.mdpi.com/article/10.3390/livers3040043/s1, Figure S1: Streamlines at Inlet (left hand side) and Outlet (right hand side) for sinusoids modelled without lymphatic drainage, Figure S2: Streamlines at Inlet (left hand side) and Outlet (right hand side) for sinusoids modelled with lymphatic drainage, Figure S3: Streamlines at Inlet (left hand side) and Outlet (right hand side) for sinusoids modelled with variable porosity (5-6-20%)

Author Contributions: Conceptualization: C.F.H.; methodology: M.B.; writing—original draft: M.B. and C.F.H.; review and editing: M.B., C.F.H. and P.A.G.M.; supervision: P.A.G.M. All authors have read and agreed to the published version of the manuscript.

Funding: This project was funded in part by Horizon 2020 MSCA ITN DeLIVER (grant no. 766181) and the Faculty of Health Sciences UiT.

Data Availability Statement: Data are available upon reasonable request from the corresponding author.

Acknowledgments: Special thanks are given to Lynn Butler for English-language revisions and Antoni Homs Corbera and Karolina Szafranska for scientific input.

Conflicts of Interest: The authors declare no conflict of interest.

References

1. Ehrlich, A.; Duche, D.; Ouedraogo, G.; Nahmias, Y. Challenges and Opportunities in the Design of Liver-on-Chip Microdevices. *Annu. Rev. Biomed. Eng.* **2019**, *21*, 219–239. [CrossRef]
2. Cogger, V.C.; Hunt, N.J.; Le Couteur, D.G. Fenestrations in the Liver Sinusoidal Endothelial Cell. In *The Liver*; Wiley: Hoboken, NJ, USA, 2020; pp. 435–443. [CrossRef]
3. Wake, K.; Motomatsu, K.; Dan, C.; Kaneda, K. Three-Dimensional Structure of Endothelial Cells in Hepatic Sinusoids of the Rat as Revealed by the Golgi Method. *Cell Tissue Res.* **1988**, *253*, 563–571. [CrossRef] [PubMed]
4. MacPhee, P.J.; Schmidt, E.E.; Groom, A.C. Intermittence of Blood Flow in Liver Sinusoids, Studied by High-Resolution in Vivo Microscopy. *Am. J. Physiol.—Gastrointest. Liver Physiol.* **1995**, *269*, G692–G698. [CrossRef]
5. Komatsu, H.; Koo, A.; Guth, P.H. Leukocyte Flow Dynamics in the Rat Liver Microcirculation. *Microvasc. Res.* **1990**, *40*, 1–13. [CrossRef]
6. Eguchi, H.; Sato, N.; Matsumura, T.; Minamiyama, M.; Kawano, S.; Kamada, T. The Microcirculatory Properties around the Hepatic Periportal and Pericentral Regions of Rats. In Proceedings of the Fourth World Congress for Microcirculation, Beijing, China, 20–22 July 1987.

7. Horn, T.; Henriksen, J.H.; Christoffersen, P. The Sinusoidal Lining Cells in "Normal" Human Liver. A Scanning Electron Microscopic Investigation. *Liver* **1986**, *6*, 98–110. [CrossRef]
8. Vidal-Vanaclocha, F.; Barberá-Guillem, E. Fenestration Patterns in Endothelial Cells of Rat Liver Sinusoids. *J. Ultrastruct. Res. Mol. Struct. Res.* **1985**, *90*, 115–123. [CrossRef] [PubMed]
9. Wack, K.E.; Ross, M.A.; Zegarra, V.; Sysko, L.R.; Watkins, S.C.; Stolz, D.B. Sinusoidal Ultrastructure Evaluated during the Revascularization of Regenerating Rat Liver. *Hepatology* **2001**, *33*, 363–378. [CrossRef]
10. Wisse, E.; De Zanger, R.B.; Jacobs, R.; McCuskey, R.S. Scanning Electron Microscope Observations on the Structure of Portal Veins, Sinusoids and Central Veins in Rat Liver. *Scan. Electron Microsc.* **1983**, *Pt 3*, 1441–1452.
11. Henriksen, J.H.; Lassen, N.A. Pressure Profile in Liver Sinusoids A Model of Localization of Sinusoidal Resistance in the Normal and Cirrhotic Liver. *Liver* **1988**, *8*, 88–94. [CrossRef] [PubMed]
12. Yoon, Y.J.; Chang, S.; Kim, O.Y.; Kang, B.K.; Park, J.; Lim, J.H.; Yun Huang, J.; Kim, Y.K.; Byun, J.H.; Gho, Y.S. Three-Dimensional Imaging of Hepatic Sinusoids in Mice Using Synchrotron Radiation Micro-Computed Tomography. *PLoS ONE* **2013**, *8*, e68600. [CrossRef]
13. Ryou, M.; Stylopoulos, N.; Baffy, G. Nonalcoholic Fatty Liver Disease and Portal Hypertension. *Explor. Med.* **2020**, *1*, 149–169. [CrossRef] [PubMed]
14. Tanaka, M.; Iwakiri, Y. Lymphatics in the Liver. *Curr. Opin. Immunol.* **2018**, *53*, 137–142. [CrossRef] [PubMed]
15. Tanaka, M.; Iwakiri, Y. The Hepatic Lymphatic Vascular System: Structure, Function, Markers, and Lymphangiogenesis. *Cell. Mol. Gastroenterol. Hepatol.* **2016**, *2*, 733–749. [CrossRef]
16. Jeong, J.; Tanaka, M.; Iwakiri, Y. Hepatic Lymphatic Vascular System in Health and Disease. *J. Hepatol.* **2022**, *77*, 206–218. [CrossRef] [PubMed]
17. Santambrogio, L. The Lymphatic Fluid. *Int. Rev. Cell Mol. Biol.* **2018**, *337*, 111–133. [CrossRef]
18. Hsu, M.C.; Itkin, M. Lymphatic Anatomy. *Tech. Vasc. Interv. Radiol.* **2016**, *19*, 247–254. [CrossRef]
19. Bonfiglio, A.; Leungchavaphongse, K.; Repetto, R.; Siggers, J.H. Mathematical Modeling of the Circulation in the Liver Lobule. *J. Biomech. Eng.* **2010**, *132*, 111011. [CrossRef]
20. Siggers, J.H.; Leungchavaphongse, K.; Ho, C.H.; Repetto, R. Mathematical Model of Blood and Interstitial Flow and Lymph Production in the Liver. *Biomech. Model. Mechanobiol.* **2014**, *13*, 363–378. [CrossRef]
21. Debbaut, C.; Vierendeels, J.; Casteleyn, C.; Cornillie, P.; Van Loo, D.; Simoens, P.; Van Hoorebeke, L.; Monbaliu, D.; Segers, P. Perfusion Characteristics of the Human Hepatic Microcirculation Based on Three-Dimensional Reconstructions and Computational Fluid Dynamic Analysis. *J. Biomech. Eng.* **2012**, *134*, 011003. [CrossRef]
22. Piergiovanni, M.; Bianchi, E.; Capitani, G.; Li Piani, I.; Ganzer, L.; Guidotti, L.G.; Iannacone, M.; Dubini, G. Microcirculation in the Murine Liver: A Computational Fluid Dynamic Model Based on 3D Reconstruction from In Vivo Microscopy. *J. Biomech.* **2017**, *63*, 125–134. [CrossRef]
23. Hu, J.; Lü, S.; Feng, S.; Long, M. Flow Dynamics Analyses of Pathophysiological Liver Lobules Using Porous Media Theory. *Acta Mech. Sin. Xuebao* **2017**, *33*, 823–832. [CrossRef]
24. Rani, H.P.; Sheu, T.W.H.; Chang, T.M.; Liang, P.C. Numerical Investigation of Non-Newtonian Microcirculatory Blood Flow in Hepatic Lobule. *J. Biomech.* **2006**, *39*, 551–563. [CrossRef] [PubMed]
25. Rohan, E.; Turjanicová, J.; Lukeš, V. Multiscale Modelling of Liver Perfusion. In Proceedings of the 15 International Conference on Computational Plasticity: Fundamentals and Applications, COMPLAS 2019, Barcelona, Spain, 3–5 September 2019; pp. 343–353.
26. Debbaut, C.; Monbaliu, D.; Casteleyn, C.; Cornillie, P.; Van Loo, D.; Van Hoorebeke, L.; Simoens, P.; Pirenne, J.; Segers, P. Multiscale Modeling of the Blood Circulation in the Human Liver Using Vascular Corrosion Casting and Micro-CT Imaging Techniques. In *Proceedings of the ASME 2011 Summer Bioengineering Conference, Parts A and B, Farmington, PA, USA, 22–25 June 2011*; American Society of Mechanical Engineers: New York, NY, USA, 2011; pp. 451–452. [CrossRef]
27. Ricken, T.; Dahmen, U.; Dirsch, O. A Biphasic Model for Sinusoidal Liver Perfusion Remodeling after Outflow Obstruction. *Biomech. Model. Mechanobiol.* **2010**, *9*, 435–450. [CrossRef] [PubMed]
28. Ahmadi-Badejani, R.; Mosharaf-Dehkordi, M.; Ahmadikia, H. An Image-Based Geometric Model for Numerical Simulation of Blood Perfusion within the Liver Lobules. *Comput. Methods Biomech. Biomed. Eng.* **2020**, *23*, 987–1004. [CrossRef]
29. Mosharaf-Dehkordi, M. A Fully Coupled Porous Media and Channels Flow Approach for Simulation of Blood and Bile Flow through the Liver Lobules. *Comput. Methods Biomech. Biomed. Eng.* **2019**, *22*, 901–915. [CrossRef]
30. Schwen, L.O.; Krauss, M.; Niederalt, C.; Gremse, F.; Kiessling, F.; Schenk, A.; Preusser, T.; Kuepfer, L. Spatio-Temporal Simulation of First Pass Drug Perfusion in the Liver. *PLoS Comput. Biol.* **2014**, *10*, e1003499. [CrossRef] [PubMed]
31. Schwen, L.O.; Schenk, A.; Kreutz, C.; Timmer, J.; Rodríguez, M.M.B.; Kuepfer, L.; Preusser, T. Representative Sinusoids for Hepatic Four-Scale Pharmacokinetics Simulations. *PLoS ONE* **2015**, *10*, e133653. [CrossRef]
32. Barléon, N.; Clarke, R.J.; Ho, H. Novel Methods for Segment-Specific Blood Flow Simulation for the Liver. *Comput. Methods Biomech. Biomed. Eng.* **2018**, *21*, 780–783. [CrossRef]
33. Rezania, V.; Coombe, D.; Tuszynski, J.A. A Physiologically-Based Flow Network Model for Hepatic Drug Elimination III: 2D/3D DLA Lobule Models. *Theor. Biol. Med. Model.* **2016**, *13*, 9. [CrossRef]
34. Ni, Y.; Li, J.-M.; Liu, M.-K.; Zhang, T.-T.; Wang, D.-P.; Zhou, W.-H.; Hu, L.-Z.; Lv, W.-L. Pathological Process of Liver Sinusoidal Endothelial Cells in Liver Diseases. *World J. Gastroenterol.* **2017**, *23*, 7666–7677. [CrossRef]

35. Horn, T.; Christoffersen, P.; Henriksen, J.H. Alcoholic Liver Injury: Defenestration in Noncirrhotic Livers-a Scanning Electron Microscopic Study. *Hepatology* **1987**, *7*, 77–82. [CrossRef] [PubMed]
36. Hilmer, S.N.; Cogger, V.C.; Fraser, R.; McLean, A.J.; Sullivan, D.; Le Couteur, D.G. Age-Related Changes in the Hepatic Sinusoidal Endothelium Impede Lipoprotein Transfer in the Rat. *Hepatology* **2005**, *42*, 1349–1354. [CrossRef]
37. Brainerd, C.; Gorti, V.; Janes, M.; Jones, K.; Khayat, S.; Liu, A.; Noonan-shueh, M.; Rao, S. Variable Fenestration of A 3D Nanoprinted Liver Sinusoid on a Chip. Dr. Ryan D. Sochol Department of Mechanical Engineering. Available online: http://hdl.handle.net/1903/24764 (accessed on 29 September 2021).
38. Heppell, C.; Roose, T.; Richardson, G. A Model for Interstitial Drainage Through a Sliding Lymphatic Valve. *Bull. Math. Biol.* **2015**, *77*, 1101–1131. [CrossRef] [PubMed]
39. Swartz, M.A. The Physiology of the Lymphatic System. *Adv. Drug Deliv. Rev.* **2001**, *50*, 3–20. [CrossRef]
40. Wisse, E.; De Zanger, R.; Charles, K.; Van Der Smissen, P.; McCuskey, R. The Liver Sieve: Considerations Concerning the Structure and Function of Endothelial Fenestrae, the Sinusoidal Wall and the Space of Disse. *Hepatology* **1985**, *5*, 683–692. [CrossRef] [PubMed]
41. Iwata, H.; Ueda, Y. Pharmacokinetic Considerations in Development of a Bioartificial Liver. *Clin. Pharmacokinet.* **2004**, *43*, 211–225. [CrossRef]

Paper III

"Highly oxidized albumin is cleared by liver sinusoidal endothelial cells via the receptors stabilin-1 and-2."

Christopher Holte, Karolina Szafranska, Larissa Kruse, Jaione Simon-Santamaria, Ruomei Li, Dmitri Svistounov, and Peter McCourt.

Scientific Reports 13, no. 1 (2023): 19121.

scientific reports

Check for updates

OPEN

Highly oxidized albumin is cleared by liver sinusoidal endothelial cells via the receptors stabilin-1 and -2

Christopher Holte[1✉], Karolina Szafranska[1], Larissa Kruse[1], Jaione Simon-Santamaria[1], Ruomei Li[1], Dmitri Svistounov[2] & Peter McCourt[1]

Oxidized albumin (oxHSA) is elevated in several pathological conditions, such as decompensated cirrhosis, acute on chronic liver failure and liver mediated renal failure. Patient derived oxidized albumin was previously shown to be an inflammatory mediator, and in normal serum levels of oxHSA are low. The removal from circulation of oxidized albumins is therefore likely required for maintenance of homeostasis. Liver sinusoidal endothelial cells (LSEC) are prominent scavenger cells specialized in removal of macromolecular waste. Given that oxidized albumin is mainly cleared by the liver, we hypothesized the LSEC are the site of uptake in the liver. In vivo oxHSA was cleared rapidly by the liver and distributed to mainly the LSEC. In in vitro studies LSEC endocytosed oxHSA much more than other cell populations isolated from the liver. Furthermore, it was shown that the uptake was mediated by the stabilins, by affinity chromatography-mass spectrometry, inhibiting uptake in LSEC with other stabilin ligands and showing uptake in HEK cells overexpressing stabilin-1 or -2. oxHSA also inhibited the uptake of other stabilin ligands, and a 2-h challenge with 100 µg/mL oxHSA reduced LSEC endocytosis by 60% up to 12 h after. Thus the LSEC and their stabilins mediate clearance of highly oxidized albumin, and oxidized albumin can downregulate their endocytic capacity in turn.

Albumin is the most abundant protein in blood (40 g/L of plasma is made up of albumin[1], and it has a correspondingly large number of functions, including binding and transporting a host of ligands including but not limited to free fatty acids, drugs (including: warfarin, salicylic acid, propofol, lidocaine) and metabolites[2]. In the blood stream albumin serves as the main antioxidant due to its readily reacting cysteine-34 residue and metal ion binding properties, and is also found extensively in the extravascular extracellular space[2,3]. Albumin is therefore a vital component in mitigation of oxidative stress throughout the body.

Oxidative stress is implicated in the pathophysiology of several diseases, such as atherosclerosis; where oxidation products are linked with plaque formation[4]; nephrotic damage in leukocyte-dependent glomerulonephritis[5]; and the development and progression of neurodegenerative diseases[6]. Ischemia-modified albumin, thought to be formed by reaction with reactive oxygen species and or hydroxyl radicals[7], therefore a form of oxidized albumin, is a marker of poor prognosis in patients reporting chest pain, and is determined clinically by assaying the cobalt binding ability of patient sera[8]. The neutrophil myeloperoxidase is one endogenous system capable of producing extremely potent oxidants such as hypochlorite, thio- and hypothiocyanite[9], thus serving as a link between inflammation and oxidative stress.

Oxidative stress and the presence of oxidized albumin is also a component of the pathogenesis of acute on chronic liver failure[10,11], a syndrome that develops from decompensated cirrhosis[12]. Elevated advanced oxidation protein products (AOPP) and modified albumins were also found in plasma samples from idiosyncratic drug-induced liver injury[13]. Oxidation of serum albumin in patients with cirrhosis and bacterial peritonitis causes decreased binding properties of albumin, predicting impaired transport function[14]. In vitro oxidized albumin has been shown to have altered affinities, both increased and decreased, to various drugs and metabolites[15,16].

Oxidised albumin is associated with a number of other pathologies. There is a correlation between the fraction of oxidized albumin and atherosclerosis development[17]. In nephrotic patients oxidized and advanced glycation end-product (AGE) albumin was found, and a reduction in oxidized albumin considered a beneficial marker after hemodialysis[18]. The oxidation products themselves have been suggested to be uremic toxins playing an active role in the development of chronic renal failure[19]. An increased fraction of oxidized relative vs. non-oxidized albumin is also characteristic of Diabetes Mellitus patients[20]. Oxidized albumin from hypoalbuminemic

[1]Vascular Biology Research Group, Department of Medical Biology, UiT The Arctic University of Norway, Tromsø, Norway. [2]Metabolic and Renal Research Group, Department of Clinical Medicine, UiT The Arctic University of Norway, Tromsø, Norway. ✉email: christopher.holte@uit.no

hemodialysis patient samples were shown to cause elevated expression of inflammatory cytokines in HUVECs[21] and primary peripheral blood leukocytes[22]. The proinflammatory effect was shown to be oxidation dependent and reversible upon chemical reduction of the albumin[21]. Oxidative modifications of HSA have been shown to induce clearance from circulation[23], showing a potential link between hypoalbuminemia and oxidative stress often observed in cirrhosis. Iwao[24] found chemically oxidized HSA (oxHSA), produced using the hypochlorite analogue chloramine-T, to be similar to oxidized albumin found in uremic patients. This oxHSA was found to be rapidly cleared from circulation in mice, primarily by the liver (51%) and spleen (23%), which are two of the major scavenging organs in the body.

Liver sinusoidal endothelial cells (LSEC) are known to take up a host of macromolecular waste from the bloodstream[25] whereas Kupffer cells (KC), the liver resident macrophages, remove larger (> 200 nm) complexes from the circulation[26]. Modified albumins such as Advanced Glycation End-products-BSA (AGE-BSA) and formaldehyde modified BSA (FSA) are taken up by the liver sinusoidal endothelium[27–29], the scavenging endothelium of the liver sinusoids. AGEs[30,31] FSA[27,32,33] were shown to be primarily endocytosed via the scavenger receptor class H[34] (SR-H), also known as stabilin-1 and -2. Oxidized low density lipoproteins oxLDL[35] and acetylated LDL[36] were also shown to be taken up by the liver sinusoidal endothelial cells via stabilin-1 and -2. Stabilin-1/2 double knockout (KO) mice exhibit glomerular fibrosis, with significant reduction to the animal lifespan, indicating that a reduction in clearance via the stabilins in the liver had downstream effects on the kidneys[37].

The stabilins are further implicated in the development of several pathologies, either caused by deficiency/insufficiency or for atherosclerosis where they seem to contribute to plaque formation. KO models of stabilin-1 or -2 showed decreased atherosclerotic plaque formation under Western diet conditions or ApoE KO[38,39]—the effect was replicated using monoclonal antibodies and suggested as a therapy against atherosclerosis in prone individuals, as antibodies would likely not greatly interfere with liver endothelial scavenging[39]. Stabilin double KOs exhibit transforming growth factor beta induced protein (TGFBI) and Periostin (POSTN) deposition in liver and in glomeruli with age[40]. Even single KO models were found to have increased inappropriate deposition of connective tissue components, and showed more severe steatosis and fibrosis in induced models[41]. Stabilin-1 was shown in a mouse model to be protective against viral myocarditis, with stabilin-1 KOs showing worse inflammation in the heart[42]. Gene correlation analysis and mouse model studies showed that stabilin-2 deficiency was associated with a prothrombotic phenotype[43]. Stabilin-2 is found to be highly expressed in cells surrounding atherosclerotic lesions in a mouse Ldlr KO model, and was suggested as a way to target these[44]. Stabilin double KO mice exhibited significant placental abnormalities, and produced few viable offspring, this was likely due to the reduced clearance of apoptotic cells during placental remodeling[45]. The liver and spleen are the main sites of stabilin 1 and 2 expression[46,47].

The ability to induce oxidative stress-like damage of oxidation protein products combined with the rapid uptake of oxHSA by the liver and the propensity for LSEC to clear modified proteins, make these cells a potential site of clearance of oxidized albumin and of injury during sustained oxidative stress.

If oxHSA binds to a scavenger receptor, as its rapid clearance suggests, this may have implications for the clearance of other waste molecules by the same. We therefore sought to determine which cell type and receptor take up oxHSA in the liver and describe the effects of oxHSA upon these cells.

Results

In vivo biodistribution

The liver took up the majority of injected oxHSA of all the organs with on average 47% of total radiation, 6.5% GI-tract, 8% head, 2.6% kidneys, 2% tail, 1.3% spleen, 1.2% lungs, 1% heart and 30% remained in the carcass. The liver and spleen took up the most radioactivity per mass, 30% and 18% per gram respectively (Fig. 1).

The majority of the injected (75%) radiation (as estimated from injected dose or total radiation in organs + carcass) was cleared before the first blood sample was collected 0:55–1:40 min post injection (Figure S2). Therefore, the $t_{1/2}$ is even lower (< 90 s).

Hepatocellular distribution

To determine the relative contribution of liver cells to oxHSA hepatocellular distribution was performed. Out of the cells of the liver the LSEC had the highest activities, compared to Kupffer cells or hepatocytes. LSEC contained activites (normalized to cell number) 15 and 11-fold higher than KC or hepatocytes respectively (Fig. 2).

In vitro uptake in isolated liver cell populations

Isolated murine LSEC showed the highest in vitro uptake with 35% uptake and degradation of added ^{125}I-oxHSA over 2 h of incubation increasing to 70% after 18 h, per 300 K cells (Fig. 3A, B). Kupffer cells (resident macrophages) took up ≈ 13% of added ^{125}I-oxHSA per 300 K cells over 2 h (Fig. 3A). Hepatocytes took up ≈10% of added ^{125}I-oxHSA per 300 K cells over 2 h, but this likely due to contamination by NPCs (Fig. 3A).

In vitro identification of the oxHSA endocytosis receptor

LSEC detergent lysates were subjected to affinity chromatography on oxHSA coupled to Sepharose. A number of proteins were eluted from this column, including stabilins-1 and -2. Stabilins-1 and -2 were not eluted from control columns; i.e. Sepharose without protein, or Sepharose coupled with native HSA. No other scavenger class receptors were eluted from the column. Importantly, the cell lysates contained all cellular proteins, and not only cell-surface proteins (Supplementary Table 1, Supplemental-MS).

To determine the potential role of the SR-H scavenger receptors stabilin-1 and stabilin-2, HEK293 cells stably over expressing mouse stabilin-1 and stabilin-2 were challenged with ^{125}I-oxHSA. Both stabilin-1 and

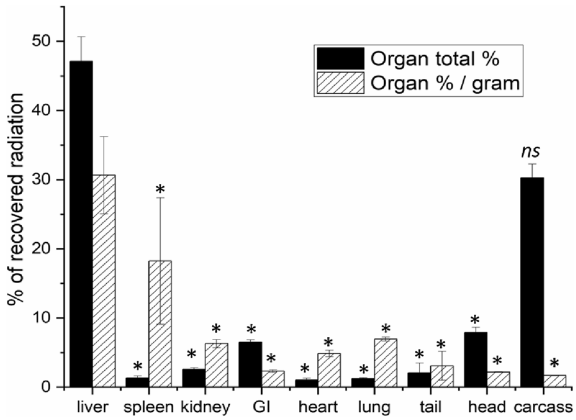

Figure 1. Biodistribution of oxHSA. 1–5 μg ^{125}I radio-labelled oxHSA was injected intravenously, and animals were sacrificed 30 min post-injection. Uptake is given as % of total recovered radioactivity (black bars) or as % of total recovered radioactivity per gram of organ (white/shaded bars). Results are given as averages ± standard deviation over bio replicates, n = 3 animals, ns = not significant, * = $p < 0.05$ compared with liver (Independent Samples Median Test).

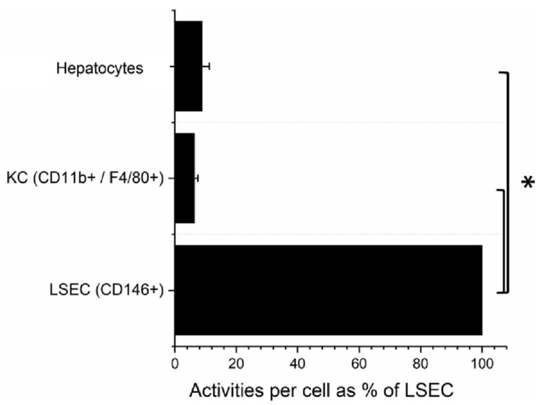

Figure 2. Hepatocellular distribution of oxHSA. Animals were injected with 1–5 μg ^{125}I radio-labelled oxHSA, sacrificed 5 min post-injection and LSEC, Kupffer cells and hepatocyte fractions were isolated. Graphs show radioactivity per cell normalized to LSEC, in isolated fractions of liver cells (selected by; CD146:LSEC, CD11b & F4/80:Kupffer cells, Percoll 45%:hepatocytes). Results are given as averages ± standard deviation over bio replicates, n = 3 animals, * = $p < 0.05$ (Independent Samples Median Test).

stabilin-2 HEK293 cells (but not the empty vector control) avidly endocytosed 48% and 67% of trace amounts of ^{125}I-oxHSA, respectively, within 4 h (Fig. 4A). Figure 4A shows the % endocytosis of added ^{125}I-oxHSA to the abovementioned HEK293 cells, as well as other known SR-H ligands: FSA; AGE-BSA and oxLDL. These other ligands were endocytosed at 29–32% and 32–55% by stabilin-1 and stabilin-2 HEK293 cells, respectively. The empty vector control cells endocytosed ≤ 12% of added ligand.

The specificity of SR-H mediated uptake of oxHSA was tested by using oxHSA to inhibit uptake of other SR-H ligands. Stabilin-1 and stabilin-2 HEK293 cells were incubated with ^{125}I-AGE-BSA (Fig. 4B) or ^{125}I-oxLDL (Fig. 4 C) and challenged with unlabelled oxHSA (0–62 μg/ml or 0–5 μg/ml, respectively). ^{125}I-AGE-BSA uptake was markedly (80% reduced relative to controls) inhibited in both SR-H expressing HEK293 cells at 7.5 μg/ml oxHSA. ^{125}I-oxLDL uptake in the same cells was somewhat (60–70% reduced relative to controls) inhibited with 5.0 μg/ml oxHSA.

Similar uptake and inhibition studies were performed on LSEC, which express both stabilin forms. LSEC challenged with 10 μg/mL Alexa488-oxHSA for 30 min showed marked uptake as determined by fluorescent microscopy (Figure S3). AGE-BSA, FSA and oxLDL inhibited the LSEC uptake of ^{125}I-oxHSA by 60–80% relative to controls (Fig. 5A). Unlabeled oxHSA inhibited the LSEC uptake of ^{125}I-FSA (50–90% reduced relative to controls), ^{125}I-AGE-BSA (30–50% reduced relative to controls) and ^{125}I-oxLDL (20–40% reduced relative to controls) (Fig. 5B–D). Unlabeled oxHSA markedly (25–90% reduced relative to controls) inhibited LSEC uptake of ^{125}I-oxHSA (Fig. 5E), but not to the same degree as it did with FSA (Fig. 5C).

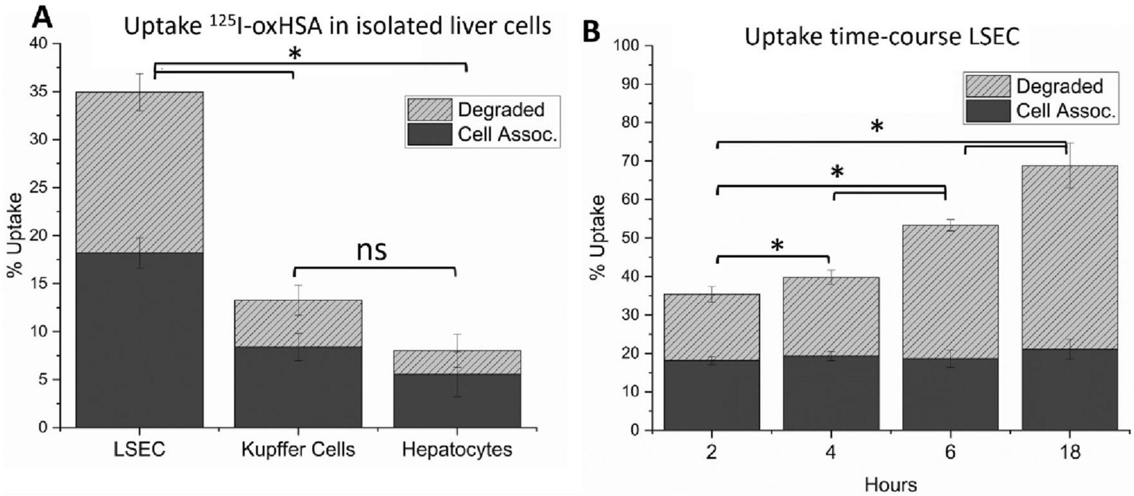

Figure 3. In vitro uptake of oxHSA by isolated liver cells. (**A**) Uptake of ^{125}I-oxHSA per 300 K cells in LSEC, Kupffer cells and hepatocytes. LSEC and hepatocytes were seeded 300K/well, Kupffer cells were counted and uptake calculated per 300K cells. (**B**) Time-course of ^{125}I-oxHSA uptake in LSEC. Uptake is given as % of added (approx. 5-15ng/well). Solid bars indicate cell associated radioactivity, shaded bars indicate acid soluble radioactivity (= degraded ligand). Results are given as averages ± standard deviation over bio replicates, n = 3 animals, ns = not significant, * = $p < 0.05$, (Independent Samples Median Test (**A**), Independent Samples Jonckheere-Terpstra Test (**B**)).

Recovery of endocytosis

To determine if the oxHSA-mediated inhibition of LSEC endocytosis was short or long term, we determined the level of FSA endocytosis after a 2-h pulse of oxHSA (100 µg/ml) followed by chases of 3, 6 and 12 h in RPMI media (Fig. 6). There was little to no recovery of LSEC FSA endocytosis to control levels even after a 12-h pulse of media (Fig. 6) where levels were at 40% of untreated levels.

Morphology and viability of LSEC challenged with oxHSA

LSEC treated with 10–160 µg/mL oxHSA for 1 h showed no morphological alterations at EM level (Figure S4). Cells treated with 0–320 µg/mL for 3–6 h showed no changes to viability as measured by LDH or resazurin assays (Figure S5).

Discussion

AOPP albumin, also known as oxHSA, is cleared from the circulation primarily by the liver and spleen[24]. We synthesized oxHSA to determine the site of its uptake in the liver and its effect on liver cells. oxHSA characterization by HPLC revealed increased size peaks relative to HSA's peak (Figure S1), this is indicative of conformational rearrangement rather than added mass, as the electrophoretic motility under denaturing conditions (SDS) do not show such dramatic changes[24]. The HPLC profile of oxHSA is furthermore a very similar profile to model ligand FSA (data not shown). These conformational changes predispose albumin to scavenger receptor mediated clearance, judging by the examples of oxHSA and FSA. The oxHSA produced in this study was not toxic for LSEC as determined by LDH and resazurin assays, and the morphology of the cells was also seemingly unaffected by oxHSA as judged by SEM (Figure S4). We show that of all the liver cells, LSEC show the highest capacity for clearance of oxHSA (Figs. 2, 3). The most likely candidate receptors mediating this process are the SR-H scavenger receptors stabilin-1 and -2. This would be consistent with the observation that the highest stabilin expression levels are in the liver and spleen[46].

We established that oxHSA is cleared by stabilins-1 and -2 by uptake and competitive inhibition studies in LSEC and HEK293 cells constitutively expressing stabilin-1 and -2. Ideally this would have been further validated by silencing stabilins in LSEC in vitro, however LSEC endocytic activity gradually decreases over time, with 60–70% reduction in uptake after 48 h and 80–85% reduction in uptake after 72 hours[48,49]. This prevents determination if reduced endocytosis after silencing would be caused directly by silencing or from a reduction in endocytic activity. For LSEC uptake of oxHSA was inhibited by FSA, AGE-BSA and oxLDL, and oxHSA in turn inhibited their uptake (Fig. 5). The uptake of FSA was completely inhibited in LSEC by oxHSA, indicating a very similar binding profile. oxHSA moderately inhibited AGE-BSA in LSEC (Fig. 5) but inhibited AGE-BSA uptake very strongly in stabilin expressing HEK293 cells (Fig. 4). oxLDL uptake/degradation was slightly inhibited by oxHSA in LSEC but very strongly in stabilin expressing HEK293 cells (Figs. 4, 5), suggesting these ligands (AGE-BSA, oxLDL) have additional receptors for endocytosis in LSEC.

We performed pulse chase experiments to determine if the effect of oxHSA on endocytosis was long lasting. Endocytosis was reduced to 40% of controls 12 h after challenge with 100 µg/mL for 2 h (Fig. 6), which is comparable to previously described effects of AGE-BSA on endocytosis mediated by stabilins-1 and -2[50]. This suggests that oxHSA depletes binding activity over a physiologically relevant timeframe. Thus, circulating oxHSA

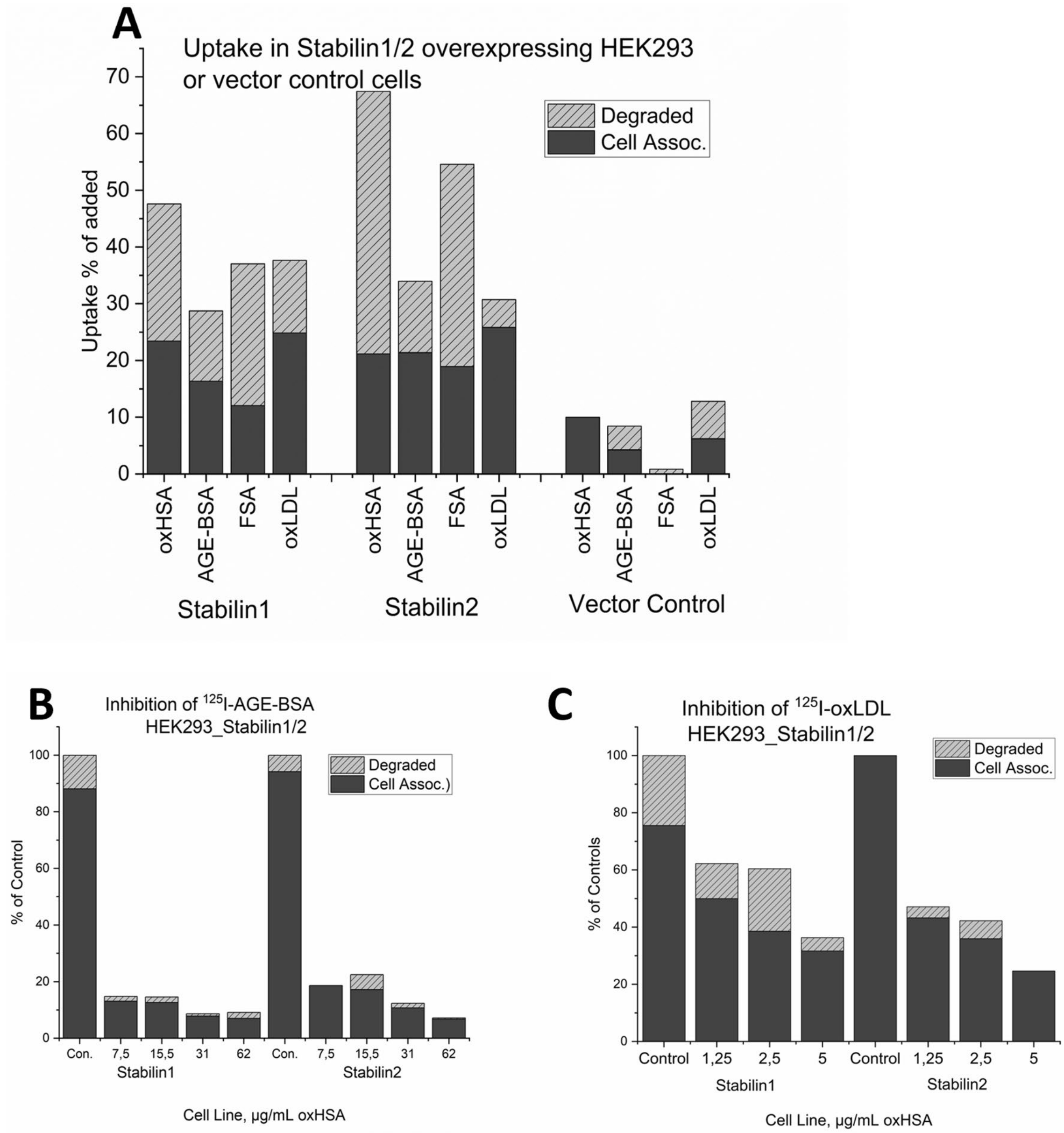

Figure 4. Uptake & competitive inhibition in HEK cells expressing stabilin-1 or -2. (**A**) Uptake of ^{125}I-labelled oxHSA compared with uptake of other ligands for stabilin-1 and -2 (AGE-BSA, FSA, oxLDL) in HEK293 cells expressing stabilin-1, -2, or transfected with the empty vector. (**B**) Inhibition of ^{125}I-AGE-BSA uptake in stabilin-1 and -2 expressing HEK cells by oxHSA. (**C**) Inhibition of ^{125}I-oxLDL uptake in stabilin-1 and -2 expressing HEK cells by oxHSA. Uptake (in **A**) is given as % of radioactivity added per well, for inhibition graphs (**B**-**C**) uptake is given as % of (untreated) controls.

may impair the clearance of other stabilin ligands, which may be of concern during pathological states with high oxidative stress. For example it has been shown that stabilins in the liver are responsible for the elimination of LPS arriving from the gut, preventing systemic inflammation[51]. It has previously been shown that SR-H deficiency causes kidney fibrosis in a mouse model[37]. This was also suggested as a link between diabetic AGE formation and diabetic reno-pathy, which also sees heightened levels of oxidation protein products[35]. Partial hepatectomy often leads to kidney injuries[52], where a reduction in clearance of scavenger receptor ligands may be a driver of these injuries. This fits with the presence of oxidized albumin in uremic patients[24] as either a marker for reduced clearance or a uremic toxicant itself.

Additionally, it has been shown that the scavenger endothelium of the liver is the main site of clearance for pro-atherogenic molecules such as oxidized LDL, and AGEs[35,53]. An increased circulation time, or accumulation of these ligands is likely to cause atherosclerotic plaques and localized inflammation in the vasculature. Oxidative stress and detection of oxidation protein products has been linked with atherosclerosis previously[4], with AOPP-Albumin been shown to cause atherosclerotic plaque formation in rabbits[54].

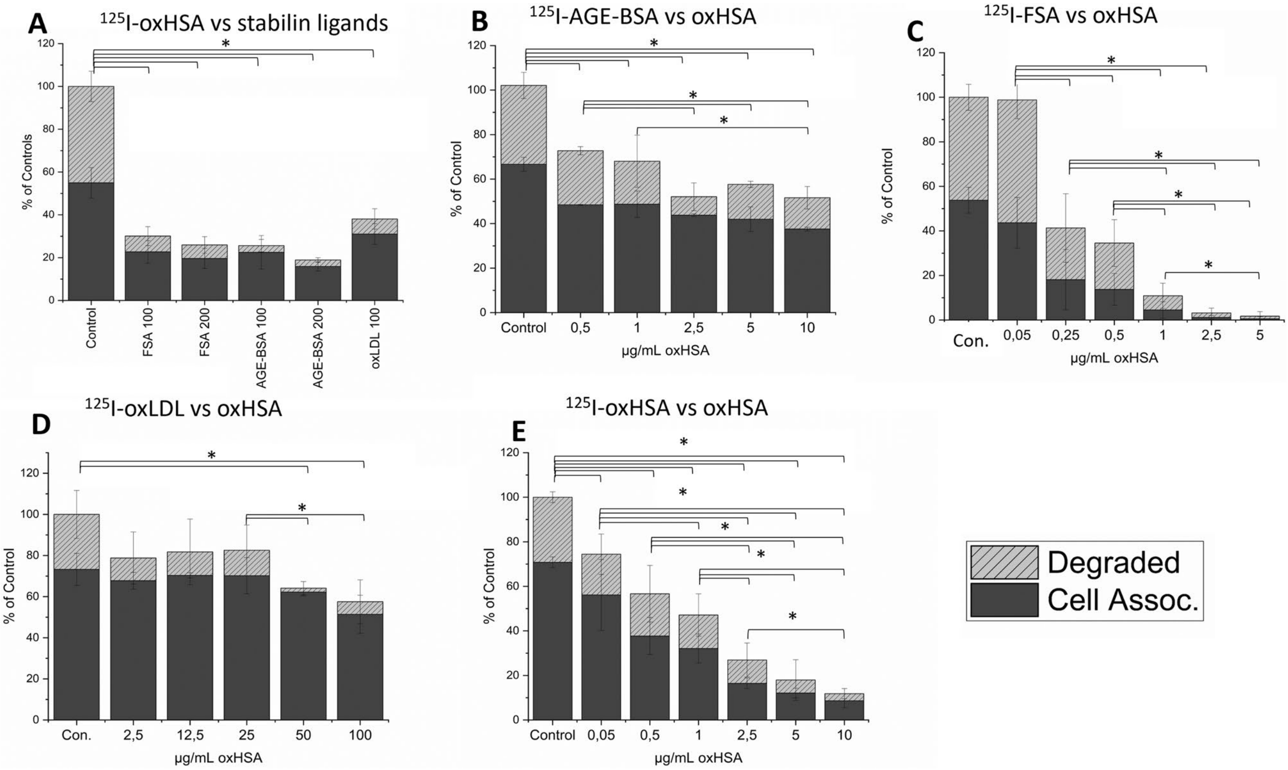

Figure 5. Competitive inhibition studies in LSEC. (**A**) Inhibition of ^{125}I-oxHSA uptake in LSEC by other ligands of stabilin-1 and -2 (FSA, AGE-BSA, oxLDL). (**B**) Inhibition of ^{125}I-FSA uptake in LSEC by oxHSA. (**C**) Inhibition of ^{125}I-AGE-BSA uptake in LSEC by oxHSA. (**D**) Inhibition of ^{125}I-oxLDL uptake in LSEC by oxHSA. (**E**) Inhibition of ^{125}I-oxHSA uptake in LSEC by unlabelled oxHSA. Uptake is given as % of (untreated) controls. Solid bars indicate cell associated radioactivity, shaded bars indicate acid soluble radioactivity (= degraded ligand). Results for are given as averages ± standard deviation over bio replicates, n = 3 animals, *:p < 0.05, (Independent Samples Median Test (**A**), Independent Samples Jonckheere-Terpstra Test (**B**-**E**)).

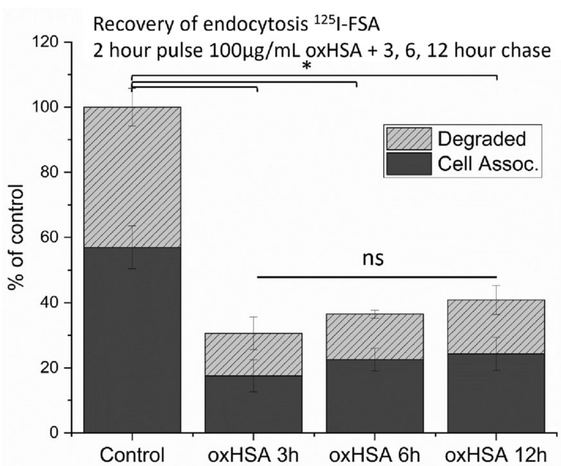

Figure 6. Pulse-chase/Recovery of endocytosis in LSEC. LSEC were treated with 100 µg/mL oxHSA × 2 h, and then the indicated number (3, 6, or 12) of hours chase in cell culture media, before endocytosis experiments with ^{125}I-FSA. Uptakes in % of matched untreated controls. Solid bars indicate cell associated radioactivity, shaded bars indicate acid soluble radioactivity (= degraded ligand). Results given as averages ± standard deviation over bio replicates, n = 3 animals, * = p = 0.025 (Independent Samples Jonckheere-Terpstra Test).

Stabilins themselves have been implicated in the pathogenesis of atherosclerosis, with amelioration of atherosclerosis development in stabilin KO models[38,39], this is indicative that binding by stabilins is part of the pathogenesis of the condition. oxHSA has a very high affinity for stabilins (greater than FSA), from this we can hypothesize that oxHSA and other stabilin ligands may, in non-scavenger sites, cause or exacerbate deleterious effects such as for example atherosclerotic lesions. Binding to stabilins may facilitate attachment by circulating immune cells and initiate inflammatory responses at the site[55]. Further stabilin-2 was found to also be a cell signalling receptor, activating the MAPK/ERK signalling pathway[56]. The implications of this signalling via stabilins especially under pro-atherogenic, or oxidative stress conditions is not well understood. Both stabilin-1 and -2 were found to bind E. coli and S. aureus in vitro[57], thus they may be involved in both attachment of immune cells, and of bacteria sensing in other non-scavenger cell types, given their signalling capabilities[56]. This could conceivably be part of the mechanism of stabilin mediated atherogenesis, with immune cell recruitment and inflammation caused by ligand activation.

The stabilins are also the receptors for clearance of apoptotic cells/ cell corpses and aged red blood cells[58,59], that circulating stabilin ligands such as oxHSA could interfere with this process therefore seems likely.

This suggests a common theme and possible feedback mechanism for these ligands, where an increase above a threshold will lead to a vicious cycle, where AOPP clearance is inhibited by their own prevalence, and their prevalence induces their own formation by an oxidative stress/ inflammation related mechanism at the sites of deposition. Thus, atherosclerosis and systemic inflammation is both driving and being driven by AOPP formation. This would all have implications for other organs, such as kidneys, as suggested by Schledzewski et al.[37].

Similarly, the pathogenic progression of liver disease or injury, would lead to a reduction in clearance of the atherogenic oxidation protein products (oxHSA, oxLDL etc.) as was indeed found by Öettl in 2013[14], which would increase their relative concentrations, circulation time, leading to deposition, plaque formation and inflammation. Plausible mechanisms driving this would be the impaired synthesis of new albumin by hepatocytes coupled with impaired clearance of modified albumins from circulation by LSECs.

In summary oxHSA is cleared in vivo by the LSEC, is a ligand for stabilins-1 and -2, and in vitro challenge of LSEC with oxHSA causes downregulation of SR-H mediated endocytosis. This has implications for the clearance of waste proteins, LPS and other ligands normally cleared by SR-H, since elevated levels of oxidized albumin are seen in diseases such as atherosclerosis, diabetes and acute and chronic liver failure.

If oxidized albumin interferes with SR-H mediated clearance, this may explain some of the downstream effects of pathological inflammation. Strategies inhibiting the formation of oxidation protein products during disease and inflammation may thus be warranted. Interventions such as those reviewed by Forman and Zhang 2021[60] may be of use in such cases.

Experimental procedures

List of reagents

Chloramine-T trihydrate (Merck, Darmstadt, Germany), Copper(II)Sulphate, Penicillin, Streptomycin, RPMI-1640 (Sigma-Aldrich, Burlington, MA, USA), RPMI-1640 (Euroclone, Pero, Italy), DMEM low glucose (Sigma-Aldrich), Trypsin–EDTA (Sigma-Aldrich), Blasticidin hydrochloride (Sigma-Aldrich), Trichloroacetic acid (Merck), Fetal Bovine Serum (Merck, Darmstadt, Germany), Iodine 125 Radionuclide (Perkin Elmer, Waltham, Mass., USA), Iodogen™ iodination reagent (Pierce, Thermo-Fischer), Alexa-488 succinimidyl ester (Thermo Fischer Scientific, Waltham, Mass., USA), Anti-CD146 microbeads, anti-F4/80 microbeads, anti-CD 11b microbeads (Miltenyi Biotech, Bergisch Gladbach, Germany), HSA Alburex (CSL Behring, King of Prussia, Penn., USA), Fetal Bovine Serum (Biowest, Nuialle, France), Resazurin (biotechne, Minneapolis, Minn., USA), Liberase™TM (Roche, Basel, Switzerland), Human fibronectin was extracted from expired human plasma donated from the hospital (University Hospital of Northern Norway, Tromsø, Norway) blood-bank, by affinity chromatography locally, using the method of Vuento 1979[61], Formaldehyde treated Serum Albumin (FSA) was prepared as described in Mego 1967[62], Blomhoff 1984[32], AGE-BSA was prepared as described in Hansen 2002[50], Oxidized Low Density Lipoprotein (oxLDL) was prepared by Copper Sulphate oxidation as previously described in Li 2011[35].

Production and characterisation of oxHSA

Oxidation of HSA was carried out as described by Iwao 2006[24]; 300 µM HSA was incubated with 100 mM Chloramine-T in oxygen saturated PBS at 37 °C for 1 h. Afterwards the oxHSA was dialyzed against pure water and kept frozen until use. HPLC separation on Superdex-200 10/300 (Amersham Pharmacia Biotech, Amersham, UK) size exclusion column was performed. Showing that the oxHSA eluted as three peaks of 837.4, 382 and 138.4 kDa (Figure S1).

Radiolabeling of oxHSA, FSA, AGE-BSA, oxLDL

oxHSA or FSA was radiolabeled using carrier free 125-Iodine (Perkin-Elmer) according to the Iodogen™(Pierce) method and free iodine separated from protein by PD-10 (Cytiva) desalting column, as previously described Blomhoff 1984[32]. Specific activity was calculated from amount of added protein and measured activity post-labeling.

Animals

C57Black/6JRj mice were ordered from Janvier, and kept at the Department of Comparative Medicine, the Faculty of Health Sciences at UiT The Arctic University of Norway, under standard conditions with water and chow (SSniff, regular chow diet) ad libitum. Mice were between 8–14 weeks old for all of the procedures. All procedures were approved by the national animal research authority under the food safety administration (Mattilsynet).

All animal procedures were performed in accordance with national and local guidelines, and are reported in accordance with ARRIVE guidelines.

Method of euthanasia, anaesthesia and analgesia

Animals were euthanized by cervical dislocation, for in vivo experiments animals were anesthetized with isoflurane gas anaesthesia, and for experiments involving manipulation beyond tail vein injection, given 0.1 mg/kg buprenorphine subcutaneously at least 15 min prior to experiments, for analgesia.

In vivo clearance, organ- and hepatocellular distribution

In vivo clearance, organ- and hepatocellular distribution was carried out as described in Santamaria-Simon 2014[63]. Briefly anesthetized mice were given intravenously 2–6 µg ^{125}I labelled oxHSA for biodistribution and hepatocellular distribution. For clearance blood samples were taken from the tail, in 2–5 µL volumes over 30 min, TCA precipitation was done to quantify intact/degraded ligand. For hepatocellular distribution animals were euthanized 5 min post-injection, and cells isolated as described in the section "Isolation of primary murine liver sinusoidal endothelial cells, Kupffer cells, hepatocytes". Organ associated activities were measured on the Perkin-Elmer Wizard[2], blood sample and isolated cell associated activities were measured on the Packard Cobra II auto-gamma.

Isolation of primary mouse liver sinusoidal endothelial cells, Kupffer Cells, hepatocytes

Primary mouse LSEC, KC or HC were isolated as previously described in Elvevold 2022[64]. Briefly livers were perfused and digested with 1.2 mg/50 mL Liberase TM™(Roche) centrifuged to separate hepatocytes from non-parenchymal cell fraction, and followed by immune magnetic separation (MACS, Miltenyi) of LSEC and KC from the non-parenchymal fraction by CD-146 and F-4/80, CD-11b respectively.

Primary cells were cultured in serum-free RPMI-1640 (Euro-Clone/Sigma) supplemented with 10,000 U/mL Penicillin, 10 mg/mL Streptomycin, 1:100 (Sigma).

HEK293 cells stably expressing stabilin 1 or 2

HEK293 cells were obtained from ATCC, HEK293 expressing mouse stabilin-1 or -2, were kindly provided by Dr Sophie Johansson (University of Uppsala, Sweden)[35], vector control cells were transfected locally by lipofectamine using the empty vector pEF6V5His-TOPO (Merck). Transfected HEK293 were grown in DMEM low glucose (Sigma) supplemented with 10,000 U/mL Penicillin, 10 mg/mL Streptomycin, 1:100, (Sigma) 7% FBS (BioWest), and 10 µg/mL Blasticidin hydrochloride for selection (Merck)[65].

Affinity chromatography

oxHSA, native HSA and FSA were coupled to cyanogen bromide activated Sepharose 4B (Pharmacia) as described in McCourt 1999[27]. Lysates from 19 million isolated LSEC were passed through the affinity columns, in 0.1% Triton TX-100 in PBS, columns were extensively washed with 0.1% TX-100/PBS and 0.1 M Acetic acid pH 3, 0.01 M EDTA.

Gel material was heated to 75 °C in SDS, and sent for mass spectrometry analysis[66].

Endocytosis experiments

Cells were seeded on human fibronectin-coated 48 well plates at 300 K cells/ well for LSEC, 300 K cells for hepatocytes, 125-320 K cells per well for KC depending on isolation yield, and allowed to adhere for 2 h before use for LSEC, KC or 4 h for hepatocytes, HEK cells were used after growing to confluence. For endocytosis experiments cells were kept in serum-free media with 1% native HSA (Alburex, CSL Behring) in RPMI-1640 (Euro-Clone) for LSEC, KC, hepatocytes and DMEM low glucose (Sigma) for HEK cells. Approximately 20,000 cpm of labelled ligand, corresponding to approximately 5–15 ng protein, was added to each well and cells were incubated for 2 h (LSEC, KC, Hepatocytes) 4 h (HEK cells) or a time course of 2, 4, 6, 18 h (LSEC). After which cell associated, non-degraded and degraded fractions were collected and measured as described in Blomhoff 1984[32].

Briefly, culture media and one wash with PBS were collected, and acid insoluble radioactivity precipitated by addition of an equal volume of 20% trichloroacetic acid and centrifugation, half of the supernatant or acid soluble radioactivity was transferred to measure the degraded fraction. Cells were dissolved using 1% SDS, to measure cell associated radioactivity. For competitive inhibition experiments several concentrations of non-radioactive ligand containing media were added to the cells immediately prior to addition of radiolabeled ligand. Iodine-125 measurements were done using the Cobra II auto-gamma (Packard).

Fluorescent microscopy

oxHSA and FSA were labelled with Alexa488 using the manufacturer's instructions (Thermo Fischer). Briefly labelling reagent was dissolved in DMSO and added to a 10 mg/mL solution of protein in 0.1 M bicarbonate buffer pH 8.3 for 1 h at room temperature, then dialyzed against PBS in a 10 K MWCO Slidealyzer dialysis cassette to remove uncoupled dye.

Cells were pre-stained with Cell Mask Orange (ThermoFischer) 1:1000 for 5 min, before addition of 10 µg/mL Alexa-oxHSA for 30 min, after which cells were washed in PBS before being viewed under the EVOS (ThermoFischer) fluorescent light microscope.

Scanning electron microscopy

Cells were seeded on human fibronectin covered glass 16 well plates at 25-40 K cells/well and allowed to attach for 2 h prior to treatment. Cells were treated with given concentrations of oxHSA in RPMI the indicated times and subsequently fixed with McDowell's fixative. Cells were post-fixed with 1% OsO4 and dried with a graded series of ethanol (30, 60, 90, 100%) washes and finally hexamethyldisilane. Cells were sputter coated with Au/Pd immediately prior to scanning.

Scanning electron microscopy was performed the Zeiss Gemini or Sigma scanning electron microscopes at the advanced microscopy core facility at UiT.

Viability experiments

Cell viability was assessed by LDH assay (Promega) or resazurin-resorufin (biotechne) assay were performed according to manufacturers instructions. For LDH LSEC were seeded 300 K cells/well in a 48 well plate and treated with varying concentrations of oxHSA. After set timepoints the supernatants were collected and analyzed. For resazurin-resorufin cells were seeded the same way, with 1:10 resazurin reagent (biotechne) added to the culture media and measurements, using the ClarioStar plate reader wavelengths excitation 530–570 nm emission 580–590 nm, done at 3 and 6 h.

Data availability

The datasets used and/or analyzed during the current study available from the corresponding author on reasonable request.

Received: 23 August 2023; Accepted: 1 November 2023
Published online: 05 November 2023

References

1. Hill, P. G. The measurement of albumin in serum and plasma. *Ann. Clin. Biochem.* **22**, 565–578 (1985).
2. Fanali, G. *et al.* Human serum albumin: From bench to bedside. *Mol. Aspects Med.* **33**, 209–290 (2012).
3. Sitar, M. E., Aydin, S. & Çakatay, U. Human serum albumin and its relation with oxidative stress. *Clin. Lab.* **59**, 945–952 (2013).
4. Kita, T. *et al.* Role of oxidized LDL in atherosclerosis. *Ann. N. Y. Acad. Sci.* **947**, 199–206 (2001).
5. Gröne, H. J., Gröne, E. F. & Malle, E. Immunohistochemical detection of hypochlorite-modified proteins in glomeruli of human membranous glomerulonephritis. *Lab. Investig.* **82**, 5–14 (2002).
6. Ramalingam, M. & Kim, S. J. Reactive oxygen/nitrogen species and their functional correlations in neurodegenerative diseases. *J. Neural Transm.* **119**, 891–910 (2012).
7. Roy, D. *et al.* Role of reactive oxygen species on the formation of the novel diagnostic marker ischaemia modified albumin. *Heart* **92**, 113–114 (2006).
8. Gaze, D. C. Ischemia modified albumin: A novel biomarker for the detection of cardiac ischemia. *Drug Metab. Pharmacokinet.* **24**, 333–341 (2009).
9. Kettle, A. J. & Winterbourn, C. C. Myeloperoxidase: A key regulator of neutrophil oxidant product. *Redox Rep.* **3**, 3–15 (1997).
10. Alcaraz-Quiles, J. *et al.* Oxidized albumin triggers a cytokine storm in leukocytes through P38 mitogen-activated protein kinase: Role in systemic inflammation in decompensated cirrhosis. *Hepatology* **68**, 1937–1952 (2018).
11. Clària, J. *et al.* Systemic inflammation in decompensated cirrhosis: Characterization and role in acute-on-chronic liver failure. *Hepatology* **64**, 1249–1264 (2016).
12. Moreau, R. *et al.* Acute-on-chronic liver failure is a distinct syndrome that develops in patients with acute decompensation of cirrhosis. *Gastroenterology* **144**, 1426-1437.e9 (2013).
13. Xiao, L. L. *et al.* Using advanced oxidation protein products and ischaemia-modified albumin to monitor oxidative stress levels in patients with drug-induced liver injury. *Sci. Rep.* **10**, 1–10 (2020).
14. Oettl, K. *et al.* Oxidative albumin damage in chronic liver failure: Relation to albumin binding capacity, liver dysfunction and survival. *J. Hepatol.* **59**, 978–983 (2013).
15. Sakurama, K. *et al.* Effects of Oxidation of Human Serum Albumin on the Binding of Aripiprazole. *Biol. Pharm. Bull.* **43**, 1023–1026 (2020).
16. Oettl, K. & Stauber, R. E. Physiological and pathological changes in the redox state of human serum albumin critically influence its binding properties. *Br. J. Pharmacol.* **151**, 580–590 (2007).
17. Fujii, R. *et al.* Oxidized human serum albumin as a possible correlation factor for atherosclerosis in a rural Japanese population: The results of the Yakumo Study. *Environ. Health Prev. Med.* **23**, 1–7 (2018).
18. Noce, A. *et al.* Hemodialysis biomarkers: total advanced glycation end products (AGEs) against oxidized human serum albumin (HSAox). *Acta Diabetol.* **56**, 1323–1331 (2019).
19. Witko-Sarsat, V., Gausson, V. & Descamps-Latscha, B. Are advanced oxidation protein products potential uremic toxins?. *Kidney Int. Suppl.* **63**, 11–14 (2003).
20. Suzuki, E. *et al.* Increased oxidized form of human serum albumin in patients with diabetes mellitus. *Diabetes Res. Clin. Pract.* **18**, 153–158 (1992).
21. Magzal, F. *et al.* In-vivo oxidized albumin-a pro-inflammatory agent in hypoalbuminemia. *PLoS One* **12**, 1–14 (2017).
22. Das, S. *et al.* Hyperoxidized albumin modulates neutrophils to induce oxidative stress and inflammation in severe alcoholic hepatitis. *Hepatology* **65**, 631–646 (2017).
23. Iwao, Y. *et al.* Oxidation of Arg-410 promotes the elimination of human serum albumin. *Biochim. Biophys. Acta Proteins Proteomics* **1764**, 743–749 (2006).
24. Iwao, Y. *et al.* The structural and pharmacokinetic properties of oxidized human serum albumin, advanced oxidation protein products (AOPP). *Drug Metab. Pharmacokinet.* **21**, 140–146 (2006).
25. Bhandari, S., Larsen, A. K., McCourt, P., Smedsrød, B. & Sørensen, K. K. The scavenger function of liver sinusoidal endothelial cells in health and disease. *Front. Physiol.* **12**, 1–23 (2021).
26. Sørensen, K. K. *et al.* The scavenger endothelial cell: A new player in homeostasis and immunity. *Am. J. Physiol. Regul. Integr. Comp. Physiol.* **303**, 1217 (2012).
27. McCourt, P., Smedsrød, B., Melkko, J. & Johansson, S. Characterization of a hyaluronan receptor on rat sinusoidal liver endothelial cells and its functional relationship to scavenger receptors. *Hepatology* **30**, 1276–1286 (1999).
28. Svistounov, D. *et al.* Hepatic disposal of advanced glycation end products during maturation and aging. *Exp. Gerontol.* **48**, 549–556 (2013).
29. Smedsrød, B. Clearance function of scavenger endothelial cells. *Comp. Hepatol.* **3**, S22 (2004).

30. Hansen, B., Arteta, B. & Smedsrød, B. The physiological scavenger receptor function of hepatic sinusoidal endothelial and Kupffer cells is independent of scavenger receptor class A type I and II. *Mol. Cell. Biochem.* **240**, 1–8 (2002).
31. Tamura, Y. *et al.* FEEL-1 and FEEL-2 are endocytic receptors for advanced glycation end products. *J. Biol. Chem.* **278**, 12613–12617 (2003).
32. Blomhoff, R., Eskild, W. & Berg, T. Endocytosis of formaldehyde-treated serum albumin via scavenger pathway in liver endothelial cells. *Biochem. J.* **218**, 81–86 (1984).
33. Politz, O. *et al.* Stabilin-1 and -2 constitute a novel family of fasciclin-like hyaluronan receptor homologues. *Biochem. J.* **362**, 155–164 (2002).
34. PrabhuDas, M. R. *et al.* A consensus definitive classification of scavenger receptors and their roles in health and disease. *J. Immunol.* **198**, 3775–3789 (2017).
35. Li, R. *et al.* Role of liver sinusoidal endothelial cells and stabilins in elimination of oxidized low-density lipoproteins. *Am. J. Physiol. Gastrointest. Liver Physiol.* **300**, 71–81 (2011).
36. Harris, E. N. & Weigel, P. H. The ligand-binding profile of HARE: Hyaluronan and chondroitin sulfates A, C, and D bind to overlapping sites distinct from the sites for heparin, acetylated low-density lipoprotein, dermatan sulfate, and CS-E. *Glycobiology* **18**, 638–648 (2008).
37. Schledzewski, K. *et al.* Deficiency of liver sinusoidal scavenger receptors stabilin-1 and -2 in mice causes glomerulofibrotic nephropathy via impaired hepatic clearance of noxious blood factors. *J. Clin. Invest.* **121**, 703–714 (2011).
38. Kayashima, Y. *et al.* Reduction of stabilin-2 contributes to a protection against atherosclerosis. *Front. Cardiovasc. Med.* **9**, 1–15 (2022).
39. Manta, C. P. *et al.* Targeting of scavenger receptors stabilin-1 and stabilin-2 ameliorates atherosclerosis by a plasma proteome switch mediating monocyte/macrophage suppression. *Circulation* **146**, 1783–1799 (2022).
40. Leibing, T. *et al.* Deficiency for scavenger receptors Stabilin-1 and Stabilin-2 leads to age-dependent renal and hepatic depositions of fasciclin domain proteins TGFBI and Periostin in mice. *Aging Cell* https://doi.org/10.1111/acel.13914 (2023).
41. Krzistetzko, J., Géraud, C., Dormann, C., Riedel, A. & Leibing, T. Association of differentially altered liver fibrosis with deposition of TGFBi in stabilin-deficient mice. *Int. J. Mol. Sci.* **24**, 10969 (2023).
42. Carai, P. *et al.* Stabilin-1 mediates beneficial monocyte recruitment and tolerogenic macrophage programming during CVB3-induced viral myocarditis. *J. Mol. Cell. Cardiol.* **165**, 31–39 (2022).
43. Michels, A. *et al.* Stabilin-2 deficiency increases thrombotic burden and alters the composition of venous thrombi in a mouse model. *J. Thromb. Haemost.* **19**, 2440–2453 (2021).
44. Lee, G. Y. *et al.* Molecular targeting of atherosclerotic plaques by a stabilin-2-specific peptide ligand. *J. Control. Release* **155**, 211–217 (2011).
45. Kim, S. Y. *et al.* Identifying stabilin-1 and stabilin-2 double knockouts in reproduction and placentation: A descriptive study. *Int. J. Mol. Sci.* **21**, 1–11 (2020).
46. Falkowski, M., Schledzewski, K., Hansen, B. & Goerdt, S. Expression of stabilin-2, a novel fasciclin-like hyaluronan receptor protein, in murine sinusoidal endothelia, avascular tissues, and at solid/ liquid interfaces. *Histochem. Cell Biol.* **120**, 361–369 (2003).
47. Hare, A. K. & Harris, E. N. Tissue-specific splice variants of HARE/Stabilin-2 are expressed in bone marrow, lymph node, and spleen. *Biochem. Biophys. Res. Commun.* **456**, 257–261 (2015).
48. Martinez, I. *et al.* The influence of oxygen tension on the structure and function of isolated liver sinusoidal endothelial cells. *Comp. Hepatol.* **7**, 1–11 (2008).
49. Li, R. *et al.* Changes in the proteome and secretome of rat liver sinusoidal endothelial cells during early primary culture and effects of dexamethasone. *PLoS ONE* **17**, e0273843 (2022).
50. Hansen, B. *et al.* Advanced glycation end products (AGEs) lower the clearance function of hepatic scavenger endothelial cells (SEC). *Int. Congr. Ser.* **1245**, 125–128 (2002).
51. Cabral, F. *et al.* Stabilin receptors clear LPS and control systemic inflammation. *iScience* **24**, 103337 (2021).
52. Peres, L. A. B., Bredt, L. C. & Cipriani, R. F. F. Acute renal injury after partial hepatectomy. *World J. Hepatol.* **8**, 891–901 (2016).
53. Hansen, B. *et al.* Advanced glycation end products impair the scavenger function of rat hepatic sinusoidal endothelial cells. *Diabetologia* **45**, 1379–1388 (2002).
54. Liu, H. & Li, J. Aging and dyslipidemia : A review of potential mechanisms. *Ageing Res. Rev.* **19**, 43–52 (2015).
55. Patten, D. A. & Shetty, S. More than just a removal service: Scavenger receptors in leukocyte trafficking. *Front. Immunol.* **9**, 2904 (2018).
56. Kyosseva, S. V., Harris, E. N. & Weigel, P. H. The hyaluronan receptor for endocytosis mediates hyaluronan-dependent signal transduction via extracellular signal-regulated kinases. *J. Biol. Chem.* **283**, 15047–15055 (2008).
57. Adachi, H. & Tsujimoto, M. FEEL-1, a novel scavenger receptor with in vitro bacteria-binding and angiogenesis-modulating activities. *J. Biol. Chem.* **277**, 34264–34270 (2002).
58. Park, S. Y. & Kim, I. S. Stabilin receptors: Role as phosphatidylserine receptors. *Biomolecules* **9**, 1–16 (2019).
59. Park, S. Y. *et al.* Rapid cell corpse clearance by stabilin-2, a membrane phosphatidylserine receptor. *Cell Death Differ.* **15**, 192–201 (2008).
60. Forman, H. J. & Zhang, H. Targeting oxidative stress in disease: promise and limitations of antioxidant therapy. *Nat. Rev. Drug Discov.* **20**, 689–709 (2021).
61. Vuento, M. & Vaheri, A. Purification of fibronectin from human plasma by affinity chromatography under non-denaturing conditions. *Biochem. J.* **183**, 331–337 (1979).
62. Mego, J. L., Bertini, F. & McQueen, J. D. The use of formaldehyde-treated 131I-albumin in the study of digestive vacuoles and some properties of these particles from mouse liver. *J. Cell Biol.* **32**, 699–707 (1967).
63. Simon-Santamaria, J. *et al.* Efficient uptake of blood-borne BK and JC polyomavirus-like particles in endothelial cells of liver sinusoids and renal Vasa recta. *PLoS ONE* **9**, e111762 (2014).
64. Elvevold, K., Kyrrestad, I. & Smedsrød, B. Protocol for isolation and culture of mouse hepatocytes (HCs), Kupffer Cells (KCs), and liver sinusoidal endothelial cells (LSECs) in analyses of hepatic drug distribution. In *Antisense RNA Design, Delivery, and Analysis* 385–402 (2022).
65. Hansen, B. *et al.* Stabilin-1 and stabilin-2 are both directed into the early endocytic pathway in hepatic sinusoidal endothelium via interactions with clathrin/AP-2, independent of ligand binding. *Exp. Cell Res.* **303**, 160–173 (2005).
66. Shevchenko, A., Wilm, M., Vorm, O. & Mann, M. Mass spectrometric sequencing of proteins from silver-stained polyacrylamide gels. *Anal. Chem.* **68**, 850–858 (1996).

Acknowledgements

Special thanks to Randi Olsen and Tom Ivar Eilertsen at the microscopy core facility, Jack Ansgar Bruun at the UiT proteomics facility, Montserrat Martin-Armas at the PET-CORE centre at UiT, Bård Smedsrød, Karen K. Sørensen, Cristina I. Øie, for advice on practical details on endocytosis assays and application forms.

Author contributions

Conceptualization: C.H.; experimental design: C.H., J.S., R.L., D.S., P.M.; experimental work: C.H., K.S., L.K., J.S., R.L., D.S.; writing original draft: C.H.; manuscript revision and editing: C.H., K.S., L.K., J.S., R.L., D.S., P.M.; supervision: P.M.

Funding

Open access funding provided by UiT The Arctic University of Norway (incl University Hospital of North Norway). KJS/PM are funded in part by the Horizon Europe EIC Pathfinder Open Grant Agreement No. 101046928. KJS/PM/LDH were funded wholly or in part by the Horizon 2020 MSCA ITN Grant Agreement No. 766181. PM is funded by the Research Council of Norway FRIPRO Grant Agreement No. 325446.

Competing interests

The authors declare no competing interests.

Additional information

Supplementary Information The online version contains supplementary material available at https://doi.org/10.1038/s41598-023-46462-9.

Correspondence and requests for materials should be addressed to C.H.

Paper IV

"Quantitative analysis methods for studying fenestrations in liver sinusoidal endothelial cells. A comparative study."

Karolina Szafranska, **Christopher Florian Holte**, Larissa Dorothea Kruse, Hong Mao, Cristina Ionica Øie, M. Szymonski, Bartlomiej Zapotoczny, and P. A. G. McCourt.

Micron 150 (2021): 103121.

Micron 150 (2021) 103121

Contents lists available at ScienceDirect

Micron

journal homepage: www.elsevier.com/locate/micron

Quantitative analysis methods for studying fenestrations in liver sinusoidal endothelial cells. A comparative study

K. Szafranska [a,b,*], C.F. Holte [a], L.D. Kruse [a], H. Mao [a], C.I. Øie [a], M. Szymonski [b], B. Zapotoczny [a,c], P.A.G. McCourt [a]

[a] Department of Medical Biology, Vascular Biology Research Group, University of Tromsø (UiT), The Arctic University of Norway, Norway
[b] Centre for Nanometer-Scale Science and Advanced Materials, NANOSAM, Faculty of Physics, Astronomy, and Applied Computer Science, Jagiellonian University, Krakow, Poland
[c] Institute of Nuclear Physics, Polish Academy of Sciences, 31-342, Krakow, Poland

A R T I C L E I N F O

Keywords:
Quantitative analysis of LSEC porosity
Machine learning
Fenestrations
Liver sinusoidal endothelial cells
Atomic force microscopy
Super-resolution microscopy

A B S T R A C T

Liver Sinusoidal Endothelial Cells (LSEC) line the hepatic vasculature providing blood filtration via transmembrane nanopores called fenestrations. These structures are 50−300 nm in diameter, which is below the resolution limit of a conventional light microscopy. To date, there is no standardized method of fenestration image analysis. With this study, we provide and compare three different approaches: manual measurements, a semi-automatic (threshold-based) method, and an automatic method based on user-friendly open source machine learning software. Images were obtained using three super resolution techniques – atomic force microscopy (AFM), scanning electron microscopy (SEM), and structured illumination microscopy (SIM). Parameters describing fenestrations such as diameter, area, roundness, frequency, and porosity were measured. Finally, we studied the user bias by comparison of the data obtained by five different users applying provided analysis methods.

1. Introduction

Liver Sinusoidal Endothelial Cells (LSEC) are the interface between the blood stream and the surrounding hepatocytes in the liver. Filtration is maintained by LSEC nanopores which are also known as fenestrations. Their diameter of 50−300 nm is crucial for size dependent passive transport of plasma soluble molecules (e.g., albumin, glucose, drugs) and small nanoparticles such as chylomicron remnants (Braet and Wisse, 2002). These nanopores are typically found in groups of 5–100 called sieve plates which are located mostly in the area outside the nuclear region. Fenestrations are dynamic structures that can react to various stimuli such as drugs or change in local environment (Braet and Wisse, 2002) and adapt their diameter and/or number within minutes or even seconds (Zapotoczny et al., 2019, 2017). Along with the passive transport of macromolecules via fenestrations, LSEC also participate in the clearing of circulating waste through active uptake via scavenging receptors. A diverse array of macromolecular waste material is constantly removed from the blood circulation by clathrin-mediated endocytosis (Sørensen et al., 2012). LSEC also play an active role in the clearance of circulating polyoma virus (Simon-Santamaria et al., 2014) and bacteriophages (Øie et al., 2020).

Both the number and diameter of fenestration are important for proper liver function. Defenestration – the loss of porous morphology is an early indication of liver fibrosis, which can cause atherosclerosis due to lack of filtration of lipoproteins from the blood stream (Rogers et al., 1992). It has been reported that porosity decreases in ageing and can be a main factor contributing for the need of increasing doses of drugs targeting hepatocytes (e.g. statins) that have to pass through the pores to reach their target (Le Couteur et al., 2002; Hunt et al., 2018a). Conversely, hepatocyte mediated detoxification of drugs from the plasma, requires porous LSEC – age related loss of porosity can result in drug doses, otherwise safe for young people, being toxic for the elderly. Moreover, hepatocytes regulate the glucose plasma concentration and LSEC are responsible for the passage of insulin (via fenestrations) to facilitate glucose disposal (Tsuchiya and Accili, 2013). All these aspects confirm that the lack of a healthy LSEC phenotype plays an important role in the development of many diseases. However, recent work has shown that the ageing related loss of LSEC fenestrations may be

* Corresponding author at: Vascular Biology Research Group (VBRG), University of Tromsø (UiT), Hansine Hansens veg 18, 9019 Tromsø, Norway.
E-mail addresses: szafranska.k.j@gmail.com, karolina.szafranska@uit.no (K. Szafranska).

https://doi.org/10.1016/j.micron.2021.103121
Received 28 March 2021; Received in revised form 1 July 2021; Accepted 14 July 2021
Available online 28 July 2021

reversible by repurposing a number of existing medicines (Hunt et al., 2018b, a). In addition, new nanomedicines show promise in this regard (Hunt et al., 2020b, 2021).

To date, in almost every article describing LSEC, the fenestration size is typically shown as a histogram of diameter distribution and/or mean value of fenestration diameter. Other parameters describing LSEC's porous morphology are fenestration frequency (number of fenestrations per area, less often per cell) and porosity (percentage of cell area covered by fenestrations). Altogether, these three features allow for complete evaluation and comparison between the LSEC phenotype in health and diseases, as well as after challenge with various drugs, with ageing, etc. However, the methods by which researchers obtain these data are often vaguely described. The lack of standardization results in cumbersome comparisons between the separate experiments conducted by different researchers.

Only a few studies proposed to standardize and automate the analysis of fenestrations using images obtained by different microscopy techniques. In 2015, Cogger et al. (2015) proposed a method for isolation, sample preparation and analysis using scanning electron microscopy (SEM). The authors suggested to manually mark the cell surface area and then measure the longest fenestration diameter using free access software such as Fiji/ImageJ (Schindelin et al., 2012). Although this method can be precise, it is time consuming and requires an assumption of fenestration circularity, which may bias the results. The magnification or pixel size issues resulted from poor image resolution are not discussed in the protocol. In 2018, Di Martino et al. (2018) proposed the analysis method for STED (Stimulated Emission Depletion) microscopy images of fenestrations using contour trace and macro programming to obtain semi-automatization of the process. The brief description suggests also that some manual steps are required. The authors made assumptions about fenestration circularity, but the exact roundness parameters for exclusion were not specified. Kong and Bobe (2021) proposed a well described semi-automated processing of human LSEC images obtained by Structured Illumination Microscopy (SIM). A Python based automated image processing macro utilizes an adaptive thresholding process and segmented images are further analysed to calculate both the number and diameter of fenestration. In 2017, we proposed the quantitative method for atomic force microscopy (AFM) image analysis of LSEC (Zapotoczny and Szafranska, 2017). Fenestration diameters were manually measured from high magnification images and, together with the manually counted fenestration number, then converted into porosity. The proposed method was precise, yet time consuming similarly to the other methods described above that involve manual measurements.

Recent developments in machine learning resulted in new possibilities for automatization or semi-automatization of the LSEC morphology analysis. Li et al. (2020) proposed an in house developed image recognition program based on a fully convolutional network for fenestration analysis. Unfortunately, many algorithms require programming skills in various programming languages, which is the main obstacle for the wide use of machine learning in biology. Recently, new software was developed with user friendly interfaces such as Weka Segmentation (Arganda-Carreras et al., 2017) or Ilastik (Berg et al., 2019). The combination of machine learning, basic image analysis and manual adjustments offers new ways to optimize the previously proposed methods and adjust them to sample size and precision needed for future experiments.

In this article we compare three different methods of image analysis: fully manual, semi-automatic (thresholding using ImageJ/Fiji) and automatic – machine learning (based on Ilastik software). We apply all three analysis methods for images obtained using each type of microscopy – AFM, SEM, and SIM. For clarity, both methods and results sections are divided according to the three imaging techniques. Finally, user bias is discussed based on the cross-correlation of image analysis performed independently by five researchers.

2. Materials and methods

2.1. Cell isolation

The cells were isolated as described in Zapotoczny and Szafranska (2017) for AFM and SIM (mouse LSECs) and in Mönkemöller et al. (2018) for SEM (cryopreserved rat LSEC). The experiments followed protocols approved by the local Animal Care and User Committees. Briefly, mice/rats were anesthetized using a mix of ketamine/xylazine and liver was perfused to remove blood and digested using Liberase™ (Roche, Germany). Thereafter, parenchymal cells were removed by a series of centrifugations. Mouse LSECs were isolated using immunomagnetic separation and CD146 conjugated magnetic beads (MACS, MiltenyiBiotec, Germany) while rat LSEC were separated by density gradient centrifugation (50/25 % Percoll gradient) followed by selective adherence to remove stellate cells and Kupffer cells, respectively. After separation, cells were seeded on glass coverslips and washed with media after 1 h incubation in 37 °C, 5 % CO_2, 5 % O_2 (cell culture media and surface coating specified for each technique below).

2.2. Sample preparation, imaging, and quantitative analysis

The differences in properties of the images obtained by each microscopy modality affect the analysis strategies. Therefore, each quantitative analysis is described separately for each imaging technique. For more detailed examples of the analysis see Supplementary Materials. The list of the parameters of interest can be found in Table 1.

2.2.1. Atomic Force Microscopy (AFM)

2.2.1.1. Sample preparation and imaging. In our analysis, we used images of samples prepared according to Zapotoczny and Szafranska (2017) and Mönkemöller et al. (2018). LSEC were cultured for 12−16 h on uncoated glass coverslips in EGM-2 full media (Lonza) and fixed for 2 min in 1 % glutaraldehyde in PBS and stored in PBS (with Mg^{2+}, Ca^{2+}) until imaging for up to two weeks. The measurements were performed using a JPK Nanowizard 3 AFM system (JPK Instruments AG, Germany) in PBS (with Mg^{2+}, Ca^{2+}) in a commercial liquid cell with the temperature control (25 °C). High magnification images were obtained using Quantitative Imaging mode with semi-soft (k = 0.03−0.06 N/m) triangular cantilevers with sharpened tips (radius <12 nm); low

Table 1
Parameters used for description of LSEC morphology.

Parameter	Definition	Unit
Cell area	(SEM/SIM) area of single cell surface (AFM) area of all cells in the image reduced by nuclei region of height above 700nm	nm^2 (μm^2)
Fenestration diameter	Max diameter – the longest diameter of single fenestration Min diameter – the shortest diameter of single fenestration For (semi-)automatic methods max and min diameter are calculated with the assumption of elliptical shape	nm
Roundness	$\frac{\text{min diameter}}{\text{max diameter}}$	0−1, unitless
Single fenestration area	(circularity assumption) $\pi \times \text{diameter}^2$ (elliptical assumption) $\pi \times$ min diameter $\times$ max diameter	nm^2
Total area of fenestrations	(Manual method, SI2) Number of fenestrations x fenestration diameter distribution ((Semi-)automatic methods) total detected area of fenestration	nm^2 (μm^2)
Porosity	$\frac{\text{total area of fenestrations}}{\text{cell area}} \times 100\%$	%
Fenestration frequency	$\frac{\text{number of fenestrations}}{\text{cell area}}$	$\frac{\text{No. of fen.}}{\mu m^2}$

magnification images of whole cells were imaged with contact mode and semi-soft triangular cantilevers with a regular tip (radius <60 nm). Precise imaging description and parameters such as loading force can be found in our previous work (Zapotoczny and Szafranska, 2017). Collected data were processed with JPK Data Processing Software and converted to tiff format for further analysis using ImageJ/Fiji.

2.2.1.2. Quantitative analysis.

1 Fenestration diameters

Single fenestration diameters were measured in three different ways from 26 high magnification images displaying a total of 625 fenestrations. A representative image is presented in Fig. 1A.

I Manual quantification was performed as follows: First, images were scaled to the scale bar individually for every image. Then, the shortest and the longest diameter of each fenestration were measured (minor and major axis respectively, assuming an elliptical shape of fenestration). Finally, the area of every pore was calculated with the assumption of an elliptical shape. The roundness parameter was defined as a ratio between the minor and major axes measured. Every fenestration was assigned with a number for further identification and comparison with another two methods. Holes on the edge of the image or clearly distorted i.e., not having a round shape or merged due to imaging or sample preparation artifacts were excluded.

II The semi-automatic method is based on the difference in contrast between the inside of fenestration and LSEC membrane. A simple threshold tool in Fiji was used to manually set cut off values for every independent image to ensure maximal precision (image from same imaging conditions are recommended when applying the same thresholding value to reduce bias). Next, the image was converted into a binary mask and then every fenestration was measured. Parameters such as fenestration area, fenestration diameter (min, max, mean), and roundness were calculated automatically (under "Analyze particles" tool in Fiji, size and circularity were set the same for all the images) and assigned to each fenestration according to the previously established order (for fenestration-by-fenestration analysis). Similarly to the manual quantification, the scale bar was used to adjust the scale for every image.

III The automatic method for the measurement of fenestrations is based on machine learning. Presented results were analyzed with Ilastik software. The algorithm was trained on a set of four representative images. A user teaches the software by marking parts of the image indicating the areas of fenestrations and the rest of the cell body area. Training is simple and takes about 30 min. Then, batch processing was applied to all 26 images to create simple segmentation binary masks (Fig. 1A, top). Finally, masks were analyzed using ImageJ/Fiji similarly to the semi-automatic method.

All 625 fenestrations were independently assigned with area, diameter (min, max, mean) and roundness obtained from three different quantitative methods and then compared.

2 Fenestration frequency and porosity

The fenestration frequency and porosity (see Table 1 for definitions) were measured from low magnification images of whole cells (Fig. 1B). 27 images of 40 μm × 40 μm size were analyzed. Initially, the image size was artificially converted (from 1024 × 1024 pixels to 2048 × 2048 pixels) with linear interpolation to digitally increase the resolution of an image ("Adjust Size" tool in Fiji). Artificially increased resolution does not bring any new information, however smaller pixel size is beneficial for better fenestration detection in all 3 analysis methods.

I Manual quantification was utilized in a two-step process. First, fenestrations were counted manually for the whole AFM images. Second, the cell area was calculated, excluding the background and nuclei areas. To achieve this, by using the 3D information about the topography of cells, regions of heights above 0.7–1.0 μm were excluded from analysis, by image contrast adjustment. We assumed that fenestrations can be formed only in flat areas of LSEC. Finally, the total area occupied by fenestrations, fenestration frequency, and porosity were calculated using the number of holes and mean diameter distribution measured from high magnification images (detailed description of calculation can be found in Supplementary information SI.1.).

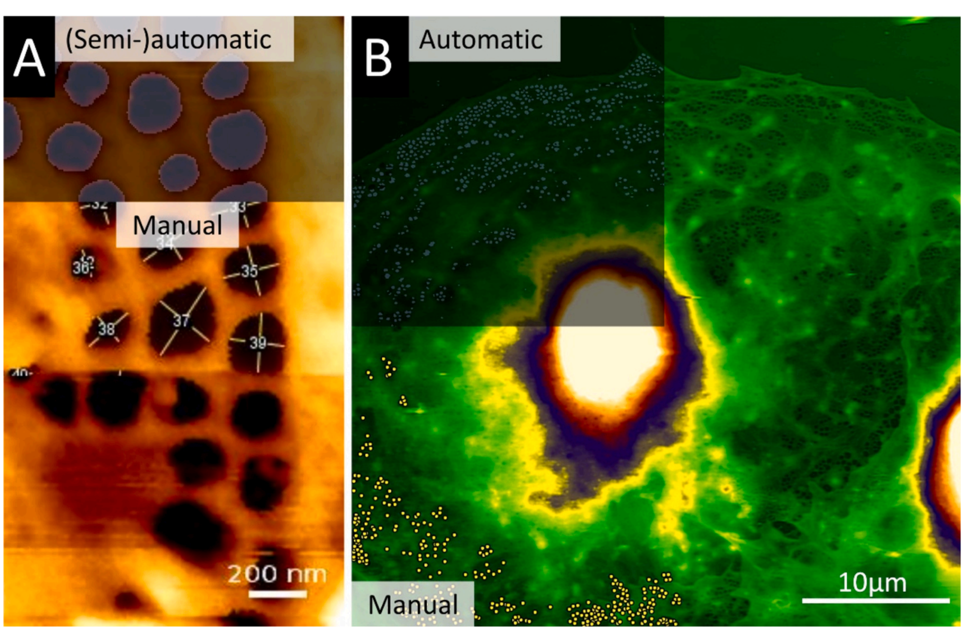

Fig. 1. Representation of the AFM image analysis. (A) High magnification AFM image of the sieve plate. Overlaid mask of fenestrations detected by (semi-)automatic methods and manually measured diameters are presented. Fixed cells were imaged using QI AFM mode and a sharp MSCT tip. (B) Low magnification AFM image of LSEC. Overlaid mask of detected fenestrations from the automatic method and marker points from manual fenestration counting are shown. Fixed cells were imaged using AFM contact mode and the MLCT tip.

II Simple thresholding could not be used for low magnification images due to the artefacts of AFM measurements that make the height (topography) images look curved/tilted. Built in image corrections are not sufficient and images require cumbersome analysis. Therefore, the semi-automatic method could not be applied to the low magnification AFM images.

III Automatic image analysis was successfully applied to measure fenestration number and area from low magnification AFM images. First, the program was trained on sets of four images (training time of around 1 h) and then all 27 images were analyzed using batch processing. Next, images were converted into simple segmentation binary masks and analyzed in ImageJ/Fiji. To avoid fenestrations merged together the watershed tool was used followed by particle analysis to exclude objects from outside of the fenestration range of 50−300 nm and circularity below 0.4. The remaining objects were automatically counted, and the total area measured to calculate porosity and fenestration frequency.

2.2.2. Nanoscopy – Structured Illumination Microscopy (SIM)

2.2.2.1. Sample preparation and imaging. Samples were prepared as previously described (Zapotoczny and Szafranska, 2017; Mönkemöller et al., 2018). Briefly, cells were seeded on fibronectin coated coverslips in RPMI-1640 medium (Sigma-Aldrich) and then fixed for 10 min with 4 % formaldehyde (FA) in PBS and stored in PBS containing 0.1 % FA. Before imaging, cells were stained using CellMask Green (ThermoFisher) 1:1000 dilution in PBS for 30 min and then mounted onto glass slides using Vectashield antifading mounting media (Vector Labs). Images were obtained using a commercial SIM microscope (OMX Blaze system, GE Healthcare) with a 60x 1.42NA oil-immersion objective (Olympus). 3D-SIM image stacks of 2−3 μm were acquired with a z-distance of 125 nm and with 15 raw images per plane (five phases, three angles). Raw datasets were computationally reconstructed using SoftWoRx software (GE Healthcare) and z-projections in tiff format were prepared for further analysis.

2.2.2.2. Quantitative analysis (Fenestration diameter, fenestration frequency and porosity). Initially, the image size was converted from 1024 × 1024 pixels to 2048 × 2048 pixels, with linear interpolation, using the adjust size tool in Fiji to digitally increase the resolution of the image.

I The scale was adjusted to the size of the image of 40.96 μm × 40.96 μm and 300 fenestrations were manually measured from the top right quarter of each of 20 images. For every fenestration, both the smallest and the largest diameters were measured to calculate mean values. For calculation of fenestration frequency, the cell area was measured using the threshold tool in ImageJ/Fiji (fenestrations area including) and fenestrations were manually counted (Fig. 2 Manual). Porosity was calculated using fenestration diameter distribution and the number of fenestrations individually for every image (for detailed calculations see Supplementary information SI.1.).

II For the semi-automatic method, images were converted into binary masks using the threshold tool with manually adjusted values for each image. A watershed function was then applied to avoid exclusion of merged fenestrations, and only objects within the fenestration size range were saved (“Analyse particles” Fiji tool, 50−300 nm diameter and circularity above 0.4). Finally, fenestration diameter, the total area and number of fenestrations were measured and used to calculate porosity and fenestration frequency (Fig. 2 Semi-automatic).

III The machine learning based automatic method was used for fast image processing. After training on four images (training time of about 1 h) all 20 images were processed and converted into simple segmentation binary masks in tiff format (Fig. 2 Automatic). Further analysis was the same as for the semi-automated method described above (analyse particles, size dependent object exclusion).

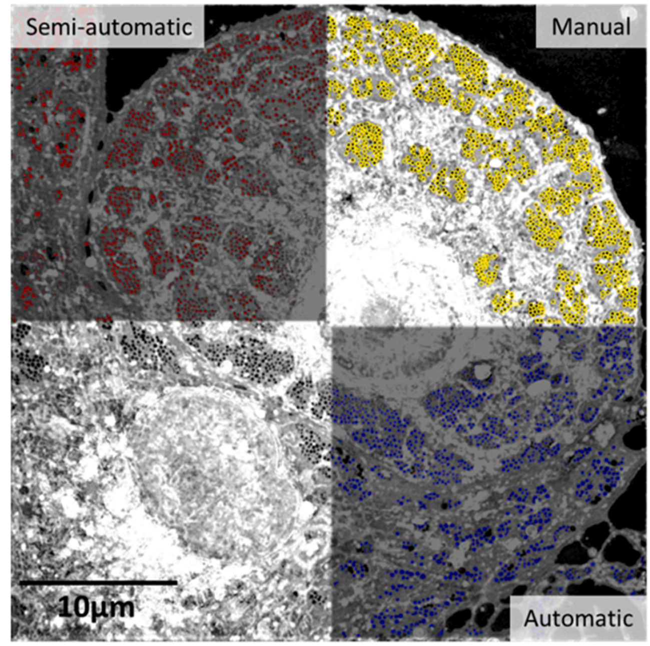

Fig. 2. Representative analysis of SIM image of LSEC stained with CellMask Green. Red - fenestrations detected by semi-automatic method, blue – fenestrations detected by automatic machine learning method, yellow marks – fenestrations counted manually.

2.2.3. Scanning Electron Microscopy (SEM)

2.2.3.1. Sample preparation and imaging. Samples were prepared as previously described (Mönkemöller et al., 2018). LSEC were seeded for 3 h on fibronection covered glass coverslips in RPMI-1640 medium (Sigma-Aldrich) and then fixed and stored in a mix of 4 % formaldehyde and 2.5 % glutaraldehyde in cacodylic buffer. Samples were then processed with 1 h treatment with freshly made 1 % tannic acid in PHEM buffer, 1 h of 1 % OsO_4 in H_2O, dehydrated in ethanol gradient (30 %, 60 %, 90 % for 5 min each, 5 times for 4 min in 100 % ethanol, and incubated twice for 10 min in hexamethyldisilane (HMDS), then left overnight to evaporate. Before imaging, samples were mounted on metal stubs using carbon tape and silver glue to reduce charging and then sputter coated with 10 nm gold/palladium. A commercial SEM system (Sigma, Zeiss) was used for imaging with a 2 kV electron beam. Low magnification images (Fig. 3B) were obtained from 5 different areas of the sample with 20 images of single cells in total. High magnification images (Fig. 3A, ~6.5 nm/pixel) were taken for each of the 20 cells.

2.2.3.2. Quantitative analysis.

1. Fenestration diameters

Contrast and brightness were adjusted for every image and the scale was set according to the scale bar.

I Fenestrations were manually measured from 20 high magnification images; assuming elliptical shape, both the smallest and the largest diameter (along minor and major axis respectively) were measured and then used for the calculation of the area and roundness.

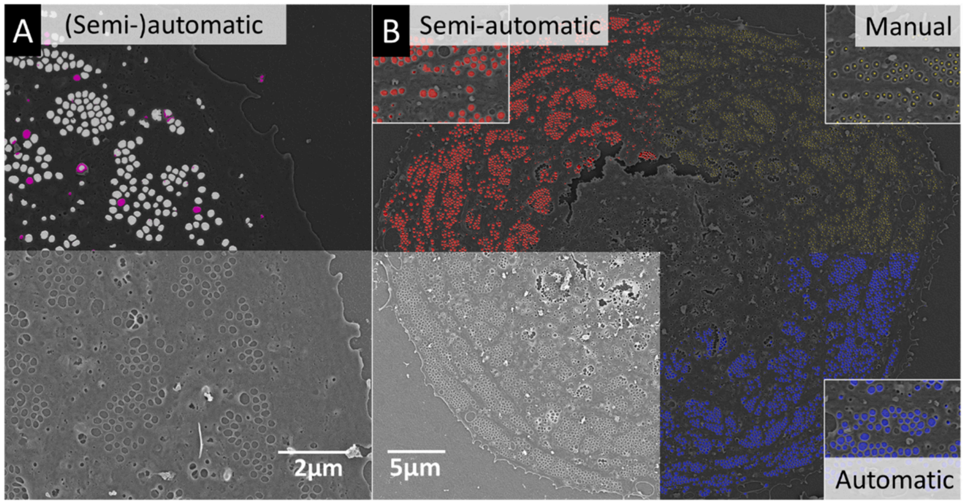

Fig. 3. Representation of the SEM image analysis. (A) High magnification of LSEC imaged using SEM. The upper panel of the image represents the overlaid mask of detected fenestration by semi- and automatic methods (white) or automatic only (magenta). (B) Low magnification of LSEC imaged using SEM. Red - fenestrations detected by semi-automatic method, blue – fenestrations detected by the automatic machine learning method, yellow – fenestrations counted manually.

II The second semi-automatic method based on the Fiji threshold function consists of few steps (detailed example in Supplementary information SI.2.). First, the contrast was adjusted to better visualize the edges of fenestrations and the image was inverted. Next, the threshold was manually set using the Huang algorithm to the point where single fenestrations but not their surrounding edges were covered. Images were then converted into binary masks and objects larger than 300 nm or smaller than 50 nm and with roundness below 0.4 were excluded. Every fenestration was then automatically measured and parameters such as area, diameters (min, max, mean) and roundness were calculated.

III For fast image processing, machine learning was applied. First, the algorithm was trained using four images (training time of about 2 h) and then all 20 images were processed and converted into simple segmentation binary images. Fenestrations were then measured the same way as described for the semi-automated method.

2. Porosity and fenestration frequency

I Fenestrations were manually counted (Fig. 3B, yellow) and the cell area was calculated from the manually marked cell shape. The total area of fenestrations was calculated using fenestration number and previously measured diameter distribution from high magnification images (details in SI.1.).

II The semi-automatic method was applied with parameters adjusted for every image individually as for the high magnification images described above (contrast adjustment, inversion, threshold and particle analysis exclusion by size) (Fig. 3B red). The total area and number of fenestrations were automatically measured after scale adjustment and used for the calculation of porosity and fenestration frequency.

III For automatic analysis, the algorithm was trained using five low magnification SEM images and then all 20 images were processed. Simple segmentation binary images were then analyzed using ImageJ/Fiji similarly to the semi-automated method.

2.3. User comparison

Five individual users with different experience with image analysis were asked to analyze one high magnification SEM and nine SIM images. For the SEM image, each user was asked to manually measure the same 700 marked fenestrations, set the scale by measuring the scale bar and perform analysis using semi-automatic and automatic methods according to the descriptions above. Then each of the 700 marked fenestrations were assigned with parameters (area of single fenestration, fenestration diameters (min, max, mean), and fenestration roundness). For SIM images, all participants were asked to manually count fenestrations from nine whole images and then analyze all images using semi-automatic and automatic methods as described above. The parameters were measured by five different users using three different analysis methods. Results were cross-correlated between each other (every single user with every other user).

2.4. Statistics

All statistical analyses were performed using OriginPro software (OriginPro 2021, OriginLab Corp., Northampton, MA). The total numbers of analysed cells and fenestrations are summarized in the Table 2. For porosity and frequency parameters, the comparison between the methods was based on the relation between the (semi-) automatic methods and manual (standard) approach. The linear correlation is necessary for the method to be useful in the experiments with expected changes in selected parameters. Therefore, linear regression was fitted to the data with the R^2 coefficient describing linearity (the closer to 1 the more linear) and slope (tangent of the angle) describing the correlation between the values. A slope of 1 is preferred as the change in porosity/frequency measured by the (semi-) automatic and manual methods would remain the same even if the absolute values vary. Slopes lower or higher than 1 mean under- or over-estimation, respectively.

Table 2
Total number of analysed images per imaging technique.

Imaging technique	Image Magnification	Number of images/cells	Number of measured fenestrations	Pixel size [nm]
AFM	High	26	(M,S-A, A) 625	4–6
	Low	27		20
SIM	Low	20	(M) 6 000 (S-A) 60 000 (A) 63 000	20
SEM	High	20	(M) 8 100 (S-A, A) 16 000	6–7
	Low	20		18–20

M – manual, S-A- semi-automatic, A - automatic.

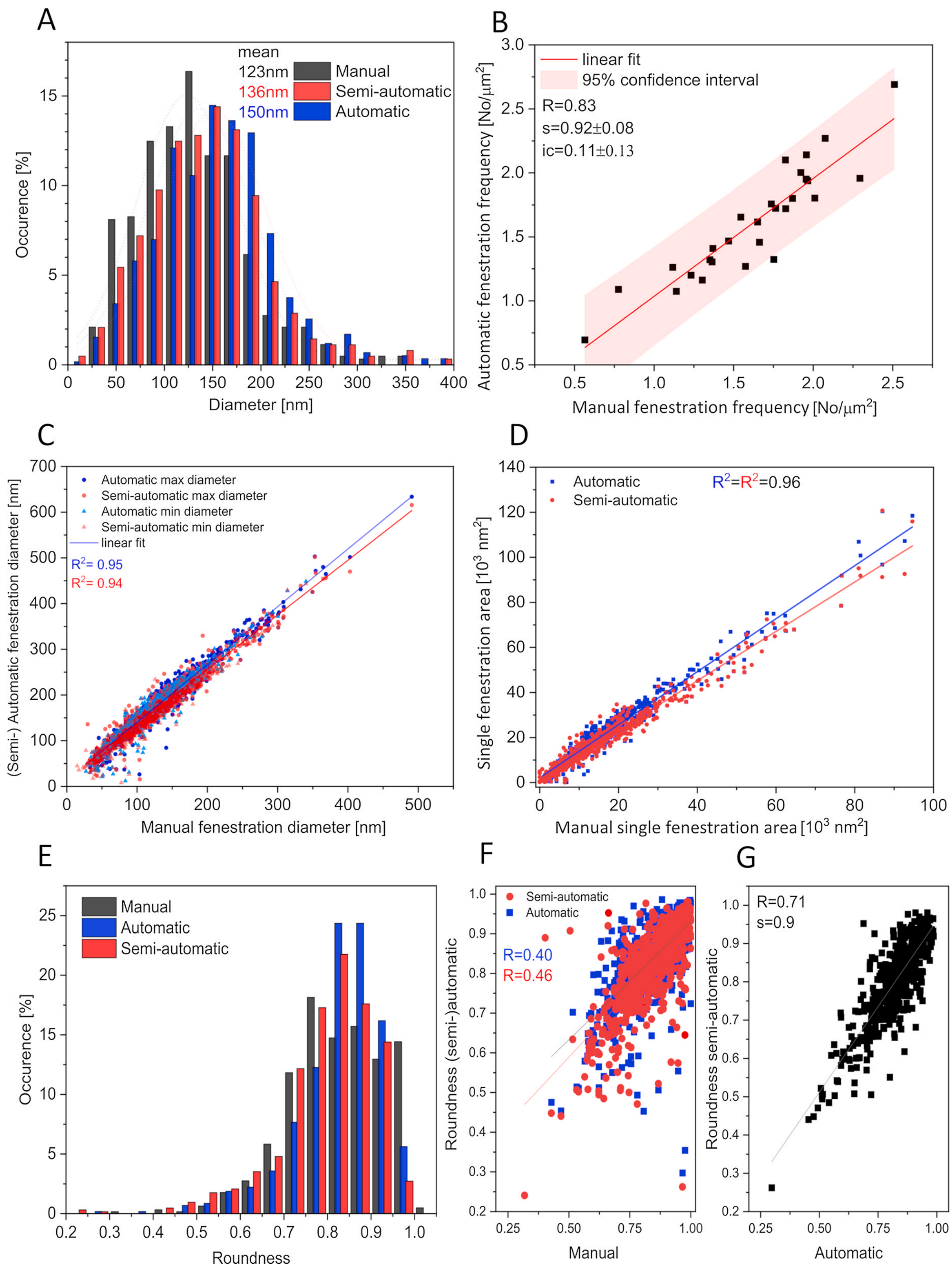

Fig. 4. Analysis of AFM images. (A) Histogram of fenestration diameter distribution. The dotted lines represent fitted Gaussian curves from which the mean values were calculated. Data comes from 625 fenestrations from 26 high magnification images of sieve plates (see Fig. 1A). (B) Correlation of fenestration frequency calculated using Automatic and Manual counting. Each dot represents a single image (see Fig. 1B), 27 images in total. S - slope of the fitted linear function, ic - intercept. (C) comparison of single fenestration diameter measured manually and automatically with the assumption of elliptical fenestration shape. Max, min diameter – major and minor axis of the ellipse. (D) comparison of single fenestration area measured manually and automatically. (C, D) each dot represents a single fenestration measured by 3 different techniques. (E) Distribution of fenestration roundness measured by different techniques (roundness = ratio of min to max diameter). (F, G) correlation of roundness parameter between manually and automatically measured fenestrations.

3. Results and discussion

In this section, the terms Manual, Semi-automatic and Automatic are used for the 3 quantitative analysis methods described in detail in the Materials and Methods section

3.1. AFM image analysis

Fenestration diameter distribution obtained from 26 high magnification AFM images show differences between the three analysis methods (Fig. 4A). Gaussian curves were fitted to calculate the mean diameter and the width of the distribution. The smallest mean diameter of 123 nm was obtained from manually measured data, semi- and automatic methods gave values of 136 nm and 150 nm, respectively. The larger diameter for non-manual methods may be related to the fenestration edge detection. Manual measurement is based on contrast and user judgement and may vary between the images. For semi- and automatic methods, the diameter is calculated back from the measured areas of single fenestrations with the assumption of circularity. Moreover, the detection of fenestrations by machine learning may require detection of the edge of the hole and it could therefore increase the total area and diameter of fenestration. This issue is related to the pyramidal shape of the AFM tip which may influence the intensity gradient corresponding with the height on the fenestration edge (more information about the AFM tip shape problems for fenestration measurement can we found in Zapotoczny and Szafranska (2017)). A pixel size of 4−6 nm would explain that difference of 13/27 nm, which correlates with 2–4 pixels between the manual and (semi-)automatic methods (Fig. 4A).

Individual analysis of each of the 625 fenestrations provides a comparison of each of the three analysis techniques for each pore. Fig. 4C shows the linear relation between the manually measured min and max diameters and the (semi-)automatic method calculated data. The fitted linear regression presents a good correlation of $R^2 = 0.94$ and 0.95 for the automatic and semi-automatic methods, respectively. The slope of the regression for both methods was 1.2 and the intercepts of 16 nm and 10 nm for the automatic and semi-automatic methods, respectively. Both the slope above 1 and the intercept values confirm that the non-manual methods detect fenestrations as larger than the manual data, however, the good linear correlation makes the measurement comparable between the samples with differences in fenestration size. The same results have been observed for fenestration-by-fenestration analysis of the areas of single pores (Fig. 4D). The linear regression slope of 1.1 and $R^2 = 0.96$ show a good linear correlation.

Most of the previously published articles dealing with the measurement of LSEC morphology assumed circularity of fenestrations. Here we show that the roundness parameter – the ratio between minimum and maximum diameter, concentrates about the value of ~0.85 for all methods (Fig. 4E). Interestingly the distribution of the manual measurements is wider and the number of nearly circular fenestrations (0.95-1) is much higher than for (semi-)automatic methods. Moreover, the comparison of roundness of single fenestrations between the three methods shows a correlation between automatic and semi-automatic (Fig. 4G) but not between manual and automatic methods (Fig. 4F). This result may suggest the user bias towards a more circular shape as the choice of min/max diameter is subjective. The roundness distribution from the automatic and semi-automatic methods is very similar and a slight increase towards more round fenestrations correlates well with the assumption that the machine learning algorithm detects the edges of the holes equally enlarging both min and max diameters and therefore increasing the roundness parameter.

The fenestration frequency calculated using automatic methods shows good correlation with the manual measurement (Fig. 4B). Almost all measured data lay within 95 % confidence interval and slope of 0.92 with $R^2 = 0.83$ indicate linear correlation.

3.2. SIM image analysis

Twenty LSEC SIM images were analyzed in three different ways. The comparison between the manual method and the (semi)automatic methods (Fig. 5A) showed a linear correlation with R^2 values of 0.85 and 0.82, respectively. The correlation for SIM is similar to the AFM images which it is enough to be useful for comparison of data from different treatment groups. There are no significant differences in the measured numbers of fenestration per image between various analysis methods (Fig. 5B). Fenestration frequency was not calculated due to difficulties in the detection of cell boundaries. The Cell Mask dyes are a group of cell membrane dyes that provide great contrast needed for detection of fenestrations but further analysis and calculations can be optimized for single cells only on non-confluent samples where only a single cell is visible in the field of view of the microscope. Alternatively, cells can be separated manually. For samples with tight cell monolayers, the cell area can be normalized according to the visible number of cells for porosity/fenestration frequency calculations by subtraction of the mean area of nuclei (10 μm is a good approximation of diameter of LSEC nuclei).

Fig. 5C shows the differences in the distribution of diameters. The semi-automatic method shifted distribution towards a larger apparent fenestration size with a mean value of 178 nm. Automatic and manual methods gave similar results with mean diameters of 138 nm and 130 nm, respectively. Machine learning showed a high number of small pores below 75 nm which may be an artifact of the detection algorithm and can be optimized by the increased training time. For all methods objects smaller than 50 nm were excluded. A pixel size of 20 nm is not sufficient for the detection of holes below 50 nm due to Nyquist's sampling criterion. The mean diameter values were calculated as centers of the fitted Gaussian distribution curves to compensate for this. The difference between semi-automatic and the other methods can be biased by the manual adjustments of the cut-off intensity value. The threshold must be set individually for every image so changes towards both smaller and larger diameters can be introduced by the users. It is not possible to use a fixed value as the intensity in the perinuclear area varies between the cells and would induce artifacts that influence the segmentation more than the manual adjustment.

Similarly to the data from the AFM images, the roundness parameter was calculated with the assumption of fenestration elliptical shape. The shift towards a more circular shape can be observed for manual measurements which is consistent with the previous observation, most probably resulting from the user bias. Also, the roundness values concentrate around a value of 0.9 for SIM images compared to 0.82 for AFM images. This difference is connected with the imaging technique – raw SIM images require reconstruction which will make small objects at the edge of achievable resolution appear more round in shape due to Wiener filtering (part of the SIM reconstruction algorithm). Adjustment of the image size using bilinear interpolation makes the shape even more circular. Nevertheless, the benefits of the decreased pixel size, which allows better precision of the quantitative analysis, outweigh the downsides.

3.3. SEM image analysis

Twenty high magnification SEM images were quantitatively analyzed using three different methods. Comparisons between manual and (semi)automatic techniques showed differences in the shape of mean diameter distribution (Fig. 6A). Mean fenestration size was calculated from the manually measured min and max diameters or for (semi-)automatic methods calculated from the detected areas, assuming circularity of holes. Only manually measured values had a simple Gaussian distribution with the center at 175 nm. The other two methods show the results with at least double Gaussian shape peaks; the first one being within the regular fenestration size range with centers at 178 nm and 191 nm for semi-automatic and automatic methods respectively,

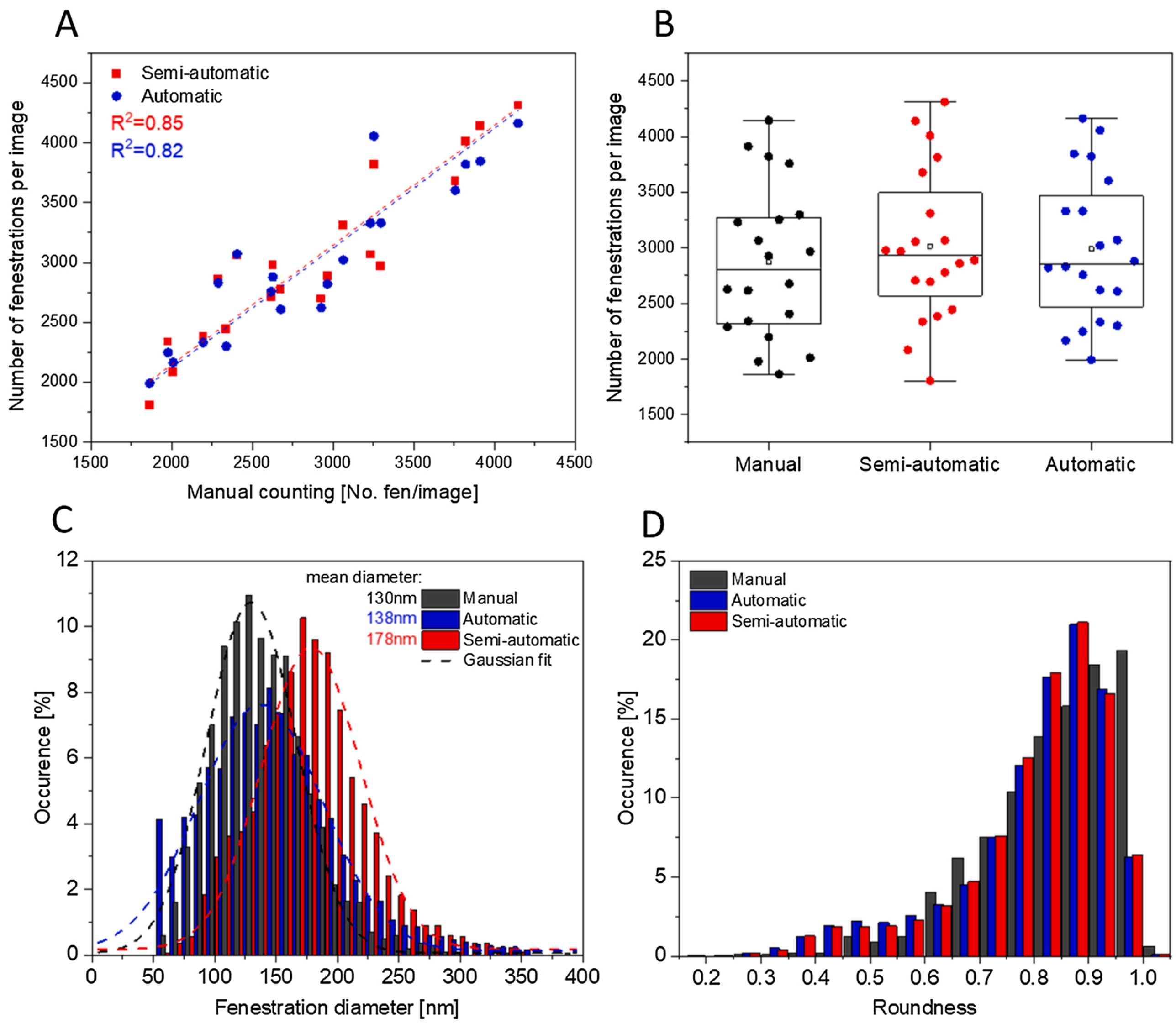

Fig. 5. Analysis of SIM images. (A) Correlation between manually and automatically counted fenestrations. Each dot represents a single image (see Fig. 2), 20 images in total. (B) Comparison of fenestration frequency between the studied groups. (C) Distribution of fenestration diameter. The dashed line represents fitted Gaussian curve from which the average value was calculated (tip of the curve). Fenestrations smaller than 50 nm were excluded due to a pixel size of 20 nm. The total number of fenestrations measured – 6 000, 60 000, 63 000 from manual, semi-automatic and automatic methods respectively. (D) Distribution of the roundness parameter calculated from measured fenestrations.

and the second maximum with centers at 100 nm and 120 nm. The additional detected objects are identified on the images as non-transmembrane protrusions in the cell membrane, most probably endocytic vesicles arising from the prominent endocytic properties of LSECs. Their size and contrast, being similar to fenestrations, make them impossible to be separated from fenestrations using threshold or Ilastik analysis, however, they can be removed from further calculations and analysis using the multi-peak Gaussian curve fitting or by cutting off all the objects below a certain size. The first approach requires more time as it should be adjusted for every cell/image but interferes less with the data. The second approach can be automated to a cut-off value set in the middle of the two maxima, but it can significantly affect the results if changes in fenestration diameters towards smaller values are expected (two peaks overlapping).

Fenestration-by-fenestration analysis with three different methods shows a good linear correlation between manual and (semi)automatic measurements with $R^2 = 0.95{-}0.96$ and a slope of 1. The automatic compared to the semi-automatic approach causes a 16 nm shift towards larger apparent fenestration size and area of 2300 nm^2. Similarly to the analysis of the AFM images, the machine learning algorithm is detecting the edge of the holes resulting in the systematic error with the value connected to the pixel size. This error would not affect the comparison between the treatment groups with expected changes in diameter but should be taken into consideration for comparison between data calculated with different methods of analysis.

Porosity and fenestration frequency were calculated from low magnification images. Both semi-automatic and automatic methods show a linear correlation of the values of porosity when compared with manual measurements, $R^2 = 0.89$ and 0.91 (Fig. 6D). However, the slopes of the linear regression are 0.63 and 0.9 respectively. The difference in slope suggests that the semi-automatic method is underestimating the value of calculated porosity. The difference in slope values between the methods can be more pronounced with the increase of cell porosity due to drug treatment. As a result, smaller changes in cell porosity can be wrongly assigned as not significant. The smaller intercept of linear regression of the semi-automatic compared to the automatic method makes it more similar to manual measurement, however, the difference in slope is more important for the usefulness as a tool for

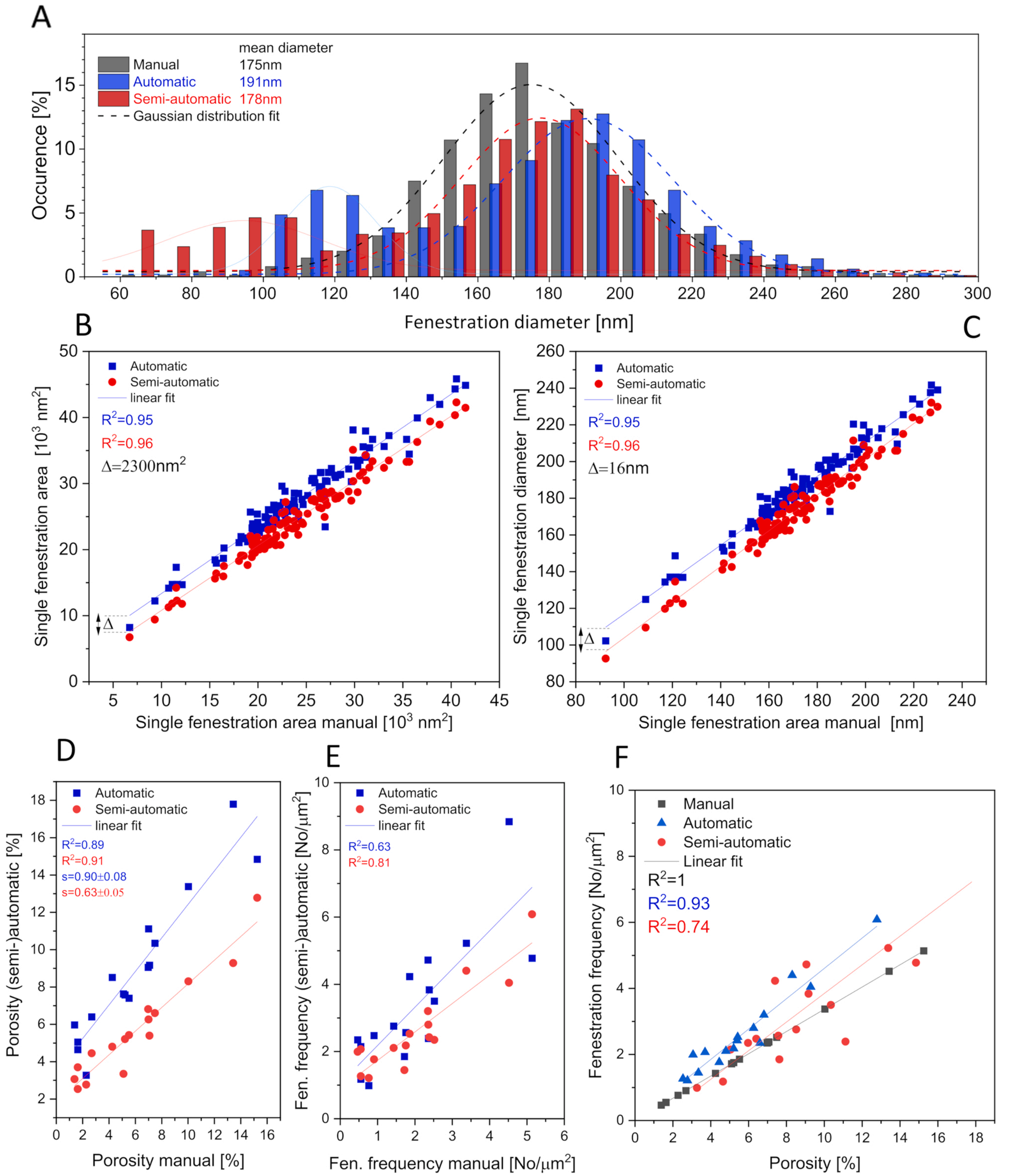

Fig. 6. Analysis of SEM images. (A) Fenestration diameter distribution measured from high magnification SEM images (see Fig. 3A). The dashed line represents fitted Gaussian curves, for semi-automatic and automatic methods a multi-peak fit was used to exclude the non-fenestration objects (thin line Gaussian curve). The total number of fenestrations measured – 8 100 from 20 images/cells for manual measurement and 16 000 from 20 images/cells for (semi-)automatic methods. Correlation of single fenestration area (B) and diameter (C) between manual and automatic methods. Δ – intercept between fitted linear functions. Comparison of porosity (D) and fenestration frequency (E) between manual and automatic methods. Each point represents a single image (see Fig. 3B), total number of images – 18. (F) the relation between frequency and porosity measured using different methods.

comparison between treatment groups.

Fenestration frequency showed a weaker linear correlation than porosity with R^2 = 0.63 and 0.81 for Ilastik and threshold respectively (Fig. 6E). These results correlate with the detection of the small fenestration-like objects shown as a second maximum on diameter distribution (Fig. 6A). Because of the small size of these structures, they do not significantly affect porosity, but their number is significant compared to detected fenestrations and this influences fenestration

Table 3
Parameters of fenestrations measured by 3 different methods from SEM images.

Parameter		Manual	Semi-automatic	Automatic
Area	Average [nm^2]	26,926 ± 2140	26,818 ± 443	26,488 ± 3767
	User comp. [%]	1.25 ± 12	0.10 ± 1.8	3.45 ± 22.6
Max diameter	Average [nm]	199 ± 7	201 ± 1.8	200 ± 13
	User comp. [%]	0.34 ± 5.25	0.03 ± 0.86	0.79 ± 10.29
Min diameter	Average [nm]	168 ± 7	166 ± 1.4	165 ± 12
	User comp. [%]	0.46 ± 6	0.03 ± 1	1.10 ± 12
Mean	Average [nm]	184 ± 7	184 ± 1.4	182 ± 13
	User comp. [%]	0.30 ± 5.7	0.02 ± 0.87	0.8 ± 10.9
Roundness	Average	0.849 ± 0.011	0.828 ± 0.001	0.830 ± 0.009
	User comp. [%]	0.000 ± 0.015	0.000 ± 0.001	0.000 ± 0.019

±SD; user comp. = comparison between users.

frequency. The above proposed approaches of removing these structures may help to reduce the effect on fenestration frequency and enable comparison between the groups if changes in frequency are expected to be independent of porosity changes (for example changes in fenestration diameter may compensate for the difference in fenestration number and show no changes in porosity). The comparison between porosity and fenestration frequency among the studied methods (Fig. 6F) shows a good correlation for manual measurement due to the direct connection between these parameters – the fenestrated area used to calculate porosity is calculated from the number of fenestrations. The automatic method shows a good linear correlation with R^2 of 0.93 while the semi-automatic method presents R^2 of 0.74 which points to the influence of detected fenestration-like objects in the calculation of fenestration number.

3.4. User comparison

To compare the differences between users and study user bias, sets of SIM and SEM images were analyzed by five researchers with different levels of imaging experience, from beginner to advanced user.

3.4.1. SEM

Firstly, 700 fenestrations from Fig. 3A were individually measured (fenestration-by-fenestration) by five users using the three studied methods and then the parameters were cross-correlated between all the users. Next, mean values were calculated for every user and the average was calculated for each method. Interestingly, the average values of parameters were similar for all techniques (Table 3). However, differences between the users (Fig. 7) and SD values of the cross-correlation show significant differences among the users. The biggest deviation is observed with the automatic method; the cross-correlation parameter for a single fenestration area was only 3.5 %, but the standard deviation of over 20 % suggested significant differences between the users. One of the main reasons for that may be the specificity of the machine learning algorithm. Each user trained the software independently and small differences can lead to different ways of detecting fenestrations. Every fenestration on a SEM image has a visible, high contrast edge which can be included or excluded from the detected area. Differences between the calculated mean values of the diameter (Fig. 7B) for manual and automatic methods are of about 6−7 nm which is similar to the pixel size of this image - 6.5 nm. The semi-automatic method is intensity and contrast based and therefore, less sensitive to user preferences about the fenestration edge. Fenestrations are detected due to high contrast edges characteristic for SEM images - steep edges give a higher signal compared to a flat cell surface or substrate in the fenestration lumen. This hypothesis was confirmed by merging binary images of detected fenestration from automatic and semi-automatic methods showing rings around the holes (see Supplementary information SI.3). Small differences in fenestration roundness among the users using the semi-automatic method (Fig. 7C) also suggest that the shape of the detected holes is the least biased by this method. A shift towards a more circular shape (roundness value closer to 1) is observed for manual measurements which (consistent with previous observations) confirms the influence of the assumption of circularity by the users.

3.4.2. SIM

Nine SIM images were analyzed independently by five users with the three methods. Each image was then cross-correlated between all users and (semi-)automatic methods were compared with manual counting.

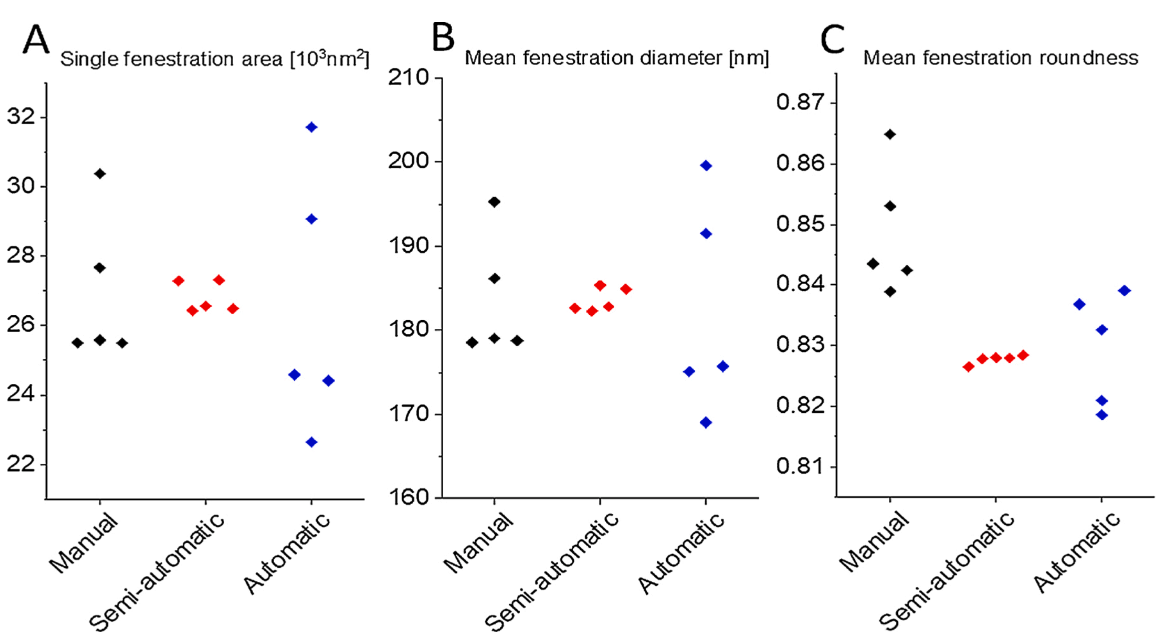

Fig. 7. Comparison of analysis methods between the users. Each point represents one user and the mean value of the presented parameter calculated from 700 measured fenestrations from SEM image.

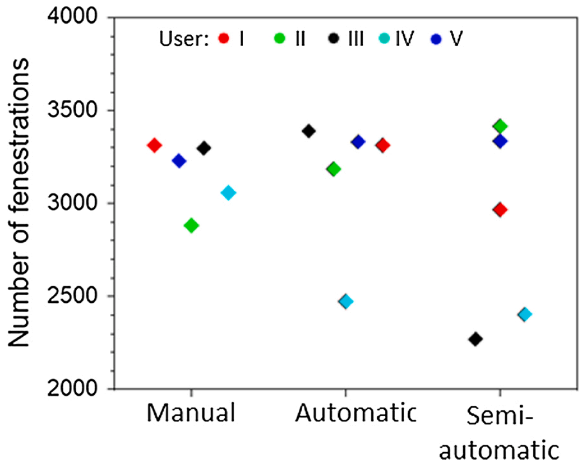

Fig. 8. Comparison between users' measurements of fenestrations number using three different techniques for one of the analysed SIM images.

Table 4
Comparison of fenestration number between the users and analysis methods for SIM images.

Change in fenestration number compared to manual counting [%]			
User	Semi-automatic	Automatic	Manual
I	10.1 ± 13	10.2 ± 12	
II	18.5 ± 9	8 ± 11	
III	−7.4 ± 15	−5.9 ± 11	
IV	−4.8 ± 13	−11.5 ± 12	
V	−4.5 ± 14	3.5 ± 13	
Cross correlation between users [%]	1.9 ± 9.5	3.3 ± 12	0.17 ± 11

The mean value of fenestration number per image was similar among the users (0.2–3.3 %), however, the difference between users within one method was about 10−12 %. An example of one of the analyzed images (Fig. 8) shows the differences between the users and methods. Manual counting has the smallest variation while (semi-)automatic methods present a wider range of calculated numbers. The main source of differences between the users using (semi)automatic methods is the large pixel size which causes the merging of fenestrations within one sieve plate during segmentation. Lowering the threshold or retraining the machine learning software leads to the presence of undetected fenestrations while the watershed function, used to split the merged holes, leads to splitting single fenestrations which causes an elevated number of detected objects (Table 4). The decision is made by each user and if it is standardized, the error can be minimized.

3.5. Discussion

In this study we investigated the use of three methods for quantitative analysis of LSEC images: manual measurement or counting of fenestrations, a semi-automatic threshold-based method and an automatic machine learning-based method. All three techniques have their advantages and disadvantages, mainly time efficiency at the cost of accuracy. The manual method was, until recently, the standard way of fenestration analysis due to the lack of proper software to semi-automate or automate the process. It was considered to be the gold standard, but the lack of scoring description prevents a proper comparison between results from different studies. Recently, attempts to apply home-made algorithms and machine learning have been reported (Di Martino et al., 2018; Kong and Bobe, 2021; Li et al., 2020), but their application requires a certain level of programming skills not available to every researcher. Here we report two methods which can be easily applied to experimental data where differences in fenestration diameter and/or number are expected.

The efficiency of each method depends mainly on the number of samples which is directly correlated with the time needed for analysis. This can be optimized in each study by designing experiments that would give minimum but sufficient sets of data for statistical analyses. The most time consuming is the manual method but the poor image quality or high number of artifacts may prevent the use of other, faster techniques. User comparison showed also that there is significant user bias for manual measurements so all analyses should be performed by one single user, ideally blind to the sample id. If there is a need for data analysis to involve more than a single person, the threshold method would introduce the smallest bias for fenestration size measurements. Fenestration frequency and porosity show similar differences among the users for all three methods so the choice can be based on to the quality of the images.

The data from all three imaging techniques suggests that the precision of both (semi-)automatic methods is similar and linear correlation allows us to use them for comparison of the parameters between experimental groups. All experiments where changes in fenestration size and/or number are expected can be analyzed using the semi-automatic or automatic method. However, the porosity calculated from SEM images using the semi-automatic method may seem underestimated. The comparison between the manual and semi-automatic methods shows a linear correlation with a slope below 1, which indicates that some fenestrated areas are not detected in the cells with higher porosity/higher number of fenestrations

The machine learning software includes a batch processing feature where, after training, tens or even hundreds of images can be automatically analyzed. The only limitation is the computer processing power which affects the speed. The main disadvantage of this approach is the requirement of images with similar contrast and brightness. In practice, each sample or group of samples may require adjustments for these parameters, and depending on the number of samples, this may reduce the time advantage over the semi-automatic method. Although, the threshold-based approach requires manual adjustment of the cut-off value for each image segmentation but still, the large number of fenestrations is analyzed for each manual step. It is a significant advantage over the fully manual approach, where single manual step gives information about only one fenestration.

For fenestration size measurements, both (semi-)automatic methods showed a systematic error that needs to be taken into consideration. The source of this error was identified and connected with the edge of the fenestration detection, related to the pixel size of the image. For the automatic method, the batch processing of all images using the same trained algorithm would solve this problem. For manual and semi-automatic methods inclusion/exclusion must be decided before the analysis.

4. Conclusions

All three proposed methods can be applied for fenestration analyses, but the best method should be selected based on the following criteria: the available imaging technique, the achievable quality of the images, the time for the analysis and the predicted outcome in measured

Table 5
Comparison of properties of the three methods of quantitative analysis.

Property	Manual	Semi-automatic	Automatic
Speed	− − − −	+	++
User bias	−/+	+	−/+
Accuracy - fenestration number	++	−	+
Accuracy - porosity	+/−	+	+
Accuracy - diameter	+/−	++	+
Artifacts sensitive	++	− −	−/+
Image quality sensitive	++	− −	−/+
User friendly	++	++	+

parameters. The pros and cons of the three selected methods are listed in Table 5.

We emphasize the need for small-scale pilot experiments to assess both the best imaging technique as well as the predicted range of changes in the LSEC morphology parameters. The time invested in the analysis of preliminary results will lead to the best possible protocol for further analysis. The combination of more than one analysis method can also be beneficial, for example, the best accuracy of diameter measurement was shown with the semi-automatic method while the number of fenestrations is most precisely detected manually.

The main limiting factor – time – can be overcome by automation, which is getting easier with the developments of new and more precise software and ongoing advancements in the field of microscopy. The results of this study show that the semi-automatic and automatic methods can be a timesaving alternative for the standard manual approach, but considerations of suitable methods are needed prior to application.

The choice of the best analysis method has to be based on the quality of every experimental data set. We suggest to first focus on obtaining the best possible image quality, within reasonable imaging time. For the fenestration size measurements, we recommend use of semi-automatic or automatic method. Automatization allows measurement of thousands of fenestrations at the same time compared to manual measurement of tens of fenestrations; it provides a better statistical overview and removes user bias manifesting as an increase in the roundness parameter. For the porosity and fenestration frequency measurements we recommend the use of the automatic method as it is the most time efficient simultaneously processing of many images. If the image quality is poor, and artifacts do not allow the use of automatic methods, the manual approach may be necessary. When using (semi-)automatic methods we recommend using the manual method for small data sets as a reference, especially if the changes in porosity or fenestration frequency between the experimental groups are small.

The above strategies for scoring LSEC porosity using SEM, SIM and AFM imaging can also be applied to other super resolution imaging modalities applied to LSEC, e.g. dSTORM (Mönkemöller et al., 2014; Mao et al., 2019) or STED (Di Martino et al., 2018). These latter two methods have the highest reported optical resolution, at 10−20 nm. (Semi-)Automation of the LSEC porosity scoring process, in combination with current and new developments in super-resolution imaging, will accelerate the evaluation of LSECs in health, disease and aging, thus aiding to development of therapies that reverse the effects on LSEC defenestration, a key phenotypic feature in various diseases and ageing.

Declaration of Competing Interest

The authors declare no competing interest.

Acknowledgements

This work received funding from the European Union's Horizon 2020 research and innovation programme under the Marie Sklodowska-Curie grant agreement no. 766181, project "DeLIVER" and Research Council of Norway, Grant no. 288565 "NANO2021". This work was supported by the Polish National Science Centre under the "SYMFONIA 3" project, grant agreement no. UMO-2015/16/W/NZ4/00070.

The authors would like to thank Randi Olsen and Tom-Ivar Eilertsen from Advanced Microscopy Core Facility at UiT for the electron microscopy expertise and Deanna Wolfson for the help with SIM imaging.

Appendix A. Supplementary data

Supplementary material related to this article can be found, in the online version, at doi:https://doi.org/10.1016/j.micron.2021.103121.

References

Arganda-Carreras, I., et al., 2017. Trainable Weka Segmentation: a machine learning tool for microscopy pixel classification. Bioinformatics 33 (15). https://doi.org/10.1093/bioinformatics/btx180.

Berg, S., et al., 2019. Ilastik: interactive machine learning for (Bio)Image analysis. Nat. Methods 16 (12). https://doi.org/10.1038/s41592-019-0582-9.

Braet, F., Wisse, E., 2002. Structural and functional aspects of liver sinusoidal endothelial cell fenestrae: a review. Comp. Hepatol. 1 (1) https://doi.org/10.1186/1476-5926-1-1.

Cogger, V.C., et al., 2015. A standardized method for the analysis of liver sinusoidal endothelial cells and their fenestrations by scanning electron microscopy. JoVE 98. https://doi.org/10.3791/52698.

Di Martino, J., et al., 2018. STED microscopy: a simplified method for liver sinusoidal endothelial fenestrae analysis. Biol. Cell 110 (7). https://doi.org/10.1111/boc.201800016.

Hunt, N.J., et al., 2018a. Novel targets for delaying aging: the importance of the liver and advances in drug delivery. Adv. Drug Deliv. Rev. 135 https://doi.org/10.1016/j.addr.2018.09.006.

Hunt, N.J., et al., 2018b. Manipulating fenestrations in young and old liver sinusoidal endothelial cells. Am. J. Physiol. – Gastrointest. Liver Physiol. 316 (1) https://doi.org/10.1152/ajpgi.00179.2018.

Hunt, N.J., et al., 2020a. The effects of metformin on age-related changes in the liver sinusoidal endothelial cell. J. Gerontol. - Ser. A Biol. Sci. Med. Sci. 75 (2) https://doi.org/10.1093/gerona/glz153.

Hunt, N.J., et al., 2020b. Rapid intestinal uptake and targeted delivery to the liver endothelium using orally administered silver sulfide quantum dots. ACS Nano 14 (2). https://doi.org/10.1021/acsnano.9b06071.

Hunt, N.J., et al., 2021. Quantum dot nanomedicine formulations dramatically improve pharmacological properties and alter uptake pathways of metformin and nicotinamide mononucleotide in aging mice. ACS Nano 15 (3). https://doi.org/10.1021/acsnano.0c09278.

Kong, C., Bobe, S., et al., 2021. Multiscale and multimodal optical imaging of the ultrastructure of human liver biopsies. Front. Physiol. 12 https://doi.org/10.3389/fphys.2021.637136.

Le Couteur, D.G., et al., 2002. Hepatic pseudocapillarisation and atherosclerosis in ageing. Lancet 359 (9317). https://doi.org/10.1016/S0140-6736(02)08524-0.

Li, P., et al., 2020. Characterizing liver sinusoidal endothelial cell fenestrae on soft substrates upon AFM imaging and deep learning. Biochim. Biophys. Acta 1864 (12). https://doi.org/10.1016/j.bbagen.2020.129702.

Mao, H., et al., 2019. Cost-efficient nanoscopy reveals nanoscale architecture of liver cells and platelets. Nanophotonics 8 (7). https://doi.org/10.1515/nanoph-2019-0066.

Mönkemöller, V., et al., 2014. Imaging fenestrations in liver sinusoidal endothelial cells by optical localization microscopy. Phys. Chem. Chem. Phys. 16 (24) https://doi.org/10.1039/C4CP01574F.

Mönkemöller, V., et al., 2018. Primary rat LSECs preserve their characteristic phenotype after cryopreservation. Sci. Rep. 8 (1) https://doi.org/10.1038/s41598-018-32103-z.

Øie, C.I., et al., 2020. Liver sinusoidal endothelial cells contribute to the uptake and degradation of entero bacterial viruses. Sci. Rep. 10 (898) https://doi.org/10.1038/s41598-020-57652-0.

Rogers, G.W.T., et al., 1992. Decreased hepatic uptake of cholesterol and retinol in the dimethylnitrosamine rat model of cirrhosis. Liver 12 (5). https://doi.org/10.1111/j.1600-0676.1992.tb00581.x.

Schindelin, J., et al., 2012. Fiji: an open-source platform for biological-image analysis. Nat. Methods 9. https://doi.org/10.1038/nmeth.2019.

Simon-Santamaria, J., et al., 2014. Efficient uptake of blood-borne BK and JC polyomavirus-like particles in endothelial cells of liver sinusoids and renal Vasa recta. PLoS One 9 (11). https://doi.org/10.1371/journal.pone.0111762.

Sørensen, K.K., et al., 2012. The scavenger endothelial cell: a new player in homeostasis and immunity. Am. J. Physiol. 303 (12) https://doi.org/10.1152/ajpregu.00686.2011.

Tsuchiya, K., Accili, D., 2013. Liver sinusoidal endothelial cells link hyperinsulinemia to hepatic insulin resistance. Diabetes 62 (5). https://doi.org/10.2337/db12-1296.

Zapotoczny, B., Szafranska, K., et al., 2017. Quantification of fenestrations in liver sinusoidal endothelial cells by atomic force microscopy. Micron 101. https://doi.org/10.1016/j.micron.2017.06.005.

Zapotoczny, B., et al., 2017. AFM reveals dynamic morphology of fenestrations in living liver sinusoidal endothelial cells. Sci. Rep. 7 (7994) https://doi.org/10.1038/s41598-017-08555-0.

Zapotoczny, B., et al., 2019. Tracking fenestrae dynamics in live murine liver sinusoidal endothelial cells. Hepatology 69 (2). https://doi.org/10.1002/hep.30232.